Università degli Studi di Messina

Dipartimento di

Scienze Chimiche, Biologiche, Farmaceutiche ed Ambientali

"Doctor of Philosophy in "Chemical Sciences"

Optimization, Evaluation and Use of Advanced Gas Chromatography-Mass Spectrometry Methods within the Context of Food Analysis

Ph.D. Thesis of:

Barbara Giocastro

Supervisor:

Prof. **Luigi Mondello**

Coordinator:

Prof.ssa **Paola Dugo**

Dottorato di Ricerca in "Scienze Chimiche" XXXIII Ciclo 2017-2020

TABLE OF CONTENTS

Chapter 1

General scope and introduction

The field of food analysis is characterized by heterogeneous samples, ranging from samples of relatively low complexity and other highly challenging ones (*e.g*. roasted coffee aroma, *etc*.) which usually contain hundreds of compounds in a wide range of concentrations. In general, food products consists of many different nutrients of organic (*e.g.* lipids, carbohydrates, proteins, vitamins *etc.*) and inorganic (e.g. water, minerals, oxygen) nature. In addition to natural constituents, food products may contain cooking-related compounds (*e.g.* Maillard reactions products), xenobiotic substances that come mainly from technological processes, agrochemical treatments or packaging materials (*e.g.* phytosanitary products, plastic derivatives, mineral oil, *etc.*) and undesired transformation products (*e.g.*, oxidization, isomerization, and hydrolysis). All of these substances present a broad molar mass range, variable polarity, and a wide range of chemical abundance. The identification of such compounds in complex food samples, remains challenging in the field of food analysis. At present, one-dimensional (1D) gas chromatography (GC) is widely exploited for the separation of volatile and semi-volatile species in food products. However, often the complexity of many naturally occurring matrices exceeds the capacity of any single separation system. Therefore, in the past years considerable research has been directed to the combination of independent techniques, with the aim of strengthening resolving power. In such a respect, to circumvent the sample complexity an advisable option is the use of multidimensional analytical techniques. In such a respect, comprehensive two-dimensional gas chromatography coupled to various forms of mass spectrometry (GC×GC-MS) is one of the most powerful analytical tools available for the separation of complex food samples. Comprehensive 2D GC was first described in 1991 [1], when Liu and Phillips employed dual-stage thermal modulation to achieve a GC×GC separation. Since its inception, many efforts have been made in the field of GC×GC in terms of hardware, software and practical/theoretical studies.

The aim of the general research, described in this Ph.D. thesis, is the optimization, evaluation and use of advanced gas chromatography-mass spectrometry methods within the context of food analysis. Moreover, focus was dedicated to various optimization aspects of GC×GC-MS. Specifically, I have been involved in a study focused on the off-line combination of normal phase high performance liquid chromatography (NP-HPLC) and GC×GC coupled with quadruple mass spectrometry detection (QMS) [2], for the detailed qualitative profiling of the entire volatile fraction of essential oils. Apart from essential oils, cryogenic-modulated (CM) GC×GC-QMS has been exploited for the chemical characterization of lipid fatty acids in unconventional palm oils [3].

A further study was related to the optimization aspects within the context of different modulator devices. Modulators are the "key" component of any GC×GC system, with cryogenic and flow modulation (FM) the two most employed devices. In such a respect, the goal of the work was to generate similar chromatography profiles using finely-tuned CM- and FM-GC×GC-MS experimental conditions, with emphasis directed to the challenge of defining an equivalent column set. In this context, a side-by-side measurement of several chromatography parameters was carried out on a sample of coconut-derived bio-oil (a food-waste sample) [4] and on a mixture of cosmetic allergens [5].

I was involved in a review article focused on the current trends in the field of GC×GC-MS [6]. Attention was devoted to various aspects of mass spectrometry, in particular to ionization processes. Later, my activity moved towards the use of "milder" electron ionization conditions in the GC×GC-QMS analysis of a variety of different molecular-mass compounds with various polarities contained in vegetable oil (*e.g.*, sterols, fatty acid methyl esters, vitamin E, squalene, and a linear alcohol) [7]. The use of "milder" ionization enhances the possibility to add a further level (or point) of identification in GC×GC-QMS, namely the molecular mass, thus facilitating the detailed profiling of several complex food samples.

In addition, I was involved in a study in the field of fast GC×GC-QMS, developing a method based on the use of micro-bore columns in both dimension for the analysis of fragrance allergens [8]. Finally, I dedicated my activity on a research focused on the evaluation of a novel form of consumable-free thermal modulation, namely solid-state modulation (SSM) [9]. Specifically, the effect of gas flow conditions on SSM performance was evaluated in relationship to different modulation column geometries.

I was involved in a research focused on the analysis of pollutants released from food cooking emissions. The research work was carried out within the context of an internship at Helmholtz Zentrum Muenchen under the supervision of Prof. Ralf Zimmermann. It must be noted that, due to the corona virus pandemic, the research work was interrupted and only a brief description of the initial research project is herein reported.

References

[1] Z. Liu, J.B. Phillips. J. Chromatogr. Sci. 29 (1991) 227.

[2] M. Zoccali, **B. Giocastro**, I. L. Bonaccorsi, A. Trozzi, P. Q. Tranchida, L. Mondello, Foods, 8 (11) (2019) 580.

[3] Y. Caro, T. Petit, I. Grondin, P. Clerc, H. Thomas, D. Giuffrida, **B. Giocastro**, P. Q. Tranchida, I. Aloisi, D. Murador, L. Mondello &L. Dufossé. Nat. Prod. Res. 34 (2020) 93.

[4] I. Aloisi, T. Schena, **B. Giocastro**, M. Zoccali, P. Q. Tranchida, E. B. Caramão, L. Mondello, Anal. Chim. Acta 1105 (2020) 231.

[5] **B. Giocastro**, I. Aloisi, M. Zoccali, P. Q. Tranchida, L. Mondello, LC-GC (Europe) 33 (10) (2020) 512.

[6] P. Q. Tranchida, I. Aloisi, **B. Giocastro**, L. Mondello, TrAC Trends Anal. Chem. 105 (2018) 360.

[7] P. Q. Tranchida, I. Aloisi, **B. Giocastro**, M. Zoccali, L. Mondello, J. Chromatogr. A 1589 (2019) 134.

[8] **B. Giocastro**, M. Piparo, P. Q. Tranchida, L. Mondello, J. Sep. Sci. 41 (2018) 1112.

[9] M. Zoccali, **B. Giocastro**, P. Q. Tranchida, L. Mondello, J. Sep. Sci. 42 (3) (2019) 691.

Chapter 2

Comprehensive two-dimensional gas chromatography: fundamentals and theoretical/practical aspects

2.1 Gas chromatography fundamentals

Gas chromatography (GC), with open-tubular capillaries (OTC), is the technique of choice for the separation of volatile and semi-volatile compounds that are thermally stable at the temperatures required for their vaporization. The milestone work focused on GC was first published in 1952 [1] when Martin and James acted on a suggestion made 11 years earlier by Martin himself in a Nobel-prize winning paper on partition chromatography [2].

In the early days, GC remained exclusively a packed-column technique and not substantially different from the initial work of Martin and James. In 1958, Golay introduced the use of the open-tubular columns, demonstrating that a tube of capillary dimensions coated with a thin film of liquid was capable of providing superior efficiency to a packed column [3]. The schematic representation of a gas chromatograph setup is shown below in *Figure 2.1*. At the heart of the system is the column, in which the crucial physicochemical process of the separation occurs. The column contains the stationary phase, while the mobile phase (the carrier gas) is flowing through this column from a pressurized gas cylinder (source of the mobile phase). A pressure and/or flow-regulating unit controls the rate of mobile-phase delivery. The introduction of the sample is performed through a unit called injector. The whole sample is transferred from the injector to the analytical column, where continuous redistributions between the mobile phase and the stationary phase occur. Due to their different affinities for the stationary phase the individual components, eventually, form their own concentration bands, which reach the column's end at different times. The analytical column is directly connected to the detector, which identify and/or quantify the single components eluting from the separating column.

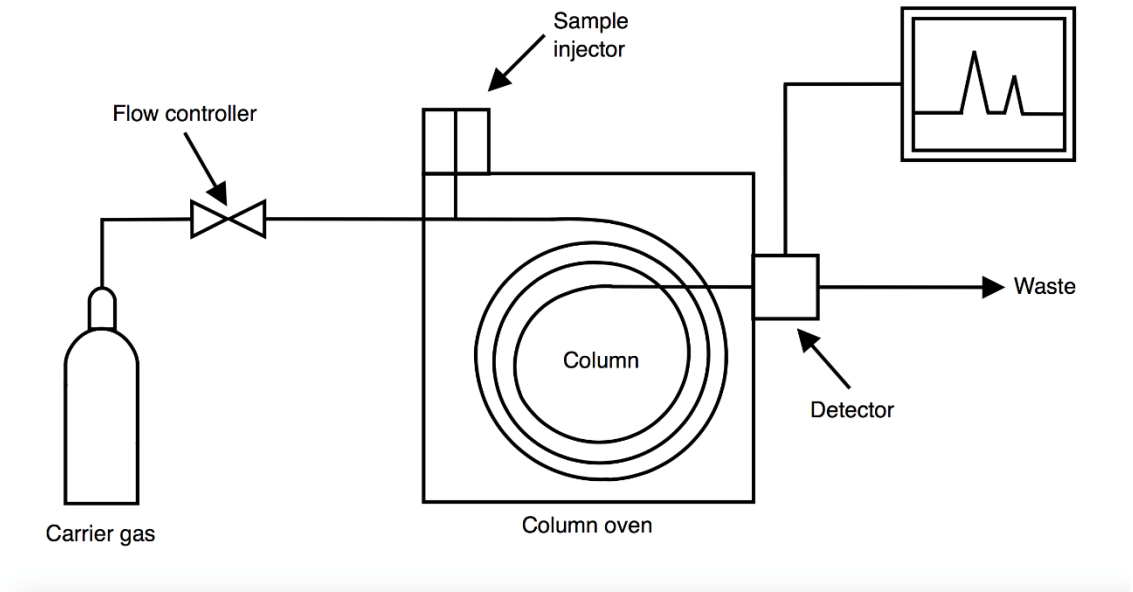

Figure 2.1. *The main components of a gas chromatograph.*

Summarizing the above, a typical gas chromatograph, essentially consist of three independently controlled thermal zones:

i) the injector zone that ensures rapid volatilization of the introduced sample;
ii) the column temperature that is controlled to optimize the separation process and
iii) the detector zone that must be at temperatures where the individual sample components are measured in the vapour phase.

2.1.1 GC terminology and figures-of-merit

- *Retention*

Separations by gas chromatography are recorded as chromatograms, of which an example is provided in *Figure 2.2.* Such a chromatogram is, basically, a plot of a series of peaks representing the separated compounds ordered by increasing time for elution (retention time) along the *x*-axis, *vs.* the detector response to the compounds as the *y*-axis.

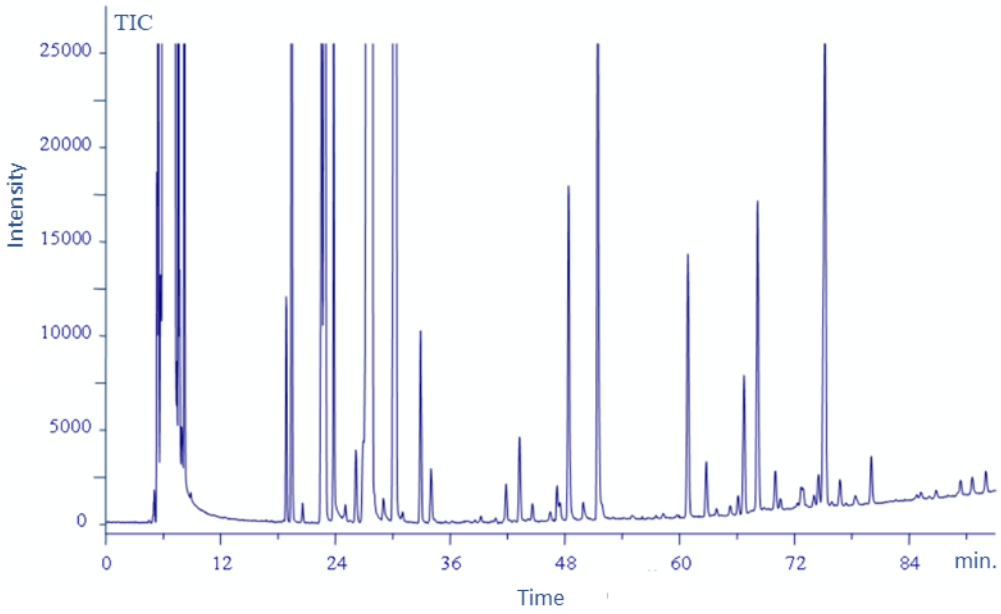

Figure 2.2. *GC chromatogram example.*

The observed retention time (t_r) contains the contribution of three components, which are related to the column and system properties:

i) the *extra column retention time* (the time to transport the sample to and from the column to accomplish sample introduction and detection);
ii) the *column holdup time*, the so-called *dead time* (the time required to transport a compound with no interactions with the stationary phase the length of the column), and
iii) the *adjusted retention time* (the additional time other than for transport each compound is delayed on account of its interactions with the stationary phase).

To characterize retention properties, regardless of the system characteristics, a useful term is the *retention factor*, *k'*, defined as:

$$k' = \frac{t_r - t_0}{t_0}$$

(Eq. 2.1)

the ratio of the time a compound engages in interactions with the stationary phase during the duration of separation, [or *adjusted retention time* $(t_r - t_0)$], and the time it takes a

completely unretained analyte in the carrier gas stream to travel the length of the column (*dead time*). Analytes with small *k'* will have little affinity for the stationary phase and shorter t_r. Analytes with large *k'* spend more time retained by the stationary phase and have longer t_r.

A measure of column selectivity is provided by the *separation factor*, *α*. The *α* value is obtained by a simple calculation corresponding to the ratio of the retention factors k', for any two compounds, with the numerator always the more retained of the two compounds. The term *α* can have values ≥1; a value of 1 corresponds to co-elution, indicating that the column has no selectivity for the separation.

The *distribution constant* K_c is a thermodynamic parameter defined as:

$$K_c = C_s/C_M$$

(Eq. 2.2)

where the terms C_s and C_M are equal to the solute concentration in the stationary and mobile phases, respectively.

The distribution constant, K_c, is connected to the *retention factor*, *k'*, by the following expression:

$$K_c = k' \times \beta$$

(Eq. 2.3)

where β is the *phase ratio* which is given approximately by dividing the column radius by twice the film thickness for open-tubular columns:

$$\beta = r_c/2d_f$$

(Eq. 2.4)

Since the early days of gas chromatography, an enormous effort has been directed at standardizing retention measurements to facilitate the use of collections of retention data for compounds identification. The retention index is the best method for documenting the GC properties of any compound. In the case of isothermal analysis, the retention index can be calculated as reported in *Eq. 2.5*. The retention index compares retention of a given solute (on a logarithmic scale) with the retention characteristics of standard solutes solution that usually are a homologous series of compounds:

$$I = 100_z + 100\frac{\log t_{r(x)} - \log t_{r(z)}}{\log t_{r(z+1)} - \log t_{r(z)}}$$

(Eq. 2.5)

The term *z* corresponds to the number of carbon atoms within a homologous series, while *x* relates to the unknown. For example, a series of *n*-alkanes can be used in this direction; each member of a homologous series (differing in a single methylene group) being assigned an index value of 100 times its carbon number (*e.g.*, 100 for methane, 200 for ethane, and 300 for propane, *etc.*). If a given solute happens to elute from the column exactly half-way between pentane and hexane, its retention index value is 550.

- *Band broadening*

The success of any GC separation is primarily dependent on maximizing the differences in retention times of the individual mixture components. Analytes are detected following the GC separation exhibiting an approximately Gaussian concentration distribution, defined by their t_r and the width at the base of the corresponding chromatographic peak, W_b.

The analyst aims to minimize peak broadening, measured as W_b in order to maximize the number of analyte peaks that can be ideally placed, side-by-side, into the available separation space, at a given resolution (*peak capacity*, n_c). Whereas the retention times are mostly related to the thermodynamic properties of the separation column, the peak width is a function of the efficiency of the solute mass transport from one phase to the other one and of the kinetics of sorption and desorption processes. In the case of OTC, the width of a chromatographic peak is determined by various processes such as molecular diffusion in the gas phase, molecular diffusion in the stationary phase, the residence time in the stationary phase, and the parabolic flow profile of the carrier gas along the column.

The most widely used, criterion of the column efficiency is the *number of theoretical plates*, *N*. *Figure 2.3* shows the measurements needed to calculate the value of *N* from a chromatographic peak.

$$\mathrm{N} = \left(\frac{\mathrm{t_r}}{\sigma}\right)^2 = \left(\frac{\mathrm{t_r}}{W_b}\right)^2 16 = 5.54\left(\frac{\mathrm{t_r}}{W_h}\right)^2$$

(Eq. 2.6)

Different terms arise because the measurement of σ can be made at different heights on the peak; at the base of the peak, W_b is 4σ, so the numerical constant is 16 (4^2); at half height, W_h is 2.35 σ, so the constant becomes 5.54 (please refer to *Figure 2.3*).

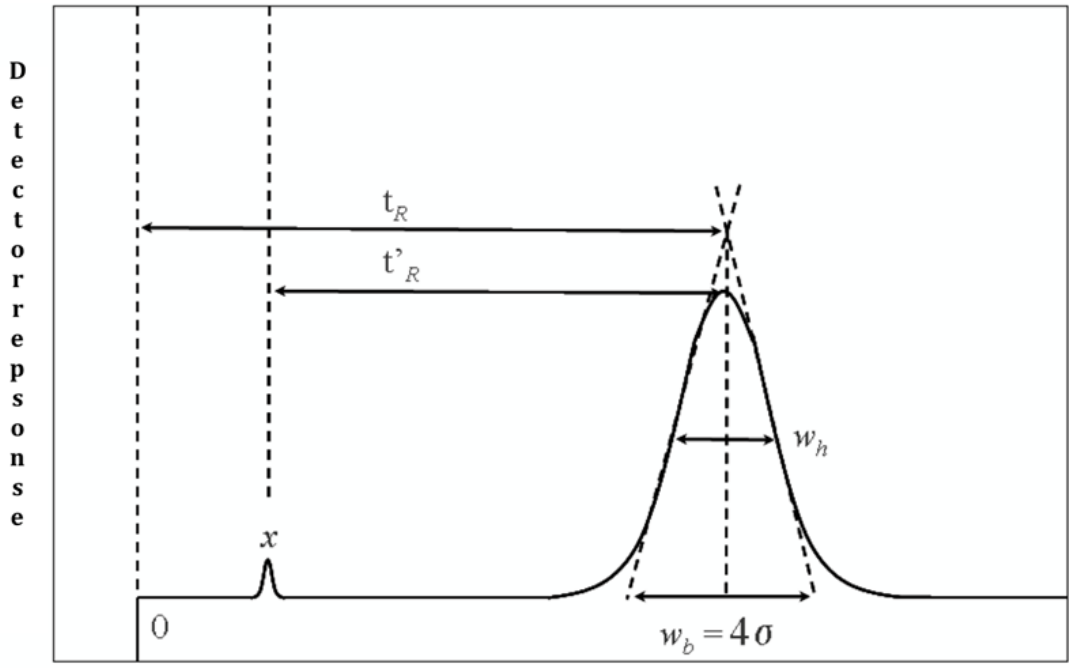

Figure 2.3. *Determination of the number of theoretical plates of a chromatographic column.*

A related parameter which express the efficiency of column is the *plate height, H*,

$$H = L/N$$

(Eq. 2.7)

where *L* is the column length. The length of a chromatographic column *L* is viewed as divided into imaginary volume units (*plates*) in which a complete equilibrium of the solute between the two phases is attained. Obviously, for a given value of t_r, narrower peaks provide greater numbers of theoretical plates than broader peaks.

For the sake of simplification, in the previous equations, the peak is assumed as perfectly symmetrical, following a Gaussian distribution, but real peaks usually exhibit some asymmetry (*Figure 2.4*), which are easily handled by peak modelling approaches [4].

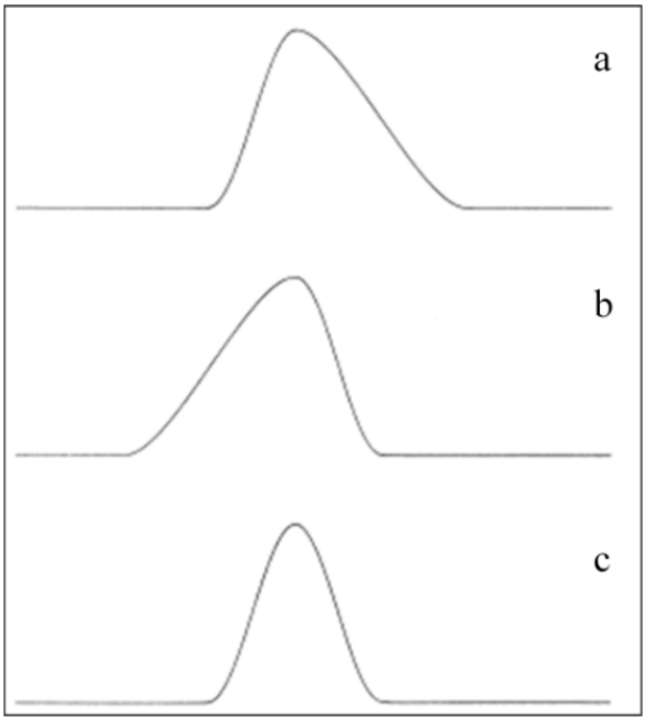

Figure 2.4. *Departures from peak symmetry: (a) slow desorption process (tailing) and (b) column overloading (fronting). (c) Gaussian distribution.*

The earliest attempts to examine the efficiency of column explain chromatographic band broadening were based on a kinetic approach described by the *van Deemter Equation*:

$$H = A + \frac{B}{\bar{u}} + C\bar{u}$$

(Eq. 2.8)

The broadening was expressed in terms of the *plate height*, *H*, as a function of the average linear gas velocity $\bar{u}$. The *van Deemter Equation* was referred to packed columns only and it identified three effects that contribute to the band broadening. The *eddy diffusion* (term *A*) describes the chromatographic band dispersion caused by the gas-flow irregularities in the column; *the longitudinal molecular diffusion* (term *B*) represents the peak dispersion due to the diffusion processes occurring longitudinally inside the column, and the *mass transfer* in the stationary liquid phase (*C*-term) which occurs due to a radial diffusion of the solute molecules. Thus, each of the three terms (*A*, *B* and *C*) should be minimized in order to maximize the number of theoretical plates, thus column efficiency.

A hyperbolic plot, the so-called *van Deemter curve* (*Figure 2.5*), represents the influence of linear gas velocity (ū) on the band broadening (*Eq. 2.8*). The curve shows the existence of an optimum velocity (ū) at which a given column exhibits its highest number of theoretical plates (*N*). Shapes of the van Deemter curves are further dependent on a number of variables: solute diffusion rates in both phases, column dimensions and various geometrical constants, the phase ratio, and retention times.

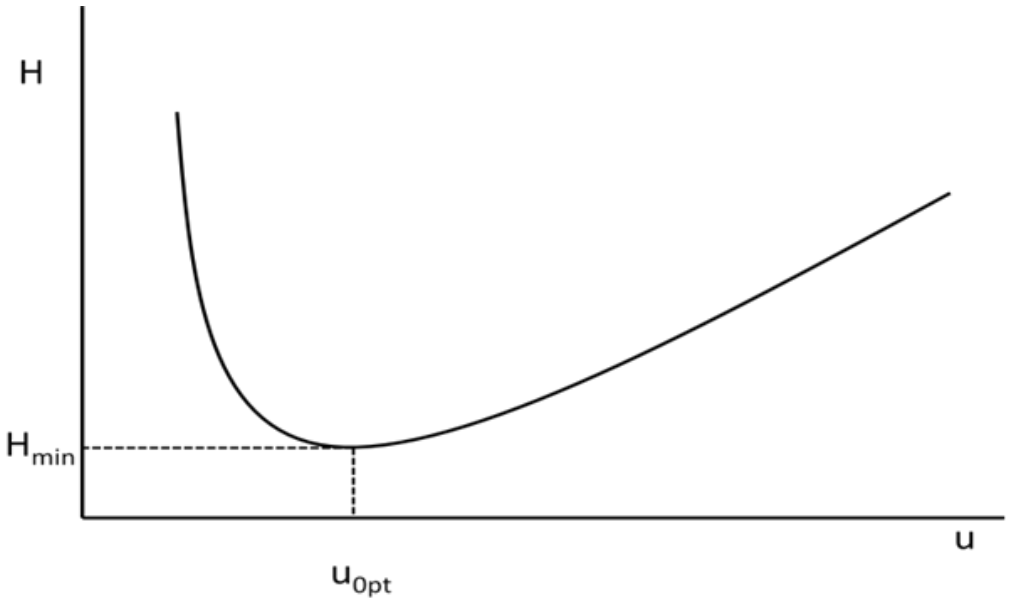

Figure 2.5. *Relationship of the plate height and linear gas velocity (van Deemter curve).*

Open-tubular columns contain no packing material inside the column and the A-term becomes zero, reducing the *van Deemter equation* to a form known as *Golay Equation* [5]. Specifically, two C-terms were introduced in the equation; one for the mass transfer in the stationary phase, C_s (similar to van Deemter), and one for mass transfer in the mobile phase, C_m. Thus the *Golay Equation* is:

$$H = \frac{B}{\bar{u}} + (C_s + C_m)\bar{u}$$

(Eq. 2.9)

where *B*-term represents the *molecular diffusion*. The equation governing molecular diffusion is:

$$B = 2D_G$$

(Eq. 2.10)

where D_G is the *diffusion coefficient* for the solute in the carrier gas. In *Eq. 2.9*, this term is divided by the linear velocity (ū), so a large velocity or flow rate will also minimize the contribution of the *B*-term to the overall peak broadening. That is, a high velocity (ū) will decrease the time a solute spends in the column and thus decrease the time available for molecular diffusion. The C_s term refers to mass transfer of the solute in the stationary phase and it is defined as

$$C_s = \frac{2kd_f^2}{3 + (1 + k)^2 D_s}$$

(Eq. 2.11)

where d_f is the average film thickness of the liquid stationary phase and D_s is the diffusion coefficient of the solute in the stationary phase. To minimize the contribution of this term, the film thickness should be small and the diffusion coefficient large. Rapid diffusion through thin films allows the solute molecules to stay closer together. Typical values for film thickness fall into the range 0.05–5 μm. Some typical performance properties for different open-tubular columns are reported in *Table 2.1*. The other part of the C_S-term is the ratio $k/(1 + k)^2$. Large values of *k* result from high solubilities in the stationary phase. This ratio is minimized at large values of k, but very little decrease occurs beyond a *k* value of about 20. Since large values of retention factor result in long analysis times, little advantage is gained by *k*-values larger than 20.

Golay‘s equation for the C_m term is:

$$C_m = \frac{(1 + 6k + 11k^2) r_c^2}{24(1 + k)^2 D_G}$$

(Eq. 2.12)

where r_C is the radius of the column. The relative importance of the two *C*-terms in the rate equation depends primarily on the film thickness and the column radius. We can say that for thin films (< 0.2 μm), mass transfer controls the *C*-term in the mobile phase; for thick films (2-5 μm), it is controlled by mass transfer in the stationary phase; and for the intermediate films (0.2 to 2 μm) both factors need to be considered. For the larger wide bore columns, the importance of mass transfer in the mobile phase in considerably greater. Finally, another consideration can be made on the *C*-terms that are multiplied by the linear velocity in *Eq. 2.9*: they are minimized at low velocities and so there is much time for the

molecules to diffuse in and out of the liquid phase and to diffuse across the column in the mobile gas phase.

Table 2.1. *Typical performance characteristics for 30 m coated OTC measured for n-undecane at 130°C.*

Internal diameter (mm)	Film thickness (µm)	Phase ratio	Column (N)
0.10	0.10	249	480000
0.10	0.25	99	328500
0.25	0.25	249	192000
0.32	0.32	249	150000
0.32	0.50	159	131300
0.32	1.00	79	102100
0.32	5.00	15	69000
0.53	1.00	132	70400
0.53	5.00	26	44000

- *Resolution*

Another measure of the efficiency of a column is the *Resolution* (R_s), which expresses the degree to which adjacent peaks are separated. The well-known Master equation for the calculation of R_s between two compounds with retention factors equal to k_1 and k_2 respectively, is:

$$R_s = \frac{\sqrt{N}}{4}\left(\frac{\alpha - 1}{\alpha}\right)\left(\frac{k_2}{k_2 + 1}\right)$$

(Eq. 2.13)

where R_s is proportional to the square root of the number of theoretical plates N (column efficiency) and is influenced by both the separation factor α (system selectivity) and the retention facor k (column retentivity). The different degrees of influence of N, α, and k on R_s can be observed in the example shown in *Figure 2.6*, where the separation of two analytes (k_1 = 4.8; k_2 = 5.0; α = 1.05) on a GC column (N = 20,000) under fixed conditions is considered. To a first approximation, the three contributions to R_s (*Eq. 2.13*) can be treated as independent and the following conclusions can be derived:

- *k:* if the column phase ratio (β) is reduced (or a lower temperature is used), leading to an increase in the retention factors, the benefits gained are very limited in terms of resolution. An increase in the retention factor (k) has a substantial effect on resolution, R_s , only for analytes with low k values (≤ 3).

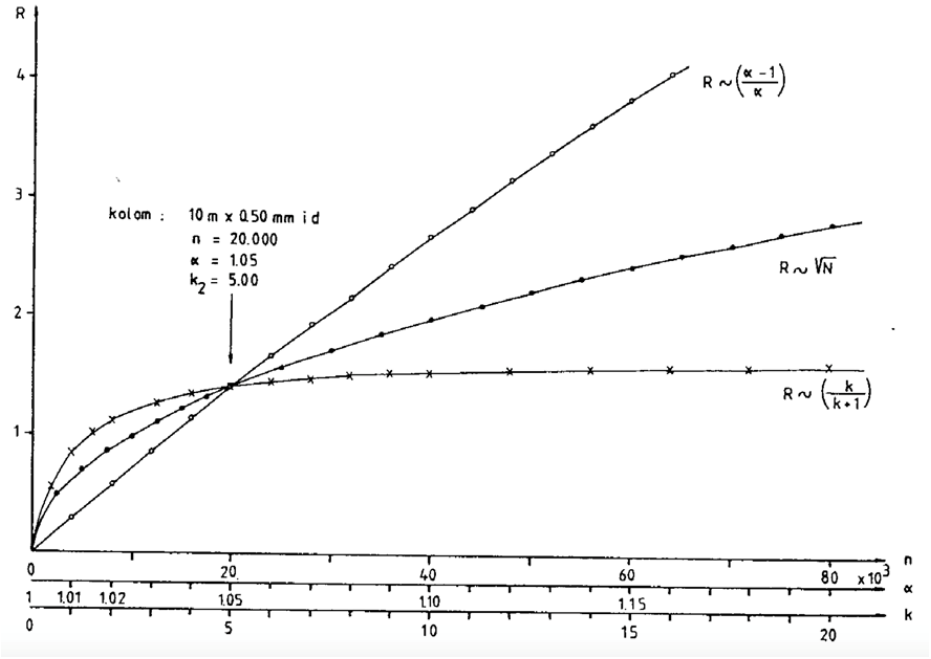

Figure 2.6. *Resolution: influence of N, α and k.*

- α: if a more selective stationary phase is employed, thus increasing k value, resolution will benefit greatly. From *Eq. 2.13* it can be concluded that at lower values, an increase in α will lead to a considerable improvement in resolution, up to an α value of about 3. At higher separation factor values, the function tends to level off. Of the three variables, selectivity has the greatest effect on resolution, and thus it is fundamental to select the most suitable stationary phase for a given separation. However, it must also be noted that *Eq. 2.13* is valid only for a single pair of analytes and not for a complex mixture of compounds; in the latter case, a stationary-phase change will often lead to an improvement in resolution for some analytes and a poorer result for others. The choice of the most selective stationary phase has the best effects only when a low-complexity sample is subjected to separation.

- *N*: if the column length is extended fourfold, leading to an increase in *N* by the same factor, resolution of the two analytes is only doubled. It follows that an evident improvement in peak resolution can only be achieved by extending the column length considerably. Such a modification is usually not desirable and certainly is not a practical solution in view of the greatly increased analysis time. However, enhancing the plate number is without doubt the best choice whenever a highly complex mixture is subjected to chromatography. In fact, an increase in *N* will lead to the same percentage increase in resolution for all the constituents of a sample.

2.2 The need for multidimensional GC

Currently, conventional 1D gas chromatography with open-tubular columns is the most common analytical method used for the analysis of volatiles and semi-volatile contained in the real-world samples. However, a satisfactory separation of all the components of a sample is often challenging when a single chromatography column is used.

A chromatographic process is governed by two main parameters:

i) peak capacity (n_c) and

ii) stationary phase selectivity.

The former (peak capacity-n_c) corresponds to the maximum number of peaks that can potentially be stacked side-by-side in the available separation space, at a given level of resolution. Such a parameter is related to the column geometry (*i.e.*, length, internal diameter, particle diameter, stationary-phase thickness) and to the experimental conditions (*i.e.*, mobile-phase flow and type, temperature, outlet pressure, *etc.*). The second parameter, stationary-phase selectivity, is mostly related to the chemistry of the stationary phase, and thus to the specific type of analyte-stationary phase interactions (*i.e.*, dispersion, dipole-dipole, electrostatic, *etc.*). Selectivity is also dependent on analyte solubility in the mobile phase, whenever this type of analyte-interactions occurs. The chromatographer aims to get the best out of a column, in order to minimize the peak broadening (W_b) and maximize the peak capacity of the chemical separation. The n_c value of a 1D GC approach can be easily estimated by dividing the retention time window (excluding the *dead time*) by the average peak width (4σ). When a conventional capillary column (30 m × 0.25 mm ID ×

0.25 µm d_f) is used the peak capacity is generally within the range 400-600. In theory, if a GC method generates a peak capacity of 600, then this means that 600 peaks could potentially be fitted side-by-side in the 1D separation space. However, GC peaks usually elute in a random manner, often leading to overcrowded parts of chromatogram, along with empty zones. The main consequence is that the n_c value must greatly exceed the number of volatiles contained in the sample if a full separation is desired. Specifically, the method peak capacity should exceed the number of the sample constituents by a factor of 100 if a resolution level of 98% is desired [6]. Consequently, to separate a 50-compounds sample, a GC method should generates a peak capacity of 5000. Such numbers indicate that the separation power of a conventional single GC column will be insufficient in many applications involving complex samples. The use of different column geometry, *i.e*. by using longer column, make it possible to increase the separation efficiency of 1D GC, but on the other hand, will increase the analysis time. The most effective way of enhancing the peak capacity and the selectivity of a GC system is to extend the separation space by adding one or more analytical dimension. When two or more GC column having different selectivity are combined together, the analytical system can be recognized as a multidimensional GC system (MDGC). In this *Chapter*, attention is focused on MDGC methodologies with emphasis directed to comprehensive two-dimensional gas chromatography (GC×GC) technology.

2.3 From MDGC to GC×GC

Widely accepted definitions of multidimensional chromatography have their roots in the concept of multidimensionality proposed by Giddings, who distinguished separations with a continuous two-dimensional separation, and coupled column with sequential zone displacements [7]. Later, Blumberg and Lee proposed the definition of "*n*-dimensional analysis as one that generates *n*-dimensional displacements" [8].

Each MDGC system has to fulfil two main conditions:

I. The components of a mixture should be subjected to two (or more) separation steps in which their displacements are governed by different factors

II. Analytes that have been resolved in the previous step should remain separated until the following separation process is completed.

When two (or more) independent separation are performed, an equal number of parameters contribute to define the identity of the analytes [9]. Taking into account two-dimensional GC, each analyte is characterised by two different retention times rather than a single one (as in 1D GC). If the dimensions are based on different analyte-stationary phase interaction (different selectivity), the separation is defined "*orthogonal*" [10]. The concept of orthogonality is illustrate in *Figure 2.7*; specifically three degrees of correlation between two separation dimensions are reported. In the case of totally orthogonal separation, the peaks are distributed over the entire two-dimensional (2D) space (*Figure 2.7a)*. The more the dimensions are correlated, the more the distribution will be centred along the diagonal (*Figure 2.7a).* In the case of total correlation, as illustrate in *Figure 2.7c,* the compounds will have the same retention in the two dimensions, thus resulting in the equivalent 1D separation along the diagonal.

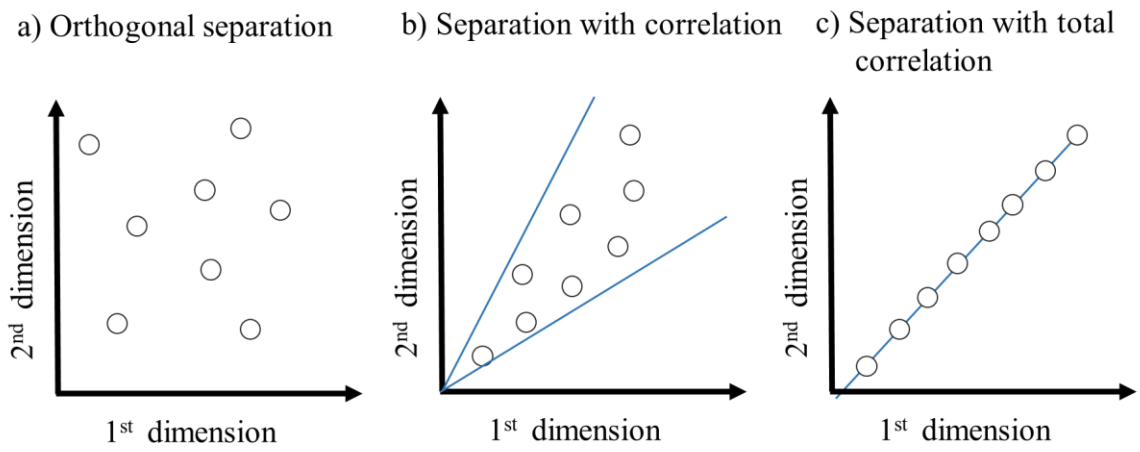

Figure 2.7. *Comparison of three degrees of correlation between two separation dimensions.*

Based on above, the analytical dimensions must be correctly selected in order to achieve ordered distributions of compounds and therefore efficient MDGC separations.

The MDGC systems can be divided in two main approaches: "heart-cutting" (or GC-GC) and comprehensive 2D GC (or GC×GC), respectively. A schematic representation of these different chromatographic modes is illustrated in *Figure 2.8.* Classical GC-GC (*Figure 2.8 a*) enables the transfer of selected bands of overlapping compounds from the first dimension (^{1}D) column ("heart-cut") into the second dimension (^{2}D). Obviously a preliminary 1D GC applications is necessary to select the first-dimension (defined as pre-column) effluent bands, that require analysis on the secondary column (defined as analytical column). The

number of heart-cuts can be increased, if only the time allowed for the separation of the cuts in the second dimension is proportionally reduced (*Figure 2.8 b*). When the number of heart-cuts gets high enough, and the time for their separation short enough, a comprehensive separation can be obtained (*Figure 2.8 c*). Consequently, one can say that GC×GC is in essence an extension of heart-cut GC, in which the entire sample is subjected to separation in both dimensions.

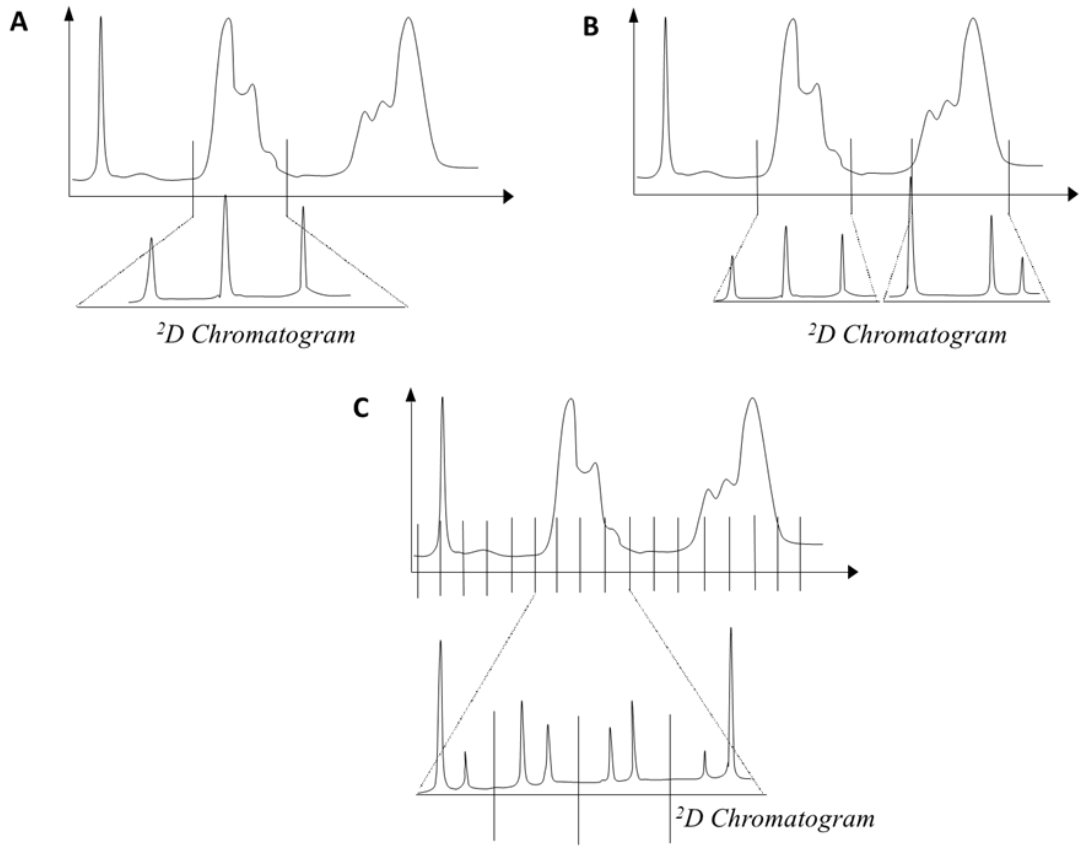

Figure 2.8. *The concept of MDGC. (A) single heart-cut GC analysis; (B) dual heart-cut GC analysis; (C) comprehensive 2D GC analysis.*

The benefits of combining two independent separation processes were recognized very early within the chromatography community. The first GC-GC experiment was described in 1958 by Simmons and Snyder [11]; a mixture of C5- C8 hydrocarbons were separated according to their boiling-points along the first-dimension; then each of four classes were subjected to a polarity-based separation along the ^{2}D, in four independent analysis. However, it was become increasingly clear that if the entire initial sample requires analysis in two different dimensions, then a different analytical route must be taken. In GC-GC, only a limited fraction of the total sample can be re-injected onto the second dimension, the

remained part is vented off or transferred to the detector without being subjected to both separations processes. In such conditions, the total number of peaks, which can be fitted in the separation space (n_c), equals the sum of that of the first and second dimensions; the latter multiplied by number (x) of heart-cuts $[n_{c1} + (n_{c2} \times x)]$ *(Figure 2.9).*

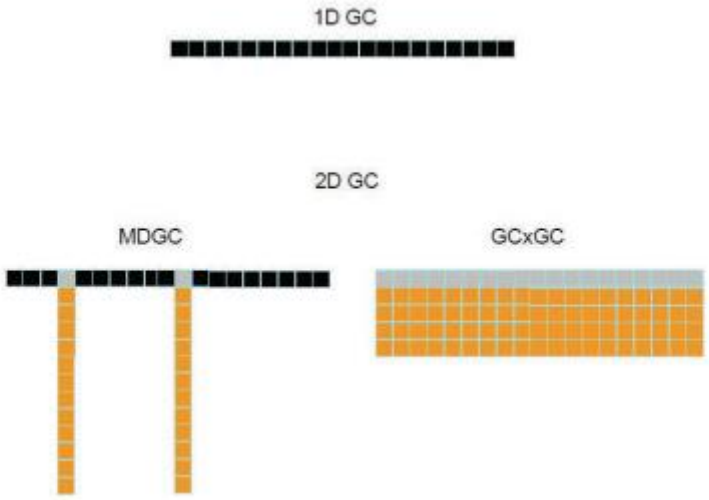

Figure 2.9. *Schematic presentation of 1D GC (on top), and the main types of 2D GC (bottom); GC-GC (left) and GC×GC (right).*

The loss of a substantial part of the primary column resolution has a significant impact on the applicability of the GC-GC technique. A more extensive occupation of the 2D separation space can be achieved by GC×GC. Ideally, in GC×GC, the total peak capacity becomes that of the first dimension multiplied by that of the second dimension $(n_{c1} \times n_{c2})$ (see *Figure 2.9*). The first example of comprehensive multidimensional chromatography was described in 1944 [12], when the chromatography pioneers reported a two-dimensional procedure for the analysis of wool amino-acids on cellulose. The authors reported as follows: "A considerable number of solvents has been tried. The relative positions of the amino-acids in the developed chromatogram depend upon the solvent used. Hence by development first in one direction with one solvent followed by development in a direction at right angles with another solvent, amino-acids (e.g., a drop of protein hydrolysate) placed near the corner of a sheet of paper become distributed in a pattern across the sheet to give a two-dimensional chromatogram characteristic of the pair of solvents used" [12].

The combination of solvents used in that analysis was chosen on the basis of R_F (retardation factor) values and in order to achieve a more extensive occupation of the 2D separation space. The amino acid R_F values for a series of solvent combinations were used both to

predict and to construct the "*dot plots".* The expected positions of a series of amino acids on 2D chromatogram, developed by using collidine in the first dimension and a phenol-ammonia in the second dimension, is illustrated in *Figure 2.10a*; a good agreement between the results predicted and the experimental results can be observed in *Figure 2.10b.* In the latter case, the comprehensive 2D chromatogram of wool hydrolysate is shown; amino acids were first separated along the dimension A-B (^{1}D), and then eluted along the dimension A-C (^{2}D).

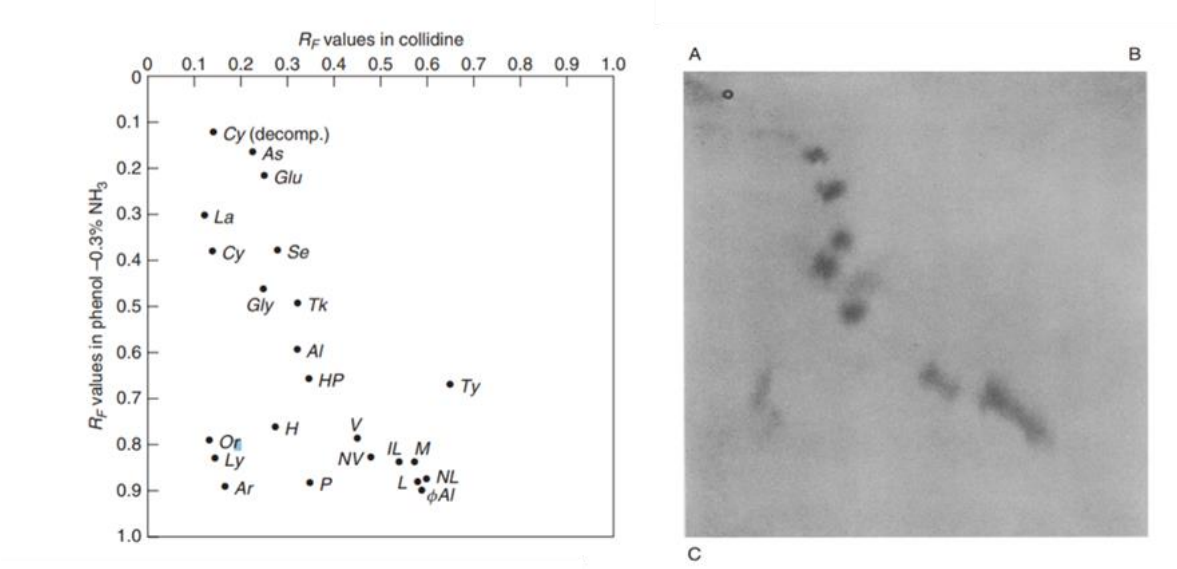

Figure 2.10. *Expected positions of a series of amino-acids on a 2D paper chromatogram (on the left) and comprehensive 2D chromatogram experimentally obtained (on the right) using collidine as ^{1}D (A-B) and a phenol-ammonia mixture in the ^{2}D (A-C).*

Pioneered by Liu and Phillips in 1991 [13] GC×GC is the most promising innovation in GC since the discovery of open-tubular columns. The leap from GC-GC to GC×GC was achieved using a special transfer device, called modulator. The latter, in a typical GC×GC experiment is located between the first and second capillary columns. In the Phillips's paper, a GC×GC separation of a mixture of standard compounds and a sample of coal liquid was achieved by employing a dual-stage thermal desorption modulator (TDM). While the follow column combination was chosen: a capillary column (with a polyethylene glycol stationary phase) of dimensions 21 m × 0.25 mm ID × 0.25 µm d_f as 1D, while the 2D was 1 m × 0.10 mm ID × 0.50 µm d_f column with a methyl silicone stationary phase.

Commercially available GC×GC systems offer several features that can not be matched by 1D GC. Specifically, the main advantages of GC×GC over conventional 1D GC can be resumed in six points:

1) enhanced separation power
2) enhanced specificity (the entire sample is subjected to a separation on two chemically different stationary phases);
3) enhanced sensitivity (the chromatography band isolation process is accompanied by analyte re-concentration, especially when using cryogenic modulation);
4) enhanced identification power due to the formation of highly organized chemical class (*e.g.*, alkanes, fatty acid methyl esters, pyrazines, etc.) patterns in the 2D chromatograms;
5) the capability to generate true sample-specific fingerprints; and
6) the generation of a higher amount of usable data per unit of time.

2.4 GC×GC: basic instrumental setup

The hardware setup of a GC×GC system (*Figure 2.11)* is quite simple and can be constructed using the same equipment employed for conventional 1D GC. A typical GC×GC experiment is carried out on two capillary columns (having different selectivity) connected through a sampling device, the so-called modulator. In most instances, both columns are placed in the same oven; or the second column can be housed in a different oven to enable more flexible temperature control. Thus, the only piece of hardware required to turn a 1D GC system into a GC×GC-one is the modulator. The latter can be mounted inside or outside any of the commercially available gas chromatographs. Specifically, the modulator acts as an on-line injector that produces very narrow injection pulses (down to 50 msec peak width) at the head of the second column, while respecting Giddings's conservation rules [7]. The entire 1D chromatogram is thus ''*sliced*'' following a modulation period (P_M) of a few seconds and re-injected into ^{2}D for a fast GC type separation (*Figure 2.11a*). Ideally, the separation of analytes in the ^{2}D has to be completed before another pulse is injected in the ^{2}D to avoid overlap of peaks issued from different modulation cycles (an effect called "wraparound").

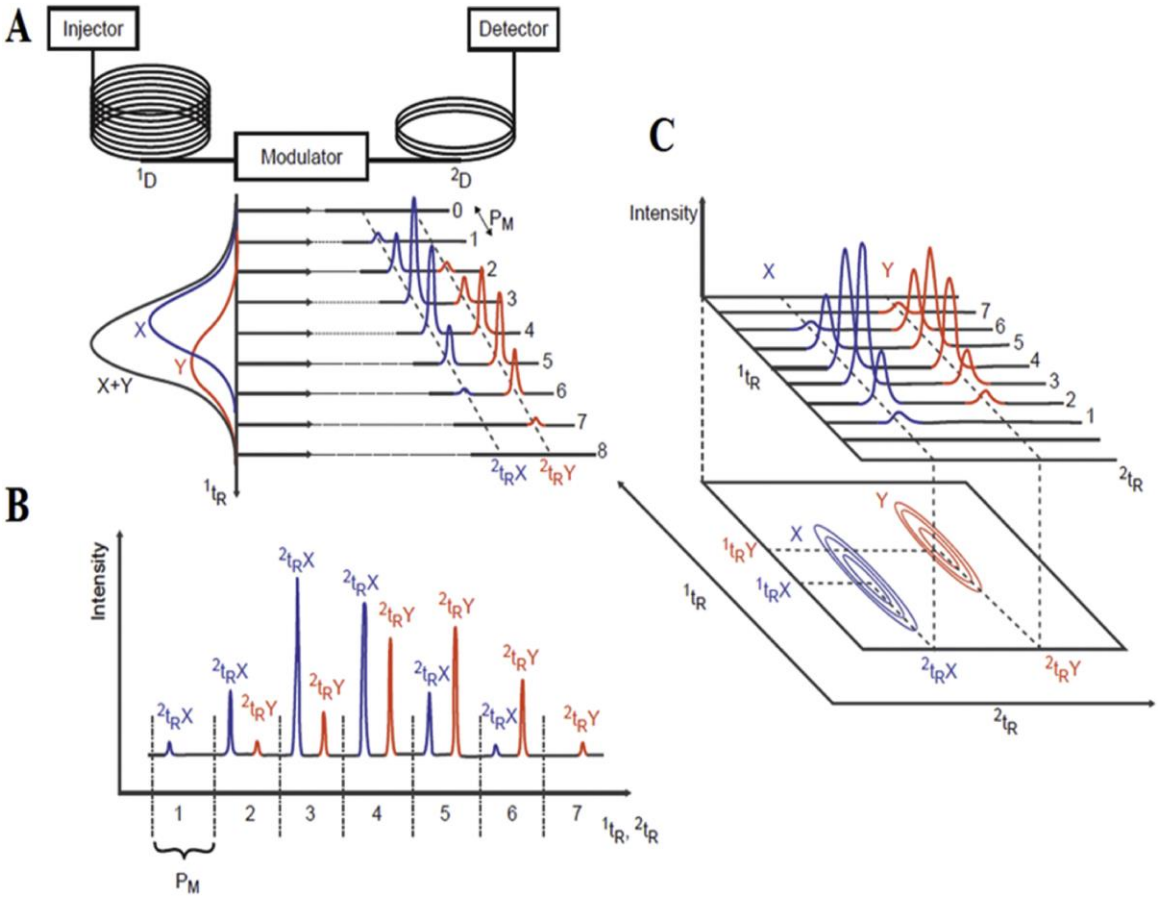

Figure 2.11a-c. *Scheme of the GC×GC setup. (a) The modulation process is illustrated for two overlapping compounds (X and Y) coming out from ^{1}D at a defined first-dimension retention time ($1t_R$). As the modulation process occurs during a defined PM, narrow bands of sampled analytes are entering into ^{2}D column and appear to have different second-dimension retention times ($2t_RY$ and $2t_RX$). (b) Raw data signal as recorded by the detector through the entire separation process. (c) Construction of the two-dimensional contour plot from (b).*

The second column analysis is much faster than the first one, thus leading to ^{2}D separation time approximately 100 times more rapid than in the ^{1}D. Although in principle, the detection occurs as in 1D GC, special requirements are needed for the detector used in GC×GC, which must be characterized by high acquisition rates, and short rise times to accurately reconstruct the narrow chromatography bands generated. Actually, a series of high-speed secondary chromatograms of a length equal to P_M (1-8 sec) are detected one after another (*Figure 2.11b*). They can at the end be combined to describe the elution pattern by means of a 2D plane (*Figure 2.11c).*

Although basic information on chromatographic performance can be deduced from the modulated raw signal, a conversion process in 2D chromatogram is necessary to elaborate and visualize the overall GC×GC separation (*e.g.* the presence of wrap-around, the amount of occupied 2D separation space, the chemical-class pattern formation *etc.*). In such a respect, the use of dedicated software packages are required. The generation of a 2D plot is a simple process, each second-dimension chromatogram is stacked side-by-side and, considering the modulation time, the first and second retention times (t_r1 and t_r2, respectively) are derived for each peaks. The resulting planar separation space contains oval-shaped peaks (intensity is related to color), each defined by two retention time (t_r1, t_r2) and an area. Although not a necessity, three-dimensional plots can also be visualized, containing cone-shape peaks projected into a space defined by a *z*-axis.

Though building a GC×GC system may seem quite simple, GC×GC method optimization is far more complicated than that in 1D-GC.

2.4.1 Column combination

Although the modulator is considered as the key component of any GC×GC system, simply installing a modulator between two column does not guarantee an efficient GC×GC separation. As in any GC system, the selection of the most appropriate chromatographic column plays significant roles to achieve a satisfactory GC separation. In such a respect, column combination optimization, including stationary phase chemistry and column geometry, is required to accomplish efficient GC×GC separation. The main aim of any GC×GC method development is to maximize the amount of exploitable separation space, which is mainly achieved by choosing a proper columns set configuration. Following the "Giddings's roles" [7], a successful multidimensional separation is achieved by combining two columns capable to generate an orthogonal setup. Theoretically, considering two completely-independent column selectivities and a fully-optimized separation, the peak capacity of a GC×GC system should be equal to the product of the peak capacity value relative to each column; however, such a result is an excessive estimation since both of the aforementioned conditions are never fully achieved. It must be emphasized, whatever stationary phases are used, complete orthogonality cannot be achieved because the volatility dimension will always generate a certain degree of correlation between the two separation mechanisms. For such a reason, it is not so common to observe analytes with a

low 1trvalue, and a high 2tr one (and vice versa). In fact, a high number of published GC×GC chromatograms are characterized by "fanshaped" analyte bands, with a left-to-right upward inclination, and with plenty of unexploited space. A typical example of low exploitation of the available 2D separation space can be observed in the cod oil fatty acid methyl ester (FAMEs) chromatogram, illustrated in *Figure 2.12*. Even though the chromatogram is well structured (C_{14} to C_{22} group-type patterns are evident), only 22.3 % of the entire 2D chromatography space is used [14]. This negative GC × GC feature can be caused by two main factors: partial correlation between the two dimensions and an excessively high second-dimension gas linear velocity. The latter aspect is discussed in depth later.

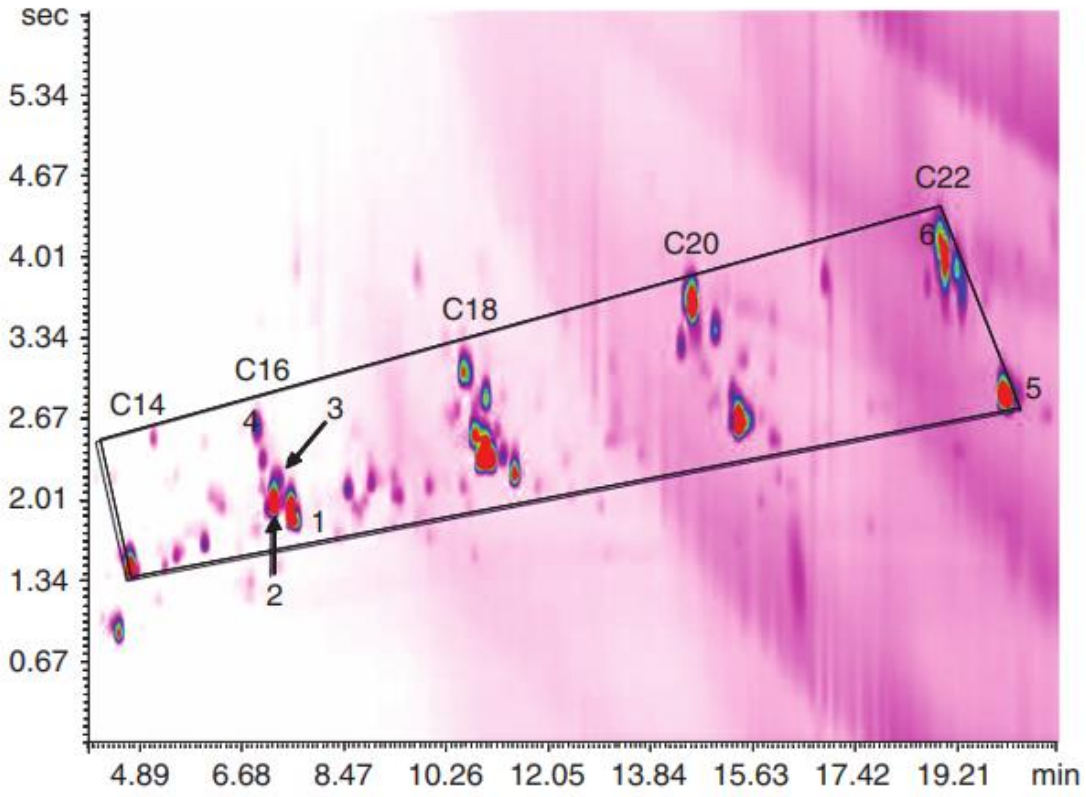

Figure 2.12. *GC×GC chromatogram of cod liver oil FAMEs. Peak identification: 1.$C_{16:0}$; 2. $C_{16:1\omega7}$; 3.$C_{16:2\omega4}$; 4.$C_{16:4\omega3}$; 5.$C_{22:1\omega9}$; 6. $C_{22:6\omega3}$.*

The most common and orthogonal column configuration combines a non-polar column as first dimension, for example, dimethylpolysiloxane, and a second column with a more polar stationary phase, for example, polyethylene glycol, phenylmethylpolysiloxane, or cyclodextrine [15, 16]. In such a case, the primary-column elution order occurs according to increasing boiling points, while the secondary-column separation is dependent on

specific polarity-based interactions (H-bond, dipole-dipole interactions, dispersion forces, etc.). Any existing stationary phase that can be used in 1D GC can also be used GC×GC. A variety of stationary phases can be selected according to the intended analyte-stationary phase interaction. Many sample-types are characterized by the presence of homologous series of constituents. The GC×GC analysis of fatty acid methyl esters (FAMEs) is a perfect example to illustrate group-type order [17]. *Figure 2.13* shows a complex human plasma fatty acid profile, in which homologues compounds are situated in a grid according to their chemical characteristics. In particular, saturated FAMEs are in the lower part of the 2D chromatogram, while an increase in the number of double bonds (DB) in the fatty acid chain intensifies retention in the second dimension. On the other hand, a reversed column set can better satisfy the aims of a specific research. Adahchour et al., studied and compared a normal and reversed column set for two different complex samples, namely diesel oil and food flavours [18]. When food flavour samples were analyzed, the reversed approach improved the peak shape of polar compounds, such as aliphatic acids and alcohols, which improved the ordered structure of the chromatogram. Seeley et al. used a high-temperature phosphonium ionic liquid column in a GC×GC application, proving that these phases can be considered as good candidates for the second dimension of a GC×GC setup [19]. Seeley himself introduced the concept of *dual-secondary GC×GC* (GC×2GC) [20]. The latter consists in the use of a dual parallel secondary column system by splitting the focused pulse towards two parallel secondary columns instead of a single one.

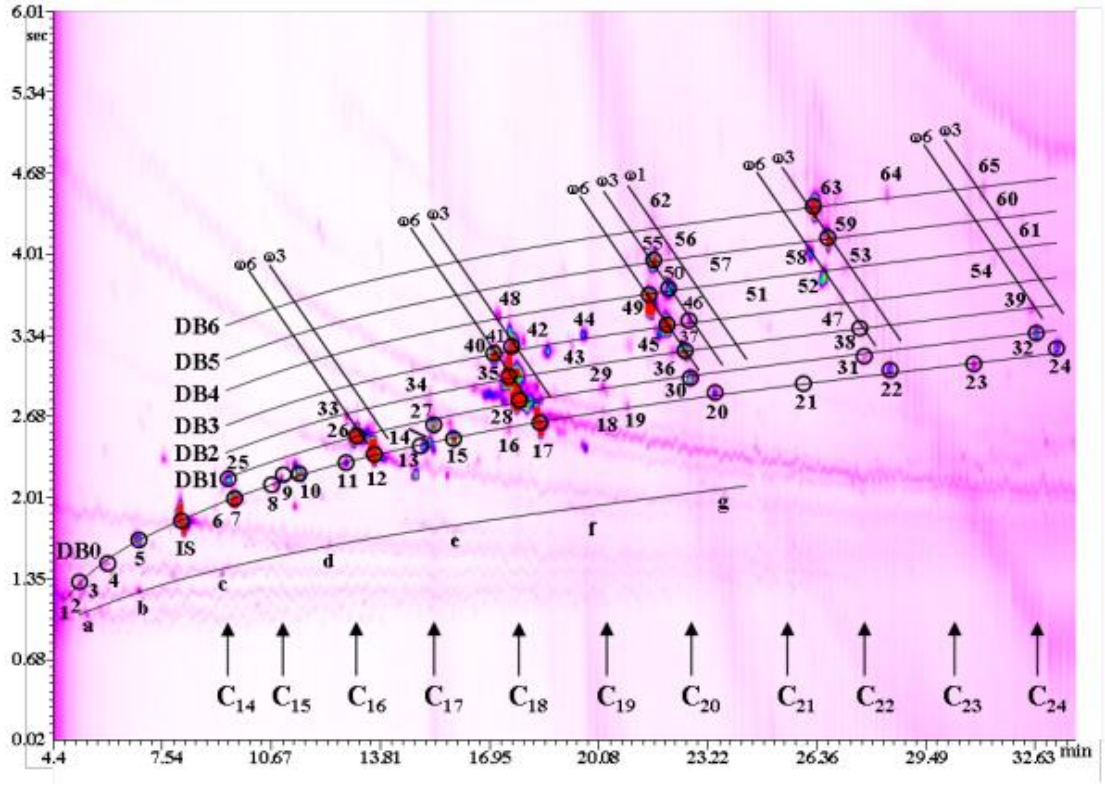

Figure 2.13. *GC×GC analysis of human plasma fatty acids. For peak identification refer to reference [17].*

Apart from the selection of the most appropriate stationary phase, the column geometry must be considered. Generally, a conventional "normal-bore" capillary column, *e.g.* 10-60 m, 0.25 mm ID, 0.25 µm d_f, is used as first dimension, while a short "micro-bore" column, 0.1mm ID, 0.1 µm d_f, is used as the second dimension. The secondary column generally measures between 80 and 200 cm long to maintain elution times that are under the modulation period (*i.e.,* 0.5-8 s) for most analytes. The direct consequence of using two capillaries with different IDs is that, under specific gas flow conditions, there will be a mismatch between the average linear gas velocity (ALV) values. In fact, it can be easily found that most GC×GC separations are carried-out at gas velocities that are ideal (or near to-ideal) in the ^{1}D and far from optimum in the ^{2}D. The reason for such gas velocity conditions is related to the fact that a single pressure source supplies gas to a long conventional and short micro-bore twin-column system. The most popular choice is the use of a ^{1}D 30 m × 0.25 mm ID × 0.25 µm d_f capillary column followed by a segment of 1m × 0.10 mm ID × 0.10 µm d_f as ^{2}D. If a such column set is used in GC×GC-FID experiment and an inlet pressure of 125 kPa (H_2) (at 50°C) is applied, then a gas flow of approximately

1.6 ml/min will be generated, corresponding to an ALV of about 30 and 265 cm/sec in the first and second dimensions, respectively. Such separation conditions are close to the ideal for a 0.25-mm ID column but far from the ideal 0.10-mm ID column (ALV to high). The GC×GC gas velocity compromise becomes less evident when the diameter of the two columns are closer. However, the proper column dimensions and column combinations, needed for a specific separation, can also be predicted by calculating the optimum flows.

2.4.2 Transfer device

As in any multidimensional system, the interface between the two dimensions is a key component in the instrumentation. The transfer device, so-called *modulator*, controls and sets fractions transit between the separation dimensions. Its role is to cut, possible re-concentrate, and to re-inject bands of eluate from the outlet of the primary column onto a short column segment, in a sequential, continuous way throughout the analysis. Since the transfer device is arguably considered the most important component of any GC×GC system, a deeper insight will be provided in section 2.5.

2.4.3 Detectors

The detector is another important GC×GC system component. GC×GC peak elution is normally very rapid and peak volumes small, requiring detector systems with a rather high sampling rate, limited internal volumes and a rapid rise time. All of these characteristics are necessary in order to reduce the effects of extra-column band broadening and to achieve a proper peak reconstruction (10 points per peaks are sufficient in the most cases). A brief discussion about detectors employed in GC×GC follows.

Flame ionization detector. The most commonly employed detector in GC×GC is the *flame ionization detector* (FID), which is capable to operate under very high sampling frequency conditions, easily above 100 Hz. It operates on the basis of decomposing the solute-neutral molecules in a flame into charged species and electrically measuring the resultant changes of conductivity. A cross-sectional view of a flame-ionization detector is shown in *Figure 2.14*. A small flame is sustained at the jet tip by a steady stream of pure hydrogen, while the necessary air (oxidant) is supplied through the diffuser. At the detector base, the column effluent is continuously introduced, mixed with hydrogen, and passed into the flame.

Conductivity changes between the electrodes are monitored, electronically amplified, and recorded. A conventional carrier gas contributes little to the flame conductivity; however, when organic solute molecules enter the flame, they are rapidly ionized, increasing the current in accordance with the solute concentration. With most flame-ionization detectors, this current increase is linear with the solute concentration up to six orders of magnitude. The flame-ionization detector is a carbon counter; each carbon atom in the solute molecule that is capable of hydrogenation is believed to contribute to the signal (compounds with C—C and C—H bonds), while the presence of nitrogen, oxygen, sulfur, and halogen atoms tends to reduce the response. The detector is most sensitive for hydrocarbons. Practically, no response is obtained for inorganic gases, carbon monoxide, carbon dioxide, and water. With such a detector, group-type 2D chromatograms can be obtained, and tentative peak classification can be achieved. The group type is assigned according to retention time correspondence with even one standard, and then FID quantification can easily be done. Biedermann and Grob exploited GC×GC-FID for the quantification of mineral oil constituents contained in a contaminated sunflower oil [21]. GC×GC-FID has been employed in several fields, such as environmental [22, 23], industrial [24], and food [25, 26]. The main drawback of using an FID, is the lack of structural information.

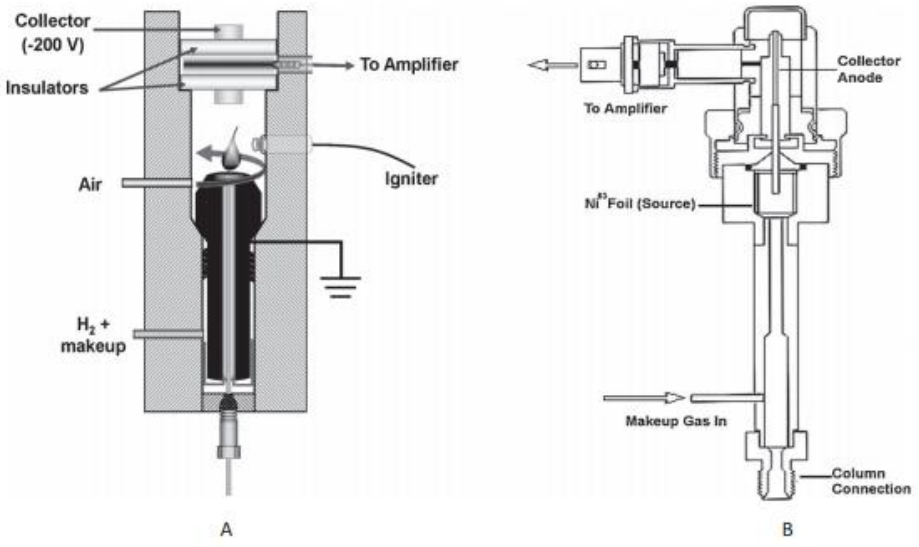

Figure 2.14. *Schematic diagram of a flame ionization detector (A) and a co-axial cylinder electron-capture detector (B).*

A variety of different other detectors have been used in the GC×GC field. The *electron capture detector* (ECD) is a concentration-dependent device and is characterized by a high specificity for organic molecules containing electronegative functional groups (halogens, phosphorous and nitro-groups). The main concern in coupling such a detector, has been related to a rather high internal volume, which can cause band broadening. The *atomic emission detector* (AED) is a device capable of measuring up to 23 elements: a He plasma chamber receives the GC effluent, and due to the high temperature encountered therein, the analytes are decomposed to their constituent atoms. Van Stee et al. reported the use of a GC × GC -AED system in petrochemical and pesticide applications [27]. The *thermionic ionization detector* (TID) is often used for the selective detection of N and P-containing compounds (in this case, it is also defined as the nitrogen phosphorous detector-NPD) and is structurally similar to the FID, apart from the presence of a ceramic bead doped with an alkali metal salt, located above the jet. Engel et al. reported the optimization and evaluation of a GC × GC –TID method for pesticides analyses [28]. The *helium ionization detector* (HID) is a sensitive and universal detector, used in particular for compounds with no or a limited FID response. The HID has been used only rarely in the comprehensive 2D GC field; the first application was reported by Winniford et al., who used a miniaturized pulsed discharge HID, in cryogenic-modulation (CM) GC × GC applications [29].

A discussion apart has to be made on mass spectrometers, the most informative detection systems, considered as an additional third dimension analysis by GC×GC users. The use of mass spectrometry (MS), as GC×GC detector dates back over 20 years ago [30], when Frysinger and Gaines reported the use of a single quadrupole mass spectrometer (QMS) system with a very low acquisition speed (2.43 scan s^{-1}). More detailed descriptions related to the use of GC×GC-MS systems in the field of food analysis, are reported in the following *Chapters*.

2.5 Modulators

As the “heart” of a GC×GC system, the modulator is located between the ^{1}D and the ^{2}D column, acting as an online injector that produces very narrow injection pluses onto the ^{2}D, generating fast secondary separations. Each modulator operates on the premise of sampling, focusing, and reinjecting portions of the ^{1}D effluent onto the head of the ^{2}D column, facilitating a comprehensive separation. The simply serial connection of two different

columns without a modulator between them, does not achieve a GC×GC separation. *Figure 2.15* explains the need for and the role of the modulator. Specifically, panels *A-C* in *Figure 2.15*. illustrates a separation with no modulator between the two columns, which essentially, will result in one-dimensional separation. In addition, there is also the possibility of the changing the elution order of the analytes due to different selectivity of the ^{2}D column (*Figure 2.15-C).* Differently, panels *D-G* illustrates a separation when the modulator interfaces the two columns. The analytes which are approaching the modulator interface (*Figure 2.15-D*) are collected or sampled for a designed period of time (according to P_M) (black in *Figure 2.15-E*). They are then re-injected as a narrow pulse onto the head of the ^{2}D column. In the meantime, the following chromatographic band is sampled (*Figure 2.15-F*). Focusing and re-injection of this analyte band allows for further separation in the ^{2}D only after the previous band had eluted from it. In the meantime the last analyte band eluting from ^{1}D is collected by the modulator (*Figure 2.15-G*).

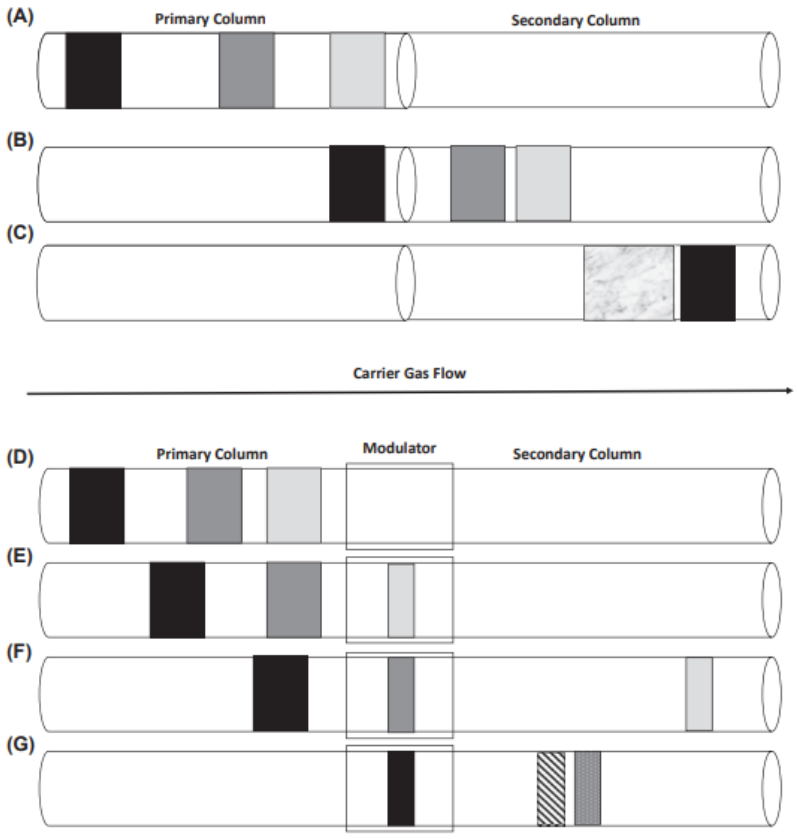

Figure 2.15. *The relevance of the modulator in GC×GC. A-C illustrate how bands separated on one column can recombine or change elution order on the second column if they flow uncontrolled from one to the other. D-G illustrate how the interface traps material from the primary column, and then allows discrete bands to pass to the second dimension column while trapping other fractions.*

Various technological improvements have been made throughout the development of modulators and they can be broadly classified in two categories: *thermal* and *valve-based*, or *flow*, modulators. Another general distinction exists between *one*- and *dual-stage* modulators: in the latter, two events in series occur in two different zones of the modulator. *Thermal modulators* can be further divided in two different classes, namely *cryogen-based* and *cryogen-free* modulators. While among *valve-based* modulators, two more approaches can be identified, namely those which employ a *differential flow modulation*, and those employ a *flow diversion modulation.*

2.5.1 Thermal modulators

The term "thermal modulator" is employed for any devices that use a positive and/or negative temperature, compared to the GC-oven temperature, to achieve a GC×GC separation. It relies on low temperatures to trap and focus analytes exiting from the ^{1}D column and re-inject them onto the ^{2}D column through rapid heating. Based on the various designs, the trapping stage can be accomplished using a thick stationary phase film, intense cooling, or combination of the two. The main advantage of thermal modulation over flow modulation is the focusing effect from the re-concentration of the analyte bands during trapping, thus leading to an enhancement of the signal-to-noise (*S/N*) ratio. In the pioneering GC×GC design, analytes eluting from ^{1}D were transferred onto the ^{2}D using a thermal modulator, namely a thermal desorption modulator (TDM). The latter, was originally developed as a sample introduction device in multiplex and high-speed gas chromatography [31-34]. It was only in 1991 [35] that Liu and Phillips, used the TDM to perform the first dual-stage modulated GC×GC separation. A dual-stage modulation was achieved by alternating two events during the entire analysis; a trapping stage based on phase-ratio focusing; and a re-injection one accomplished by thermal desorption. A scheme of TDM-GC×GC system proposed by Phillips is below reported, *Figure 2.16*. The TDM interface was constructed by coating the initial part of the secondary column with a film of electrically conductive material, namely gold paint, and by looping it outside the GC oven, at room temperature. The modulator was 15 cm in length, divided equally between two stages.

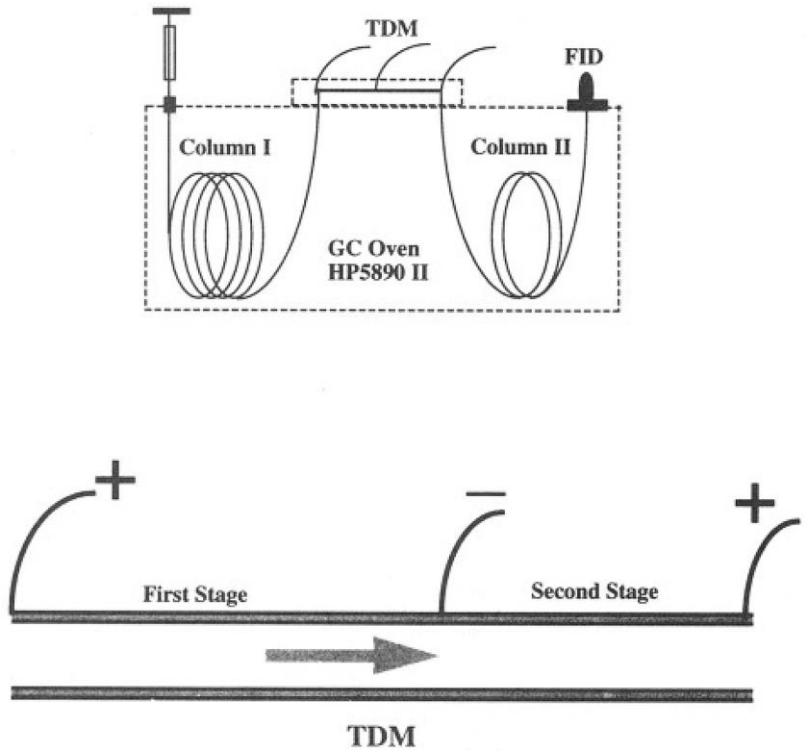

Figure 2.16. *Scheme of TDM-GC×GC-FID system employed by Liu et al. [35]. An expansion of the modulator is shown in the bottom part.*

The principal of its operation is shown in *Figure 2.17* and it consists on the following steps:

(1) analytes eluting from the ^{1}D column were entrapped in the thick film of stationary phase outside the GC oven (band compression I), at ambient temperature (step 1a);

(2) the application of an electrical pulse to the conductive capillary tube resulted in heating of the stationary phase and drove the analytes back into the gas phase, thus leading to their re-mobilization ending the first modulation stage (step 1b);

(3) the re-mobilized fraction, transported by the carrier gas, reach the second "cold" segment of the modulator (band compression II);

(4) another narrow chromatography plug begins to be accumulate at the modulator head, which has rapidly cooled down to ambient temperature (step 2a);

(5) at this point, another electrical pulse is directed to the second modulator segment, launching the narrow band onto the secondary column (step 2b), thus ending the second modulation stage

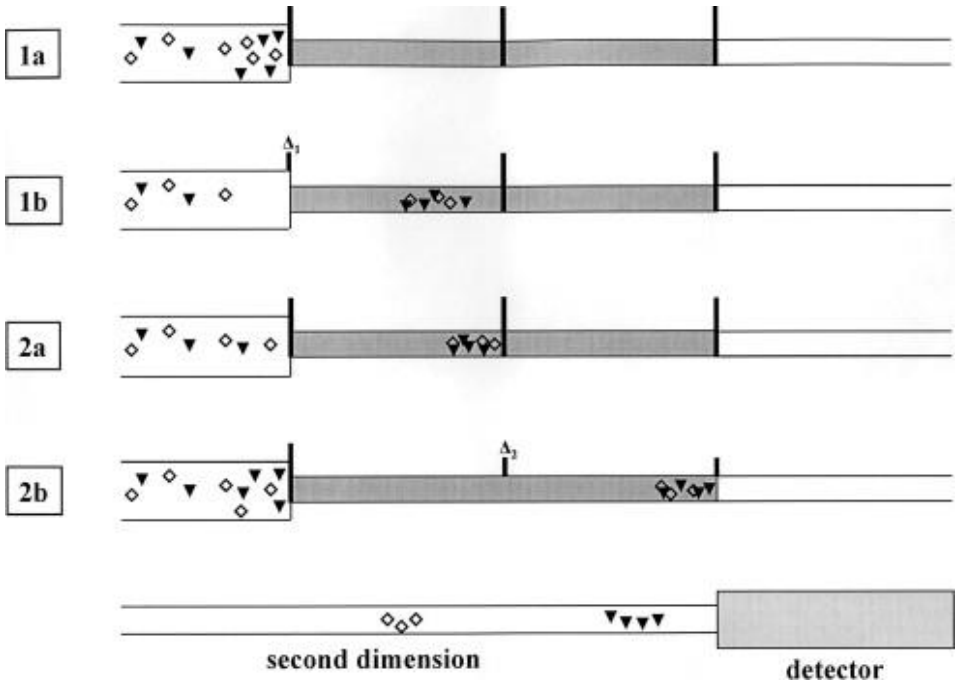

Figure 2.17. *Dual-stage thermal desorption-modulation process on two compounds, co-eluting in first dimension.*

(6) the different secondary-column selectivity will enable the delivery of two separated compounds to the detector; and

(7) 2 s the first electrical pulse, the next modulation process was initiated.

Although successful in accomplishing the first GC×GC separation, the design was not very robust due to frequent burnouts and the delicate nature of the thin conductive films. Many efforts have been made on the designs of thermal modulator over the years, and today they can be further broken down into two subcategories: *cryogen-based*, and *cryogen-free* modulator, which are often further divided into *movable* and *static* modulators, respectively.

2.5.1.1 Cryogen-based modulators

Cryogen-based modulators use cryogens to provide cooling in order to trap the solutes at temperatures significantly lower than the oven temperature. The re-mobilization step is achieved once that the cooled section of the modulator is brought back to or higher than the GC oven temperature. Although the use of cryogens (LN_2 or CO_2) for thermal modulation added a consumable cost to the system, it remains popular and continues to be further developed.

Longitudinal movement design. Cryogen-based modulation was first described in 1998 [36] when Kinghorn and Marriott reported the use and the basic principles of the *longitudinally modulated cryogenic system* (LMCS). A schematic representation of the LMCS device can be displayed as in *Figure 2.18.* The end part of a 30 m×0.22 mm ID×0.25-μm d_f non-polar capillary column was linked to a movable 5-cm cryo-trap which entrapped/focused effluent fractions by means of an internal CO_2 flow which generated intense cooling. The longitudinally motion of the CO_2-cooled cryo-trap towards two different position (marked as "R" and "T") along the head of the second dimension, allowed the modulation process. Specifically, analytes exiting from the first dimension were cold-trapped in a small region of the column (position marked as "R"). In the following step, the cooled spot of the column was exposed to the GC oven temperature via the longitudinal motion of the trap to the downstream region (position marked as "T") of the column. The desorbed band, transported by carrier gas flow, were moved along the column to be subject to a second trapping stage in the bottom segment ("T"). The motion of the cryo-trap back its original position, "R", allowed the trapped analytes to be re-injected onto the secondary column, while preventing any potential analyte breakthrough.

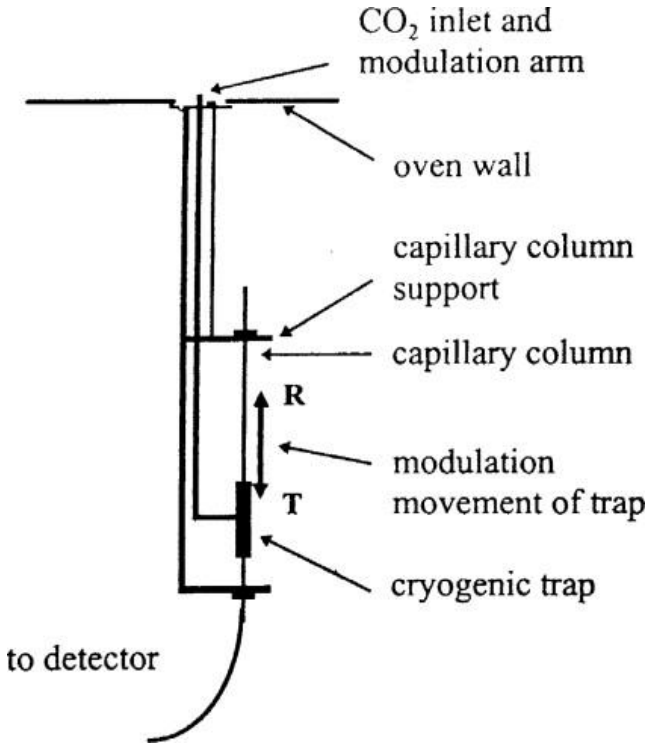

Figure 2.18. *Device for longitudinally modulated cryogenic system (LMCS). Analytes are sampling when the trap is in the T position, and re-injected when the trap reach the R position.*

The longitudinal motion of the trap was driven by a pneumatic, electrical, or stepper motor actuator through a modulator arm connected to the trap. The LMCS offered significant advantages over the thermal sweeper: *i)* more efficient entrapment, owing to the low trapping temperature; *ii)* no GC-oven-temperature limitation, except that related to the less thermally-stable stationary phase employed; and, *ii)* less elaborate construction. On the other hand, there were some limitations to this approach. The first was the consumption of liquid CO_2 employed as a cryogenic agent, boosting the cost/analysis. Another limitation was the use of a moving trap, which could damage the column or cause other problems.

Static jets design. The moving parts were eliminated from the design of CMs when Ledford et.al. [37] described a *dual stage static modulator*, namely *quad-jet modulator*. As shown in *Figure 2.19*, this modulator used two hot jets and two cold jets situated at the head of the second column, to achieve a dual stage modulation. These jets were positioned to provide a transverse gas flow onto the head of the second column and were pulsed in an alternative mode.

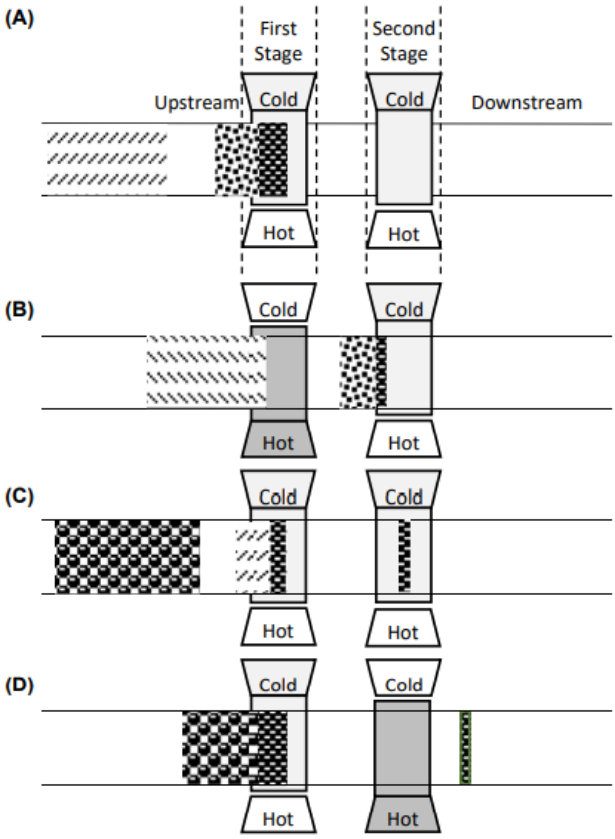

Figure 2.19. *Modulation process of the dual stage quad jet thermal modulator.*

Specifically, one pair of heating/cooling jets was located at the upstream point of the second column, while the other pair was located at a downstream point. The first stage of cooling (liquid N_2) enables the trapping of a primary column chromatography band by the activation of the cold jet upstream [the hot jet (air) downstream was simultaneously activated] (*Figure 2.19-A*). The upstream hot jet was then pulsed (and downstream cold jets were activated), remobilizing the trapped analytes to the second stage where the downstream cold jet would refocus the band of analytes and prevent any breakthrough (*Figure 2.19, B-C*). At the end of the second re-concentration process, the upstream cold and downstream hot jets were turned on (*Figure 2.19-D)* allowing the first-stage entrapment of another chromatography band and the re-injection of the previously entrapped chromatography band onto the second-dimension. A commercial version of this modulator utilizing liquid nitrogen as the cooling agent is now available on GC×GC instruments provided from LECO Corporation.

Beens *et.al*. [38] proposed a simplified version of the quad-jet system, obtained by eliminating the use of the hot jets. Specifically, the trapping stage was performed by using pressurized CO_2 as cooling agent. The not-excessively low trapping temperatures generate by pressurized liquid CO_2 minimized the need for heating jets. Thus making possible the only use of GC-oven temperature for analyte re-mobilization. On the other hand, it did not enable the entrapment of highly volatile compounds, such as C_5 and C_6. The original Beens modulator was commercialized by Thermo Fisher Scientific.

More recently, effort has been devoted to reduce the consumption rate of cryogens while still maintaining the performance of the quad-jet thermal modulator. In such a respect, Mostafa and Gòrecki developed a single stage jet trap modulator [39]. The liquid nitrogen, used as cryogen, was provided from a pressurized Dewar. A piece of deactivated fused silica tubing (0.10 m × 0.32 mm ID) was used as the modulator capillary. The use of a (3-4 mm) plug of compressed fused silica wool inside the trapping capillary, serves as a restriction at the point of the cold jet to increase trapping efficiency by slowing the gas flow during the single-stage modulation process, thus preventing the breakthrough of the analytes. The performance of the modulator, evaluated on a broad (C_5 to C_{24}) range of compounds, was similar to the quad-jet modulator proposed by Ledford but featured by a significant reduction of liquid cryogen consumption.

Static dual-jet loop design. Shortly after the introduction of the quad-jet modulator, Ledford and co-workers proposed a single cryo-jet interface, capable of dual-stage modulation, with the use of a delay loop [40]. This modulator type is commercially available from Zoex Corporation [41] in two variants: with liquid nitrogen cooling (model ZX1) and as a cryogen-free modulator (model ZX2). The latter, employs a closed cycle refrigerator/heat exchanger to produce a -90°C cold jet (N_2) capable of modulating C_7+. In this design, the two stages were created by looping a segment (1-1.5 m) of capillary column through the pathway of a cold jet (*Figure 2.20*). The modulator loop can be created by looping the last part of the first dimension, or the initial segment of the second, or a more advisable choice is to use an uncoated column or a segment of stationary-phase coated capillary. The cold jet is continuously directed vertically downward onto the modulator loop, thus generating two cold spots; one in the upstream and one in the downstream portion of the loop. The cold jet is diverted from the cold spots by activating a hot jet, which is activated for a brief period (*e.g.*, 200-600 msec), in a periodic manner (according to the modulation period). Specifically, the hot jet, which can produces temperatures of 475°C, is positioned perpendicularly to the cold one, and by heating the cold spots, allows the remobilization of the entrapped analytes into the looped capillary.

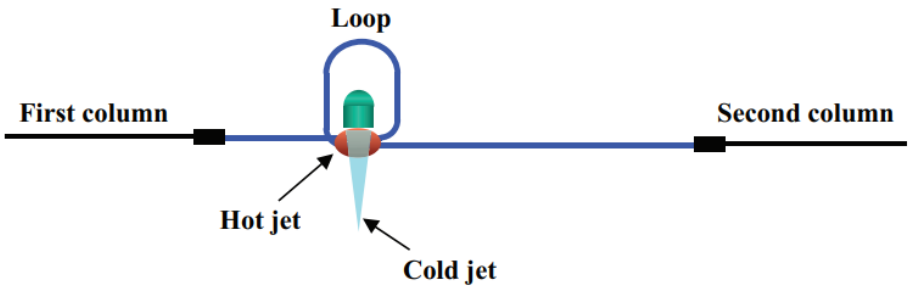

Figure 2.20. *Loop-type modulator. The cold flow is directed downwards, while the hot jet is located perpendicularly to the cold one.*

The remobilized analytes, transported by the gas carrier flow, will reach the downstream cold spot, where they will be refocused together with any potential breakthrough from the first stage. In the meantime, the next fraction of analytes eluting from ^{1}D are trapped at the upstream cold spot. The re-activation of the hot jet allows two events; the re-injection of the refocused chromatography band into the ^{2}D column and the release of the trapped analytes from the upstream cold spot into the loop. The temperature range, and the

minimum P_M of 1 sec, may limit the applicability of such modulator in the analysis of highly volatile analytes (< C_7). Additionally, the length of the loop and the velocity of the carrier gas have to be carefully adjusted whenever the chromatographic conditions change. If the flow of the carrier gas is not adjusted properly, the band traveling through the delay loop might not reach the trapping spot at a time when it is cold, and therefore it might not be refocused.

2.5.1.2 Cryogen-free modulators

While cryogen-based jet modulators have proven to be highly reliable, recent innovations have been directed toward providing simpler and more cost-effective thermal modulator designs. In this respect, a major thrust is the research, development and commercialization of cryogen-free thermal modulators, which does not require the use of any cryogenic liquid to generate GC×GC data. In this regard, the TDM introduced by Liu and Phillips [35] can also be recognized as the first cryogen-free device. Since its inception, many efforts have been made on the development of cryogenic-free designs. Presently, few cryogenic-free modulators are commercially available and they can be further divided into *static* modulators and *movable* modulators. The designs proposed from Ledford, and previously described, is available in both a liquid nitrogen variant with a modulation range of C_4 to C_{40} and a cryogen-free variant with a modulation range of C_8 to C_{40} [42]. The cryogen-free variant uses a closed loop chiller instead of liquid nitrogen to cool the heat exchanger.

Solid-state modulator. Luong *et.al* recently introduced a new cryogen-free moving thermal modulator [43]. The transfer device, defined "*thermal independent modulator*" (TiM), was located on top of the GC oven and was based on thermally independent heating and cooling stages. Specifically, the device consisted of three independent temperature zones, a cold zone in the middle and two heated zones named as "entry" and "exit" zone, respectively. A motion of a modulation column between these three independent thermal zones, allowed a dual-stage modulation. The modulator position and its cryogen-free nature were the main features in common with the "Phillips" modulator [35]; analyte remobilization induced by column movement was the main characteristic shared with the LMCS [36]. The TiM modulator is commercially available and is defined with the term *solid-state modulator* (SSM). A schematic representation of the SSM can be displayed as in *Figure 2.21*. Specifically, the SSM consists of a thermo-electrical cooling (TEC) device

located between two heated aluminum chambers (hot entry and hot exit). The two chambers are each linked to two transfer lines, enabling connections to the GC oven and to the TEC device. Specifically, the two heated areas could be temperature programmed from ambient temperature to greater than 350°C for remobilization, while the TEC in the middle could be programmed from -51 to 50°C. The modulation column (MC) is looped inside each chamber, is held by a gripper at the hot entry side, and is linked to the ^{1}D and ^{2}D columns (inside the GC oven). The dual-stage modulation is achieved by the mechanically motion of the MC back and forth in a fashion opposite to LMCS, in which a cold trap was moved along the column [33]. *Figure 2.22* reports a schematically representation of the SSM mechanism. For the sake of simplification, let consider a single chromatography elution band. In first stage, the gripper is in the de-energized (forward) position (state *Ia* in *Figure 2.22*), and the compounds eluting from the ^{1}D column will reach the TEC device held at a temperature of −51°C and will be subjected to a first entrapment process (blue circle inside the TEC device).

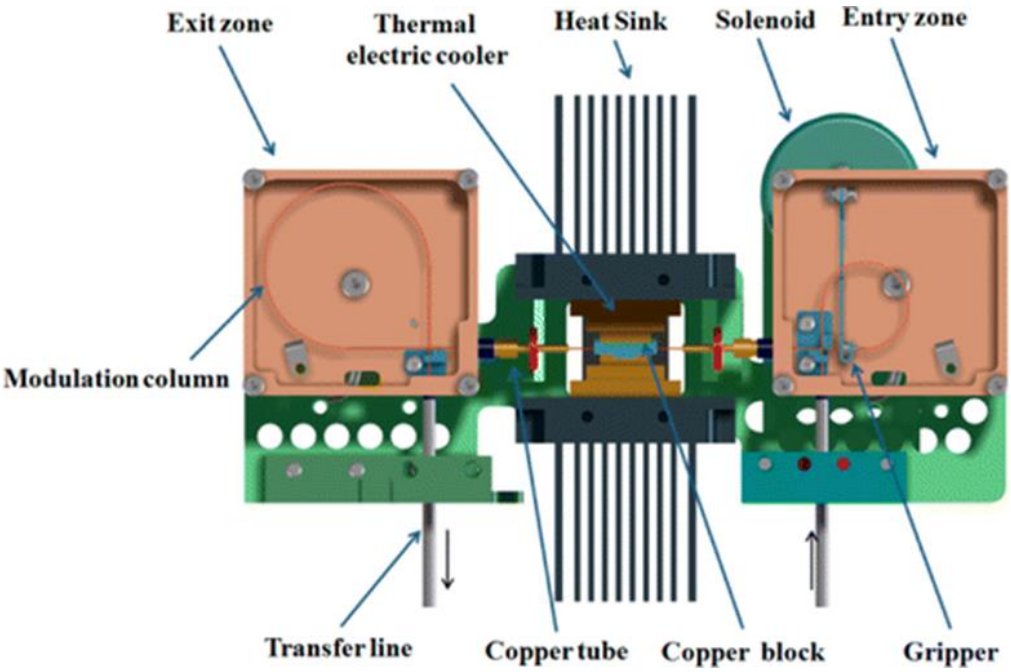

Figure 2.21. *Schematic representation of solid-state modulator (SSM)-(Luong, et al., Anal. Chem., 88(17), 2016, 8428-8432)*

When the gripper is in the energized (backward) position (state *IIa-b* in *Figure 2.22*), the previously cooled part of the MC will be moved back into the hot entry zone, will be

subjected to a first heating process (state *IIa*). Thus enabling the remobilization of the chromatography band (red circle in the hot entry zone), which will again be directed to the TEC device (state *IIb*), to be entrapped a second time. Afterward, the gripper will be again de-energized back to the initial state (*Ib*), enabling the entrance of the entrapped band into the exit zone, where a second heating/remobilization process occurs. At the same time, a new entrapment process will begin (stage *Ia*).

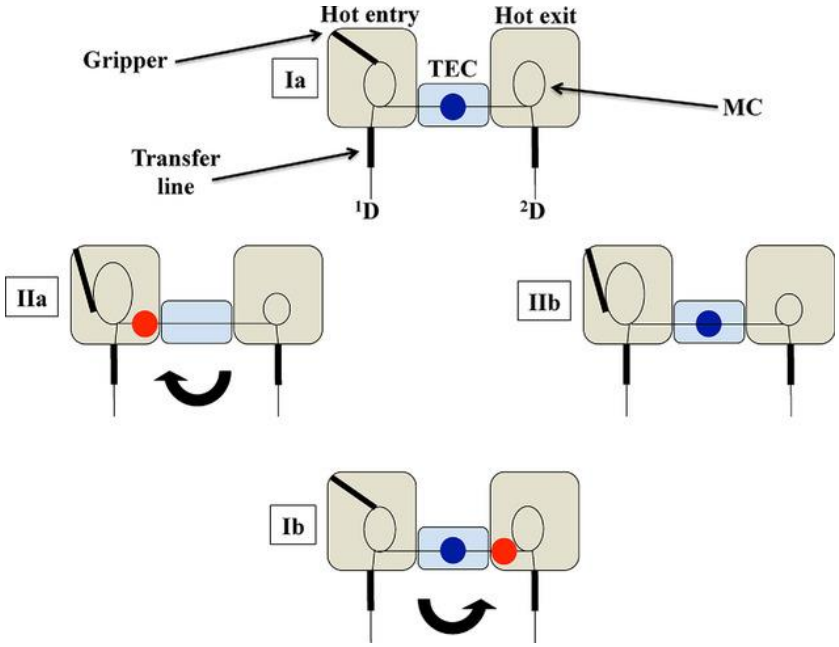

***Figure 2.22**. Scheme of the solid-state modulation (SSM) process.*

Other designs. Muscalu *et.al* proposed a single-stage cryogen-free thermal modulator [44], which uses a coated stainless steel capillary trap. Focusing of the analytes within this trap was accomplished through compression of the trap between two ceramic cooling blocks. While, the re-injection of focused chromatographic bands into the ^{2}D was achieved by using a capacitive discharge power supply to resistively heat the trap. Another cryogen-free approach was developed by Mucédola *et.al.* who described a modulator named as "*Do-It-Yorself*" [45]. The latter was a segmented loop-based thermal modulator that applies the principles of a resistively heated trap similar to the original Liu and Phillips design [35]. Trapping of the analytes was achieved by using a delay loop composed of a metallic modulation loop (1 m) with a 0.50 µm stationary phase film thickness located in the oven. The application of a short heat pulse (provided by a 32-45 W power source) to the metal

column cause the desorption of entrapped chromatographic bands. Kurabayaski *et al.*, described a dual-stage microfabricated thermal modulator, named as *micro thermal modulator* (*μTM*) [46]. The two stages of the μTM were made of micro-channels etched onto a silicon wafer and doped with boron. The walls of the micro-channels were dynamically coated with polydimethylsiloxane, and Pyrex glass was anodically bonded to the wafer to seal the micro-channels. Micro-heaters and temperature sensors were patterned onto the Pyrex glass, and microfabricated silicon spacers were used to create an air gap between the thermoelectric cooler and the μTM. Both stages were cooled by the thermoelectric cooler while heating alternated to provide dual-stage modulation.

Two key issues for application of cryogen-free thermal modulators remain a challenge. First, there is the challenge to properly modulate C_3-C_7, and second the relatively long PM provided negate the opportunity to apply this modulation platforms for high speed GC×GC applications.

2.5.2 Valve-based modulators

The category of the *valve-based modulator* or *flow modulator* (FM) is referred to any modulator that uses gas flow to control and isolate fractions of primary-column eluate and pulses them onto the head of the secondary analytical column. Depending on the direction of flow, the modulator can be considered a forward fill/flush modulator (FFF), when the flush (re-injection) occurs in the same direction as the originally fill stage; or a reversed fill/flush (RFF), if the flush occurs on the opposite direction of the fill stage. Specifically, the injection pulse width is dominated by the amount of time the flow of gas containing the eluate from the ^{1}D column is directed towards the ^{2}D. A further distinction can be made on the basis of the possible paths that the ^{1}D effluent may take while the ^{2}D separation is taking place. In a low duty cycle, the ^{1}D effluent is directed to an exhaust pathway during this stage, ultimately never reaching the ^{2}D column. In a full transfer mode the ^{1}D effluent is stored during the accumulation stage, which is subsequently flushed onto the ^{2}D column during an inject stage. The modulation approaches used in a valve-based modulator can further be divided into two categories, namely *differential flow modulation* and *flow diversion modulation.*

2.5.2.1 Differential flow modulation

The first flow modulator was described in the same year as the first cryogen-modulator, namely LMCS [36]. In an investigation focused on chemometrics, Bruckner *et.al.* [47] employed a six-port diaphragm valve to achieve a single-stage FM GC×GC analysis (*Figure 2.23*). Specifically, in the original design only four of the six available ports were employed to diverted eluate from the ^{1}D to the ^{2}D column. While, the other two valve ports were connected to an auxiliary pressure source and to a waste line. This valve interface was placed between a wide-bore PDMS-coated ^{1}D column and a narrow-bore poly (ethylene glycol) ^{2}D column. Excessively high gas flows in the second dimension were avoided by using a split line (0.5 m × 0.18 mm ID used-silica column). In the original work, a 0.5 s modulation period and a 0.1 duty cycle were employed. To perform modulation, the valve was actuated twice per second, and the chromatography band was pulsed onto the secondary column for a 50 ms period at the beginning of each modulation process. At the end of the brief pulsed period, the valve was switched to the other position, and the primary-column effluent was directed to waste (450 ms). While the ^{2}D injection peaks were very narrow owing to rapid actuation, only about 10% of the eluate from ^{1}D separation was transferred to the ^{2}D analytical column. Apart the sensitive issue, a further disadvantage was the restricted operational temperature of the valve. The latter, was placed inside the GC-oven and had several internal parts that was not designed to be operated at temperatures above 175°C, thus causing a temperature constraint on the GC×GC separations.

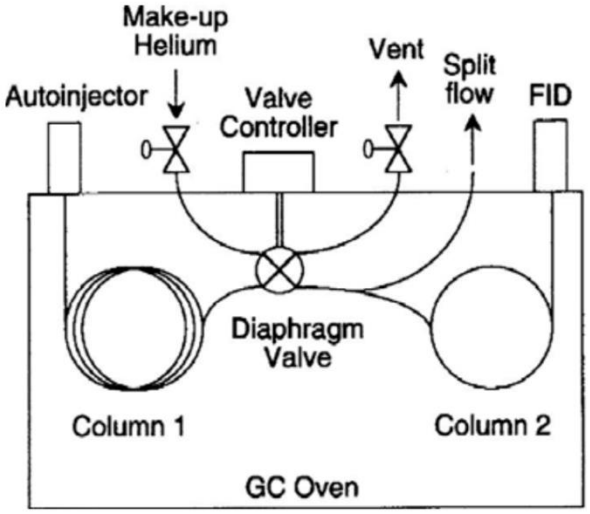

Figure 2.23. *The first FM device (in the ‘‘waste’’ mode).*

An early solution to the temperature concerns was to have the valve-face mounted outside the GC oven. Seeley and co-workers, inspired by the original design proposed by Bruckner, reported the first dual-stage valve FM device, defining the approach as *differential flow modulation* [48]. To address the low duty cycle, Seeley introduced the use of a sampling loop (20-μL) to collect fractions of the ^{1}D eluate and transfer them to the ^{2}D column (*Figure 2.24*). The FM device was designed in order to protect the temperature-sensitive parts of the valve and allowing the wetted portions of the valve to reach much higher temperatures. In this respect, the portions of the valve containing non-wetted components was housed outside the GC oven and was maintained at 125°C by using a heater block. Inside the oven, the interface was attached to a 10 m × 0.25 mm ID × 1.4 μm d_f primary column and a 5 m × 0.25 mm ID × 0.25 μm d_f capillary or a 5 m × 0.25 mm ID × 0.50 μm d_f capillary. The dual-stage modulation occurred through two stages: accumulation and injection. In the original work, the valve was used in the accumulation and injection states for 80% and 20% of the modulation period, respectively. Once the sampling loop was filled to its maximum volume (20-μL), the excess effluent was vented to the atmosphere (0.75 mL/min), and the previously accumulated chromatography plug was launched onto the second dimension exploiting a high gas flow (15 mL/min). The disadvantage related to the high secondary-column flows was partially resolved in a series of later FM-GC×GC studies by splitting the primary flow between two secondary analytical capillaries (GC×2GC) [49, 50].

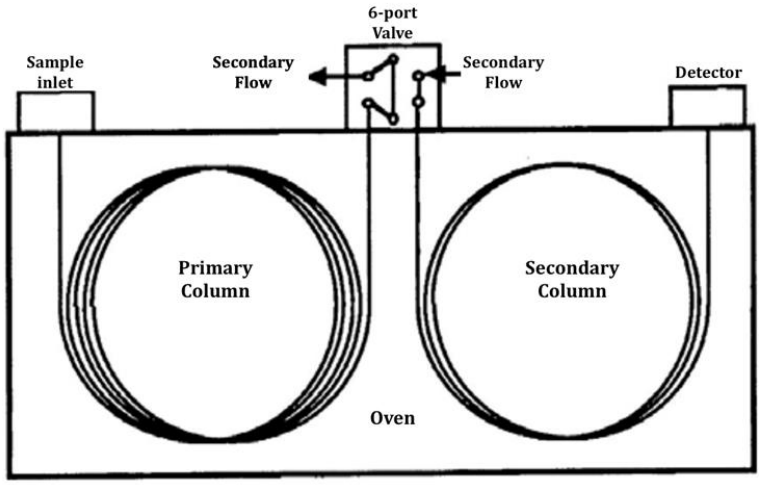

***Figure 2.24**. The first FM GC×GC device equipped with a sampling loop.*

Recent improvements to commercially available diaphragm valves have resulted in higher temperature limit. Specifically, the original temperature limit of 175°C was overcame by replacing the temperature sensitive O-ring with a perfluoroelastomer-based-O-ring, allowing reliable function up to 325°C. This "high temperature" diaphragm valve, characterized by a very simple design, allowed the modulation of a wide range of volatility compounds (*e.g.* C_1 to C_{40}+) [51].

2.5.2.2 Flow diversion modulation

Flow diversion is a technology that originated with heart cutting (GC-GC) originally performed with pneumatic valves. The concept of flow diversion came with the introduction of the Deans' switch [52]. Flow diversion modulation technology employs the use of solenoid valves to control gas pressures that lead to control the of transfer of eluate from first column to the second one. In 2006, Seeley *et al.* introduced an interesting and simple dual-stage design based upon a Deans' switch and featured of a high duty cycle (*Figure 2.25*) [53]. The design consisted of three deactivated fused- silica columns, two micro-volume T-unions and a two-way solenoid valve (housed outside the GC oven) connected to an auxiliary pressure source. The output ports of the solenoid valve were connected to the unions by using two fused-silica segments. One of the T-unions was linked to the primary-column outlet, while the other directed the flow to the second dimension. The two T-unions were connected by a sampling loop (volume = ~24 μL). The ^{1}D column effluent entered the modulator device at the upper T-union, while the auxiliary flow (20 mL/min) entered at the common port of the valve. The modulator operated in two stages, fill and flush. When the modulator was in the ''*fill*'' stage, the auxiliary flow was directed to the ^{2}D, and the primary-column effluent flowed freely within the loop. Prior to the effluent reaching the bottom union, the valve was switched to the "*flush*" state. In this state, the auxiliary carrier gas flushed the content of the loop onto the head of the second dimension. The pressure pulse, during the injection stage, temporarily stopped, or even slightly reversed the flow at the outlet of the ^{1}D, which prevented analytes breakthrough. This system was featured by: *i)* stability at high GC temperatures; *ii)* simple construction; *iii)* duty-cycle = 1. The main drawbacks were related to the complexity of method optimization, the rather high second-dimension gas linear velocity, and the low modulation

period. However, the novel modulator was very promising and was exploited successfully in FM-GC×GC applications [54, 55].

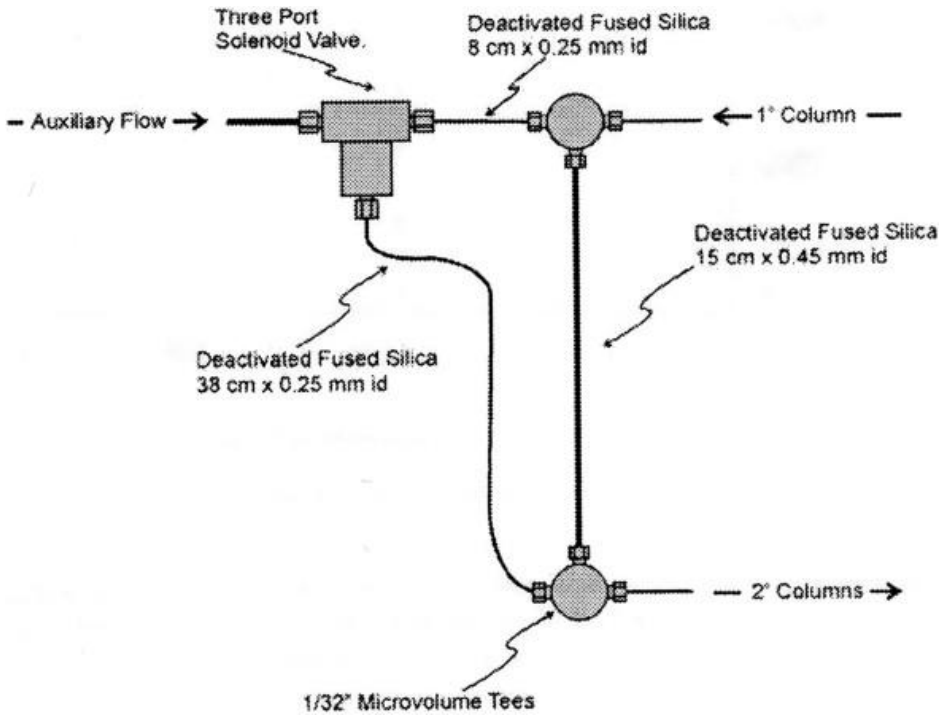

***Figure 2.25**. The dual-stage FM device introduced by Seeley.*

In 2011, Tranchida *et al.*, developed a differential flow modulator using a seven port valve (wafer-chip) with a flexible loop to accumulate sample [56]. *Figure 2.26* shows the seven-port valve device. The interface comprised a metallic disc (2.5 cm diameter, 7 mm thickness), and internal rectangular channels (250 μm width/75 μm depth), connecting ports 1-2-3 and 4-5-6/7. A two-way electrovalve was located outside the GC oven and was connected to an advanced pressure control (APC) unit. Two metallic branches connected the valve to the interface in positions 2 and 5. The primary and secondary columns were linked to positions 1 and 6, respectively. Positions 3 and 4 were connected via a 40μL stainless-steel loop (20 cm × 0.71 mm OD × 0.51 mm ID). The size of the loop is chosen considering the modulation period, first-column flow and second-column dimensions. It is noteworthy that the flow exiting the loop was divided between the channels linked to ports 6 and 7. A needle-valve connected to a waste line at the head of the 2D column was used to reduce the flow rate to ~2.5 ml/min, resulting in a low duty cycle estimated at~5%.

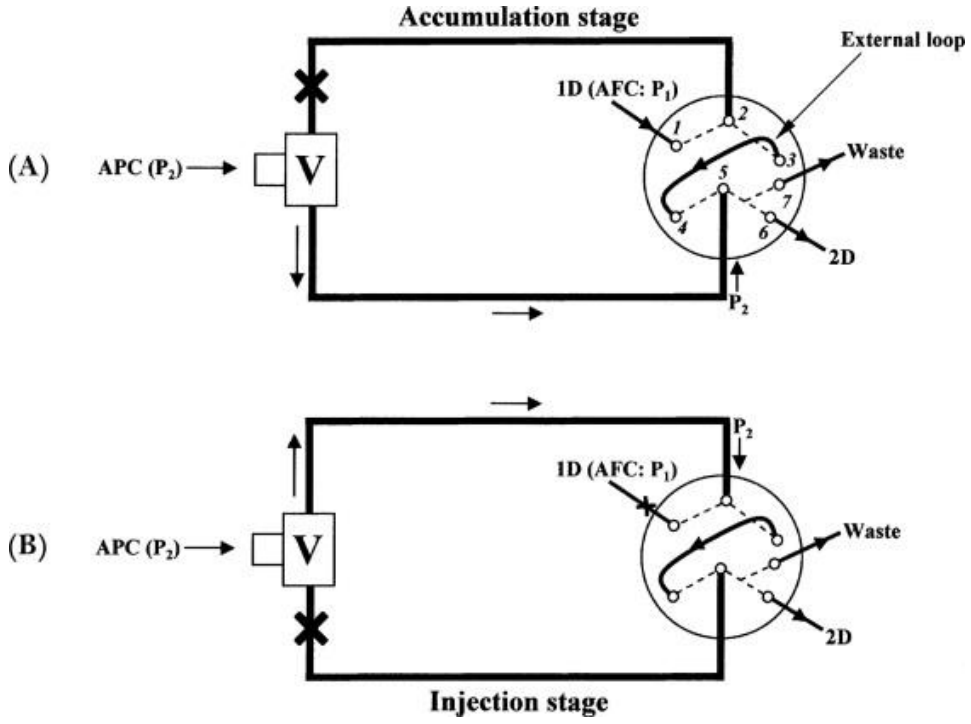

Figure 2.26. *Seven-port FM device in the accumulation (A) and injection (B) modes. Abbreviations: V: two-way solenoid valve; AFC: Advanced flow controller.*

The same 7-port modulator was coupled with high resolution time-of-flight mass spectrometry (HR-ToFMS) to perform a proof-of-principle study [57]. Specifically, the experimental conditions were modified resulting in an initial flow rate of 3.4 ml/min and a duty cycle of 40% at the beginning of the analysis. While, at the end of the run separation the flow rate was 2.1 ml/min with slightly lower duty cycle. A key issue with many valve-based modulator, either differential flow and flow diversion, is the high flow rates generated on the ^{2}D column, posing compatibility issues for mass spectrometry (MS) detection due to the connection to a vacuum system. A typical approach to address this issue is to split the flow exiting the modulator prior to MS detection. In this regard, the flow could be splitted either to a bleed column or to an additional detector, typically an FID. However, this ultimately compromises the sensitivity of the analysis. Mondello group used missmatched length of deactivated fused silica, to allow lower gas flow rates (6-8 ml/min) on the ^{2}D column compared to the typical flow rate of~20 ml/min, while still providing an efficient re-injection onto the secondary-column. For such purpose, a longer pulse time was required to totally clear the sampling loop [58]. The design and flow conditions were found to be compatible with the most commonly used mass spectrometer used in GC×GC-MS (qMS, ToFMS), without the need to divert the flow to another detector [57, 58].

Shortly, after Seeley, Agilent Technologies introduced their flow diversion modulator constructed by using *Capillary Flow Technology* (CFT) [53]. The modulator, housed in the GC oven, was based upon a Deans' switch compatible with most forms of MDGC. SepSolve Analytical introduced the so-called INSIGHT, which is a RFF modulator type. The use of both CFT and INSIGHT modulators rely upon application of split flow to reduce the flow rate on the ^{2}D column to facilitate the coupling with MS detectors. To address this issue, Seeley has introduced a novel flow diversion modulation, in which the use of a high-speed Deans' switch allows to generate sub 50 msec pulse widths at low flow of 2 ml/min on the ^{2}D column, resulting in narrow ^{2}D peak widths and reproducible $2t_r$ [59]. In an effort to alleviate the need to choose between a low duty cycle modulator or full transfer modulator, Seeley himself designed a multi-mode modulator (MMM) that is capable to perform heart cutting (GC-GC) low duty cycle GC×GC, and total transfer GC×GC [60]. The MMM device consisted of a three-port solenoid valve, a cross union, a T-union, and a joining capillary (*Figure 2.27*). The latter was connected, through the cross union, to the ^{1}D column and, through the T-union to the ^{2}D column, thus keeping the two columns (^{1}D and ^{2}D) in close proximity to one other. Auxiliary carrier flow entered through the three-port solenoid valve, and by flow switching through the selection of the output of the valve, the divert or inject state occurs. The normally closed out port was connected to the cross union, while the normally opened out port was connected to the T-union. A flow restrictor was connected to the fourth port of the cross union. The prior state for both low duty cycle and full transfer modulation occurred when the auxiliary flow of the valve was directed to the T-union toward the ^{2}D column. In such a case, the auxiliary flow (F_A) must be greater than the ^{2}D flow (F_2) in order to prevent ^{1}D column effluent (F_1) from entering the second-dimension column. The injection state, was achieved by directing the auxiliary flow to the cross union towards the ^{1}D column. It the magnitude of the ^{1}D column flow compared to the ^{2}D flow to determine if the MMM will operates as a low duty cycle modulator or a full transfer modulator. Specifically, when the ^{1}D flow (F_1) is greater than the ^{2}D flow (F_2) the device will operates as a low duty cycle modulator. While, when the ^{1}D flow (F_1) is lower than the ^{2}D flow (F_2), the device will operates as a full transfer modulator. Research in the development of valve-based modulator technology has a significant number of research groups working to advance this modulator type, for a deeper examination of current research the reader is encouraged to review several modulators developed in the last few years [61-69].

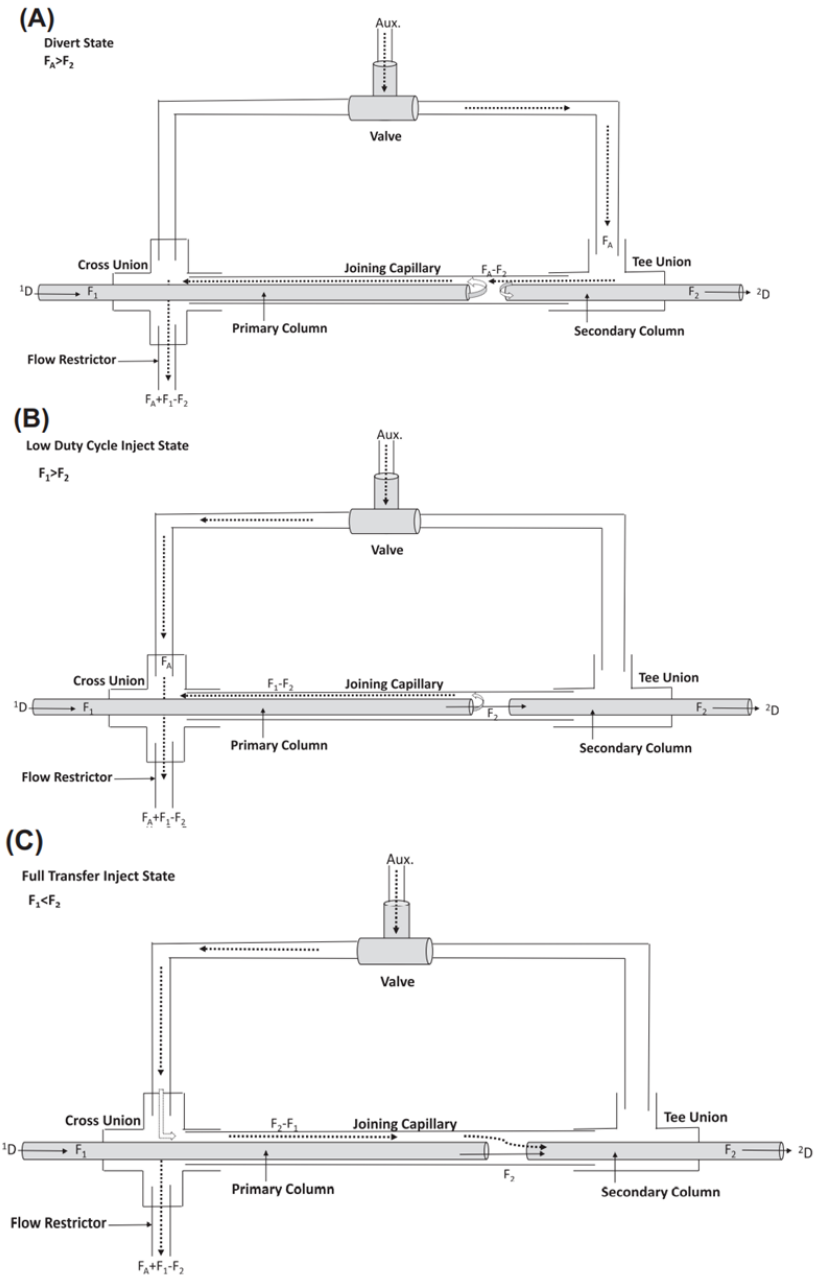

***Figure 2.27**. Schematic of layout of the multi-mode modulator (MMM). A) The divert state for both the low duty cycle and full transfer modes. B) The injection state for low duty GC×GC modulation mode. C) The injection state for the full transfer GC×GC modulation mode.*

2.5.3 Optimization aspects

2.5.3.1 Modulation parameters

The time taken to complete a single cycle of modulation events is called *sampling frequency* or *modulation period (P_M)*, and it represents a critical choice during GC×GC method optimization. The main theory on the impact of modulation was put forward by Murphy and co-workers with their studies involving LC×LC separations [70]. They demonstrated that the sampling frequency has a direct effect on the resolution of a 2D chromatogram. They demonstrated empirically that each first dimension peak must be sampled at least 3-4 times to obtain optimum resolution. Consequently, Murphy's criterion is often used as a basis when developing methods in 2D chromatography. More recently, Khummueng et al. [71, 72] studied the influence of GC×GC modulation on symmetrical and non-symmetrical peaks. They introduced the notion of "*modulation ratio*" (M_R) which is defined as in *Eq.2.15*,

$$M_R = \frac{4\sigma}{P_M} = \frac{W_b}{P_M} = \frac{W_h \times 1.6985}{P_M} \qquad \textit{(Eq. 2.15)}$$

where the peak width at the base (W_b), defined as 4 times the ^{1}D column peak standard deviation (σ) or 1.6985 times the width at half height of the peak (W_h), is divided by the modulation period (P_M). They therefore concluded that, for a quantitative analysis of trace compounds, a modulation ratio of at least 3 must be applied, while a M_R of 1.5 is adequate for semi-quantitative analysis or for major components only. The degree of resolution and reconstructed peak widths of the analytes eluting from ^{1}D are also affected by another parameter, the *phase of modulation* [73]. This is defined as the difference between the center of the ^{1}D peak and the mean of the peak region sampled by the modulator. Two limiting scenarios can be distinguished:

i) *in-phase modulation (Figure 2.28-A)*, if a symmetric pulse sequence with a single maximum peak is observed, and

ii) a *180 degrees out-of-phase* modulation *(Figure 2.28-B)*, if the pulse sequence still symmetric but has two (equal) maxima.

In general, any phase between these two limiting cases may be observed in actual two-dimensional separations due to the random nature of the distribution of peaks emerging from the ^{1}D column *(Figure 2.28-C)*.

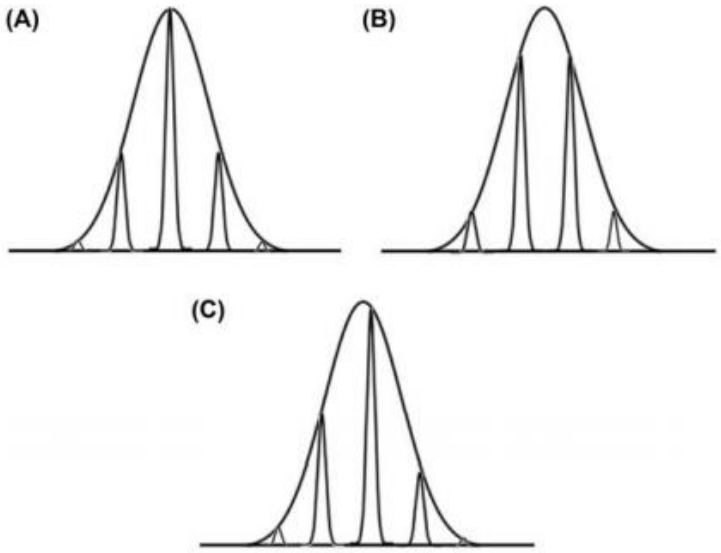

Figure 2.28. *(A), in-phase modulated GC peak pulses in GC×GC (B), and 180° out-of-phase modulated GC peak pulses in GC×GC. (C) any other phase modulation.*

Another important criterion to be checked is the quantitative aspect related to the modulator. The "duty cycle" is defined as the effluent fraction from the first dimension which is sampled and collected during modulation period. This corresponds to the modulator transfer rate. Most modulators collect first dimension effluent throughout the modulation period (duty cycle = 1), e.g., thermal modulators. Other modulators, such as valve-based, sample less than 100% during modulation cycle (transfer rate < 1) [74]. When the transfer rate is less than 1, the product loss generates quantification problems, for trace analysis in particular. For most GC×GC quantitative applications, the effluents must be fully and quantitatively transferred to the second dimension. In flow modulator applications, low duty cycle devices are excluded for trace compound analysis, due to the sensitivity losses.

2.5.3.2 Modulator type

For thermal modulators, some additional temperature parameters must be kept in mind. In fact, to accomplish effective thermal modulation, the modulator must generate sharp and symmetrical injection bands at the head of the ^{2}D column. Remobilization of analytes is

accomplished through the application of high temperatures to rapidly flush the focused zone out of the modulator region and re-inject it to the ^{2}D column. Therefore, the control of trapping and re-injection temperatures is important to get effective modulation. Specifically, the trapping temperature must be low enough to trap and focus the analyte bands. At the same time, it should not be excessively low, as it might retard analyte band remobilization, generating a band streak on the ^{2}D plot. Once the analyte bands are trapped, the cold region must then be heated rapidly to a temperature which permits remobilization of the trapped bands (i.e. trapped compounds should have a retention factor on the trapping capillary of zero) [75]. Other parameters are unique to the design of each thermal modulator. For the commercial dual-stage jet modulators, a carefully optimization of the hot pulse duration is also required. As the total time for the heat pulse and the cold pulse is equal to half the modulation period (for the quad-jet system), increasing the heat pulse time reduces the cold pulse time. The heat pulse time must be sufficiently long for efficient reinjection of high boiling point compounds into the ^{2}D column, while not reducing the cold pulse time to the point where low boiling point compounds are not adequately trapped. Very short hot pulse times were found to degrade first-dimension separation. Apart from the temperatures issues, the distance between the two jets and the linear gas carrier velocities, must be considered. In fact, when the distance between the two jets is not long enough, or the linear gas velocity is too high, breakthrough can occur (*Figure 2.29*). In the loop-type modulator, an additional parameter that needs to be carefully optimized is the length of the delay loop. The typical length of the loop is 1 m. If the loop is too short, the band travelling through it might not reach the second trapping spot at a time when it is cold, and may therefore not be refocused, allowing breakthrough to occur. Conversely, if the loop is too long, multiple injections from the first cold spot could be present within the loop simultaneously. Overall, it should be kept in mind that the length of the loop might need to be adjusted every time the GC×GC parameters (especially carrier gas flow rate and modulation period) are changed. A model for GC×GC systems using a loop modulator was developed to determine the optimum length of the loop capillary [76].

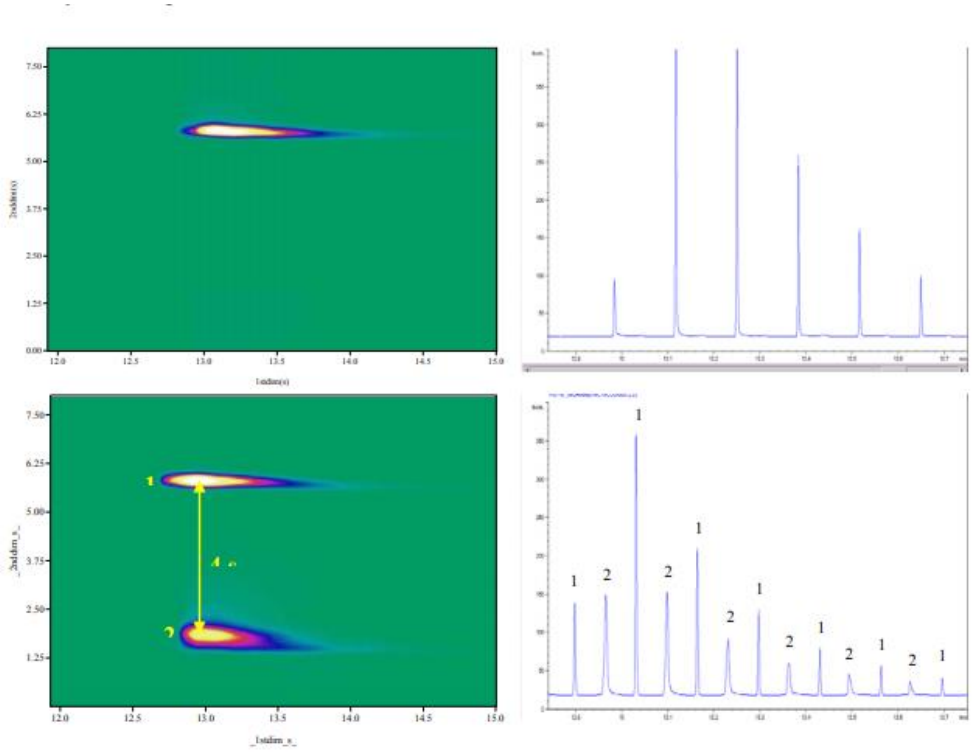

Figure 2.29. *Breakthrough effect in a dual-jet cryogenic modulator by a too high carrier gas velocity or a too short distance between the nozzles.*

Regarding the quad-jet design proposed by Ledford, since the construction is such that the two cold and the two hot jets are placed quite close together in the same small chamber, they may influence each other. Applying the hot jet for a too long time, will prevent proper focusing of the analytes by the other cold jet, allowing breakthrough to occur.

Taking into account the valve-based modulators, the installation can be quite difficult when considering the number of connections and steps required to complete method development and optimization. Ensuring that all connections are leak-free along the column path is vital, especially when coupling to a mass spectrometer. Determining the proper lengths of primary, secondary, and auxiliary or transfer lines, as well as flows required for every stage, should be done prior to installation. If the original instrumental setup is not precisely measured, proper modulation cannot be performed. Method development and optimization of low duty modulators generally differ from those of full transfer modulators, but both include a calculator to assist in determining the correct pressures and flows for the entire column set.

References

[1] A. T. James and A. J. P. Martin, Biochem. J. 50 (1952) 679.

[2] A. J. P. Martin and R. L. M. Synge, Biochem. J. 35 (1941) 1358.

[3] M. J. E. Golay, Gas Chromatography 1958 (Amsterdam Symposium), ed. D.H. Desty, Butterworth, London (1958) 36.

[4] C. F. Poole, The Essence of Chromatography, Elsevier, Amsterdam, 2003.

[5] L. S. Ettre, LC-GC (Europe) 15 (2002) 364.

[6] J. C. Giddings, J. Chromatogr. A 703 (1995) 3.

[7] J. C. Giddings, J. High Resolut. Chromatogr. 10 (1987) 319.

[8] L. Blumberg and M.S. Klee, J. Chromatogr. A. 1217 (2010) 99-103.

[9] L. Mondello, A.C. Lewis, K.D. Bartle (Eds.), Multidimensional chromatography, Chichester, John Wiley & Sons, 2002.

[10] C.J. Venkatramani, J. Xu and J.B. Phillips, Anal. Chem. 68 (1996) 1486.

[11] M.C. Simmons, L.R. Snyder, Anal. Chem. 30 (1958) 32.

[12] R. Consden, A.H. Gordon, A.J.P. Martin, Biochem. J. 38 (1944) 224.

[13] Z. Liu and J. B. Phillips, J. Chromatogr. Sci. 29 (1991) 227.

[14] P.Q. Tranchida, A. Casilli, P. Dugo, G. Dugo, L. Mondello, Anal. Chem. 79 (2007) 2266.

[15] P. Korytár, P. Haglund, J. de Boer, U.A.Th. Brinkman, Trends Anal. Chem. 25 (2006) 373.

[16] J. Dallüge, J. Beens, U.A.Th. Brinkman, J. Chromatogr. A, 1000 (2003) 69.

[17] P.Q. Tranchida, R. Costa, P. Donato, D. Sciarrone, C. Ragonese, P. Dugo, G. Dugo, L. Mondello, J. Sep. Sci. 31 (2008) 3347.

[18] M. Adahchour, J. Beens, R.J.J. Vreuls, A.M. Batenburg, U.A.Th. Brinkman, J. Chromatogr. A 1054 (2004) 47Z. Liu, J.B. Phillips, J. Microcolumn Sep. 1 (1989) 249.

[19] J.V. Seeley, S.K. Seeley, E.K. Libby, Z.S. Breitbach, Anal. Bioanal. Chem. 390 (2008) 323.

[20] J.V. Seeley, F.J. Kramp and K.S. Sharpe, J. Sep. Sci. 24 (2001) 444.

[21] M. Biedermann, K. Grob, J. Sep. Sci. 32 (2009) 3726.

[22] G.S. Frysinger, R.B. Gaines, L. Xu, C.M. Reddy, Environ. Sci. Technol., 37 (2003) 1653.

[23] G.F. Slater, H.K.White, T.I.Eglinton, C.M. Reddy, Environ. Sci. Technol. 39 (2005) 2552.

[24] C. Vendeuvre, F. Bertoncini, L. Duval, J.L. Duplan, D. Thiébaut, M.-C. Hennion, J. Chromatogr. A 1056 (2004) 155.

[25] P.Q. Tranchida, A. Giannino, M. Mondello, D. Sciarrone, P. Dugo, G. Dugo, L. Mondello, J. Sep. Sci. 31 (2008) 1797.

[26] B. Vlaeminck, J. Harynuk, V. Fievez, P.J. Marriott, Eur. J. Lipid Sci. Technol. 109 (2007) 757.

[27] L.L.P. van Stee, J. Beens, R.J.J. Vreuls, U.A.T. Brinkman, J. Chromatogr. A 1019 (2003) 89.

[28] E. Engel, J. Ratel, P. Blinet, S.-T. Chin, G. Rose, P.J. Marriott, J. Chromatogr. A 1311 (2013) 140.

[29] B.L. Winniford, K. Sun, J.F. Griffith, J.C. Luong, J. Sep. Sci. 29 (2006) 2664.

[30] G.S. Frysinger, R.B. Gaines, J. High Resolut. Chromatogr. 22 (1999) 251.

[31] Z. Liu, J.B. Phillips, J. Microcolumn Sep. 1 (1989) 249.

[32] Z. Liu, J.B. Phillips, J. Microcolumn Sep. 1 (1989) 159.

[33] Z. Liu, J.B. Phillips, J. Microcolumn Sep. 2 (1990) 33.

[34] J.B. Phillips, D. Luu, J.B. Pawliszyn, Anal. Chem. 57 (1985) 2779.

[35] J.B. Phillips, Z. Liu, J. Chromatogr. Sci. 29 (1991) 227.

[36] P.J. Marriott, R.M. Kinghorn, Anal. Chem. 69 (1998) 2582.

[37] E.B. Ledford Jr., In 23rd International Symposium on Capillary Chromatography, Riva del Garda, Italy, 5-10 June 2000.

[38] J. Beens, M. Adahchour, R.J. Vreuls, K. van Altena, U.A. Brinkman, J. Chromatogr. A 919 (2001) 127.

[39] A. Mostafa, T. Gòrecki, Anal. Chem. 88 (2016) 5414.

[40] E.B. Ledford Jr., C.A. Billesbach, J.R. Termaat, Pittcon 2002, New Orleans, LA, USA, 17e22 March 2002.

[41] Zoex Corporation, Products, Zoex Corporation, [Online]. Available: http://zoex.com/products/.

[42] P. Stevens and J. Binkley, [Online]. https://www.leco.com/images/e-seminar_archive/posters/MiscGeneral/Liquid_CryogenFree_Thermal_Modulator_GCxGC-TOFMS_PS_Pcon09_LPSS-010.pdf

[43] J. Luong, X. Guan, S. Xu, R. Gras, R.A. Shellie, Anal. Chem. 88 (2016) 8428.

[44] A.M. Muscalu, M. Edwards, T. Go´recki, E.J. Reiner, J. Chromatogr. A 1391 (2015) 93.

[45] V. Mucèdola, L.C.S. Vieira, D. Pierone, A.L. Gobbi, R.J. Poppi, L.W. Hantao, Talanta 164 (2017) 470.
[46] S.-J. Kim, S.M. Reidy, B.P. Block, K.D. Wise, E.T. Zellers, K. Kurabayashi, , Lab Chip 10 (2010) 1647.
[47] C.A. Bruckmer, B.J. Prazen, R.E. Synovec, Anal. Chem. 70 (1998) 2796.
[48] J.V. Seeley, F. Kramp, C.J. Hicks, Anal. Chem. 72 (2000) 4346.
[49] J.V. Seeley, F.J. Kramp and K.S. Sharpe, J. Sep. Sci. 24 (2001) 444.
[50] J.V. Seeley, F.J. Kramp, K.S. Sharpe and S.K. Seeley, J. Sep. Sci. 25 (2002) 53.
[51] C.E. Freye, L. Mu, R.E. Synovec, J. Chromatogr. A 1424 (2015) 127.
[52] D.R. Deans, Chromatographia 1 (1968) 18.
[53] J.V. Seeley, J. N. Micyus, J.D. McCurry, S.K. Seeley, Am. Lab. 38 (2006) 24.
[54] M. Poliak, A.B. Fialkov, A. Amirav, J. Chromatogr. A 1210 (2008) 108.
[55] P. McA. Harvey, R.A. Shellie, P.R. Haddad, J. Chromatogr. Sci. 48 (2010) 245.
[56] P.Q. Tranchida, G. Purcaro, A. Visco, L. Conte, P. Dugo, P. Dawes, G. Dugo, L. Mondello, J. Chromatogr. A 1218 (2011) 3140.
[57] P.Q. Tranchida, S. Salivo, F.A. Franchina, L. Mondello, Anal. Chem. 87 (2015) 2925.
[58] P.Q. Tranchida, F.A. Franchina, P. Dugo, L. Mondello, J. Chromatogr. A 1359 (2014) 271.
[59] A. Ghosh, C.T. Bates, S.K. Seeley, J.V. Seeley, J. Chromatogr. A 1291 (2013) 146.
[60]J.V. Seeley, N.E. Schimmel, S.K. Seeley, J. Chromatogr. A 1536 (2018) 6.
[61] Y.V. Patrushev, V.N. Sidelnikov, J. Chromatogr. A 1426 (2015) 183.
[62] F.A. Franchina, M. Maimone, P.Q. Tranchida, L. Mondello, J. Chromatogr. A 1441 (2016) 134.
[63] J. Krupcik, R. Gorovenko, I. Spanik, P. Sandra, D.W. Armstrong, J. Chromatogr. A 1280 (2013) 104.
[64] J. Krupcik, P. Màjek, R. Gorovenko, I. Spanik, P. Sandra, D.W. Armstrong, J. Chromatogr. A 1286 (2013) 235.
[65] P.Q. Tranchida, F. A. Franchina, P. Dugo, L. Mondello, J. Chromatogr. A 1372 (2014) 236.
[66] F. A. Franchina, M.E. Machado, P.Q. Tranchida, C.A. Zini, E.B: Caramao, L. Mondello, J. Chromatogr. A 1387 (2015) 86.
[67] P.Q. Tranchida, M. Maimone, F. A. Franchina, T.R. Bjerk, C.A. Zini, G. Purcaro, L. Mondello, J. Chromatogr. A 1439 (2016) 144.

[68] F. A. Franchina, M. Maimone, D. Sciarrone, G. Purcaro, P.Q. Tranchida, L. Mondello, J. Chromatogr. A 1402 (2015)102.

[69] M. Zoccali, K.A, Schug, P. Walsh, J. Smuts, L. Mondello, J. Chromatogr. A 1497 (2017) 135.

[70] R.E. Murphy, M.R. Schure, J.P. Foley, Anal. Chem. 70 (1998) 1585.

[71] W. Khummueng, J. Harynuk, P.J. Marriott, Anal. Chem. 78 (2006) 4578.

[72] W. Khummueng, P.J. Marriott, LC-GC Eur. 1 (2009) 40.

[73] P. Haglund, M. Harju, C. Danielsson, P.J. Marriott, J. Chromatogr. A 962 (2002) 127.

[74] J.V. Phillips, J. High Res. Chromatogr. 23 (2000) 253.

[75] R.B. Gaines, G.S. Frysinger, J. Sep. Sci. 27 (2004) 380.

[76] J. Harynuk, T. Górecki, J. Chromatogr. A 1086 (2005) 135.

Page intentionally left blank

Chapter 3

GC×GC-mass spectrometry hyphenation

3.1 Introduction

Shortly after the introduction of comprehensive two-dimensional gas chromatography, Phillips et al. made an original comparison between GC×GC, and GC-MS [1]. The authors highlighted as follow: “in both of these instruments, gas chromatography first disperses the sample's components in time presenting them to the secondary analytical instrument either individually or at least in greatly simplified sub-mixtures.” In GC-MS, the ion source generally transforms such individual components, into a much more complex mixture of ions, increasing data density for each compound (especially when electron ionization is involved). In GC×GC, the modulator does not alter molecular structures, even though it does increase data density (each compound, is divided into several fractions), to a much lower extent than an ion source. In *Figure 3.1,* a comparison between general GC-MS and GC×GC setups is reported. The positioning of the ion source and mass analyzer, beside the modulator and ^{2}D column, is very interesting, because it highlights the fact that these instrumental parts have many aspects in common [1]. Specifically, an ion source (plus accessories, such as means for ion acceleration) can be seen as an ultra-high speed modulator, which receives analytes from a GC dimension, and then ionizes, fragmentates, and injects them onto a further analytical dimension. In such a respect, the multidimensional nature of GC-MS has been recognized in several occasions, including the first description of the technology in a scientific journal, published in 1959 [2]. Although GC×GC is a powerful technique for the physical separation of volatile mixtures, it can realistically only give a broad indication of the nature or chemical class of many of the resolved components. When the characterization of individual components and their structural elucidation are needed, the most advisable options is the extension of the technique, by coupling GC×GC with MS detection.

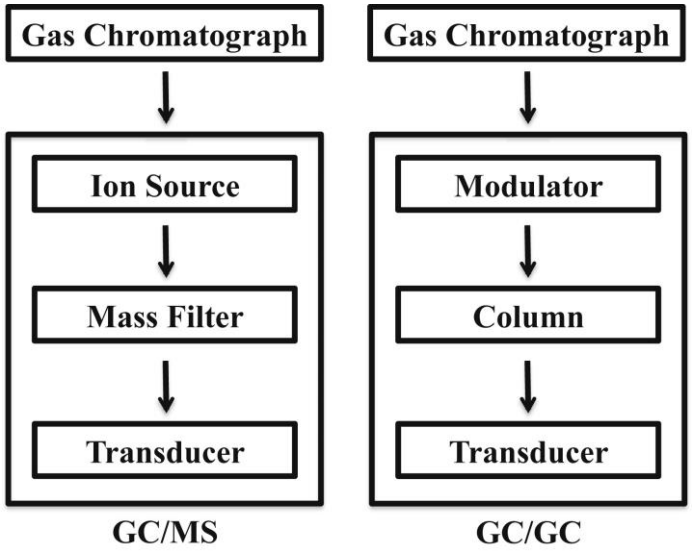

Figure 3.1. *A side-by-side representation of GC-MS and GC×GC processes [1].*

GC×GC-MS is the most powerful analytical tool today available for the analysis of complex mixtures of volatile and semi-volatile compounds. The first published GC×GC-MS research appeared in 1999 [3]: the authors used a thermal sweeper to perform modulation, and single quadrupole (Q) MS for compound structural elucidation. Since 1999, a great deal of evolution has occurred in the GC×GC-MS field, with it being described in a series of review articles [4-6]. The combination of GC×GC with various forms of MS forms a three-dimensional system. Typically, co-eluting compounds at the ^{1}D column outlet (*x*-axis separation) are characterized by the same or similar vapour pressure (if a low polarity column is used); such overlapping analytes are subjected to a ^{2}D analysis (*y*-axis separation) during which specific interactions with the stationary phase prevail (dipole-dipole, H-bonding, etc.). In the case of persisting co-elution, this can be unravelled by the mass analyzer on a mass-over-charge (*m/z*) basis (z-axis separation). Consequently, GC×GC-MS can potentially generate a cubic separation space, with four possible levels (or points) of identification: I and II) retention values on the two GC columns; III) the formation of chemical class patterns; IV) the entire mass spectral fingerprint. In this *Chapter*, principles and instrumentations of GC×GC-MS are described, with emphasis directed to the ionization modes and to the most popular types of mass analyzers.

3.2 Mass spectrometry fundamentals

Thomson, Aston and Dempster are recognized as the pioneers of mass spectrometry [7-11]. The aim of any MS system is to generate ions from either inorganic or organic compounds by any suitable method, to separate these ions by their mass-to-charge ratio and to detect them qualitatively and quantitatively by their respective *m/z* and abundance. Only a brief description of the basic concepts of mass spectrometry technology is herein reported.

Three basic steps are involved in mass spectrometry analysis: ionization, separation and detection of ions in the gas phase. This leads to a basic setup that all mass spectrometers have in common (*Figure 3.2*).

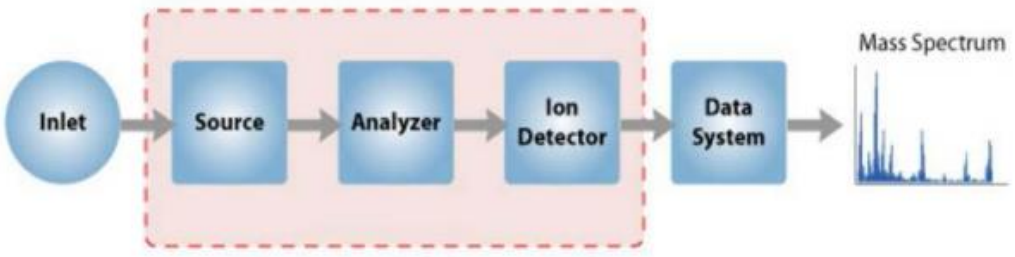

Figure 3.2. *Basic components of a mass spectrometer*.

Generally, a MS system consist of a *sample inlet,* which operates under atmospheric pressure conditions, while the other components, namely *ion source*, *mass analyzer* and *detector* operate under high vacuum conditions. A vacuum system maintains a very low pressure in the mass spectrometer; the ion source region is usually maintained at a pressure of 10^{-4} to 10^{-8} torr; somewhat lower pressure is required in the mass analyzer region (around 10^{-8} torr). Most instruments use a differential pumping system to maintain an optimal vacuum. In such a respect, an essential requirement is to maintain the integrity of the sample molecules during their transfer from atmospheric pressure (sample inlet) to the ion-source (vacuum). When the mass spectrometer is employed as a detector for a GC×GC system, the secondary column is usually directly connected to the MS after passing through a heated metal transfer line. The ^{2}D is joined to the transfer line in a vacuum-sealed manner. The temperature of the transfer line must be high enough to avoid analyte condensation, and is often set at a value equal to or just slightly below the maximum GC analysis temperature. The low-pressure conditions, present in the end portion of the column,

contribute to the complete and rapid transfer of the analytes into the ion source. The *ion source* converts the neutral sample molecules into gas-phase ions, which are then separated and mass analyzed by the *mass analyzer*. The *detector* measures and amplifies the ion current of mass-resolved ions. Finally, the *data system* records, processes, stores, and displays data in form of a mass spectrum. A *mass spectrum* of a molecule is represented as a plot of ion abundance (ordinate) *vs.* mass-to-charge ratio, *m/z* (abscissa). Sometimes, the peak at highest *m/z*, which is called *base peak*, results from the detection of the entire ionized molecule, the so-called *molecular ion* (MI), $M^{+\bullet}$. The *base peak* is arbitrarily assigned the relative abundance of 100%. The *molecular ion peak* is usually accompanied by several peaks at lower *m/z*, *i.e.*, the *fragment ion peaks*, which are given as percentages of the base peak. The *relative intensity* for expressing ion abundances helps to make mass spectra more easily comparable. The *m/z* is a dimensionless term in which the mass of the ion, expressed in *atomic mass units* (u) corresponding to $^{1}/_{12}$ of the mass of the most abundant ^{12}C isotope, and synonymous of dalton (Da), is divided by the number of carried charges. The mass spectrum is represented as a bar graph *Figure 3.3*, usually referred TO as centroid view, which derives from the data reduction of the initially acquired profile data by the mass spectrometer.

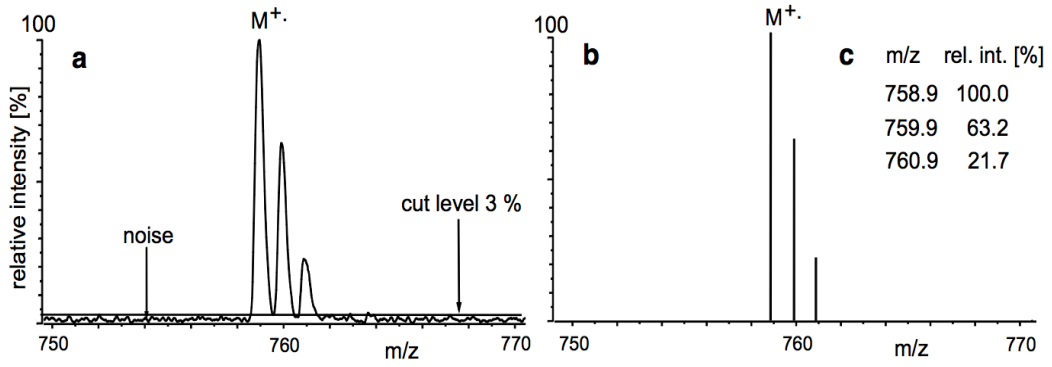

Figure 3.3. *Tetrapentacontane, $C_{54}H_{110}$: representations of the molecular ion signal as (b) centroid, (a) profile spectrum.*

When a mass spectrometer is coupled to a GC or GC×GC system, its output must provide a series of mass spectra each one ideally corresponding to an eluted compound. In this regard, the *total ion chromatogram* (TIC) represents a plot of the total ion current *vs.*

retention time obtained from a chromatography experiment with mass detection, and it results from the summation of the entire separated ion currents carried by the different ions contributing to a mass spectrum. Differently, the *extracted ion chromatogram* (EIC) refers to a plot of the intensity of the signal observed at a chosen (or a set) *m/z* as a function of retention time. Finally, the *base peak chromatogram* (BPC) is a chromatogram obtained by plotting the signals of the base peak ions as a function of retention time.

3.2.1 Mass resolution and mass accuracy

The resolution and mass accuracy of a mass spectrometer are the primary features to be considered for determining whether an instrument suits the demanded tasks. The *resolution, R*, refers to the ability of a mass spectrometer of separating two narrow mass spectral peaks. While, the term (Δ*m/z*), reported in the *Eq. 3.1*, represents the *resolving power*, namely the ability of an instrument to distinguish between ions differing by a small increment in their *m/z* value:

$$R = \frac{m}{\Delta m} = \frac{m/z}{\Delta m/z}$$

(*Eq. 3.1*)

Instruments capable of *low resolution* (LR) operate at values of *R* in the range 500-2000. While, instruments capable of *high resolution* (HR) operate at *R* > 5000. *Mass accuracy* tends to improve as peak resolution is improved. Although, resolution and accurate mass measurements are closely related to each other, an HR measurement does not necessarily imply the measurement of the accurate mass, as the former aims to separate adjacent signals, while accurate mass measurements can deliver molecular formula determination [12,13]. The *mass accuracy* indicates the deviation of the instrument's response between the measured *accurate mass* and calculated *exact mass*. It can be expressed as *absolute mass accuracy*, *Δm/z*:

$$\Delta\, m/z = m/z_{experimental} - m/z_{calculated}$$

(*Eq. 3.2*)

or, alternatively, as relative mass accuracy, *δ m/m, i.e.,* the *absolute mass accuracy* divided by the *exact mass*, and expressed as parts per million (*ppm*):

$$\delta\, m/m = (\Delta m/z)/(m/z) * 10^6$$

(*Eq. 3.3*)

Accurate mass measurements allow to determine the elemental composition of an analyte, and thereby to confirm the identification of target compounds or to support the identification of unknowns. Assuming perfect mass accuracy, we should be able to assign the molecular formula of any ion simply through its exact mass. In reality, deviations between the accurate and exact mass of an ion always exist to some extent and, thus, we normally deal with errors in the order of one to several *ppm* depending on the type of instrument and the mode of its operation.

3.3 Ionization modes

In the present section, focus will be devoted to ionization methods most used in GC×GC-MS. The aim of the *ion source* is to perform the ionization of the analytes exiting from the ^{2}D GC column, before the mass analyzer. The mass analyzer of any mass spectrometer can only handle charged species, *i.e.*, ions that have been created from atoms or molecules, more seldom from radicals, zwitterions or clusters. The task of any *ion source* is to generate these charged species. Specifically, analytes exiting the GC column are subjected to an ionization process consisting in the addition or loss of an electron, in protonation or deprotonation, *etc*. and is followed by fragmentation. The extent to which fragmentation occurs depends on the amount of energy transferred to the analytes, and by its physic-chemical properties. In this respect, some ionization techniques, so-called "*hard*", are very energetic and cause extensive fragmentation of the analyte with even the loss of its intact ion. *Electron ionization (EI)* belongs to such a group of sources. The latter is by far the most common ionization mode employed in GC- and GC×GC-MS; in such a respect a detailed description of EI process will be reported below. On the contrary, so-called "*soft*" ion sources, *e.g., chemical ionization* (*CI*), do allow for generating intact ions of the molecular species. However, it is worthy to say that both *EI* and *CI* sources are only suitable for gas phase ionization, and thus their use is limited to sufficiently volatile and thermally stable compounds.

3.3.1 Electron ionization

Electron ionization was introduced in 1921 by Dempster, who used it to measure lithium and magnesium isotopes [14]. Ionization is effected by shooting energetic electrons onto a neutral that must have been transferred into the gas phase before. *Figure 3.4* shows a schematic representation of the electron ionization source. It consists of a chamber, so-called *ionization chamber*, which is region of the ion source block where analyte molecules are directly introduced and ionized. The beam of ionizing electrons is generated by thermionic emission from a resistively heated metal *filament*, typically made of rhenium or tungsten. The high-energy electrons produced are accelerated towards an anode and collide with the gaseous molecules to affect their ionization. In this regard, it must be highlighted that the electrons do not "*impact*" molecules. For this reason the term "*electron impact*" has been correctly re-named as *electron ionization*.

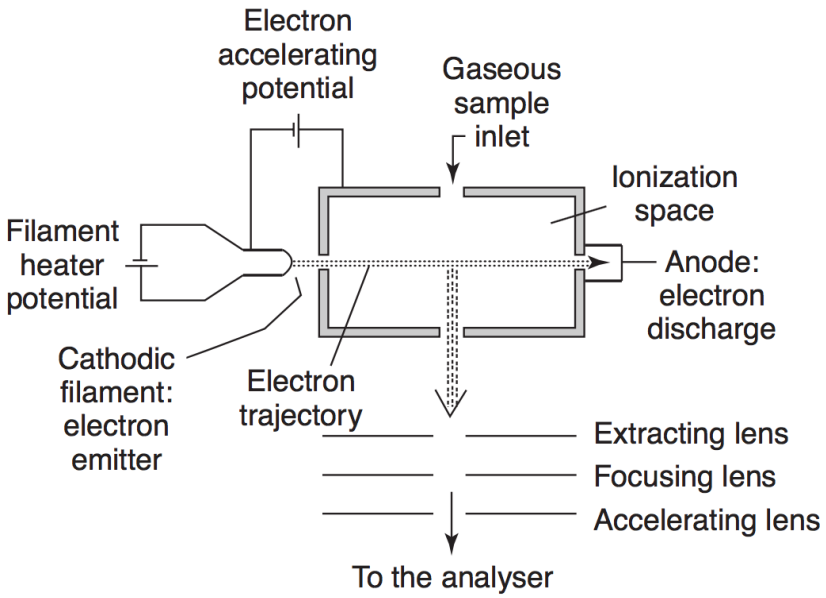

Figure 3.4. *Schematic representation of an electron ionization source.*

Each electron has a given wavelength. If one of the frequencies has an energy corresponding to a transition in the molecule, an energy transfer that leads to various electronic excitations can occur. When enough energy is transferred, then an electron can be expelled (*Eq. 3.4*), thus generating a positive radical ion $M^{+\bullet}$

$$M_{(g)} + e^- \rightarrow M_{(g)}^{+\bullet} + 2e^-$$

(*Eq. 3.4*)

where $M_{(g)}$ represents the neutral molecule in the gas phase. In the most cases the neutral is a molecule, and a *radical cation* or an *odd-electron (open-shell)* ion is generated, *e.g.,* for methane we obtain:

$$CH_4 + e^- \rightarrow CH_4^{+\bullet} + 2e^-$$

(*Eq. 3.5*)

In the rare case the neutral is a radical, the ion created by electron ionization would be *even-electron, e.g.,* for nitric oxide:

$$NO^{\bullet} + e^- \rightarrow NO^+ + 2e^-$$

(*Eq. 3.5*)

In addition, depending on the analyte and on the energy of the primary electrons, doubly (M^{2+}) and even triply charged ($M^{3+\bullet}$) ions can also be observed, with the former being an *even-electron ion* and the latter an *odd-electron* one. There are several other events possible from the electron-neutral interaction, *e.g.,* a less effective interaction will bring the neutral into an electronically excited state without ionizing it. The minimum energy required to ionize a neutral compound is defined as *ionization energy* (IE), and is in the range 7-15 eV for most molecules. *Figure 3.5* illustrates a generalized ionization efficiency curve for EI, showing a plateau around 70 eV. More specifically, below an EI energy of 50 eV the ionization efficiency falls very rapidly, while it reaches a maximum at around 70 eV.

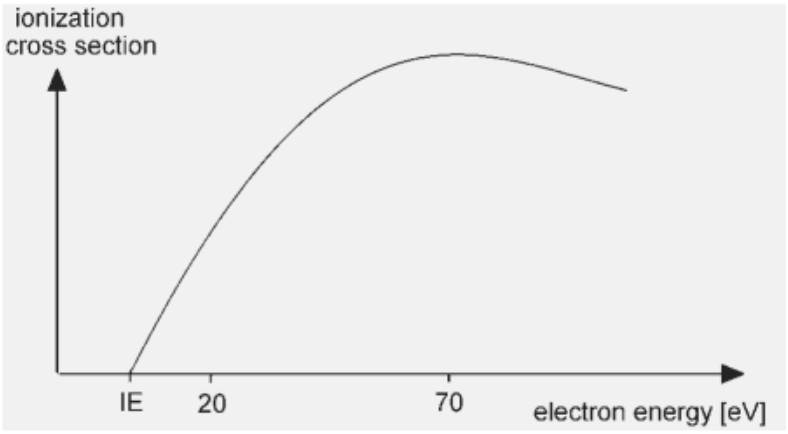

Figure 3.5. *Ionization efficiency curve for EI; ionization cross section versus electron energy.*

For positive ions the electron energy is in most cases set to 70 eV. However, between only 10 and 20 eV energy is transferred to the molecules during the ionization process. The obvious consequence is that the excess energy leads to extensive fragmentation, which can be advantageous in providing structural information for the elucidation of unknown analytes. In any case, EI mass spectra are excellently reproducible when measured under standard conditions (70 eV, ion source at 150–250°C), in both cases of measurements performed on the same or different types or brand of instruments. This fact has triggered the construction of mass spectral databases, commonly named as libraries. The most comprehensive EI mass spectral databases are those provided by the National Institute of Standards and Technology (NIST), and the Wiley/NBS. Furthermore, the 2017 version of the NIST/EPA/NIH mass spectral database is equipped with a compilation of linear retention index (LRI) values determined on non-polar and polar columns.

3.3.2 Chemical ionization

Chemical ionization was first reported in 1960 [15], is considered as a *soft* ionization technique with respect to conventional EI; in fact, a lower amount of energy is required for the ionization of neutral molecules. CI technique, in comparison to EI, presents the advantage of yielding a spectrum with less fragmentation in which the molecular species is preserved. Ionization in CI is the results of one or several competing chemical reactions. Specifically, new ionized species are formed when gaseous molecules interact with ions.

The ionization process may involve the transfer an electron, proton, or other charged species between the reactants. These reactants are:

i) the neutral analyte, and

ii) ions from a reagent gas.

CI ion sources exhibit close similarity to EI ones and the latter can usually be switched to CI operation, by the presence of an excess of reagent gas over the analytes. *Figure 3.6* reports a schematic layout of a typical CI ion source. As can be observed, the reagent gas is introduced directly into the ion volume to ensure maximum pressure inside at minimum losses to the ion source housing. During CI operation, the pressure in the ion source housing typically rises by a factor of 20-50 as compared to those used in the EI.

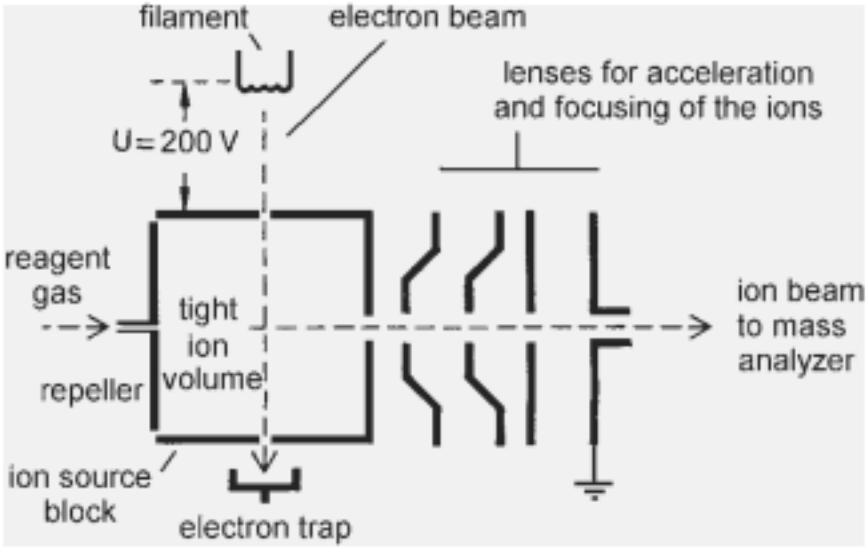

Figure 3.6. *Schematic representation of an chemical ionization (CI) source.*

Such intra-source conditions, ensures that an electron entering the source block will preferentially ionize the reagent gas molecules, generating the so-called "*ion-reagent*". The latter interact with the neutral analyte molecule leading to the formation of ionized species. It must be noticed that, CI differs from EI, because the ionization process is enabled by *bimolecular processes* (ion-molecular reactions), rather than unimolecular (electron-molecule) ones. This subsequent ion-molecule interactions, will produce positive and

negative ions of the substance, the latter particularly useful to analyze highly electronegative compounds.

Apart from the most commonly employed ionization modes, other two ionization processes can be used in GC field, atmospheric pressure CI and single photon ionization (SPI), respectively. must be cited. Atmospheric pressure chemical ionization (APCI) is perceived as a novel form of *soft* ionization in the GC field, most probably due to its recent burst of popularity in GC-MS experiments [16], and most certainly not to its invention date [17]. APCI process produces mass spectra with a limited amount of fragmentation, and most often with the presence of molecular ion (MI). In recent years, it has gained a certain popularity in a variety of GC-MS applicational field, such as petrochemical [18], food contamination [19] environmental [20] and metabolomics. Single photon ionization (SPI) is enabled by a pulsing laser, which generates vacuum ultraviolet (VUV) photons, with sufficient energy to induce soft and universal ionization. Welthagen et al. used a SPI [21] characterized by the use of a pulsing laser (5 Hz) to generate vacuum ultraviolet (VUV) photons with sufficient energy (10.5 eV; 118 nm wavelength) to promote universal analyte ionization. It was reported that, under the applied SPI conditions, only small aliphatic molecules (as well as the mobile phase) were not ionized.

3.4 Mass analyzers

A mass analyzer is a device that enables to separate the gas phase species produced according to their mass-to-charge ratio, *m/z*. There are wide varieties of mass analyzers available to current-day GC- and GC×GC-MS food analysis. Mass analyzers use different physical principles, the selection of an MS system depends on different factors, with ease-of-use along price representing key aspects next to the technical differences. In general, they can be divided in two broad classes on the basis of many properties. Scanning analyzers allow only the ions of a given mass-to-charge ratio to go through at a given time. They are either magnetic sector or quadrupole instruments. On the contrary, mass analyzers such as time-of-flight, ion trap, ion cyclotron resonance or orbitrap, allow the simultaneous transmission of all ions across a given mass range. Analyzers can be also grouped on the basis of other properties, for example ion beam *vs.* ion trapping types, or continuous beam *vs.* pulse based. Another trend in mass analyzer development is to combine different analyzers in sequence in order to allow multiple experiments to be performed. For example,

triple-quadrupoles and more recently hybrid instruments such as quadrupole-time-of-flight (TOF) allow the generation of fragments over several decomposition experiments. The main characteristics for measuring the performance of a mass analyzer are: 1) the mass range limit; 2) the analysis speed; 3) the transmission; 4) the mass accuracy and finally 5) the resolution.

3.4.1 Single quadrupole

The principle of the quadrupole mass analyzer was first described by Paul and Steinwegen in 1953 [22]. Linear single-quadrupole analyzers are made up of four parallel cylindrical or hyperbolically shaped rod electrodes (*Figure 3.7*). The mass separation is accomplished by the stable vibratory motion of ions in a high-frequency oscillating electric field that is created by applying a combination of direct-current (DC) and radio frequency (RF) potentials to these electrodes [23-25]. Opposite rods are connected electrically in pairs. The two pairs will, at any given time, have potentials of the same magnitude, but of opposite sign. As an ion enters in the space between the rods oscillates in the directions *x* and *y*, whose amplitude depending on the frequency of the potential applied and the masses of the ion. A positive ion will be attracted towards a negative rod. If the potential changes sign, the ion will change direction avoiding discharging itself on the rod. Acting as a scanning device, at given values of the DC and RF potentials, only ions within a certain narrow *m/z* range will have stable trajectories and be allowed to reach the detector, while all others are eliminated. The motion of an ion traveling through the quadrupole is described by the theory of the *Mathieu equations* [26].

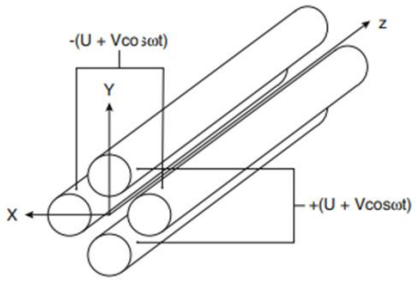

Figure 3.7. *Schematic of the quadrupole analyzer.*

As illustrated in *Figure 3.7,* the DC potential applied to the electrodes of the *x-z* plane is positive, while that applied to the electrodes of the *y-z* plane is negative. To fully understand how the potential influences the trajectory of the ions, the *x-z* and *y-z* planes must be considered separately. Taking into account the *x-z* plane (*Figure 3.8*), at positive (DC) potentials, ions will be rejected and focused toward the central axis of the electrodes. Once the potential is switched to negative value, the positive ions will be accelerated towards the electrodes. If the potential at the electrodes changes rapidly, high-mass ions will preferably be pushed to move towards the middle between the electrodes. On the contrary, in the presence of lighter ions the negative, tough brief, potential can be sufficiently intense to attract and lead them to collide with the electrode. In this way, the rods act as a "high pass mass filter".

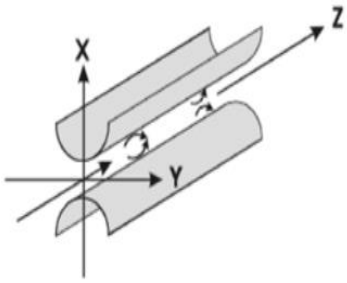

Figure 3.8.. *Schematic representation of the motion of the ions inside the quadrupole analyzer.*

In the *y-z* plane, the situation is very similar except from the fact that the DC potential is negative. Which means that heavy ions will be pushed to hit one of the electrodes. Conversely, low-mass ions will be pushed back towards the middle between the electrodes. In such conditions, the rods will act as a "low pass mass filter". Those ions which have a stable trajectory through both the high pass and low pass filter are successfully detected. Figure *3.9* illustrates a diagram in which is represented the stability areas. Specifically, four stability areas are labeled I to IV for x- and y- motion.

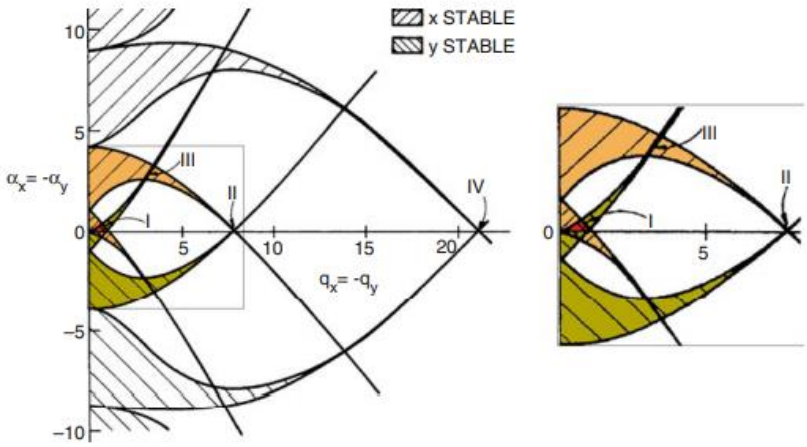

Figure 3.9. *Stability diagram for a linear quadrupole analyzer showing four stability regions (I–IV) for x- and y-motion. The portion within the square frame is zoomed to double size on the right (Adapted from Ref. [27]).*

The quadrupole is a real mass-to-charge ratio analyzer. It does not depend on the kinetic energy of the ions leaving the source. The only requirements are:

i) the time for ions to go through the analyzer is short compared with the time necessary to switch from one mass to the other, and

ii) the interscan delay, *i.e.*, the time between one scan and the next, has to be small.

Single quadrupole mass spectrometers (QMS) are the most common devices employed in the field of GC-MS. The devices offers the advantages to perform well in both untargeted and targeted analysis, by two different operational modes, namely scan and SIM (selected ion monitoring). However, as mentioned previously, linear quadrupole analyzers (QMS) are the second most common form of mass spectrometry used in the GC×GC field (see *Figure 3.7*), with such a situation depending on a technological characteristics. In fact, QMS is a scanning device, capable to monitor *m/z* one at a time, across an applied mass range (typical m/z ranges are 25 to 2000 u), thus decreasing the sensitivity (low duty cycle ≈0.1%). The sensitivity, can be vastly improved when scanning a narrow *m/z* range, or operating in single ion monitoring (SIM) mode, namely choosing only on or few ions to be detected. In such an operation mode, the quadrupole mass spectrometer has a duty cycle of 100%. QMS technology has evolved greatly over recent years, to the extent that such instrumentation can now be used for analyte quantification in GC×GC analyses.

3.4.2 Time-of-flight

In 1946, Stephens introduced the principle of TOF analysers [28]. It was only in 1955 that Wiley and McLaren published the design of a linear TOF mass spectrometer, which later became the first commercial instrument [29]. The concept of TOF is rather straightforward: ions of different *m/z* are dispersed in time during their flight along a field-free drift path of known length. *Figure 3.1o* shows a scheme of a linear TOF instrument. After being formed by continuous or pulsed ion source and accelerated by an electric field, ions arrive at the interface of the TOF in the form of *ion packages.* These ions are then accelerated towards the flight tube by a difference of potential applied between an electrode and the extraction grid. When leaving the acceleration region, all the ions whit the same charge will ideally possess an equal kinetic energy, and will enter into a field-free region, and reach the detector positioned at the other extremity of the flight tube at different velocities according to their masses. Which means that all ions start at the same time or at least within a sufficiently short time interval and the lighter ones will arrive earlier at the detector than the heavier ones.

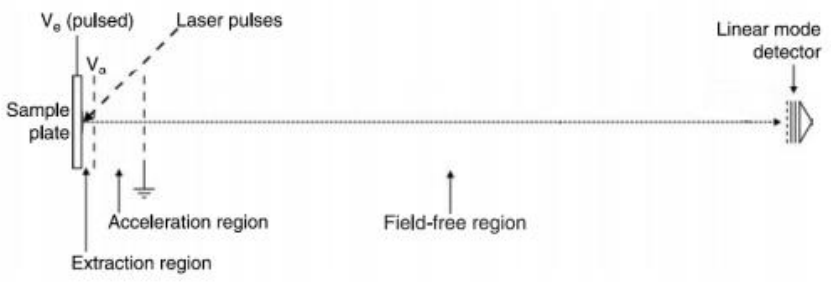

Figure 3.10. *Schematic representation of a linear TOF mass spectrometer.*

Such an instrumental setup where the ions are traveling on a straight line from the point of their generation towards the detector is called "*linear*" TOF. The time difference between the starting signal of the pulse and the time at which an ion hits the detector is the time of flight and can be expressed as:

$$t_{tof} = \frac{L}{v} = L\sqrt{\frac{m}{2qU_a}} \propto \sqrt{m/z}$$

(*Eq. 3.6*)

where *L* is the length of the field-free region, *v* is the ion velocity after acceleration, *m* is the mass of the ion, *q* the charge of the ion, U_a the accelerating electric potential difference, and *z* the charge state. This equation shows that, higher is the mass of an ion slower it will reach the detector, and vice versa.

-*Orthogonal acceleration*

As aforementioned, TOF analyzers are directly compatible with pulsed ionization techniques. However, to fully exploit the capabilities of such a mass analyzers, it is interesting to combine them also with continuous ionization techniques, *e.g.*, EI and any type of API. The major breakthrough in the technological development of TOF analyzers arose from the design of the orthogonal acceleration TOF analyzer. In an oaTOF analyzers, pulses of ions are extracted orthogonally from a continuous ion beam. Specifically, ions fill the first stage of the ion accelerator in the space between the extraction plate and a grid. A pulsed electric field is then applied at a frequency of several kilohertz, which force ions to assume a direction orthogonal to their original trajectory, and then begin to fly towards the analyzer. It is worthy to say that the duty cycle of an oaTOF is far from 100% and it is generally lower than that of classical TOF analyzer. That is because the time required for the ion beam to fill the orthogonal acceleration region is lower than the time required for the sampled ions to hit the detector, and since new ions cannot be injected until the ions from the previous injection have reached the detector, the logical consequence is that a part of the ions produced in the source are lost in the first stage of the orthogonal accelerator. The most significant advantages of oaTOF analyzers are: *i*) high mass resolving power, and *ii*) mass accuracies even up to or below 1 ppm. Therefore, it is not surprising that oaTOF instruments are currently widespread used in combination with GC and fast GC

-*Reflectron*

The mass resolving power of a TOF analyzer is mass dependent, and is also a function of the length and geometry of the flight path of the instrument. A way to improve mass resolution is to use an electrostatic reflector also called a *reflectron.* The reflectron,

introduced by Mamyrin [30], has the aim to create a retarding field that acts as an ion mirror by deflecting the ions and sending them back through the flight tube. The simplest type of reflectron, which is called a single-stage reflectron (ReToF), consists of a series equally spaced grid electrodes or more preferably ring electrodes connected through a resistive network of equal-value resistors. As shown in *Figure 3.11* the reflectron is situated behind the field-free region opposed to the ion source while detector is positioned on the source side of the ion mirror to capture the arrival of ions after they are reflected. The reflectron corrects the kinetic energy dispersion of the ions leaving the source with the same *m/z* ratio. Consequently, ions with more kinetic energy and hence with more velocity will penetrate the reflectron more deeply than ions with lower kinetic energy. Consequently, the faster ions will spend more time in the reflectron and will reach the detector at the same time than slower ions with the same *m/z*. Although the reflectron increases the flight path, though without increasing the dimensions of the mass spectrometer, the beneficial increase in mass resolution comes at the expense of sensitivity and mass range limitation.

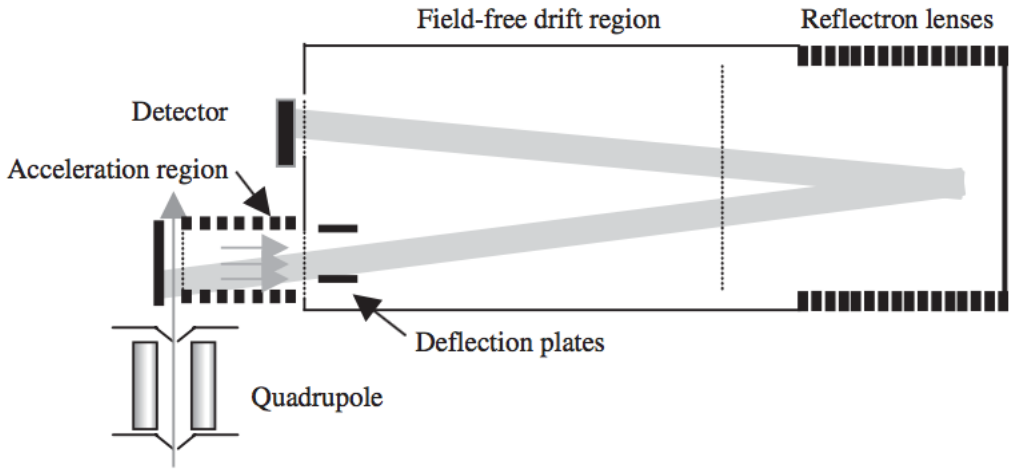

Figure 3.11. *The working principle of a single-stage reflectron.*

The choice of operating TOF instruments in “linear” or “reflectron” mode heavily depends on the species to be detected. For example, when operating in linear mode, the aim is usually to detect larger species, which will not be stable enough to survive along the strong electric field of the reflectron. Therefore, the given resolving power is much lower, as the width of the isotopic envelope do not allow for its decent resolution. The opposite is the case of

ReTOF, because especially in the presence of metastable fragmentations (*i.e.*, in tandem MS), only fragments still having kinetic energies close to that of the precursor can be successfully and sensitively detected. The use of TOF as a mass analyzer, presents several advantages. In principle, the upper mass range has no limit, thus making it especially suitable for analyzing large molecules and differently to the scanning devices, all the mass range is simultaneously analyzed leading to a very high sensitivity compared to quadrupole analyzer. Generally, the TOF analyzer is very fast, and a spectrum over a broad mass range can be obtained in the microseconds time interval. Thus making possible, theoretically, the production of several thousand mass spectra over a very wide mass range in 1 second.

3.4.3 Triple quadrupole

Triple quadrupole (QqQ) MS instruments follow a basic principle. The first quadrupole (Q1) is set to transmit a particular *m/z*. The second quadrupole (q) is normally an octapole or hexapole, and contains a gas-filled collision cell, within which fragmentation occurs through low energy collision induced dissociation (CID). In the third quadrupole (Q3), the product ions produced from the precursor ion are analyzed (*Figure 3.12*).

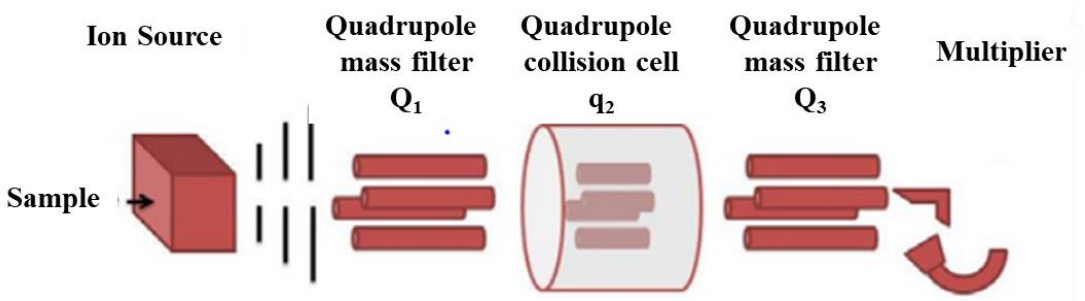

Figure 3.12. *Schematic of a triple quadrupole mass spectrometer.*

Considering a precursor ion, m_1^+, which decomposes to give a product ion, m_2^+, and a neutral loss, *N:*

$$m_1^+ \rightarrow m_2^+ + N$$

(*Eq. 3.7*)

MS/MS experiments can be classified according to which of these species (precursor,

product ions or neutral loss) is detected. Therefore, four types of scanning mode are most commonly used, namely the product ion scan, precursor ion scan, neutral loss scan and selected reaction monitoring (*Figure 3.13*).

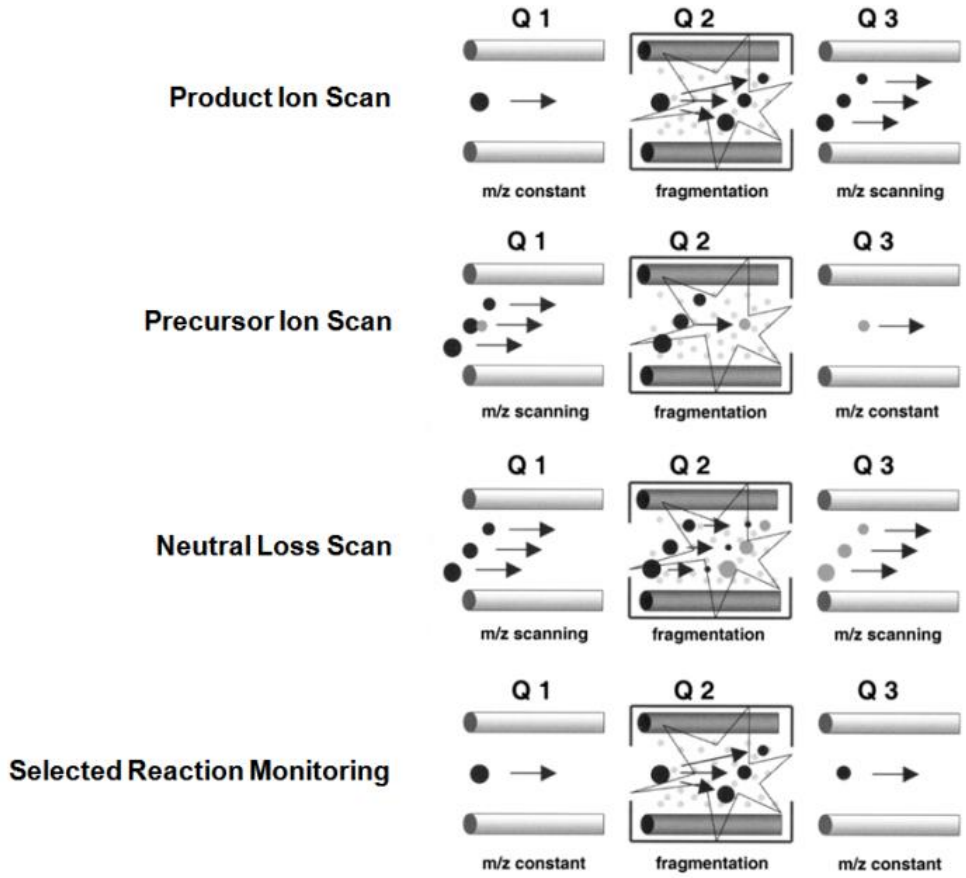

Figure 3.13. *Schematic of operation modes of a triple quadrupole mass spectrometer.*

The *product ion scan* is accomplished by setting the first analyzer (MS_1) to a particular m/z value, and performing a scan on a range of m/z values in the second analyzer (MS_2). This is the most common and well-known MS/MS mode, which is generally used for structural elucidation tasks. *Precursor ion scan* is achieved by performing a scan in MS_1, while a specific m/z is set at MS_2. This mode is particularly useful when a given product ion, characteristic of a compound class, is known and thus all the compounds belonging to that class can be identified. To perform a *neutral loss scan*, the two mass analyzers operate at the same scan speed, but MS_2 is shifted by a determined m/z value respect to MS_1. In this way, only ions which lose a neutral mass, corresponding to the m/z difference between the two analyzers, can be revealed.

In *selected reaction monitoring*, transitions of m/z values from a precursor to a particular ion produced upon dissociation are monitored. Since one or more pair of transitions can be monitored in the same time interval, that is a precursor to one or more product ions, this technique is often referred to as multiple reaction monitoring.

All these operating modes may be used for both qualitative and quantitative applications, depending on the specific case and needs. Concerning qualitative applications, they aims to two main purposes: i) the identification of unknown compounds compared to reference through the recognition of common fragmentation patterns, and ii) mapping the fragmentation paths that lead to a certain mass spectrum. Furthermore, the scanning of a precursor ion and that of a neutral loss are particularly useful in screening experiments. In the context of quantitative analyses, the major reduction of chemical background is certainly a significant advantage. Additionally, the very rapid duty cycle (10 to 50 ms) of the QqQ also makes it particularly suitable for high throughput analysis.

3.5 Evolution and current state of GC×GC-MS

In a recent review paper, Tranchida et al. [31] reported on evolution and trends in the field of GC×GC-MS, over a period spanning from 2014 to 2017, and covering a total number of 343 papers (*Figure. 3.14*).

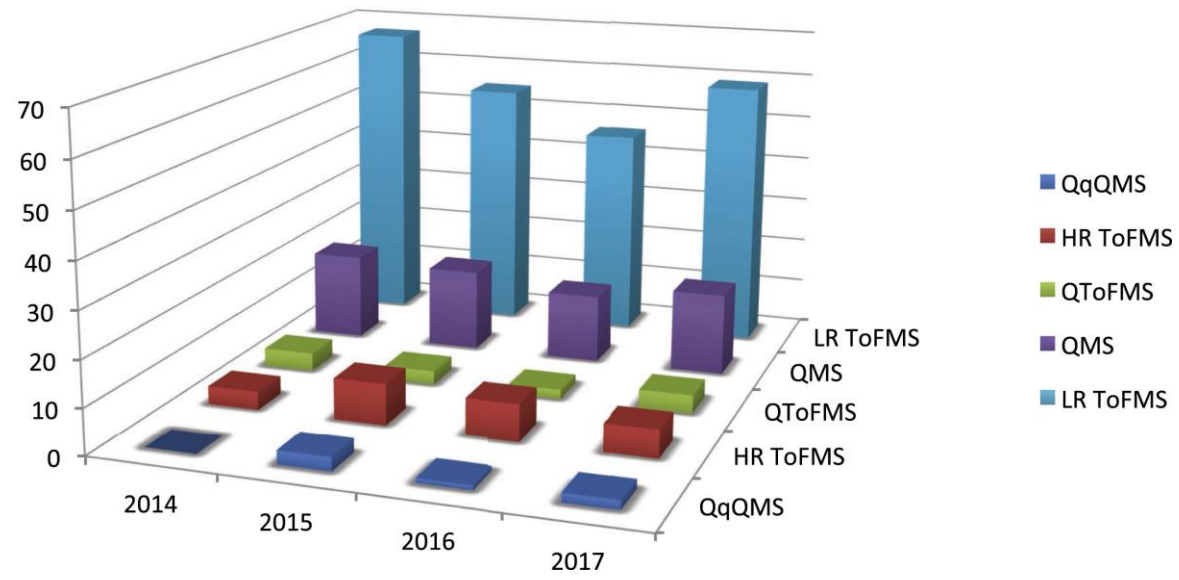

Figure 3.14. *Graph constructed by using GC×GC-MS data, related to the 2014-2017 period (number of papers is reported along the z-axis) [31].*

The authors found that the number of GC×GC-MS papers per year was rather stable (on average 86 papers per year), with these reporting on the use of five forms of MS. The use of LR ToFMS was by far the most popular choice, it being present in about 66% of the contributions. The use of QMS it was reported in approx. 20% of the applications, while, HR ToFMS was involved in approx. 8% of the research work. Such MS instrumentation can generate database-searchable full spectra, along with exact identification, in particular if the molecular ion species is preserved. Two remaining forms of mass spectrometry (both multi-analyzer types), namely QToF and QqQMS, have been reported in only 12 and 6 investigations, respectively (*Figure. 3.14*). Taking into account the ionization modes, one can say that the use of EI to induce analyte fragmentation has been exploited almost exclusively. As already mentioned, the ion source has the main roles to receive analytes from the GC column, to ionizes and fragmentates them, and transfer the ions into a further analytical dimension, namely the mass analyzer. In the case of scanning devices, such as in QMS, the mass analyzer transmits packets of ions to the detector, at one *m/z* value at a time, across a specific mass range. Such analyzers basically perform an extraction process: only ions with a stable trajectory reach the detector, while all others are eliminated. True ion separations in space occur in ToFMS systems: the ions formed in the source are pulsed rapidly and sequentially (orthogonal acceleration) into the flight tube; herein, ions are separated in a field-free region on a flight-time basis (heavier ions travel slower compared to lighter ones). The following concept can be applied to both GC×GC-QMS and GC×GC-LR ToFMS: if a mass range of m/z 50-450, at nominal mass resolution, is applied, then potentially 400 different masses could fit in the MS separation space. If, hypothetically, 3 compounds overlap completely at the GC outlet, with 50 ions generated per compound, then a great increase in data density, and overall disorder, will be attained: many of the resulting m/z values will be unique to each compound, while others will overlap. Reliable peak identification under such circumstances is highly complicated, to the least.

The situation would be entirely different with an ideal *soft-ionization (SI) approach*, namely a universal process capable of generating an abundant molecular ion per analyte, along with a low number of less intense ions (*e.g.*, 10). Each compound would be then characterized by four types of information: two retention times (along ^{1}D and ^{2}D respectively), MM and a database-searchable mass spectrum (if an SI MS database was available).

Some SI GC×GC-MS applications have appeared over the last decade: in 2007, Welthagen et al. used a form of SI named single photon ionization (SPI) [32], characterized by the use of a pulsing laser (5 Hz) to generate vacuum ultraviolet (VUV) photons with sufficient energy (10.5 eV; 118 nm wavelength) to promote universal analyte ionization. It was reported that, under the applied SPI conditions, only small aliphatic molecules (as well as the mobile phase) were not ionized. In 2011, Eschner et al. reported on the use of a GC ×GC-LR ToFMS instrument, with the capability to generate EI and SPI MS spectra, in an alternate mode, throughout the same analysis [33]. An EI SPI spectral production frequency of 80 Hz was applied, with the summed data used to create a TIC GC×GC-LR ToFMS chromatogram (*Figure 3.15 a*). Hard and soft ionization spectra for an alkane (compound 1), a saturated cyclic hydrocarbon (compound 2), and an aromatic hydrocarbon (compound 3), are illustrated in *Figure 3.15 b*.

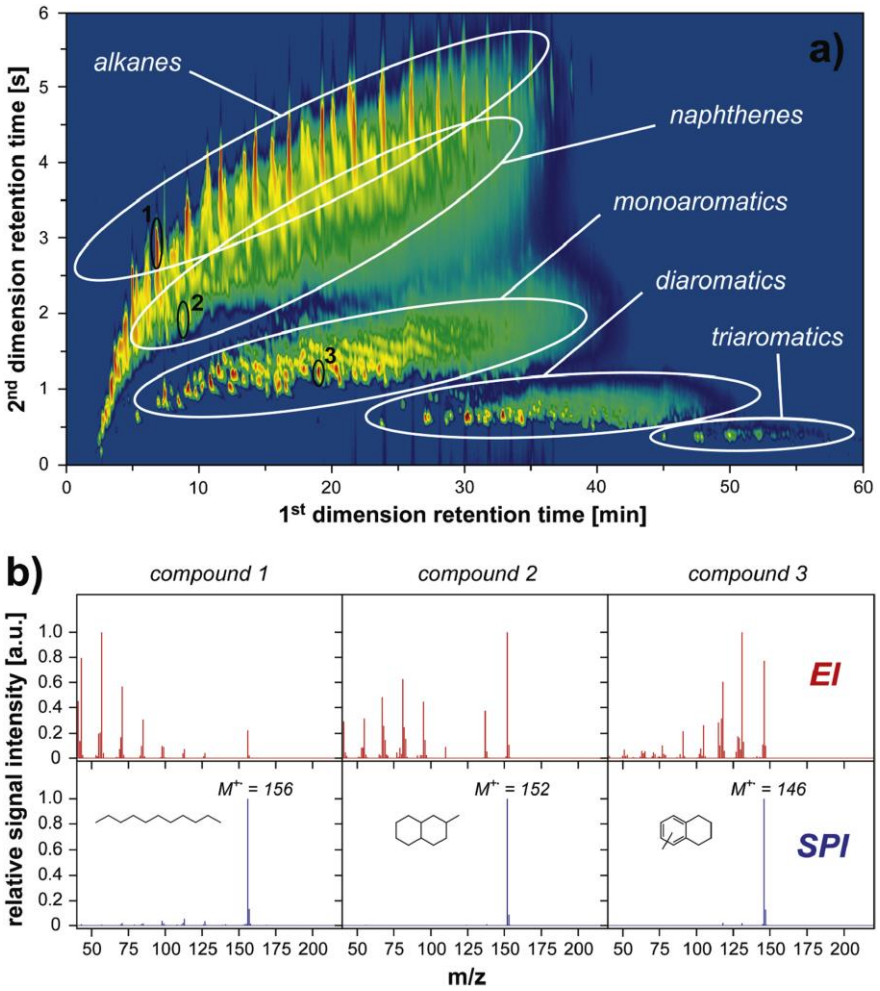

Figure 3.15. a) *GC ×GC -LR ToFMS analysis of diesel (the TIC chromatogram was generated by using both EI and SPI data); (b) EI and SPI spectra for the numbered peaks (1-3).*

As can be readily seen, molecular ions dominate the SPI spectra, accompanied by a few low-intensity fragments. Five different types of information, per analyte, were available: two retention times, MM, along with hard and soft fragmentation spectra. If one also considers the potential deconvolution capabilities, then the identification power of the technology becomes outstandingly high. Atmospheric pressure (AP*) CI* is perceived as a novel form of SI in the GC field [34], capable to produces mass spectra with a limited amount of fragmentation, and most often with the presence of MM and/or protonated MM ion information. In recent years, it has been used in a variety of GC-MS applicational fields, such as petrochemical (hydrocarbon biomarkers) [35], food contamination (pesticide residues) [36], environmental (brominated flame retardants in dust) [37], and metabolomics [38]. Megson et al. used GC×*GC* hyphenated with APCI QToFMS, for the analysis of fresh and used plane engine oil to highlight the presence of health-hazardous organophosphates [39].

Variable EI is a form of SI, of recent introduction, which has been used in GC×*GC* -LR ToFMS experiments involving engine lubricating oils [40]. In such MS instrumentation, the ionization energies can be varied between 10 and 70 eV, with values of 14 and 70 eV selected for the investigation. The emphasized strength of the variable EI approach is that sensitivity is maintained at an acceptable level, even under very low ionization energy conditions. In conventional GC-EI MS, on the other hand, a drastic sensitivity fall can be expected at ionization energies [41]. As an example, the 70 eV, the 14 eV, and the NIST spectral results for methyleicosane isomers (nominal mass ¼ 296) are shown in *Figure 3.16*. The MM ion is always present in the 14 eV spectra, along with diagnostic ions, enabling a clear differentiation between the isomers. On the contrary, if present, the MM ion is barely visible in the 70 eV and NIST spectra, while the fragmentation patterns are similar.

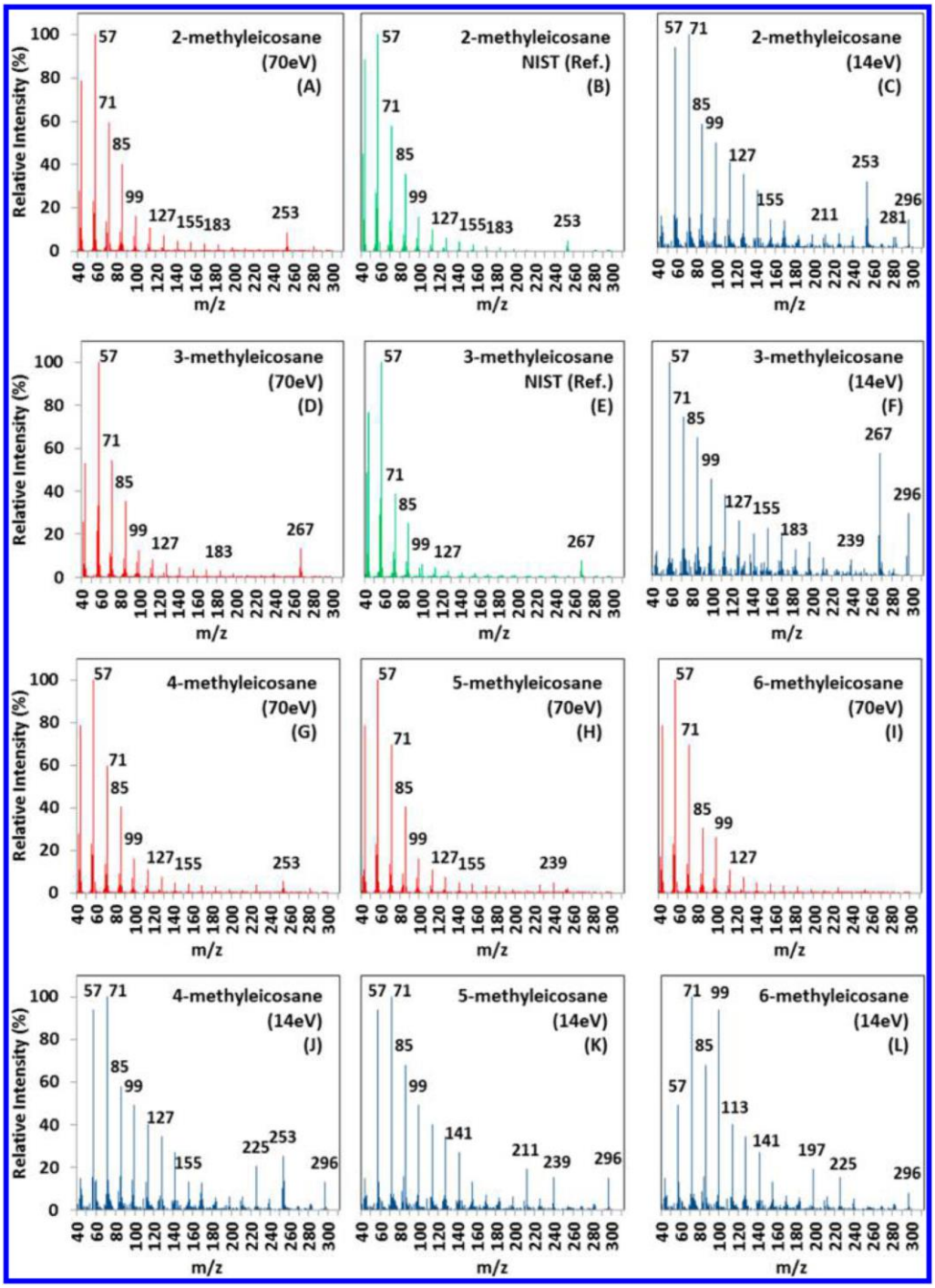

Figure 3.16. *Spectra of methyleicosane isomers generated by using ionization energies of 14 and 70 eV, along with the NIST result.*

References

[1] J.B. Phillips, J. Xu, J. Chromatogr. A 703 (1995) 327.

[2] R.S. Gohlke, Anal. Chem. 31 (1959) 535.

[3] G.S. Frysinger, R.B. Gaines, J. High Resol. Chromatogr 22 (1999) 251.

[4] M. Adahchour, J. Beens, R.J.J. Vreuls, U.A.Th. Brinkman, TrAC Trends Anal. Chem. 25 (2006) 540.

[5] M. Adahchour, J. Beens, U.A.Th. Brinkman, J. Chromatogr. A 1186 (2008) 67.

[6] P.Q. Tranchida, F.A. Franchina, P. Dugo, L. Mondello, Mass Spectrom. Rev. 35 (2016) 524.

[7] J.J. Thomson, Philos. Mag. 44 (1897) 293.

[8] J.J. Thomson, Philos. Mag. 13 (1907) 561.

[9] F.W. Aston, Philos. Mag. 38 (1919) 709.

[10] A.J. Dempster, Phys. Rev. 11 (1918) 316.

[11] A.O. Nier, Int. J. Mass Spectrom. Ion Proc. 100 (1990) 1.

[12] M.P. Balogh, Spectrosc. 19 (2004) 34.

[13] A.W.T. Bristow, Mass Spectrom. Rev. 25 (2006) 99.

[14] A. J. Dempster. Phys. Rev. 18(1921) 415.

[15] M.S.B. Munson, F.H. Field, J. Am. Chem. Soc. 88 (1966) 2681.

[16] A. Carrasco-Pancorbo, E. Nevedomskaya, T. Arthen-Engeland, T. Zey, G. Zurek, C.Baessmann, A.M. Deelder, O.A. Mayboroda, Anal. Chem. 81(2009) 10071.

[17] E.C. Horning, M.G. Horning, D.I. Carroll, I. Dzidic, R.N. Stillwell, Anal. Chem. 45 (1973) 936.

[18] V.V. Lobodin, E.V. Maksimova, R.P. Rodgers, Anal. Chem. 88 (2016) 6914.

[19] T. Portoles, J.V. Sancho, F. Hernandez, A. Newton, P. Hancock, J. Mass Spectrom. 45 (2010) 926.

[20] D. Megson, M. Robson, K.L. Jobst, P.A. Helm, E.J. Reiner, Anal. Chem. 88 (2016) 11406.

[21] C.J. Wachsmuth, M.F. Almstetter, M.C. Waldhier, M.A. Gruber, N. Nürnberger, P.J. Oefner, K. Dettmer, Anal. Chem. 83 (2011) 7514.

[22] W. Paul, H. Steinwedel, Z. Naturforsch. A 8 (1953) 448.

[23] P. H. Dawson, Quadrupole mass analyzers: performance, design, and some recent applications, Mass Spectrom. Rev. 5 (1986) 1.

[24] J. E. Campana, Elementary theory of quadrupole mass spectrometry, Int. J. Mass Spectrom. Ion Proc. 33 (1980) 101.

[25] P. E. Miller, M. Bonner Denton, The quadrupole mass filter: basic operating concepts, J. Chem. Educ. 63 (1986) 617.

[26] D.W. McLachlan. Theory and Applications of Mathieu Functions. Oxford, Clarendon Press (1947).

[27] Dawson PH (1986) Quadrupole Mass Analyzers: Performance, Design and Some Recent Applications. Mass Spectrom Rev 5:1–37

[28] Stephens, W. Phys. Rev. 69 (1946) 691.

[29] W.C. Wiley, and J.B. McLaren, Rev. Sci. Instrum., 16 (1955) 1150.

[30] B.A. Mamyrin, V.I. Karataev, D.V. Schmikk, and V.A. Zagulin, Sov. Phys. JETP, 37 (1973) 4.

[31] P.Q. Tranchida, I. Aloisi, B. Giocastro, L. Mondello, TrAC Trends Anal. Chem. 105 (2018) 360.

[32] W. Welthagen, S. Mitschke, F. Mühlberger, R. Zimmermann, J. Chromatogr. A 1150 (2007) 54.

[33] M.S. Eschner, T.M. Groger, T. Horvath, M. Gonin, R. Zimmermann, Anal. Chem. 83 (2011) 3865.

[34] A. Carrasco-Pancorbo, E. Nevedomskaya, T. Arthen-Engeland, T. Zey, G. Zurek, C. Baessmann, A.M. Deelder, O.A. Mayboroda, Anal. Chem. 81 (2009) 10071.

[35] V.V. Lobodin, E.V. Maksimova, R.P. Rodgers, Anal. Chem. 88 (2016) 6914.

[36] T. Portoles, J.V. Sancho, F. Hernandez, A. Newton, P. Hancock, J. Mass Spectrom. 45 (2010) 926.

[37] D. Megson, M. Robson, K.L. Jobst, P.A. Helm, E.J. Reiner, Anal. Chem. 88 (2016) 11406.

[38] C.J. Wachsmuth, M.F. Almstetter, M.C. Waldhier, M.A. Gruber, N. Nürnberger, P.J. Oefner, K. Dettmer, Anal. Chem. 83 (2011) 7514.

[39] D. Megson, X. Ortiz, K.J. Jobst, E.J. Reiner, M.F.A. Mulder, J.-C. Balouet, Chemosphere 158 (2016) 116.

[40] M.S. Alam, C. Stark, R.M. Harrison, Anal. Chem. 88 (2016) 4211.

[41] E. de Hoffmann, V. Stroobant, Mass Spectrometry Principles and Applications Third Edition, John Wiley & Sons, Chichester, 2007.

Chapter 4

Research in the field of advanced chromatography-mass spectrometry technologies for food samples analysis

4.1 In-depth qualitative analysis of essential oils using LC// GC×GC-QMS*

The present research is focused on the in-depth qualitative analysis of three types of lime essential oil (EO), *viz.*, Key (A and B) and Persian, using the off-line combination of normal phase high performance liquid chromatography (NP-HPLC) and comprehensive two-dimensional gas chromatography–quadrupole mass spectrometry (GC × GC-QMS). The first analytical dimension (NP-HPLC) was exploited for the isolation of the hydrocarbon constituents from the oxygenated ones. Each fraction was then reduced in volume and analyzed using (cryogenic modulation) GC × GC-QMS. Peak assignment was carried out through the combined use of mass spectral database and linear retention index matching processes. The powerful four-dimensional technology enabled the separation and identification of a very high number (153) of lime essential oil volatile compounds.

Two varieties of sour lime are mostly used in the flavor industry, namely Key (*Citrus aurantifolia* Swingle) and Persian (*Cistrus latifolia* Tanaka). Distilled Key lime oil is the most common product, with its aroma deriving from transformation processes (hydration, elimination, rearrangement reactions) which occur during the distillation process.

*This section has been adapted from the following publication: M. Zoccali, **B. Giocastro**, I. L. Bonaccorsi, A.Trozzi, P. Q. Tranchida, L. Mondello in *"In-Depth Qualitative Analysis of Lime Essential Oils Using the Off-Line Combination of Normal Phase High Performance Liquid Chromatography and Comprehensive Two-Dimensional Gas Chromatography-Quadrupole Mass Spectrometry." Foods 2019, 8(11), 580-589.*

Cold-pressed lime oil is characterized by a fragrant citrus aroma and is used in perfumery, as well as in the flavor industry. Different types of cold-pressing processes provide different types of lime oils: (I) a screw press is used to attain a juice–oil–pulp mixture, followed by centrifugation to isolate the essential oil. Such a procedure is used only for Key limes and yields the type A oil; (II) the peel is subjected to gentle grating, with the oil washed away through the application of water. After, the oil is recuperated through centrifugation. Such a process is applied to both Key (type B oil) and Persian limes [1]. The volatile fraction of lime oils is lower than other cold-pressed citrus oils (e.g., 85% against 99% of sweet orange oil), and is composed of a variety of mono- and sesquiterpenes (both hydrocarbons and oxygenated), along with aliphatic alkanes, alcohols, and aldehydes [2]. Gas chromatography-mass spectrometry (GC-MS) is certainly the prime analytical choice for the qualitative untargeted analysis of the volatile fraction of lime essential oil; identification is often achieved through MS database matching, the use of linear retention index (LRI) information, and the co-injection of pure standard compounds. The GC-MS analysis is commonly performed using a conventional (*i.e.*, 30 m × 0.25 mm ID × 0.25 µm d_f) low-polarity column and a unit-mass resolution mass spectrometer [2,3]. Even though the utility of GC-MS is not herein doubted, it has been previously shown that the on-line combination of normal phase liquid chromatography (NP-LC), and GC-MS is of high analytical usefulness within the context of lime essential oil analysis, and more in general in that of essential oils. The NP-LC process achieves a polarity-based separation, thus isolating the hydrocarbons from the oxygenated compounds. After each fraction is subjected to a GC-MS analysis, reducing the chance of co-elution, and thus increasing the number of separated compounds [4]. A great increase in the number of separated compounds can also be attained by using comprehensive two-dimensional GC-MS (GC × GC-MS). In GC × GC analyses, a dedicated transfer device (a cryogenic modulator in the majority of cases) is used to first cut, and then transfer fractions of effluent from a first analytical column (usually a conventional column) onto a second one (usually a short micro-bore column segment (1-2 m) with a different stationary phase. Such a transfer (or modulation) process occurs sequentially, and in a continuous manner, throughout the analysis. The superiority of GC × GC, over conventional GC, is due to the: (I) enhanced selectivity; (II) increased separation power; (III) high sensitivity due to analyte re-concentration (if cryogenic modulation is used); (IV) pattern formation of homologous series of compounds (e.g., alkanes, fatty acid methyl esters, etc.), enhancing the reliability of identification. Comprehensive 2D GC was first introduced in 1991 [5], can now be considered as a well-known technology [6], and

has been used both for the analysis of non-citrus and citrus essential oils [7, 8]. With the aim of exploiting the benefits of both LC and GC × GC (with single quadrupole (Q) MS), in previous off-line research the two technologies were combined (LC//GC × GC-QMS) and used for the highly-detailed qualitative analysis of sweet orange and bergamot essential oils [9]. Later studies were focused on a highly specific albeit minor chemical class (sesquiterpene hydrocarbons) of lemon, bergamot, sweet orange, clementine, bitter orange, mandarin (green, yellow, red), pink grapefruit, and lime (Key A, Key B, and Persian) essential oils [10], and on the oxygenated constituents of green, yellow, and red mandarin oils [11].

4.1.1 Experimental

- **Sample and sample preparation**

A standard mixture of C_7-C_{30} *n*-alkane was kindly provided by Merck Life Science (Merck KGaA,Darmstadt, Germany) and used for the calculation of LRI values. Three genuine cold-pressed samples of lime (Key A, Key B, and Persian) oils were provided by Citrojugo S.A. de C.V. Tecomán (Colima, Mexico). Prior to LC analyses, the oils were diluted 1:2 (*v/v*) in *n*-hexane.

- **Instrumentation**

LC pre-separation. LC pre-separations were carried out by using a Shimadzu 5D Ultra-e system (Kyoto, Japan) consisting of:

- An LC system, equipped with a CBM-20A communication bus module, two LC-30AD dual-plunger parallel-flow pumps, a DGU-20A online degasser, an SPD-M20A photodiode array detector, a CTO-20A column oven, and an SIL-30AC autosampler. Data were acquired by the LC solution v.5.92 software (Shimadzu).
- An AOC-5000 auto injector equipped with a dedicated dual side-port syringe, employed as a transfer device (not used in the present investigation).

LC fractions were collected by disconnecting the transfer line (linking the outlet of the LC detector to the syringe) from the syringe side. A 100 × 3 mm ID × 5 µm d_f silica column (SUPELCOSIL LC-Si, Merck Life Science) was operated under the following gradient conditions (flow: 0.35 mL min^{-1}): 0-4.5 min (100% hexane); from 4.5 to 6.0 min 100% MTBE (until the end of the analysis). Injection volume: 20 µL. LC fractions: hydrocarbons were collected from 1.5 to 3 min (525 µL); oxygenated compounds were collected from

7.3 to 14 min (2345 µL). Prior to GC × GC-QMS injection, the fractions were reduced to a volume of 100 µL (under a gentle stream of nitrogen).

CM GC×GC-QMS analysis. All applications were performed on a system consisting of a GC2010 gas chromatograph and a QP2010 Ultra quadrupole mass spectrometer (Shimadzu). The primary column (^{1}D) was an SLB-5 ms [(silphenylene polymer which can be considered equivalent in polarity to poly (5%diphenyl/95% dimethylsiloxane)] with dimensions 30 m × 0.25 mm ID × 0.25 µm d_f column. The secondary column (^{2}D) was a segment of Supelcowax-10 (100% polyethylene glycol) with dimensions 1.0 m × 0.10 mm ID × 0.10 µm d_f column. A 1.5 m × 0.18 mm ID segment of uncoated capillary column, was used to create the modulator loop. All the columns used were kindly provided by Merck Life Science. The connections between the ^{1}D and ^{2}D columns, and the modulator loop, were made by using two SGE SilTite mini unions (Trajan, Ringwood, Victoria, Australia).

GC×GC conditions: modulation was carried out every 5 s by using a cryogenic fluid-free modulator (under license from Zoex Corporation, Houston, TX, USA). The duration of the hot pulse (400°C) was 400 ms.

GC oven temperature program: 50°C to 250°C at 3°C min^{-1}; carrier gas, helium, was supplied at an initial pressure of 173.5 kPa (constant linear velocity). Injection temperature: 250°C.

- Injection mode and volume for monoterpene hydrocarbons: split (1:150), 0.4 µL.
- Injection mode and volume for sesquiterpene hydrocarbons: split (1:20), 1.0 µL.
- Injection mode and volume for oxygenated compounds: split (1:20), 1.0 µL.

Mass spectrometry conditions: the temperature of the interface was 250°C; the ion source temperature was 200°C, with analyte fragmentation induced by electron ionization (70 eV).The samples were analyzed in the scan mode using a mass range of 40-360 m/z; spectra generation frequency: 33 Hz.

Data were acquired by using the GCMS Solution v.4.45 software (Shimadzu, Kyoto, Japan) bidimensional chromatograms were generated by using the ChromSquare v.2.3 software (Shimadzu). The MS database employed was the FFNSC 3.0 (Shimadzu).

4.1.2 Results and Discussion

As performed in previous research [9], peak identification was carried out through the combined use of MS database spectral searching and LRI information (comparison between the MS database and experimental LRI values). Three levels of identification were defined: level I—a similarity match ≥90% and an experimental LRI value within a ± 5 LRI tolerance window, with respect to the database result; level II—either a similarity match ≥90%, or an experimental LRI value within a ± 5 LRI tolerance window, with respect to the database result (a compound identified in such a manner cannot be characterized by a similarity match <80%, or an experimental LRI value outside a ± 10 LRI tolerance range); level III—a similarity match >75% and an experimental LRI value within a ± 15 LRI tolerance window, with respect to the database result. It must be emphasized that pure standard compounds were not used in the present research to confirm peak identity. However, the combined use of LRI data and MS information is nowadays accepted for the identification of essential oil constituents [13]. Finally, the main scope of the research was to demonstrate the power of the off-line four-dimensional (4D) method for this type of food sample. After the LC pre-separation step, the two fractions (hydrocarbons and oxygenates) were reduced in volume (to 100 µL) and then subjected to three GC×GC-QMS analyses; the hydrocarbon fraction was analyzed twice, for the monoterpene (M) and sesquiterpene (S) hydrocarbons. For the latter compounds, present in lower quantities compared to the M hydrocarbons, a higher sample volume and lower split ratio were used. Fifty hydrocarbons were identified, considering the three oils: 46, 47, and 47 hydrocarbons in the Key A, Key B, and Persian lime oils, respectively, as shown in *Table 4.1*. With regard to the oxygenated compounds, an overall number of 103 constituents were identified: 77, 82, and 48 compounds in the Key A, Key B, and Persian lime oils, respectively, as shown in *Table 4.2*. The GC×GC-QMS chromatogram of the oxygenated fraction of the Persian lime oil is shown in four expansions in *Figure 4.1 A-D*. As can be seen, more than half of the detected peaks in *Figure 4.1 A-D* were not assigned. Considering both the hydrocarbons and oxygenates, a total number of 153 constituents were identified in the three oils: 123, 129, and 95 compounds in the Key A, Key B, and Persian lime oils, respectively, as shown in *Tables 4.1* and *4.2*.

The off-line combination of HPLC and GC × GC–QMS, and its application to the detailed qualitative analysis of lime Essential oils (EOs), gave origin to compound-rich chromatograms, due to the possibility of concentrating the two pre-separated fractions

(hydrocarbon and oxygenated compounds), and the two fundamental GC×GC characteristics, namely, the enhanced separation power and sensitivity. As mentioned previously, fifty hydrocarbons were identified with the distribution of M, S, and aliphatic hydrocarbons illustrated in *Figure 4.2.*

Table 4.1. *Hydrocarbons identified in the three types of cold-pressed lime essential oils, along with experimental and database linear retention index (LRI) values (exp./data LRI).*

Peak	Hydrocarbon	Exp./Data LRI	Identification Level			
			Key A	Key B	Persian	Class
1	Nonane [a, b]	902/900	-	I	-	Ali
2	*α*-Thujene [c]	927/927	I	I	I	M
3	*α*-Pinene [c]	933/933	I	I	I	M
4	Camphene [c]	953/953	I	I	I	M
5	Sabinene [c]	973/972	I	I	I	M
6	*β*-Pinene [c]	980/978	I	I	I	M
7	Myrcene [c]	988/991	I	I	I	M
8	*α*-Phellandrene [c]	1009/1007	I	I	I	M
9	*α*-Terpinene [c]	1018/1018	I	I	I	M
10	*p*-Cymene [c]	1025/1025	I	I	I	M
11	Limonene [c]	1030/1030	I	I	I	M
12	β-Phellandrene	1045/1031	II [c]	II [d]	II [c]	M
13	(E)-β-Ocimene [c]	1047/1046	I	I	I	M
14	γ-Terpinene [c]	1059/1058	I	I	I	M
15	Terpinolene [c]	1087/1086	I	I	I	M
16	Undecane [e]	1100/1100	II	II	-	Ali
17	Tridecane	1299/1300	I [c]	I [c]	I [a]	Ali
18	*δ*-Elemene [c]	1336/1335	I	I	I	S
19	*α*-Cubebene [a]	1353/1349	II	II	-	S
20	*α*-Copaene [a]	1381/1375	II	II	II	S
21	*β*-Elemene [c]	1387/1390	I	I	I	S
22	Tetradec-1-ene [e, b]	1391/1392	-	-	II	Ali
23	Tetradecane [e]	1398/1400	I	II	I	Ali
24	*cis*-*α*-Bergamotene [a]	1416/1416	I	I	I	S
25	*α*-Santalene [a]	1422/1418	I	II	I	S
26	(*E*)-Caryophyllene [c]	1426/1424	I	I	I	S
27	*γ*-Elemene	1434/1432	I [c]	I [c]	I [e]	S
28	*trans*-*α*-Bergamotene	1436/1432	I [a]	I [a]	I [c]	S
29	*α*-Himachalene [a]	1440/1449	I	II	I	S

Table 4.1.
Cont.

Peak	Hydrocarbon	Exp./Data LRI	Identification Level			
			Key A	Key B	Persian	Class
30	(*E*)-*β*-Farnesene [c]	1452/1452	I	I	I	S
31	*α*-Humulene [c]	1462/1454	II	II	II	S
32	Sesquisabinene [a]	1456/1455	I	II	I	S
33	*β*-Santalene [c, b]	1464/1459	-	-	II	S
34	*β*-Chamigrene [a]	1476/1479	II	II	II	S
35	*γ*-Curcumene [a]	1481/1482	I	I	I	S
36	*α*-Curcumene [a]	1483/1480	-	-	II	S
37	*Germacrene D* [a]	1487/1480	II	II	II	S
38	*trans-β-Bergamotene* [a]	1488/1483	II	II	I	S
39	*Valencene* [a]	1490/1492	I	I	I	S
40	*β*-Selinene	1497/1492	I [c]	I [c]	I [a]	S
41	*Pentadecane* [e]	1498/1500	III	III	I	Ali
42	*(Z)*-*α*-Bisabolene [a]	1503/1503	I	I	I	S
43	*(E, E)* -*α*-Farnesene[c]	1505/1504	I	I	I	S
44	*β*-Bisabolene [c]	1509/1508	I	I	I	S
45	*(Z)*-*γ*-Bisabolene [a]	1511/1515	I	I	I	S
46	*(E)*-*γ*-Bisabolene [a]	1530/1528	I	II	I	S
47	*(E)*-*α*-Bisabolene [a]	1541/1540	I	I	I	S
48	*Germacrene B* [c]	1556/1557	I	I	II	S
49	*Hexadecane* [e]	1598/1600	II	II	I	Ali
50	*Heptadecane* [e]	1699/1700	I	I	I	Ali

Abbreviations: M: monoterpene; Ali: aliphatic; S: sesquiterpene. [a] Compound not yet identified in cold-extracted laboratory oils [2,10].[b] Compound identified in only one of the samples. [c] Compound identified previously in industrially cold-extracted lime oils and cold-extracted laboratory oils, reported since 1980 [2,10]. [d] Compound identified previously only in cold-extracted laboratory oils [2,10].[e] Compound, to the best of the authors' knowledge, identified for the first time in an industrially cold-extracted lime oil.

Table 4.2. *Oxygenated compounds identified in the three types of cold-pressed lime essential oils, along with experimental and database LRI values (exp./data LRI).*

Peak	Hydrocarbon	Exp./Data LRI	Identification Level			
			Key A	Key B	Persian	Class
51	Pinacol [a]	862/858	III	III	-	AliA
52	6-methyl-5-hepten-2-one [b]	985/986	I	II	-	AliK
53	Octanal [c]	1006/1006	I	I	-	AliAld
54	Eucalyptol [a]	1036/1032	II	-	II	MA
55	cis-Sabinene hydrate [c]	1074/1069	II	II	II	MA
56	Octanol [c]	1074/1076	II	-	-	AliA
57	Linalool [c]	1101/1101	I	I	I	MA
58	trans-Sabinene [c]	1105/1099	II	-	-	MA
59	Nonanal [c]	1106/1107	II	II	II	AliAld
60	trans-Pinene hydrate [a]	1111/1121	-	II	II	MA
61	Endo-fenchol [b, d]	1126/1119	-	II	-	MA
62	trans-p-Mentha-2,8-dien-1-ol [a]	1128/1122	II	III	-	MA
63	trans-*p*-Menth-2-en-1ol	1129/1139	III [b]	II [b]	II [c]	MA
64	(*3E,6Z*) -Nonadienol [a, d]	1141/1152	-	III	-	AliA
65	cis-Limonene oxide [c]	1142/1134	II	-	II	MO
66	trans -Limonene oxide [c]	1142/1138	II	-	-	MO
67	cis-p-Mentha-2,8-dien-1-ol [a, d]	1142/1138	-	II	-	MA
68	(*E*)-Myroxide [a]	1147/1141	III	-	-	MO
69	trans-Pinocarveol [b]	1147/1141	-	II	II	MA
70	Citronellal [c]	1154/1152	II	II	II	MAld
71	Camphor [a, d]	1154/1149	-	III	-	MK
72	Isopulegol [a]	1154/1149	III	II	II	MA
73	cis-Non-3-en-1-ol [a, d]	1163/1153	-	III	-	AliA
74	Camphene hydrate [a, d]	1163/1156	-	II	-	MA
75	Pinocarvone [a]	1168/1164	II	II	-	MK
76	Non-(*2Z*)-enol [a, d]	1171/1170	-	III	-	AliA
77	Rose furan oxide [a]	1172/1169	II	II	-	MO
78	Borneol	1179/1173	II [b]	II [b]	II [c]	MA
79	Isogeranial [a]	1182/1179	III	II	II	MAld
80	cis-Pinocamphone [b, d]	1182/1176	II	-	-	MK
81	Terpinen-4-ol [c]	1186/1180	II	II	II	MA
82	cis-Pinocarveol [a]	1188/1186	-	II	-	MA
83	p-Cymen-8-ol	1192/1189	II [a]	II [b]	III [a]	MA
84	Non-(*6Z*)-enal [a, d]	1196/1206	III	-	-	AliAld
85	α-Terpineol [c]	1200/1195	I	I	I	MA
86	Dec-(*4Z*)-enal [a, d]	1196/1196	-	II	-	AliAld
87	cis-Piperitol [a]	1207/1198	III	II	-	MA

Table 4.2.
Cont.

Peak	Hydrocarbon	Exp./Data LRI	Identification Level			
			Key A	Key B	Persian	Class
88	neo-Dihydro carveol [a, d]	1203/1198	II	-	-	MA
89	Decanal [c]	1207/1208	III	II	II	AliAld
90	trans-Piperitol [e, d]	1216/1208	-	II	-	MA
91	Nerol [c]	1231/1229	I	II	II	MA
92	3,7-dimethyl-Oct-7-enol [a, d]	1231/1228	-	-	III	AliA
93	Neral [c]	1242/1238	I	II	I	MAld
94	Carvone [a]	1249/1246	II	-	II	MK
95	Linalyl acetate [a]	1250/1250	III	II	-	ME
96	Geraniol [c]	1256/1255	II	II	II	MA
97	Piperitone [b]	1260/1267	II	II	-	MK
98	Geranial [c]	1272/1268	I	II	II	MAld
99	Perilla aldehyde [c]	1282/1278	I	II	II	MAld
100	Dihydro-linalool acetate [a, d]	1286/1275	-	II	-	ME
101	Dec-2-en-1-ol [a, d]	1284/1270	III	-	-	AliA
102	iso-Isopulegyl acetate [a]	1289/1286	II	II	-	ME
103	Thujyl acetate [a]	1289/1298	-	II	II	ME
104	cis-Verbenyl acetate [a]	1290/1278	III	II	-	ME
105	trans-Pinocarvyl acetate [a]	1298/1296	II	II	-	ME
106	Geranyl formate [d, e]	1298/1300	II	-	-	ME
107	Undecanal [c]	1307/1309	II	II	II	AliAld
108	Isoascaridole [a]	1309/1306	II	II	II	MO
109	Deca-(*2E*,*4E*)-dienal [a]	1321/1322	III	II	-	AliAld
110	Methyl geranate [a]	1322/1326	II	II	-	ME
111	Myrtenyl acetate [a]	1326/1326	II	II	-	ME
112	Citronellyl acetate [c]	1349/1350	II	II	-	ME
113	neo-iso-Carvomenthyl acetate [a, d]	1349/1350	-	-	II	ME
114	Neryl acetate [c]	1359/1361	II	II	II	ME
115	trans-Myrtanol acetate [a, d]	1372/1387	II	-	-	ME
116	Geranyl acetate [c]	1378/1380	I	II	II	ME
117	(*Z*)-Trimenal [a, d]	1435/1424	-	III	-	AliAld
118	Dodecanal [c]	1411/1410	II	II	II	AliAld
119	trans-Nerone [a, d]	1435/1440	III	-	-	MK
120	(*E*)-Trimenal [a, d]	1435/1424	-	III	-	AliAld
121	Geranyl isobutyrate [a]	1506/1507	III	III	-	ME
122	Tridecanal	1512/1516	II [b]	II [a]	II [c]	AliAld
123	(*Z*)-Nerolidol [a]	1544/1531	-	III	-	SA
124	(*E*)-Nerolidol	1551/1561	III [e]	II [e]	III [a]	SA

Table 4.2.
Cont.

Peak	Hydrocarbon	Exp./Data LRI	Identification Level			
			Key A	Key B	Persian	Class
125	Hedycaryol [a]	1554/1544	II	II	-	SA
126	Longipinanol [a]	1558/1572	III	III	-	SA
127	trans-Sesquisabinene hydrate [a]	1584/1576	II	II	-	SA
128	Caryophyllene oxide [c]	1592/1587	III	II	-	SO
129	Dodecyl acetate	1607/1610	II [e]	II [c]	II [a]	AliE
130	Tetradecanal [c]	1614/1614	II	II	II	AliAld
131	Humulene epoxide II [a, d]	1619/1613	III	-	-	SO
132	(*Z*)-Sesquilavandulol [a]	1623/1610	III	III	III	SA
133	(*E*)-Sesquilavandulol [a]	1639/1633	II	II	II	SA
134	trans-Tetradec-2-enal [a, d]	1668/1673	-	-	III	AliAld
135	(*Z*)-Nerolidyl acetate [a, d]	1664/1665	II	-	-	SE
136	epi-α-Bisabolol [a, d]	1664/1679	-	III	-	SA
137	Isobornyl isobutanoate-8-hydroxy [a]	1668/1676	II	II	-	ME
138	neo-Intermedeol [a]	1668/1661	II	II	-	SA
139	β-Bisabolol [a]	1677/1677	II	II	II	SA
140	(*Z*)-Apritone [a]	1688/1687	I	II	II	SK
141	α-Bisabolol [c]	1693/1688	II	I	II	SA
142	(*E*)-Apritone [a]	1713/1710	II	II	-	SK
143	(*2E,6Z*) - Farnesal [a, d]	1713/1714	-	-	II	SAld
144	Tridec-2-en-1-ol acetate [a]	1715/1705	III	III	III	AliE
145	Hernianin [a, d]	1735/1720	-	III	-	Other
146	(*E, E*) -Farnesal [a]	1739/1737	II	II	II	SAld
147	Hexadec-(*11Z*)-enal [a]	1817/1808	II	II	II	AliAld
148	Farnesyl acetate [a, d]	1832/1832	-	III	-	SE
149	Hexadec-(*11E*)-en-1-ol [a, d]	1879/1869	-	III	-	AliA
150	Cyclohexadecanolide [a]	1920/1935	III	III	III	AliE
151	Citropten [a]	1991/1982	II	II	II	Other
152	Octadec-(*13Z*)-enal [a]	1998/2010	III	III	III	AliAld
153	Isopimpinellin [a, d]	2239/2239	-	-	II	Other

Abbreviations: Ali, aliphatic; K, ketone; Ald, aldehyde; E, ester; O, oxide; A, alcohol. [a] Compound, to the best of the authors' knowledge, identified for the first time in an industrially cold-extracted lime oil.[b] Compound not yet identified in cold-extracted laboratory oils [2]. [c] Compound identified previously in industrially cold-extracted lime oils and cold-extracted laboratory oils, reported since 1980 [2]. [d] Compound identified in only one of the samples. [e] Compound identified previously only in cold-extracted laboratory oils [2].

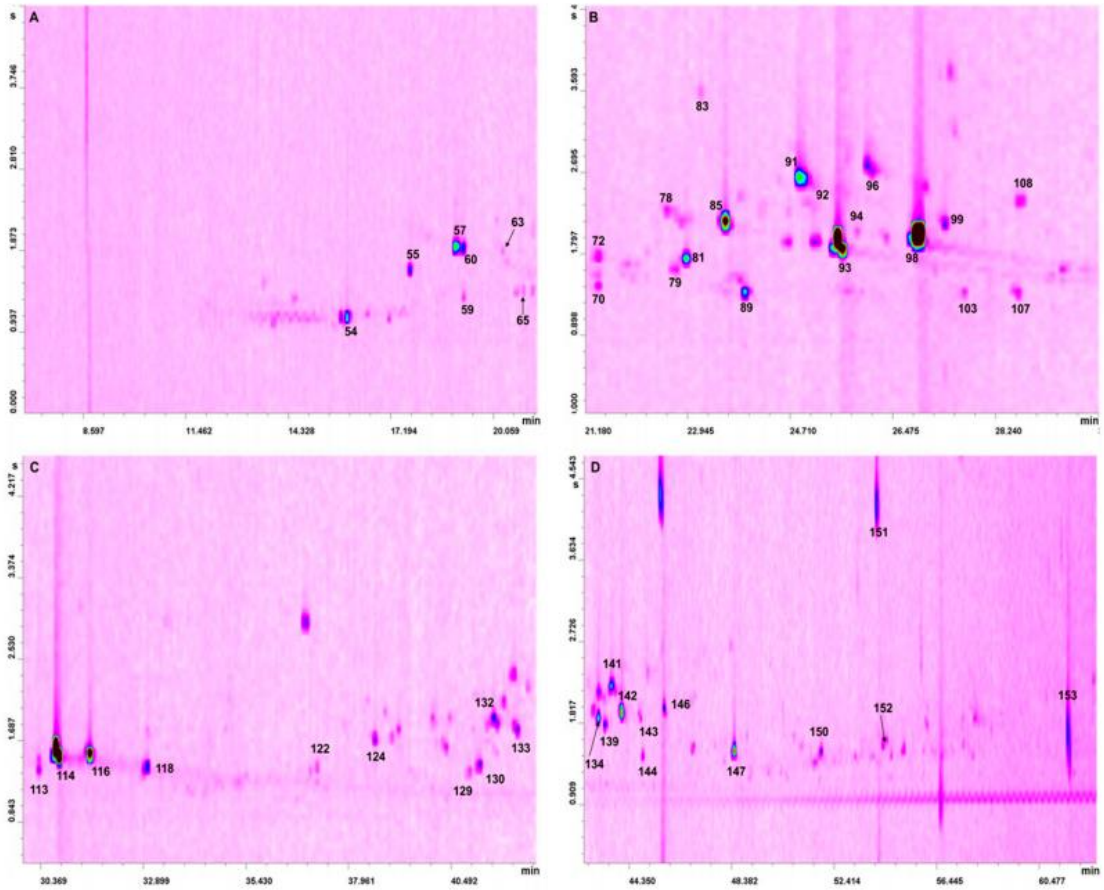

Figure 4.1. *Four GC × GC-QMS chromatogram expansions (A-D) relative to the analysis of the oxygenated fraction of Persian lime oil (refer to Table 4.2 for peak identification).*

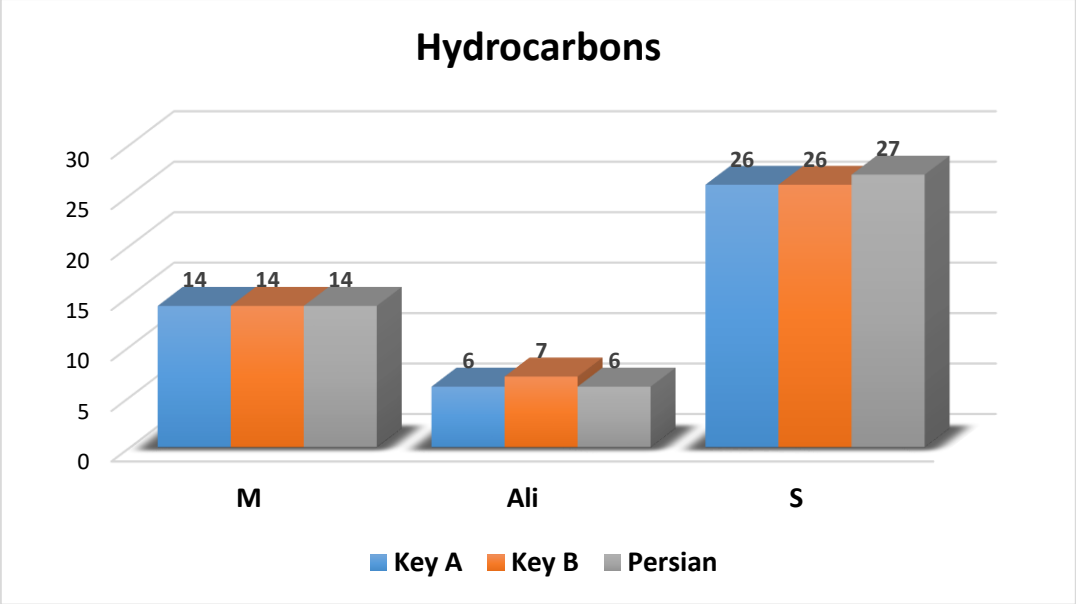

Figure 4.2. *Graph illustrating the number and chemical class of the hydrocarbons identified in the three lime oil samples.*

As can be observed, also in *Table 4.1*, the hydrocarbon profiles in the three types of lime oils were very similar. Considering the Key A oil, a number of compounds corresponding to 36, 9, and 1 were identified at levels I, II, and III, respectively; with regard to the Key B oil, a number of compounds corresponding to 32, 14, and 1 were identified at levels I, II, and III, respectively; finally, in the Persian oil, 38 and 9 compounds were identified at levels I and II, respectively. It is noteworthy that the LRI values were calculated by considering the total retention time (sum of the first and second dimension retention times) of the most intense modulated peak of both the alkanes and the lime oil hydrocarbons. Furthermore, the MS database LRI values were derived from analyses performed on the same (low polarity) column, as that used in the first analytical dimension. The retention of both the alkanes and the lime oil hydrocarbons, on the short medium-polarity (100% polyethylene glycol) second dimension, was negligible; for such a reason, there was a general good agreement between experimental and database LRI values. Six hydrocarbons (all aliphatic) reported in *Table 4.1*, to the best of the present authors' knowledge, have not been previously reported in the literature (an in-depth investigation was carried out) in a cold-extracted lime oil. Furthermore, γ-elemene (a sesquiterpene) was found for the first time in Persian oil, even though it has been reported in Key A and B oils [2, 10]. Five hydrocarbons were found in both types of Key oils (undecane, tetradecane, pentadecane, hexadecane, heptadecane), while six (tetradec-1-ene, tetradecane, γ-elemene, pentadecane, hexadecane, heptadecane) were present in the Persian oil. The chemical class distribution

of the 103 oxygenated compounds identified in the lime oils is illustrated in the graph shown in *Figure 4.3.*

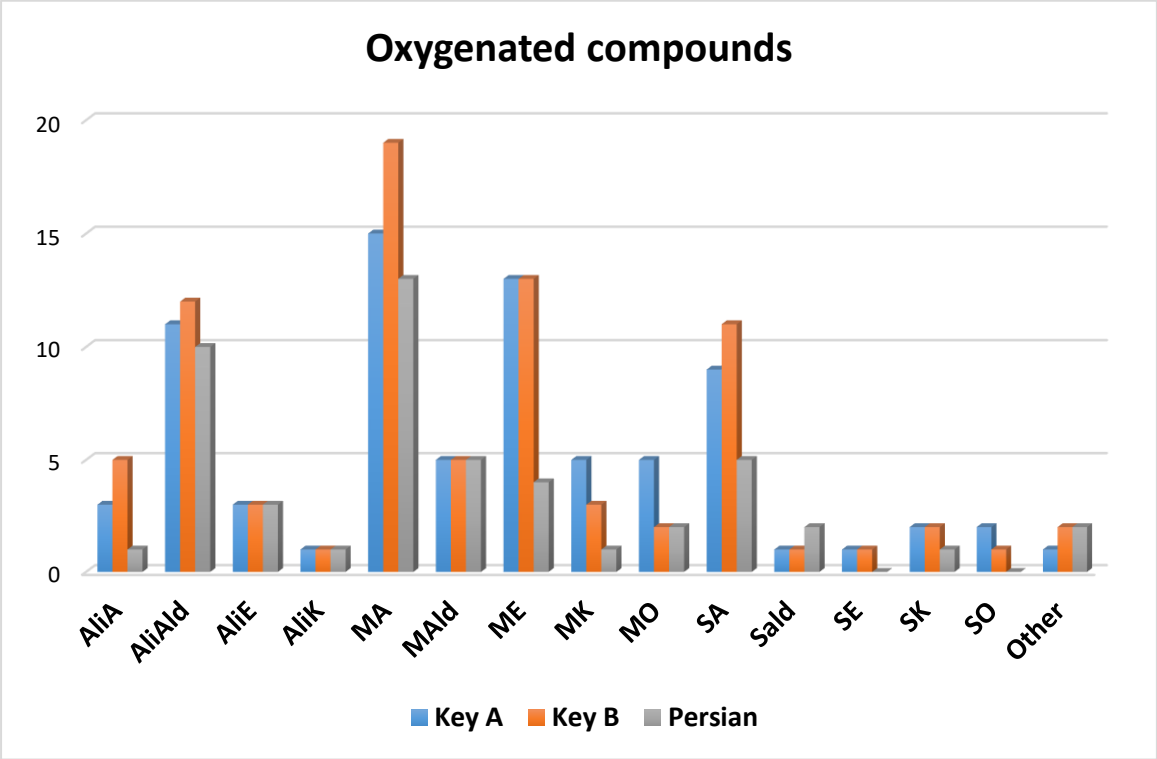

Figure 4.3. *Graph illustrating the number and chemical class of the oxygenated compounds identified in the three lime oil samples.*

The number of identified compounds was higher in the Key oils compared to the Persian one. Considering the Key A oil, a number of compounds corresponding to 46, 54, and 23 were identified at levels I, II, and III, respectively; with regard to the Key B oil, a number of compounds corresponding to 36, 73, and 20 were identified at levels I, II, and III, respectively; finally, in the Persian oil, 41, 46, and 8 compounds were identified at levels I, II, and III, respectively. Compared to the hydrocarbons, and in percentage terms, many more compounds were identified at levels II and III. Such an occurrence was, in part, due to the strong interaction of specific oxygenated compounds (*e.g.*, alcohols) on the second dimension column, causing an increased divergence between the experimental and database LRIs. After an in-depth investigation in the literature, no information was found on 65 compounds present in *Table 4.2* and related to cold-pressed lime oil. Additionally, no previous description was found for the presence of tridecanal in Key B oil, even though it was identified in all the three oils [2]. Finally, (E)-nerolidol (a sesquiterpene alcohol) and dodecyl acetate were found in all the three oils, even though they have not been previously

related to Persian lime oil [2]. To conclude, the applied LC//GC × GC-QMS method has enabled the in-depth elucidation of the chemical profile of three types of cold-pressed lime essential oils. The proposed method allows the formation of highly informative and ordered elution patterns that can be exploited for the creation of a fingerprint database as a support for quality assurance. To the best of the authors' knowledge, many volatiles are here related to such samples for the first time. It cannot obviously be excluded that, in cases, peak identification may not be correct (especially for level III identifications), and that compounds present in the literature related to cold-pressed lime oil have been missed. Even so, the 4D method herein proposed is a powerful analytical not only for citrus (and non-citrus) essential oil analysis, but also in other areas of food research. For example, the 4D technology has been used for the determination of mineral oil contamination in baby foods [13].

4.2 Chemical characterization of lipid profile in unconventional palm-oils using CM-GC×GC-QMS†

The present work is focused on the characterization of lipid profiles in three endemic species of *Arecaceae* from Reunion Island: *Hyophorbe indica*, *Dictyosperma album* and *Latania lontaroides* for the first time. Specifically, the analysis of the fatty acid profiles of the seed oils were performed by using a cryogen-modulated comprehensive two-dimensional gas chromatography system coupled with a single quadrupole mass spectrometer (CM-GC×GC-QMS). The carotenoids determination was carried out by high performance liquid chromatography-photo diode array detector-mass spectra (HPLC-PDA-MS).

The plant kingdom contains various bioactive hydrocarbon compounds such as lipids with an incredible variety of structures and functions. In this respect, vegetable seeds are original and abundant sources of valuable lipids (fatty acids, carotenoids, etc.). Polyunsaturated fatty acids (PUFAs) are found mostly in plant seed oils and are important substrates for the biosynthesis of cellular hormone-like compounds (eicosanoids) at least.

† This section has been adapted from the following publication: Y. Caro, T. Petit, I. Grondin, P. Clerc, H.Thomas, D. Giuffrida, **B. Giocastro**, P. Q. Tranchida, I. Aloisi, D. Murador, L. Mondello &L.Dufossé in "*Chemical characterization of unconventional palm oils from Hyophorbe indica and two other endemic Arecaceae species from Reunion Island*."*Natural Product Research, 2020, 34, 93-101*.

A large number of studies have shown positive health benefits associated with consumption of Omega-3 (ω3) PUFAs on infant development, coronary artery and cardiovascular diseases [14, 15], arthritis [16], inflammatory and autoimmune disorders [17], and cancer [18, 19].

Some particular seed oils are also rich in unsaponifiable derived lipids with varying biological properties, such as the carotenoids. Carotenoids are fat-soluble pigments found in seed oils. They are isoprenoidic type of compound usually consisting of a forty carbon atoms skeleton [20]. Carotenoids that contain oxygen in their structure are known as xanthophylls, whereas those that lack oxygen are called carotenes. Some carotenes, such as α- and β-carotene, are converted by the body into retinol, or vitamin A1. Some carotenoids can act as antioxidants by scavenging oxygen and peroxyl radicals. Recently, their importance has grown due to the beneficial health properties that have been ascribed to them [21, 22].

Five vegetable oils dominate the world market, e.g. palm, soybean, canola, sunflower seed, and palm kernel oil. Edible palm oil is derived from the fruit of the oil palm tree, primarily the African palm *Elaeis guineensis*. In its natural, unprocessed state, crude palm oil is dark red in color due to a high content of carotenoids, including β-carotene and lycopene [23]. Recent literature has emphasized the necessity of investigating unconventional, or underutilized minor plant oils, like those from rice bran [24], Allanblackia [25, 26], pequi [27], and pistachio oil [28] to meet the increasing global demand for edible oils and biodiesel [23]. Furthermore, consumers are looking for novel vegetable oils that have unique health-promoting properties. Unconventional oils are often harvested from wild plants, and each unconventional oil has its own challenges that must be overcome to enable large-scale production: low seed yield or oil content, strong flavor of the oil, presence of minor toxic compounds, etc. [23].

Reunion Island in the western Indian Ocean arose two million years ago from a volcanic hot spot and its diversity of habitats and microclimates have encouraged the diversification of a highly endemic flora. Given that the presence of bioactive polyunsaturated fatty acids and valuable carotenoids in plant seeds could offer new additional values to a prospective crop, we investigated the chemical characteristics (e.g. fatty acid and carotenoid contents) of novel seed oils, yet not investigated, from ripe fruit of three endemic plant species of Reunion Island belonging to the *Arecaceae* family. *Arecaceae* are part of a botanical family of perennial plants. These are climbing plants, shrubs, trees and stemless plants, all

commonly known as ‘palms’ such as the well-known African species *Elaeis guineensis* (Jacq.) producing the edible palm oil. To date, over 181 genera including around 2600 species are listed, most of them restricted to tropical and subtropical climates. In Reunion island, 55 species of *Arecaceae* were identified and some of them are endemic, including the following three species: *Hyophorbe indica Gaertn* (local name: ‘palmiste poison’), *Dictyosperma album* (Bory) Scheff. (local name ‘palmiste blanc’), and *Latania lontaroides* (Gaertn.) H.E. Moore (local name: ‘latanier rouge’) (*Figure 4.4*). As far as we know, the chemical characterization of the seed oil (i.e. the oil content, fatty acid composition, carotenoid content…) extracted from these three endemic palms which grow inside the forest or along the coasts of the Reunion Island have not been previously investigated.

Figure 4.4 *Photograph of the plant, ripe fruit, seeds and extracted seed oil of the three endemic Arecaceae species of Reunion island: a) Hyophorbe indica Gaertn.; b) Dictyosperma album (Bory) Scheff.; c) Latania lontaroides (Gaertn.) H.E. Moore.*

4.2.1 Experimental

- **Samples collection**

The ripe fruits from the three endemic plant species were wild-collected from January 2015 to 215 December 2017 in the forest area of the Reunion Island. The endemic species were authenticated by the botanist Hermann Thomas of the National Park of La Réunion.

- **Oil extraction from seeds**

The ripe fruits were cleaned and oven-dried at 60°C during 24 to 48 hours. The shell was

cracked to remove the seeds (kernels) and dried at 60°C for 2 hours. The seeds were first milled in a laboratory grinder for 30 seconds in order to obtain a fine powder. Oil extraction was then carried out using cyclohexane (99.8% purity, Carlo Erba) from 50-60g of dried seed powder by pressurized liquid extraction with a Dionex ASE^{TM}300 apparatus (Dionex, USA). The following experimental conditions were applied for ASE extraction: temperature 90°C, cells were preheated 6 min, 17 min static time, 5 min dynamic time. The cycle was repeated 5 times. This program ensures complete extraction of the neutral lipids from the sample at 90°C under 100 bars. A flush volume of 100% of the cell was used and finally the cell was purged for 120 sec with nitrogen to collect the extract in the collection vial. The solvent was finally driven off at 40 °C using a rotary evaporator (RC 600, KNF Neuberger, France) to obtain the extracted lipids. All quantitative determinations were performed in triplicate.

4.2.1.1 Fatty acids (FAs) analysis

Derivatization of fatty acid methyl esters (FAMEs) was performed as follows: 100 μL of a solution of KOH/MeOH 2N was added to 10 mg of oil sample, dissolved in 1 mL of *n*-hexane 235 and was left to react for 5 min at room temperature. The reaction mixture was shaked for 2 min using a vortex mixing. The upper hexanic phase, containing FAMEs, was subjected to CM GC×GC-QMS analysis.

CM GC×GC-QM. All applications were carried out using a system consisting in two independent Shimadzu GC-2010 gas chromatographs, and a QP2020 quadrupole mass spectrometer (Kyoto, Japan). The first gas chromatograph (GC1) was equipped with an AOC-20i auto-injector, and a split-splitless injector (310°C). The first column was an SLB-5ms [(silphenylene polymer, which can be considered equivalent in polarity to poly (5%diphenyl/95% dimethylsiloxane)] with dimensions 30 m × 0.25 mm ID × 0.25 μm d_f. The second column was an SLB-35ms [(polymer which can be considered equivalent in polarity to poly (35%diphenyl/65% dimethylsiloxane)] with dimensions 3 m × 0.25 mm ID × 0.25 μm d_f. A 1.5 m segment of the column was used to create the modulator loop, leaving a 1.5 m segment for the analytical separation. All the columns used were kindly provided by Merck Life Science (Merck KGaA, Darmstadt, Germany). The connections between first and second columns, were made by using two SilTite mini unions (Trajan, Ringwood, Victoria, Australia). Helium was supplied at the GC1 inlet at a pressure of 60.3 kPa; volume

and mode of injection: 1 µL in the split mode (30:1). GC1 and GC2 temperature program were set as 110- 320°C and 3°C/min. Modulation was performed by using a cryogenic fluid-free modulator (under license from Zoex Corporation); modulation period was 2.5 sec (the heating step was performed at 340°C, for 0.5 s). For quadrupole MS analysis, the sample was analyzed in the full scan mode with a scan speed of 20,000 amu/sec, a mass range of 45-500 m/z and a sampling frequency of 33 spectra/sec. The temperature of the interface was set at 310°C and the ion source temperature was set at 200°C, with analyte fragmentation induced by electron ionization (70 eV). Data were acquired by using the GC-MS solution software (Shimadzu). The MS database used was the Lipids GC-MS library v.1.0 (Shimadzu). Bidimensional chromatograms were generated using the ChromSquare software v. 2.3 (Shimadzu).

1D GC-FID. Quantitative analysis of FAMEs, according to the standard NF T60-233 and ISO standard 12966-4, was performed by gas chromatography-flame ionization detection (1D GC-FID) using a model Clarus 580 GC (Perkin Elmer), after methylation of the FAs: the derivatized fatty acid methyl esters (FAMEs) were prepared from 350 mg of oil sample with 28 mg of C17 internal standard (e.g., 0.08 mg of internal standard per mg of oil), and then extracted by 4 mL of n-heptane (99%, Carlo Erba). The upper heptanic phase, containing FAMEs, was subjected to 1D GC-FID internal calibration analysis. The sample (injection: 1 µL; split ratio: 100:1) was injected on a capillary column TR-FAME^{TM} (grafted cyanopropylphenyl-based phase of 30 m and diameter of 0.25 mm). The stationary phase had a film thickness of 0.25 µm. Helium was used as carrier gas with a flow rate of 1 mL/min. The injector and FID detector temperature were set at 250 °C. The column was preheated at 120 °C for 5 min and a temperature profile (3 °C/min) was applied until 200 °C and finally kept for 6 min at 200 °C. All quantitative determinations were performed in triplicate.

4.2.1.2 Carotenoids analysis

Carotenoids analyses were performed on the unsaponifiable fractions of the oils. Firstly, the unsaponifiable fraction was extracted from oils using diethyl ether after saponification of the oil by using KOH/EtOH 1M under reflux according to ISO standard 3596-1. The organic phase was dried over anhydrous sodium sulfate, filtered and the solvent was removed on a rotary evaporator at 40 °C to obtain the unsaponifiable fraction of the oil. All quantitative determinations were achieved in triplicate.

HPLC-PDA-MS: the oil samples were fully diluted in 1 mL of a MeOH/MTBE (1:1) mixture, and then, if necessary, they were further diluted with the same solvent mixture; then filtered in a nylon 0.2 µm filter before injection into the HPLC-PDA-MS system. The carotenoids analyses were carried out using a Nexera X2 liquid chromatography system (Shimadzu, Milan, Italy), consisting of a CBM-20A controller, four HPLC-30AD dual-plunger parallel-flow pumps, a DGU-20 A5R degasser, a CTO-20AC column oven and a SIL-30AC autosampler. 0.1 mm I.D. stainless steel tubing (zero dead volume) was employed for column connection and a SPD291 M30A photo diode array detector (PDA). The HPLC system was coupled to an LC-qMS-2020 mass spectrometer through an APCI source (Shimadzu, Kyoto, Japan). Data acquisition was performed by means of the LabSolutions software (Version 5.91, Shimadzu Corporation). Separations were carried out on a YMC C30 column (250 mm × 4.6 mm i.d., 5 µm particle size). The mobile phases were A (MeOH/MTBE/H_2O, 81:15:4) and phase B (MeOH/MTBE/ H_2O, 16:80.4:3.6); a linear gradient was used changing from 99 to 66% A in 30 min, maintaining this condition for 5 min, changing from 66 to 44% A in 15 min, keeping this condition for 5 min, changing from 44 to 22% A in 15 min and from 22 to 0% A in 5 min, returning to the initial conditions (99% A) in 5 min, and keeping this condition for 5 min. The flow rate was set at 0.8 mL/min, the column temperature was maintained at 35°C, the UV/vis spectra were acquired between 220 and 700 nm and the chromatograms were processed at 450 nm. The LC-qMS-2020 detection was achieved through an APCI interface operated in positive and negative mode; detector voltage, 1.05 kV; interface temperature: 350°C; DL temperature, 300 °C; heat block temperature, 300°C; nebulizing gas flow (N_2), 2.0 L/min; drying gas flow (N2), 5.0 L/min; full scan range (positive and negative mode), 300-1200 m/z; event time, 0.2 s. The different carotenoids were characterized using their UV-vis and mass spectra, their available standards and their elution order. Quantitative data were obtained by HPLC-DAD using external calibration curves from carotenoids standards, in the concentration range from 1 to 100 µg/mL at five concentrations levels. The results were obtained from the average of three determinations and the CV% was below 7% in all the LC measurements. Standard purity was above 98% and the R coefficient for the calibration curves was always above 0.9992, with LOD and LOQ values of respectively for β-carotene 0.07 and 0.1, for lutein of 0.06 and 0.18, for lycopene of 0.08 and 0.3, µg/mL. The carotenoid concentrations are expressed in ppm (mg/kg $^{-1}$ of oil).

4.2.2 Results and Discussion

The chemical characteristics of the seed oils extracted using a pressurized liquid extraction process with cyclohexane are presented in *Table 4.3.* The kernels of *Dictyosperma album* (Bory) Scheff. showed the highest oil content (8.8 %) whereas *Hyophorbe indica* Gaertn. seeds had the lowest oil content (3.1 %) among the studied *Arecaceae* species despite it exhibited the highest content of unsaponifiable fraction (13.41 g/100 g oil). The content of unsaponifiable lipids from commercial vegetable oils generally reaches 0.2 to 2.0 g/100g oil.

Table 4.3. *Compositional characteristics of the oils extracted from the three endemic Arecaceae species from Reunion Island.*

Plant species	Seed oil content (g/100g seed DM)[a]	Color of the extracted oil	Unsaponifiable content in oil (g/100g oil DM)[a]
Hyophorbe indica Gaertn.	*3.09 ± 0.19*	*dark orange-red*	*13.41 ± 1.50*
Dictyosperma album (Bory) Scheff.	*8.81 ± 0.08*	*dark green*	*2.76 ± 0.22*
Latania lontaroides (Gaertn.) H.E. Moore	*8.68 ± 0.29*	*pale green*	*0.74 ± 0.31*

[a]*Mean value and standard deviation of triplicate samples. DM: Dry material.*

For example, the study conducted on oil extracted from Phoenix canariensis date seeds (Arecaceae) indicated that the unsaponifiable matter content was 1.8 g/100g of seed oil [29].The level of unsaponifiable fraction of the seed of *H. indica* Gaertn was thus considered as very exceptional; in fact, a value around 13.4 (g/100g oil) is higher than the unsaponifiable fraction content of the avocado oil and shea butter (from 10 to 12 g/100g oil) which are commonly used in cosmetics for their moisturizing and softening properties (hair, scalp, skin, face, etc.). Interestingly, oil from *H. indica* Gaertn. also presented a dark orange-red color indicating the presence of different pigments (carotenoids).

- **Fatty acids profile**

The analysis of the fatty acid profile of the three investigated seed oils was performed using cryogenic-modulation comprehensive two-dimensional gas chromatography-quadrupole mass spectrometry (CM GC×GC-QMS). One of the major beneficial characteristics of CM GC×GC-QMS was the high sensitivity making this technique particularly suitable for trace-level fatty acids detection in oil from fruits [30] or seeds.

The bidimensional plot of the fatty acids detected in the endemic *H. indica* seed oil is shown in *Figure 4.5.* Results indicated that twenty-five fatty acid methyl esters (FAMEs) were identified in the *H. indica* seed oil, attained through CM GC×GC-QMS (instead of 13 by 1D GC-FID; data not shown).

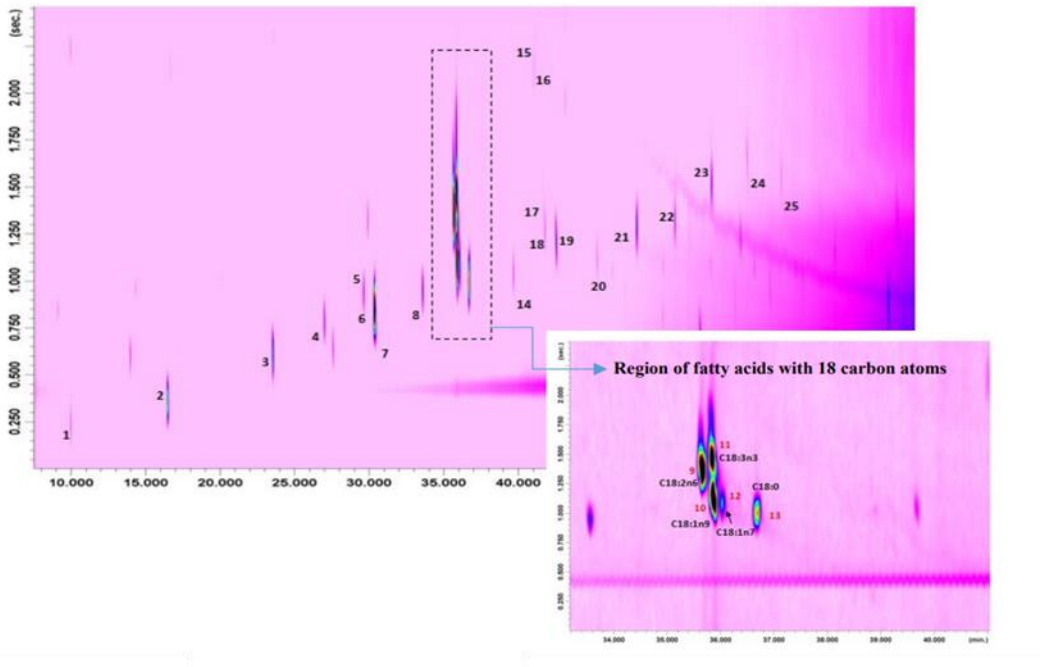

Figure 4.5. *Bidimensional plot of the fatty acids detected in the endemic Hyophorbe indica Gaertn. seed oil and peak identification.*

The fatty acid compositions of *H. indica* seed oil and the two other unconventional palm oils, obtained by relative quantification from CM GC×GC-QMS peak areas, are shown in *Table 4.4.* To the best of the authors knowledge, this is the first report on the seed oil composition of these three endemic *Arecaceae* species from Reunion island. Interestingly, *H. indica* seed oil contained approximately 50% polyunsaturated fatty acids (PUFAs), 23% monounsaturated fatty acids (MUFAs), and only 27% saturated fatty acids (SFAs). Results indicated that fatty acids with 18 carbon atoms were predominant.

H. indica seed oil contained mainly linoleic acid (C18:2 ω6; 33.7%), oleic acid (C18:1 ω9; 20.3%), *alpha*-linolenic acid (C18:3 ω3; 16.5 %), palmitic acid (C16:0; 15.8%) and stearic acid (C18:0; 122 4.5%). These findings are quite unusual and possibly a unique fatty acids composition in species belonging to the *Arecaceae* family. In fact, previous studies conducted on seed oil extracted from different palm species, including the African oil palm (*Elaeis guineensis*), indicated that palm oils are often rich in palmitic acid (43.5%) and

oleic acid (36.6 %), and contain some traces of omega-3 PUFAs (<0.5% to total fatty acids) [31]. Another study conducted on oil extracted from *Phoenix canariensis* date seeds, belonging to Arecaceae family as well, indicated that the main fatty acids of oil were oleic (50.1%), linoleic (19.2%), lauric (10.2%), palmitic (9.8%) and stearic (7.5%) acids [29].

Table 4.4. *Fatty acids identification and composition (%) of three seed oils obtained from endemic Arecaceae species from Reunion Island*

Peak number (Fig.S2)	Fatty acid methyl ester (FAMEs) identification	*H. indica*	*D. album*	*L. lontaroides*
		(%)	*(%)*	*(%)*
n.i	C6:0, Caproate	*n.d*	*n.d*	*n.d*
n.i	C8:0, Caprylate	*n.d*	*n.d*	*1.77*
1	C10:0, Caprate	*0.14*	*0.93*	*1.05*
2	C12:0, Laurate	*1.89*	*20.93*	*34.14*
3	C14:0, Myristate	*1.18*	*16.14*	*22.96*
4	C15:0, Pentadecanoate	*0.39*	*0.08*	*n.d*
7	C16:0; Palmitate	*15.80*	*13.62*	*9.90*
8	C17:0: Heptadecanoate	*0.51*	*0.10*	*0.04*
13	C18:0; Stearate	*4.49*	*5.4*	*4.20*
14	C19:0; Nonadecanoate	*0.17*	*n.d*	*n.d*
19	C20:0; Arachidate	*0.61*	*0.21*	*0.09*
20	C21:0; Heneicosanoate	*0.10*	*n.d*	*n.d*
21	C22:0; Behenate	*0.74*	*0.10*	*0.03*
22	C23:0; Tricosanoate	*0.26*	*0.007*	*n.d*
23	C24:0; Lignocerate	*0.52*	*0.35*	*0.09*
24	C25:0; Pentacosanoate	*0.08*	*n.d*	*n.d*
25	C26:0; Cerotate	*0.04*	*0.18*	*n.d*
	∑ SFAs	**26.9 %**	**58.0 %**	**74.3 %**
	- MUFA Omega-9:			
5	C16:1ω9; cis-7 hexadecenoate	*0.07*	*0.06*	*n.d*
10	C18:1ω9; Oleate	*20.29*	*22.49*	*21.01*
17	C20:1ω9; Gondoate	*0.08*	*0.32*	*0.09*
	- MUFA Omega-7:			
12	C18:1ω7; cis-Vaccenate	*1.78*	*0.38*	*0.04*
18	C20:1ω7; Paulinate	*0.05*	*0.24*	*0.10*
	- MUFA Omega-5 & Omega-11			
6	C16:1ω5; 11(Z)-hexadecenoate	*0.43*	*0.38*	*n.d*
	∑ MUFAs	**22.7 %**	**23.9 %**	**21.2 %**
	- PUFA Omega-6:			
9	C18:2ω6; Linoleate	*33.70*	*16.91*	*4.46*
16	C20:2ω6; Eicosa-(11Z,14Z)-dienoate	*0.11*	*0.05*	*n.d*
	- PUFA Omega-3:			
11	C18:3ω3; alpha-Linolenate	*16.46*	*1.13*	*0.03*
	- Other PUFA :			
15	C20:2ω4; Eicosa (13,16)-dienoate	*0.12*	*n.d*	*n.d*
	∑ PUFAs	**50.4 %**	**18.1 %**	**4.5 %**
	ω6/ω3-PUFA ratio	**2 : 1**	**15 : 1**	**n.d**
	Edible oil equivalent	Oil rich in ω3	Oil rich in SFA	Oil rich in SFA

n.i.: not identified; n.d: not quantified/not detected; Peak numbers only refer to the identifications reported in Figure 4.4. relative to the bidimensional plot of H. indica seed oil. SFAs: saturated fatty acids. MUFAs: monounsaturated fatty acids. PUFAs: polyunsaturated fatty acids (unsaturation ≥2). ω6/ω3-PUFA ratio: ratio between omega-6 and omega-3 PUFA fatty acids.

Furthermore, the *H. indica* seed oil investigated here presented an optimal ω6/ω3-PUFAs ratio close to 2:1. Ideally, a fatty acid profile rich in PUFAs with a ω6/ω3-PUFAs ratio lower than 4:1 in diet is recommended to reduce the risk of chronic diseases [32]. By comparison, edible palm oil showed an ω6/ω3-PUFAs ratio of about 47:1 because the palm

oil contained only 10% ω 6-PUFAs and <0.5% ω 3-PUFAs (and approximatively 50% SFAs and 40% MUFAs) [31]. Some trace-level long-chain MUFAs and PUFAs fatty acids (*e.g.,* the (E)-vaccenic acid (C18:1ω7; 1.8%), the eicos-(11Z)-enoic acid or gondoic acid (C20:1ω9; 0.08%), the eicos (13)-enoic acid or paulinic acid (C20:1 7; 0.05%), the eicosa-(11,14) dienoic acid (C20:2ω6; 0.11%), and the eicosa-(13,16)-dienoic acid (C20:2ω4; 0.12%) were also identified by CM GC×GC-QMS in H. indica seed oil, with others long-chain SFAs like arachidic acid (C20:0;141 0.61%), behenic acid (C22:0; 0.74%), and lignoceric acid (C24:0; 0.52%). Some of these long-chain fatty acids, in particular, gondoic acid, paulinic acid and the eicosa-(13,16)-dienoic acid, can rarely be found in seed oils. The high content of ω6-PUFAs (linoleic acid; 34%), ω3-PUFAs (alpha-linolenic acid; 17%) and MUFAs (oleic acid; 20%), made the *H. indica* oil attractive for its potential use in healthy formulations, paint and coatings, or oleochemical applications. However, from a nutraceutical point of view, research on the chemical composition of the H. indica seed oil was very limited, if any at all, and it could be considered to be reasonably foreseeable that this unconventional palm oil might be toxic by ingestion (the toxicological profile of this oil was not known). For example, some ornamental palms, for instance sago and betel nut palms, both belonging to Arecaceae family as well, were poisoning, due to the presence of cycasin and arecoline [33, 34]. So, clinical trials are needed before the H. indica seed oil can be recommended to treat any health conditions. The seed oil extracted from *Dictyosperma album* (Bory) Scheff. (8.8% dry weight of oil) had a similar fatty acid composition to edible palm oil. In fact, *D. album* seed oil contained approximately 58% saturated fatty acids, 24% monounsaturated fatty acids, and 18% polyunsaturated fatty acids. The seed oil contained mainly lauric acid (C12:0; 158 20.9%), myristic acid (C14:0; 16.1%), palmitic acid (C16:0; 13.6%), oleic acid (C18:1ω9; 22.5%), and linoleic acid (C18:2 ω6; 16.9%). The *Latania lontaroides* (Gaertn.) H.E. Moore seed oil (8.7% dry weight of oil) showed even higher SFA content (74% w/w of total fatty acids) (*Table 4.4*), and its fatty acid composition was approaching the one of the palm kernel oil. These findings suggested that unconventional seed oils of *D. album* and *L. lontaroides* can be useful for oleochemical applications at least, like the palm oil already used in Europe for these purposes.

- **Seed carotenoids composition**

  The HPLC carotenoids profiles of the three investigated seed oils are shown in *Figure 4.6*, and their relative carotenoids composition (%) in oil are shown in *Table 4.5*.

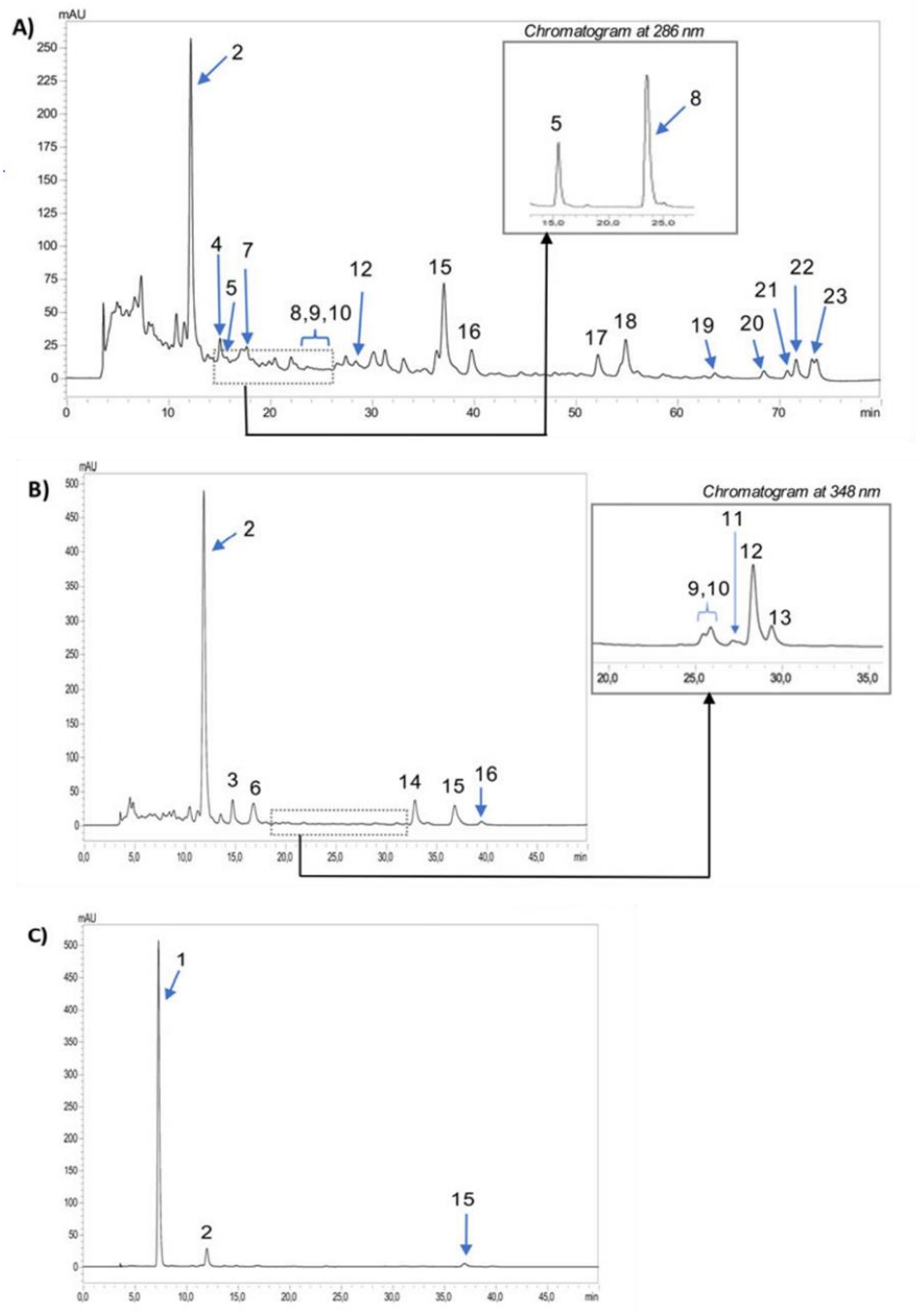

Figure 4.6. *HPLC-PDA chromatograms (extracted at · 450 nm) of the carotenoids in the three seed oils obtained from endemic Arecaceae species from Reunion Island: Hyophorbe indica Gaertn. (A), Dictyosperma album (Bory) Scheff. (B),and Latania lontaroides (Gaertn.) H.E. Moore (C).*

Lutein was by far the most abundant carotenoid in the seed oils of *H. indica* (A) and *D. album* (B), respectively 41% and 70% to total carotenoids, followed in both oils by also a good percentage of β-carotene (21% and 7%, respectively, in *H. indica* and *D. album* seed oil); this is in agreement with the generally reported higher content of lutein compared to the other carotenoids in oilseeds of many plants that often store carotenoids in specialized plastids [35]. Lutein was considered extremely important in the prevention of macular diseases and cognitive function [36, 37], while β-carotene was being the most important provitamin A carotenoid. The seed oil of *L. lontaroides* also showed the presence of lutein and β-carotene, but its main carotenoid (88%) was a very early eluting compound which has not yet been identified. The author hypothesis is that it might be an apocarotenoid. Further work is in progress aimed at its structure elucidation.

Table 4.5. *Carotenoids content and relative carotenoids composition (%) of the three seed oils obtained from endemic Arecaceae species from Reunion Island.*

				H. indica		*D. album*		*L. lontaroides*	
Unsaponifiable content in oil (g/100g)				13.41 ± 1.50		2.76 ± 0.22		0.74 ± 0.31	
Oil color:				orange-red		dark-green		pale-green	
Peak number	**t_R (min)**	**Carotenoids**	**[M]$^{\cdot-}$ (m/z)**	**Quantification in mg kg^{-1} oil** (rel.% in brackets)					
1	7.3	n.i. (unknown compound)	411	n.d.	–	n.d.	–	5.1	(87.9%)
2	**12.2**	**all-*trans*-lutein**	**568**	**45.2**	**(41.1%)**	**14.2**	**(70.0%)**	**0.5**	**(8.6%)**
3	14.7	9-*cis* or 9′-*cis*-lutein	568	n.d.	–	1.2	(5.9%)	n.d.	–
4	15.1	n.i. (unknown compound)	n.d.	n.q.	–	n.d.	–	n.d.	–
5	15.5	phytoene isomer-1	n.d.	n.q.	–	n.d.	–	n.d.	–
6	16.6	9-*cis* or 9′-*cis*-lutein	568	n.d.	–	1.5	(7.4%)	n.d.	–
7	17.2	phytofluene isomer-1	542	n.q.	–	n.d.	–	n.d.	–
8	23.5	phytoene isomer-2	n.d.	n.q.	–	n.d.	–	n.d.	–
9	25.4	phytofluene isomer-2	542	n.q.	–	n.q.	–	n.d.	–
10	25.8	phytofluene isomer-3	542	n.q.	–	n.q.	–	n.d.	–
11	27.2	phytofluene isomer-4	542	n.q.	–	n.q.	–	n.d.	–
12	28.4	phytofluene isomer-5	541	n.q.	–	n.q.	–	n.d.	–
13	29.4	phytofluene isomer-6	541	n.q.	–	n.q.	–	n.d.	–
14	33.0	*all*-trans-α-carotene	536	n.d.	–	1.5	(7.4%)	n.d.	–
15	**37.1**	***all*-trans-β-carotene**	**536**	**22.9**	**(20.8%)**	**1.5**	**(7.4%)**	**0.2**	**(3.4%)**
16	39.8	9-*cis*-β-carotene	536	7.1	(6.4%)	0.4	(2.0%)	n.d.	–
17	52.2	n.i. (unknown compound)	536	n.q.	–	n.d.	–	n.d.	–
18	**54.9**	***cis*-lycopene isomer-1**	**536**	**11.5**	**(10.4%)**	n.d.	–	n.d.	–
19	63.7	*cis*-lycopene isomer-2	536	2.5	(2.3%)	n.d.	–	n.d.	–
20	68.5	*cis*-lycopene isomer-3	536	3.1	(2.8%)	n.d.	–	n.d.	–
21	70.8	*cis*-lycopene isomer-4	536	2.9	(2.6%)	n.d.	–	n.d.	–
22	71.7	*cis*-lycopene isomer-5	536	5.8	(5.3%)	n.d.	–	n.d.	–
23	73.2	*cis*-lycopene isomer-6	536	9.1	(8.3%)	n.d.	–	n.d.	–
	Total carotenoids (mg kg^{-1} oil):			**110.1**		**20.3**		**5.8**	

n.i.: not identified; n.d: not detected; n.q.: detected, but not quantified; Peak numbers refer to the identifications reported in Figure 4.6.

Interestingly, only in the seed oil of *H. indica* was detected a good amount (34.9mg/kg oil, *i.e.* 23% to total carotenoids) of different lycopene isomers; both D. album and L.

lontaroides did not show the presence of lycopene. Lycopene has been related to the prevention of some type of cancer and cardiovascular diseases [38]. Furthermore, the HPLC carotenoid profile relative to *H. indica* seed oil shows the detection of different isomers of phytofluene (carotenoid precursor) and two isomers of one other 'invisible' carotenoid precursor, phytoene (detected, but not quantified). Phytoene has lately received greater attention in the literature [39] as evidence is accumulating that it may provide health and cosmetic benefits. So, the health beneficial properties attributed to lutein, β -carotene, lycopene, and phytoene, certainly provide very interesting properties to the studied seed oils, especially the H. indica one which contained 110mg of total carotenoids per kg of crude oil (*Table 4.5*).

The roles of carotenoids in oilseeds are less clear than in other tissues, but there are evidences of their important role for the abscisic acid (ABA) production, seed dormancy and their contribution to the antioxidant system in the oilseeds [35]. For example, the crude red palm oil from *E. guineensis* [40] and the unconventional crude seed oils of Brazilian Passiflora species [41, 42] have been reported to contain very high amounts, in the order of several hundred mg/kg oil, of total carotenoids content.

Then taking into consideration that according to the classification proposed by Britton and Khachik [20], the carotenoid content in fruits and vegetable can be regarded as low (0-100 mg/100 g), moderate (100-500 mg/100 g), high (500-2000 mg/100 g) and very high more than 2000 mg/100 g, the high content of carotenoids determined in *H. indica* oil (110mg/kg oil, i.e. approximatively 357 mg/100 g seeds, taking into account the oil yield), provides evidence for the potential use of these natural compounds in healthy formulations. From a nutraceutical point of view, and provided that this endemic palm oil was not toxic for humans, these high-value carotenoids in *H. indica*, in particular, lutein, β-carotene, and lycopene, which were detected in a high content (respectively 45.2, 22.9 and 34.9mg/kg oil in crude oil) might be use to formulate new nutraceutical and pharmaceutical products.

4.2.3 Conclusions

The works presented in this study investigated for the first time the chemical characterization of three unconventional seed oils from endemic *Arecaceae* species from Reunion Island. First, results revealed the particular composition of the unconventional red seed oil from the ripe fruits of *Hyophorbe indica* Gaertn. This seed oil contained a high degree of unsaturation (50% of polyunsaturated fatty acids), which is possibly a unique

fatty acid composition in the Arecaceae family. The crude H. indica seed oil was interesting because it is high in ω6-PUFAs (linoleic acid; 34%), in ω3-PUFAs (alphalinolenic acid; 17%), in MUFAs (oleic acid; 20%), and very rich in valuable carotenoids, such as lutein, β-carotene and lycopene, that could be exploited due to their beneficial properties on human health. However, the food safety and toxicology of the red oil from this endemic palm species of Reunion Island was not known, and clinical trials are needed before the H. indica oil can be recommended to treat any health conditions.

Then, the two other unconventional *D. album* and *L. lontaroides* seed oils contained high level of saturated fatty acids very similar to that of the palm and palm kernel oil, respectively. So, they can be useful for oleochemical applications at least, like the palm oil used in Europe for these purposes. Although unconventional seed oil crops could offer new opportunities, properties and functionalities for the global market, they lack the years of research, improvements, and experience that have been invested in conventional oilseeds. An important need for any industrial applications is to increase productivity, and enhance the oil and unsaponifiable yields.

4.3 GC×GC-HR-TOF MS: exploring the chemical signature of food cooking emissions[i]

It has long been known that emissions from food cooking are a significant source of indoor air pollution [43-50]. Cooking involves a wide range of chemical reactions leading to the release of different cooking-related compounds including *n*-alkanes, fatty acids, polycyclic aromatic hydrocarbons (PAHs), dicarboxylic acids, aldehydes, *n*-alkanones, lactones, and sterols. Such releases could have negative impacts on the environment and human health depending on many factors including types of food, fuel and stoves, as well as cooking styles and methods, which can lead to different chemical profile emissions. The scope of this study is the untargeted assignment of significant differences in the emission of cooking aerosols. For this purpose, the chemical composition of several extracts of collected aerosols under different cooking conditions were investigated by using a GC×GC-HR-TOF MS system.

[i] The work reported in this section has been carried out at Helmholtz Zentrum Muenchen-Comprehensive Molecular Analytics (CMA). Only a brief description of the research project is herein reported.

The samples were collected from different types of commonly used cooking methods either by using electrical or natural gas stoves (*e.g.* pan-frying, stir-frying, deep-frying, oven roasting, oven broiling and oven baking) as well as foods (*e.g.* breakfast meats, beef, pork, chicken, fish fillets, and vegetables).

Non-targeted statistical compare will be applied for the first time to GC×GC-HR-TOF MS data. Statistical comparison and further multivariate analysis on peak tables of GC×GC-data will allow us to identify significant signatures of compounds for the different foods as well as cooking conditions.

- Experimental

Aerosol sampling. In order to sample, exclusively, cooking emissions in a quantitative manner, cooking experiments were conducted in an isolated environment where all air flows (in and out) were controlled and the in-flowing make-up air was purified to minimize potential contamination. For that purpose, an environmental chamber was designed (the inside dimensions of the environmental chamber were: 4 m in length, 3 m wide, and 2.5 m high with a volume of about 27 m^3). Altogether more than 140 cooking experiments were conducted in the chamber with the purpose to simulate the most common residential cooking procedures, and the $PM_{2.5}$ was measured. Two particle samplers were mounter on holding units in the chamber and operated concurrently during each cooking experiments. For each $PM_{2.5}$ sampling system, a $PM_{2.5}$ virtual impactor was mounted onto specially designed holding unit made of stainless steel. *Figure 4.7* shows, schematically, the $PM_{2.5}$ sampling unit. The total flow rate through each $PM_{2.5}$ virtual impactor was 425 L min^{-1}, and it was kept constant during the experiments by adjustment in the pressure gauges P_1 and P_2 (*Figure 4.6*). In addition, , each $PM_{2.5}$ sampler was followed by a canister made of stainless steel loaded with three polyurethane foam (PUF) units to allow the collection of semi-volatile and volatile organic emissions. Each PUF was cylindrical in shape, 7 cm in diameter and 4.5 cm in lenght. Here, exclusively quartz fiber filters (2500 QAO-UP, size 8 × 10 inches) were used for sampling of particulate matter. Subsequently, the $PM_{2.5}$ samples and PUF-samples were subjected to GC×GC-HR-TOF-MS.

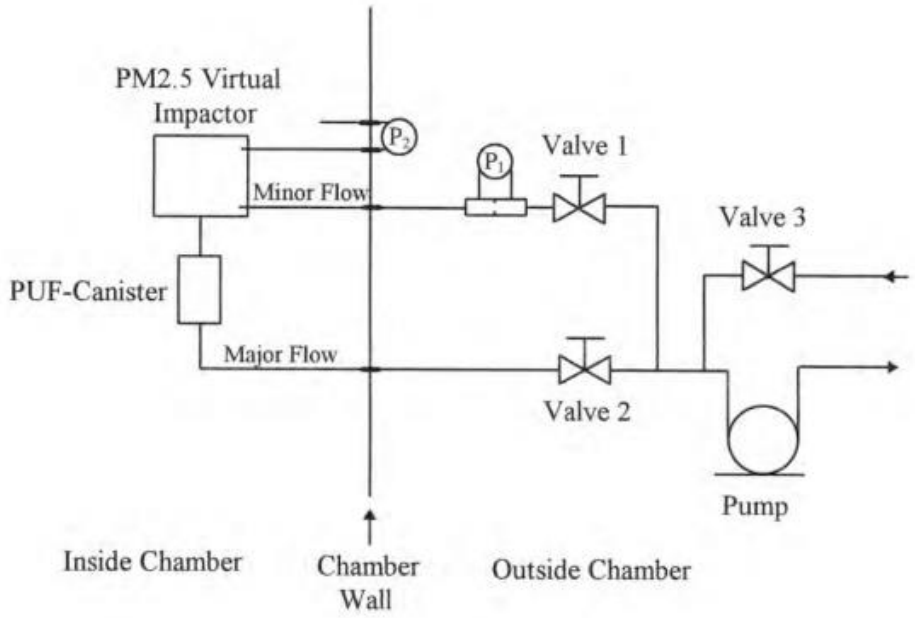

Figure 4.7. $PM_{2.5}$ sampling system.

Sample and sample preparation. Immediately prior to sample extraction, the filters and PUF-samples were spiked with the internal standars (ISs) (*n*-decanoic- d_{19} acid, *n*-tetradecanoic-d_{27} acid, *n*-eicosane-d_{42}, *n*-tetracosane-d_{50}, and *n*-triacontane-d_{62}, 1-phenyldodecane). All the ISs, dichloromethane and 1-methyl-3-nitro-1-nitrosoguanidine, were kindly provided by Merck Life Science (Merck KGaA, Darmstadt, Germany). The presence of the ISs for the scope of quantification was not exploited in the present research. The spiked filters were subsequently extracted for 12 hours with a Soxhlet extraction system using dichloromethane as solvent. After extraction, the filtered extract was reduced by rotary vacuum distillation to a volume of 3 to 5 mL and then by solvent evaporation with a stream of high purity N_2 to a volume of 1 mL. Diazomethane was prepared from 1-methyl-3-nitro-1-nitrosoguanidine. Following the volume reduction, each extract was reacted with freshly produced diazomethane to convert organic acids to their methyl ester analogues and acid hydroxyl compounds to their methoxy analogues. After the derivatization, sample extracts were stored at –21°C until analysis by GC×GC-HR-TOF MS.

GC×GC-HR-TOF MS measurements. All the applications were performed on a Pegasus GC-HRT 4D system (LECO, St. Joe, USA). The first dimension was an apolar 5% phenyl polysilphenylene-siloxane column (BPX5, SGE, Analytical Science, Australia) with

dimensions 24 m × 0.25 mm ID × 0.25 μm d_f. A medium-polar 50% phenyl polysilphenylene-siloxane column (BPX50, SGE) with dimensions 1.5 m × 0.10 mm ID × 0.10 μm d_f was used as second dimension. An uncoated capillary column with dimensions 0.8 m × 0.1 mm ID was used in the transfer line. The connection between the columns was made through the use of two Siltite micro unions (Trajan, Ringwood, Victoria, Australia). Modulation was achieved by using a dual stage four-jet cryogenic (liquid N_2) modulator, using the first 0.1 m of the second analytical column as modulation capillary. The carrier gas was He and was used under a constant flow of 1.2 mL min^{-1}. An Optic 3 injection system was also used. During the thermal desorption step the oven was kept at 50°C for 2 min before to increasing to 300°C at 6°C min^{-1}, which was held for 5 min. A secondary oven offset of +10 °C was applied. Transfer line temperature was 300 °C. The modulation period was set at 3 s: the hot pulse was held for 1 s, and the cold jet for 0.5 s. Modulation heating temperature: +15 °C offset with respect to the temperature of the main GC oven. The HR TOFMS was operated at 100 Hz with an acquisition range from *m/z* 15 to 500. Electron ionisation occurred at 70 eV at a source temperature of 300°C. Data collection was performed using the LECO ChromaToF-HRT software (v. 5.20.36). Mass spectral matching was performed by using the NIST 2017 Mass Spectral Library.

- Discussion

The samples set chosen for statistical evaluation comprised 35 samples (with three replicates each) collected from different types of commonly used cooking methods either by using electrical and natural gas stoves, as well as different foods. Specifically, 5 different cooking methods were chosen: pan-frying, stir-frying, deep-frying, oven roasting and oven broiling. Food items cooked included bacon, sausages, steaks, chicken, pork chops, scramble eggs, breaded and unbreaded fish fillets. Many of the food items mentioned were characterized by different fat contents, such as sausages (42% and 17% on fat content). The bidimensional chromatogram obtained by GC×GC-HR-TOF MS analysis of a sample collected from cooking sausages with a content of 42% in fat (the cooking experiment was carried out by using pan-frying as a cooking method, and employing an electrical stove) is shown in *Figure 4.8*. Fresh mixed vegetable and frozen mixed vegetable were stir-fried, while deep frying was used as cooking method for 3 food items including chicken wings, breaded fish fillets, and French fries. Both, beef and pork cooked by oven roasting were considered. Broiling is a common cooking methods to prepare steaks. Here, T-bone steaks, ribeye steaks and round steaks were considered. In addition, during the simulated

residential cooking, different types of vegetable oils and butter and shortenings were used. While the vegetable oils were used for cooking in most of pan-frying and stir-frying experiments, shortenings mixed with vegetable oils were used for deep frying, and butter was used only for pan-frying fresh and defrosted fish.

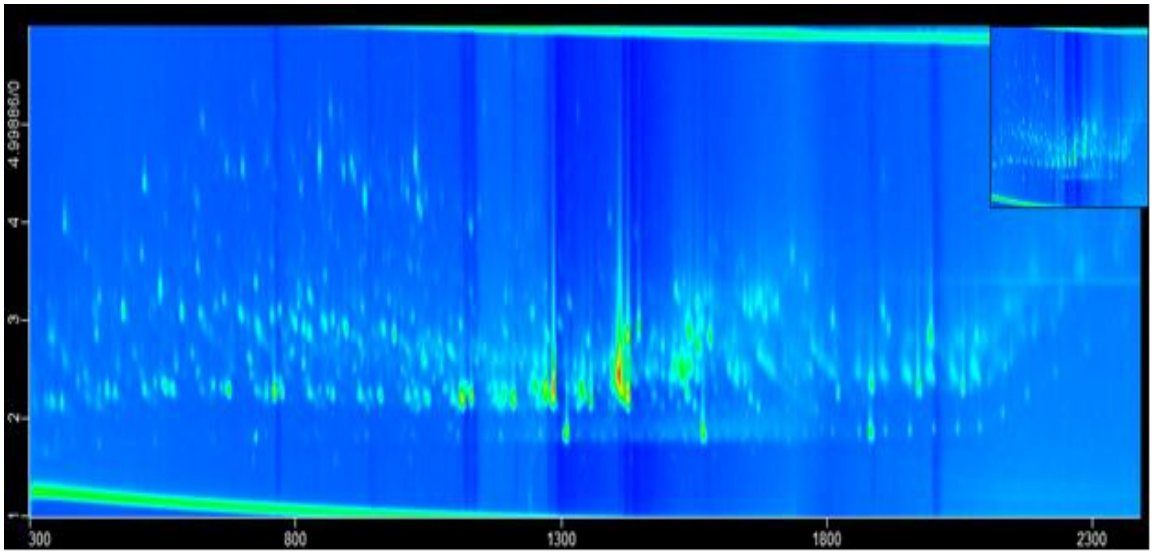

Figure 4.8. *Bidimensional chromatogram of a sample collected from a food cooking emission (food sample: sausages; cooking method: pan-frying; stove: electrical stove).*

Different cooking styles emit different compound profiles. For the comparison of replicate chromatograms of different samples (or the same sample), peak alignment prior to data analysis is an indispensable step, as retention time of the same component can vary between replicate chromatograms. Subsequently, the generated data matrix is used for further statistical analysis to identify significant differences between samples or sample classes followed by multivariate data analysis. The generated data set was processed with Leco ChromaTOF and MatLab (MathWorks). An alignment of peak tables was (semi-) automatically performed by ChromaTOF build-in Statistical Compare toolbox, which, additionally, offers the calculation of Fisher values. For further statistical compare evaluation, the aligned peak tables were imported into PLS-Toolbox (Eigenvector Research, Inc). The main aim of this study is to demonstrate that GC×GC-HR-ToF MS is an efficient tool to analyze large data sets with subsequent statistical analysis.

References

[1] W. Feger, H. Brandauer, H. Ziegler, Flavour Fragr. J. 15 (2000) 281.

[2] G. Dugo, A. Cotroneo, I. Bonaccorsi, A.Trozzi, G. Dugo, L. Mondello, Eds.; CRC Press: London, UK, 2010; pp. 1–162. ISBN 978-1-4398-0028-7.

[3] M.G. Chisholm, M.A. Wilson, G.M. Gaskey, Flavour Fragr. J. 18 (2003) 106.

[4] L. Mondello, P. Dugo, K.D. Bartle, G. Dugo, A. Cotroneo, Flavour Fragr. J. 10 (1995) 33.

[5] Z. Liu, J.B. Phillips, J. Chromatogr. Sci. 29 (1991) 22.

[6] P.J. Marriott, S.-T. Chin, B. Maikhunthod, H.-G. Schmarr, S. Bieri TRAC Trends Anal. Chem. 34 (2012) 1.

[7] J.J. Filippi, E. Belhassen, N. Baldovini, H. Brevard, U.J. Meierhenrich, J. Chromatogr. A 1288 (2013) 127.

[8] L. Mondello, A. Casilli, P.Q. Tranchida, P. Dugo, G. Dugo, Flavour Fragr. J. 20 (2005) 136.

[9] P.Q. Tranchida, M. Zoccali, I. Bonaccorsi, P. Dugo, L. Mondello, G. Dugo, J. Chromatogr. A 1305 (2013) 276.

[10] M. Zoccali, I.L. Bonaccorsi, P.Q. Tranchida, P. Dugo, L. Mondello, G. Dugo, Flavour Fragr. J. 30 (2015) 411.

[11] M. Zoccali, P.Q. Tranchida, I.L. Bonaccorsi, P. Dugo, L. Mondello, G. Dugo, Food Anal. Method. 10 (2017) 1106.

[12] B. D'Acampora Zellner, C. Bicchi, P. Dugo, P. Rubiolo, G. Dugo, L. Mondello, Flavour Fragr. J. 23 (2008) 297.

[13] L. Mondello, M. Zoccali, G. Purcaro, F.A. Franchina, D. Sciarrone, S. Moret, L. Conte, P.Q. Tranchida, J. Chromatogr. A 1259 (2012) 221.

[14] P.C. Calder, Eur. J. Lipid Sci. Technol. 116 (2014)1280.

[15] K.J. Bowen, W.S. Harris, P.M. Kris-Etherton, Curr Treat. Options Cardiovasc. Med. 18 (2016) 16.

[16] J.M. Kremer, Am. J. Clin. Nutr. 71 (2000) 349.

[17] J.C. Maroon, and J.W. Bost, 2006. Surg. Neurol. 65 (2006) 326.

[18] R. Zárate, N. El Jaber-Vazdekis, N. Tejera, J.A. Pérez, C. Rodríguez, Clin. Transl. Med. 6 (2017) 19.

[19] H.J. Lee, Y.M. Han, J.M. An, E.A. Kang, Y.J. Park, J.Y. Cha, K.B. Hahm, Expert Rev. Anticancer Ther. 18 (2018) 1189.

[20] G. Britton, and F. Khachik, in: Carotenoids, Birkhäuser (2009).

[21] R.K. Saini, S.H. Nile, S.W. Park, Food Res Int. 76 (2015) 735.

[22] E.M. Yahia, J. de Jesús Ornelas-Paz, T. Emanuelli, E. Jacob-Lopes, L.Q. Zepka, B. Cervantes-Paz, in: Fruit and vegetable phytochemicals: chemistry and human health, John Wiley & Sons Ltd (2017).

[23] L. Cassiday, Inform. 29 (2018) 6.

[24] M. Friedman, J. Agric. Food Chem. 61 (2013) 10626.

[25] D.A. Ofori, K. Kehlenbeck, M. Munjuga, R. Jamnadass, E.K. Asaah, C. Kattah, F. Rutatina, Acta Hortic. 979 (2013) 311.

[26] S.L. Crockett, Int. J. Mol. Sci. 16 (2015) 22333.

[27] A.M.M. Guedes, R. Antoniassi, A. Ferreira de Faria-Machado, OCL. 24 (2017) 507.

[28] R.M. Ojeda-Amador, G. Fregapane, M.D. Salvador, Food Chem. 240 (2018) 123.

[29] I. Nehdi, S. Omri, M.I. Khalil, S.I. Al-Resayes, Ind. Crops Prod. 32 (2010) 360.

[30] P.Q. Tranchida, A. Giannino, M. Mondello, D. Sciarrone, P. Dugo, G. Dugo, L. Mondello, J. Sep. Sci. 31(2008) 1797.

[31] V. Dubois, S. Breton, M. Linder, J. Fanni, M. Parmentier, OCL. 15 (2008) 56.

[32] A.P. Simopoulos, Nutrients 8 (2016) 128.

[33] A.P. Simopoulos, Nutrients 8 (2016) 128.

[34] A.D: Kinghorn, in: Handbook of natural toxins, Marcel Dekker (1983).

[35] G.M. Williams, Food Addit. Contam. 1 (1984) 173.

[36] C.A. Howitt, and B.J. Pogson, Plant Cell Environ. 29 (2006) 435.

[37] N.I. Krinsky, J.T. Landrum, R.A. Bone, Annu. Rev. Nutr. 23 (2003) 171.

[38] M. Le, and L. Xiao-Ming, J. Sci. Food Agric. 90 (2010) 2.

[39] L. Arab, and S. Steck, Am. J. Clin. Nutr. 71 (2000) 1691.

[40] A. Melendez-Martinez, P. Mapelli-Brahm, C.M. Stinco, J. Food Comp. Anal. 67 (2018) 91.

[41] J.M. Lecerf, OCL. 20 (2013) 147.

[42] F.C. De Santana, F.B. Shinagawa, E.D.S. Araujo, A.M. Costa, J. Mancini-Filho, J. Food Sci. 80 (2015) 2647.

[43] R. Kamens, C.-t Lee, R. Wiener, D. Leith, Atmos. Environ. 25 (1991) 939.

[44] H. Ozkaynak, J. Xue, J. Spengler, L. Wallace, E. Pellizzari, P. Jenkins, J.Expo. Anal. Environ. Epidemiol. 6 (1996) 57.

[45] C.Y. Chao, E.C. Cheng, Indoor Built Environ. 11 (2002) 27.

[46] M. Lazaridis, V. Aleksandropoulou, J. Smolík, J.E. Hansen, T. Glytsos, N. Kalogerakis, E. Dahlin, Indoor Air, 16 (2006) 282.

[47] W.X. Zhao, P. K. Hopke, E. W. Gelfand, N. Rabinovitch, Atmos. Environ. 41 (2007) 4084.

[47] G. Buonanno, L. Morawska, L. Stabile, Atmos. Environ. 43 (2009) 3235-3242.

[48] S.C. Lai, K. F. Ho, Y. Y. Zhang, S. C. Lee, Y. Huang, S.C. Zou, AAQR, 10 (2010) 472.

[49] M.-P. Wan, C.-L. Wu, G.-N. Sze To, T.-C. Chan, C.Y.H. Chao, Atmos. Environ., 45 (2011) 6141.

[50] D. Massey, A. Kulshrestha, J. Masih, A. Taneja, Build. Environ. 47 (2012) 223.

[51] USEPA, 1999. Emissions from Street Vendor Cooking Devices (Charcoal Grilling). US Environmental Protection Agency, Washington, DC, pp. 1-551.

Chapter 5

Towards the determination of an equivalent standard column set between cryogenic and flow modulated GC×GC-MS

5.1 Analysis of coconut-derived bio-oil by using flow- and cryogenic-modulation comprehensive 2D gas chromatography-mass spectrometry [i]

This preliminary research is focused on the task of defining an equivalent standard column set between cryogenic and flow-modulation comprehensive two-dimensional gas chromatography (GC×GC) combined with mass spectrometry (MS). Cryogenic modulation (CM) was carried out by using a loop-type device, while the flow modulator used was a seven-port wafer chip, equipped with an external accumulation loop.

Initially, a common low-polarity + mid-polarity CM GC×GC column set was selected (30 m × 0.25 mm ID × 0.25 μm d_f + 1.5 m × 0.25 mm ID × 0.25 μm d_f), a method was developed, and a GC×GC-MS fingerprint was attained (on a sample of bio-oil derived from coconut fibers). After, a column set with the same stationary phases was selected for the flow modulation GC×GC-MS method (20 m × 0.18 mm ID × 0.18 μm d_f + 5 m × 0.32 mm ID × 0.25 μm d_f), with the capability to provide a-similar-as-possible separation. A side-by-side measurement of several chromatography parameters (efficiency, peak capacity, resolution, peak widths, retention factors, elution temperatures) was made.

[i] This section has been adapted from the following publication: I. Aloisi, T. Schena, **B. Giocastro**, M. Zoccali, P. Q. Tranchida, E. B. Caramao, L. Mondello in "*Towards the determination of an equivalent standard column set between cryogenic and flow-modulated comprehensive two-dimensional gas chromatography" Analytica Chimica acta, 2020, 1105, 231-236.*

5.1.1 Introduction

Comprehensive two-dimensional GC (GC×GC) separations are carried out on two columns linked in sequence, with a modulator located at some point between them [1]. The modulator, it being either flow or cryogenic, enables continuous (throughout the analysis) processes of isolation and re-injection of chromatography bands from the first to the second column. Several cryogenic and flow modulation devices have been described over the past two decades, with thorough details reported in the literature [2,3]. Focus will be herein given to cryogenic loop-type modulation [2,3], and to a flow modulation (FM) model, stemming from an approach introduced by Seeley et al. in 2006 [4]; the latter transfer device was constructed by using two T-unions (one upstream, and the other downstream), three fused-silica capillary columns, and a two-way solenoid valve (positioned outside the GC oven), with the latter linked to an auxiliary gas source. Two capillaries linked the unions to the valve outlet ports, while the remaining capillary bridged the two unions and acted as accumulation loop. The remaining port of each union was connected to the first dimension column (1D- upstream), and to a 10 cm segment of 0.25 mm ID capillary tubing (downstream union), which in turn was linked to a T union, this being connected to two second dimension (^{2}D) columns. During the accumulation step, the gas flow from the auxiliary source was directed to the downstream union allowing the ^{1}D effluent to enter the loop. At the end of the accumulation process, the gas flow from the auxiliary source was directed to the upstream union, enabling the rapid flushing of the loop (re-injection step). The accumulation and re-injection steps were performed in 1.4 s and 0.1 s, respectively. A gas flow of 20 mL min^{-1} was used for efficient loop flushing, and was split equally between two 2D 5 m × 0.25 ID columns, each connected to a flame ionization detector (FID). In later research, and following the FM model proposed by Seeley et al., a seven-port wafer chip, with internal micro-channels and an external accumulation loop, was evaluated in FM GC×GC- FID applications [5]. In this and other FM studies, high ^{2}D gas flows were used [5-8]. The generation of high gas flows can be considered as a main drawback, especially if mass spectrometry (MS) detection is required.

In recent work, it has been shown that an efficient re-injection process can be performed at greatly reduced gas flows (6-8 mL min^{-1}) simply by extending the re-injection period [9]. The straightforward concept is that a re-injection period of 100 ms, at a gas flow of 24 mL min^{-1}, is equivalent to a re-injection period of 300 ms, at a gas flow of 8 mL min^{-1}. In following related FM GC×GC-MS research, a 0.53 mm ID ^{2}D column was used to benefit

from the vacuum outlet conditions, leading to the introduction of the term "low-pressure comprehensive 2D GC" (GC×LP GC). Additionally, it was demonstrated that the use of a longer accumulation loop, enabling two accumulation + two re-injection processes (dual stage), had a beneficial effect on peak shape [10].

This preliminary investigation is based on the task of determining an equivalent standard column set between cryogenic- and flow-modulation GC×GC. Cryogenic modulation (CM) was carried out by using a loop-type device; the FM device used was a seven-port wafer chip, with the seventh port closed [the seventh port is normally used if dual detection (e.g., MS and FID) is required]. The flow modulator used can be considered as a compact version of the device introduced by Seeley et al. [4].

5.1.2 Material and methods

5.1.2.1 Sample, standard compounds, and sample preparation

A sample of bio-oil (produced through pyrolysis of coconut fibers) was diluted in dichloromethane at a concentration of 10,000 and 20,000 ppm (v/v). Two internal standards (ISs) were used (naphthalene- d_8 and acenaphthene- d_{10}), each at a concentration of 166 mg L^{-1}. The presence of the ISs for the scope of quantification was not exploited in the present research. The standard compounds were purchased from Merck Life Science (Merck KgaA, Darmstald, Germany).

5.1.2.2 Instrumentation

Cryogenic-modulation GC×GC-MS

The CM GC×GC-MS analysis was performed on a loop-type modulator Shimadzu GC×GC-MS system, consisting of two independent (GC2010) gas chromatographs (GC1 and GC2) [11], and a QP2010 Ultra single quadrupole mass spectrometer (Kyoto, Japan). The first GC system was equipped with a split/splitless injector, which was maintained at a temperature of 280°C. Injected volume was: 1 μL (of the 10,000 ppm solution), at a split ratio of 20:1. The capillary columns used were: 30 m × 0.25 mm ID × 0.25 μm d_f [SLB-5ms-silphenylene polymer with similar polarity to poly (5% diphenyl/95% dimethyl siloxane)] in the 1D and 1.5 m × 0.25 mm ID × 0.25 μm d_f [SLB-35ms - proprietary polymer with similar polarity to poly (35% diphenyl/65% dimethyl siloxane) in the ^{2}D. An uncoated capillary column, with dimensions 1.5 m × 0.18 mm ID, was used as delay loop. The columns were heated as follows: 50°C-330°C at 6°C min^{-1} (in both GC ovens). Such a

choice was also related to the fact that the FM GC×GC-MS instrument was composed of a single GC oven.Carrier gas (He) conditions: constant linear velocities of approx. 18.5, 80.4, and 103.9 cm s^{-1}, were generated in the first dimension, the delay loop, and the second dimension, respectively. Gas flow was approx. 0.41 mL min^{-1} (injection pressure: ≈ 9 kPa) at the beginning and 0.35 mL min^{-1} (injection pressure: ≈ 72 kPa) at the end of the analysis. Such gas velocity and flow values can be calculated as previously described [12], by considering the pressures at the ^{1}D column inlet and outlet (or inlet of the delay loop), and the ^{2}D column inlet (or outlet of the delay loop) and outlet (vacuum conditions) (*Figure 5.1*). A simple alternative, exploited in this case, was to use a dedicated software (GC×GC flow calculation software, Shimadzu).

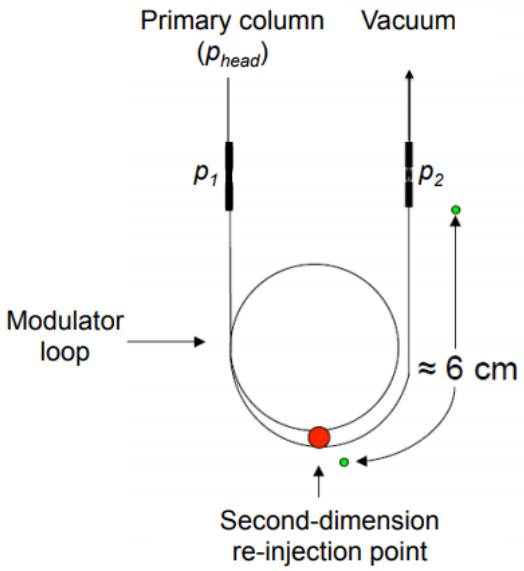

Figure 5.1. *Scheme of the loop-type cryogenic modulator. Absolute inlet pressure at the injector: p_{head}; absolute inlet pressure at the loop: p_1; absolute outlet pressure at the loop: p_2.*

Modulation was carried out by using a liquid nitrogen free chiller unit (ZX2 - under license from Zoex Corporation). The loop-type modulator is characterized by a vertical cold jet, which operates continuously throughout the GC×GC-MS analysis, and a horizontal hot jet which is activated for a specific time at pre-determined intervals. Both jets are directed onto two overlapping points of the delay loop, one upstream and the other downstream (*Figure 5.1*). Modulation period was 4.0 s, with a hot pulse (280°C) duration of 0.2 s. Mass spectrometry conditions: interface and ion source temperatures were maintained at 250°C;

ionization was performed through electron ionization (70 eV), over the mass range m/z 35-500. Spectral generation frequency was 33 Hz.

Data processing was performed by using the ChromSquare software v. 2.3 (Shimadzu). Mass spectral databases used were FFNSC 3.0 and Wiley registry 11th edition/NIST 2017 mass spectral library.

Flow-modulation GC×GC-MS

The FM GC×GC-MS applications were carried out on a Shimadzu GCMS-TQ8040 system. The GC system was equipped with a split/splitless injector, which was maintained at a temperature of 280°C. The injected volume was: 1 μL (of the 20,000 ppm solution), at a split ratio of 10:1. The capillary columns used were: 20 m × 0.18 mm ID × 0.18 μm d_f (SLB-5ms) in the first dimension and 5 m × 0.32 mm ID × 0.25 μm d_f (SLB-35ms) in the second dimension. The columns were heated as follows: 50°C-330°C at 6°C min^{-1}.

A seven-port wafer chip was located inside the GC oven and was connected to a three-way solenoid valve by using two symmetric 1.07 m stainless steel tubings of dimensions 0.97 m × 0.51 mm ID + 0.10 m × 0.25 mm ID. Gas flow was supplied to the solenoid valve through an auxiliary pressure control (APC) unit. The modulator loop (stainless steel) was of dimensions 40 cm × 0.51 mm ID (volume = 78.6 μL). The seventh port was blocked. A scheme of the modulator is shown in *Figure 5.2* and for a better representation is shown with all 7 ports on the front side. However, the modulator used in the present study was characterized by 5 ports on the front face and by 2 ports on the back, with the latter connected to the valve via the stainless steel tubing. Carrier gas (He) conditions: average ^{1}D gas velocity was 12.3 cm s^{-1} [gas flow was approx. 0.24 mL min^{-1} (injection pressure: ≈ 61 kPa) and 0.20 mL min^{-1} (injection pressure: ≈ 155 kPa) at the beginning and at the end of the analysis, respectively]; loop gas velocity was about 1.9 cm s^{-1} during accumulation and approx. 68.0 cm s^{-1} during re-injection; the average ^{2}D gas velocity was approx. 257 cm s^{-1} [gas flow was approx. 8.4 mL min^{-1} (re-injection pressure: ≈ 13 kPa) and 7.1 mL min^{-1} (re-injection pressure: ≈ 79 kPa), at the beginning and at the end of the analysis, respectively]. Approximate gas flows (and velocities) were derived with the support of the HP flow calc. 2.0 (Hewlett–Packard) software, and were calculated as follows: ^{1}D gas flow: ^{1}D column inlet pressure and the APC pressure (as outlet pressure), with a pressure reduction due to the 0.10 m × 0.25 mm ID stainless steel tubing linked to the modulator (the contribution of the 0.97 m × 0.51 mm ID portion on the APC pressure drop was considered to be negligible); ^{2}D gas flow: the APC pressure as inlet pressure, with a

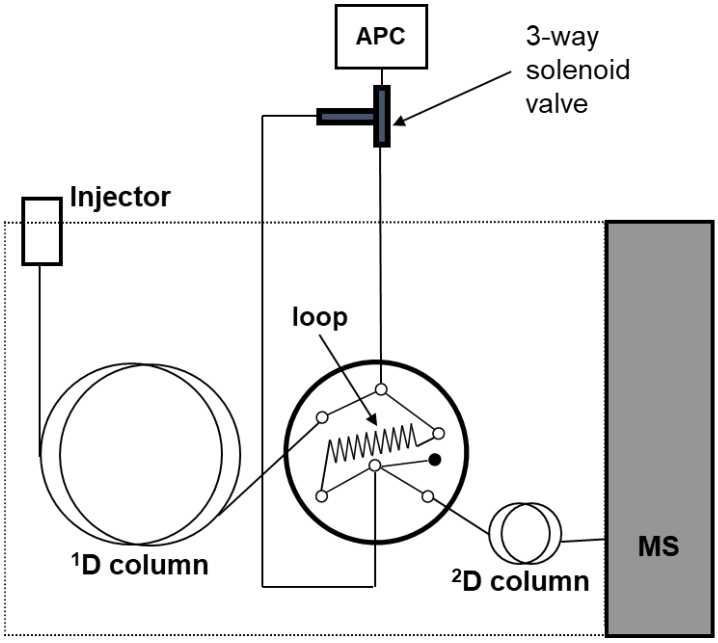

Figure 5.2. *Scheme of the GC×GC system equipped with the seven-port flow modulator.*

pressure reduction due to the 0.10 m × 0.25 mm ID stainless steel tubing linked to the modulator (the contribution of the 0.97 m × 0.51 mm ID portion on the APC pressure drop was considered to be negligible) and the outlet vacuum conditions; loop flow during accumulation: ^{1}D gas flow; loop flow during re-injection: ^{2}D gas flow. It is noteworthy that the calculations were made by not considering restrictions inside the wafer chip (internal channels). Modulation period was 4.0 s, with a re-injection period of 0.4 s.

Mass spectrometry conditions (the triple quadrupole mass spectrometer was used in the scan mode): interface and ion source temperatures were maintained at 220°C; ionization was performed through electron ionization (70 eV), over the mass range m/z 45-450. Spectral generation frequency was 33 Hz.

5.1.3 Results and Discussion

The CM GC×GC-MS applications were carried out by using a single quadrupole mass spectrometer, whereas a triple quadrupole one (in the scan mode) was used in the FM ones. The ion sources in the two MS systems were the same. Furthermore, in the triple quadrupole MS instrument the first quadrupole and the collision cell were operated only as “fly through” zones, while the second quadrupole was operated by using the same acquisition frequency as that of the single quadrupole MS instrument. Such a procedure was considered

as acceptable because the objective of the research was to define an equivalent standard column set, in terms of the overall separation performance.

Very simply, and initially, a standard CM GC×GC-MS column set was selected, a method was developed, and a GC×GC-MS fingerprint was attained (on a sample of bio-oil derived from coconut fibers). After, a column set was selected for the FM GC×GC-MS method, with the capability to provide a-similar-as-possible separation. With the FM column combination providing a comparable result with respect to that of the standard CM column set, then these can be considered (to a certain degree) as equivalent. In view of the results hereafter reported, the FM set of columns is proposed as a possible standard column combination.

The CM GC×GC-MS method

Cryogenic-modulation GC×GC-MS analyses are usually carried out by using a 30-60 m × 0.25 mm ID column in the first dimension and a 1-2 m ^{2}D column characterized by a 0.1 mm ID or the same ID as that of the 1D column [13]. Such a selection can be considered as a standard choice.

In the present study, a (low-polarity + mid-polarity) 30 m × 0.25 mm ID × 0.25 μm d_f + 1.5 m × 0.25 mm ID × 0.25 μm d_f combination of columns was used, with a 1.5 m × 0.18 mm ID uncoated column used as delay loop, to enable two accumulation and two re-injection processes (dual-stage modulation). The phase ratio of both analytical dimensions equalled approx. 250. The GC×GC-MS system was operated in the constant average linear velocity (ALV) mode: the ^{1}D gas ALV was approx. 18.5 cm s^{-1} (void-time: ≈ 162 s), the intra-loop one about 80 cm s^{-1}, and the ^{2}D gas ALV circa 100 cm s^{-1} (void-time: 1.5 s).

The He ^{1}D velocity was lower than the ideal value (≈ 30-40 cm s^{-1}), with a potential highest column efficiency of about 120,000 theoretical plates (N). Concerning the ^{2}D, a 1.5 m × 0.25 mm ID × 0.25μm d_f column, operated under optimum GC-MS conditions, should generate about 6000 N [14]. The modulation period was 4.0 s, with a re-injection time of 0.2 s (280°C). Both columns were heated from 50°C to 330°C, at 6°C min^{-1}.

The developed CM GC×GC-MS method was applied to the analysis of bio-oil, the resulting chromatogram of which is shown in *Figure 5.3-A*. Considering an analyte elution time window of 40 min (2400 s), corresponding to 600 modulations, this would lead to an overall potential N value of: 600 × 6000 = 3,600,000. In this approximate calculation, the ^{1}D N value has not been included.

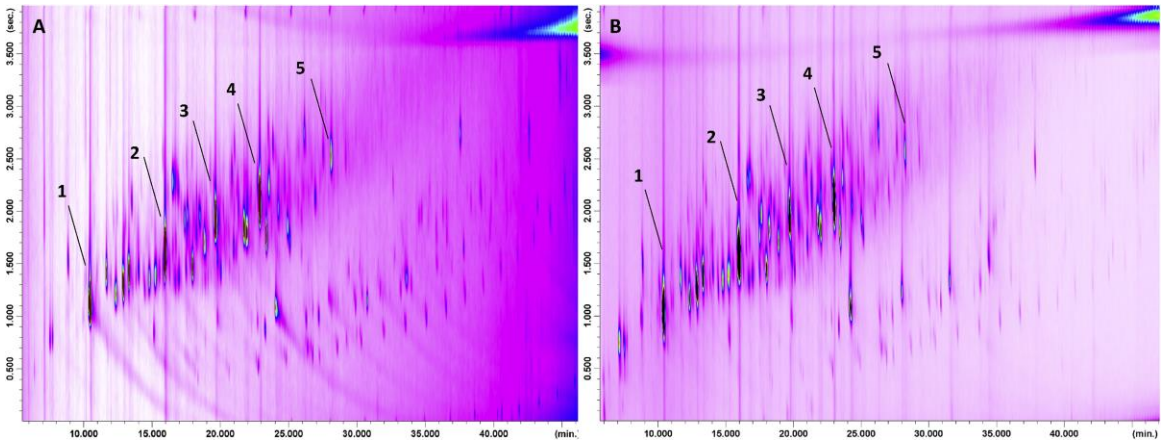

Figure 5.3. *A cryogenically-modulated (in A) and a flow-modulated (in B) GC×GC-MS chromatogram of coconut-derived bio-oil. Peak identity can be found in Table 5.1.*

The FM GC×GC-MS method

In FM applications, it is widespread practice to use a rather long wider-bore column in the second dimension [5-10], to accommodate the rather large sample volumes deriving from the modulator loop. Even so, there is no real standard set of columns used in FM GC×GC. In the present study, a 20 m × 0.18 mm ID × 0.18 μm d_f column was used in the first dimension and a 5 m × 0.32 mm ID × 0.25 μm d_f one in the second dimension. The types of stationary phase and the temperature program were obviously the same as used in the CM analysis.

The phase ratio of the ^{1}D column was approx. 250, while that of the second column was approx. 320. Ideally, and if available in the laboratory, a ^{2}D column with a phase ratio of 250 would have been used. A sample amount 4× higher was introduced onto the ^{1}D column in the FM analysis, to compensate for the higher sensitivity of CM. Such a choice was made purely on the basis of previous experience made on the two types of modulators. The injector pressure applied generated a ^{1}D ALV of approx. 12.3 cm s^{-1} (a flow of about 0.24 mL min^{-1} at the beginning of the analysis), corresponding to a void time of about 163 s. The ^{1}D outlet pressure considered was that provided by the APC unit during accumulation (with a pressure reduction due to the stainless steel tubing linked to the modulator; see *section 5.1.2.2*).

With regards to the ^{2}D, a constant ALV of approx. 260 cm s^{-1} was generated by the auxiliary pressure, corresponding to a void time, in this case, of about 1.9 s. The ^{2}D outlet pressure was obviously that of the mass spectrometer. The ^{1}D void times in the CM and FM applications can be considered as equal. On the other hand, the ^{2}D void time in the FM method was slightly higher (1.9 s *vs.* 1.5 s), a factor in part counterbalanced by the higher phase ratio (retention factors will slightly decrease).

The ^{2}D column used was operated at a very high gas linear velocity, and presumably far from its ideal separation potential (≈ 15,600 *N*). On the other hand, the use of low ^{1}D gas flow conditions is related to the necessity to avoid the occupation of an excessive volume of the loop, during the accumulation step (a factor leading to breakthrough). Such ^{1}D He velocity conditions were again lower than ideal, with a potential highest column efficiency of ≈ 110,000 *N*. The ^{2}D gas flow was calculated to be 8.4 and 7.1 mL min^{-1}, at the beginning and at the end of the analysis, respectively. Such values are admittedly high, but well within the pumping capacity of the mass spectrometer used (15 mL min^{-1}). Moreover, the use of a relative long accumulation loop (40 cm × 0.51 mm ID) enabled two accumulation and two re-injection processes, with the scope of improving peak shape as previously demonstrated [10]. Modulation period was 4.0 s, with a pulse time of 0.4 s. More specifically, an accumulation (3.6 s) ➔ re-injection (0.4 s) ➔ accumulation (3.6 s) process occurred within the loop, prior to the final re-injection step (0.4 s) which enabled the transfer of the chromatography band onto the ^{2}D. On the basis of flow calculations (see section 2.2.2) it was anticipated that the leading edge of the chromatography band, at the end of the second accumulation step, could have been released from the loop leading to breakthrough. Such a factor, visible as a baseline raise prior to the sharp modulated peak, was not observed. It is noteworthy that such tuning of the FM flow conditions (^{1}D, accumulation loop, ^{2}D), which has been previously described [9,10], must be considered as a useful approximation, also because restrictions inside the wafer chip (internal channels) were not considered.

The developed FM GC×GC-MS method was applied to the analysis of coconut bio-oil, the resulting chromatogram of which is shown in *Figure 5.3 B.* In this case, an overall potential *N* value of about 9,360,000 (600 × 15,600) could be attained.

Comparison of the results

Considering the combined potential efficiency of the columns used in the FM GC×GC-MS analyses, then this was nearly three times higher than that of the CM GC×GC-MS set of columns. However, two advantages must be accounted for in the CM method, compared to the FM one: I) the gas flow conditions were nearer to optimum in the second dimension; II) the re-injection conditions are much better due to chromatography band re-concentration.

The CM and FM GC×GC-MS chromatograms reported in *Figures 5.3 A-B* have been aligned (as will be seen ^{2}D retention times differed a little), after being corrected for wrap-around.

In first instance, the elution temperatures were very similar for the 5 numbered peaks in *Figures 5.3 A-B*, as can be seen from the information listed in *Table 5.1*. The elution temperatures were calculated from the total (^{1}D + ^{2}D) retention times provided by the GC×GC-MS software used (the most intense modulated peak is considered). Across the elution temperature range 112.3-219.7°C, corresponding to a time period of approx. 18 min, the maximum difference was 0.8°C for peak 5, corresponding to 8 s. The elution temperature for phenol was slightly higher in the CM application (0.5°C, corresponding to 5 s) and, on the other hand, slightly lower for the other four compounds. Such differences can also be related to the modulation phase and, hence, to the position of the most intense modulated peak for a specific compound. Peaks widths (at half height - w_h) for the five compounds listed in *Table 5.1* were derived by considering only non-overloaded modulated peaks. The measured values were rounded to the first ten due to the fact that one data point every 30.3 ms was acquired. Consequently, the w_h results listed in *Table 5.1* are to be considered as approximations. In general, the w_h values were similar, even though always lower in the flow modulation experiments (apart from phenol), with an average value of 188 ms against 224 ms. The peak capacities, calculated using the two average w_h values and the modulation period, were approx. 18 and 21 in the CM and FM applications, respectively. Besides peak capacity, peak-to-peak resolution is a further important factor, and was found to be generally similar in both types of applications. For example, CM and FM chromatogram expansions between approx. 15.1 and 15.4 minutes are shown in *Figures 5.4-A* and *5.4-B*, with the (spectrally-similar) compounds indicated by a asterisk characterized by resolution values of 1.4 and 1.5, respectively.

***Table 5.1**. Information related to compound identity, elution temperatures (Elution temp.), ^2D retention times (t_R), peak widths at half height (w_h), and signal-to-noise ratios (s/n) for the 5 compounds indicated in the cryogenic modulation and flow modulation applications (Figure 5.3 A-B).*

Peak/Compound	**Cryogenic modulation**			**Flow modulation**		
	Elution temp. (°C)	*^2D t_R (s)*	*w_h (ms)*	*Elution temp.*	*^2D t_R*	*w_h*
1. Phenol	112.8	4.16	190	112.3	3.47	190
2. Naphthalene-d_8	146.1	4.67	230	146.4	4.01	190
3. 2,6-Dimethoxyphenol	168.1	4.97	220	168.4	4.43	180
4. Acenaphthene-d_{10}	187.7	5.18	230	188.4	4.52	200
5. Syringylacetone	218.9	5.63	250	219.7	5.06	180
Average			*224*			*188*

Retention factors were measured for the 5 compounds numbered in *Figure 5.3*, and were obviously found to be higher in the CM analysis, with all compounds characterized by a difference of approx. a single *k* unit (*Table 5.2*). Column efficiencies were also calculated for the 5 compounds (^{2}D separations can be considered as isothermal), with them being altogether comparable (*Table 5.2*): the average *N* values were approx. 2700 and 3000 in the CM and FM analyses, respectively.

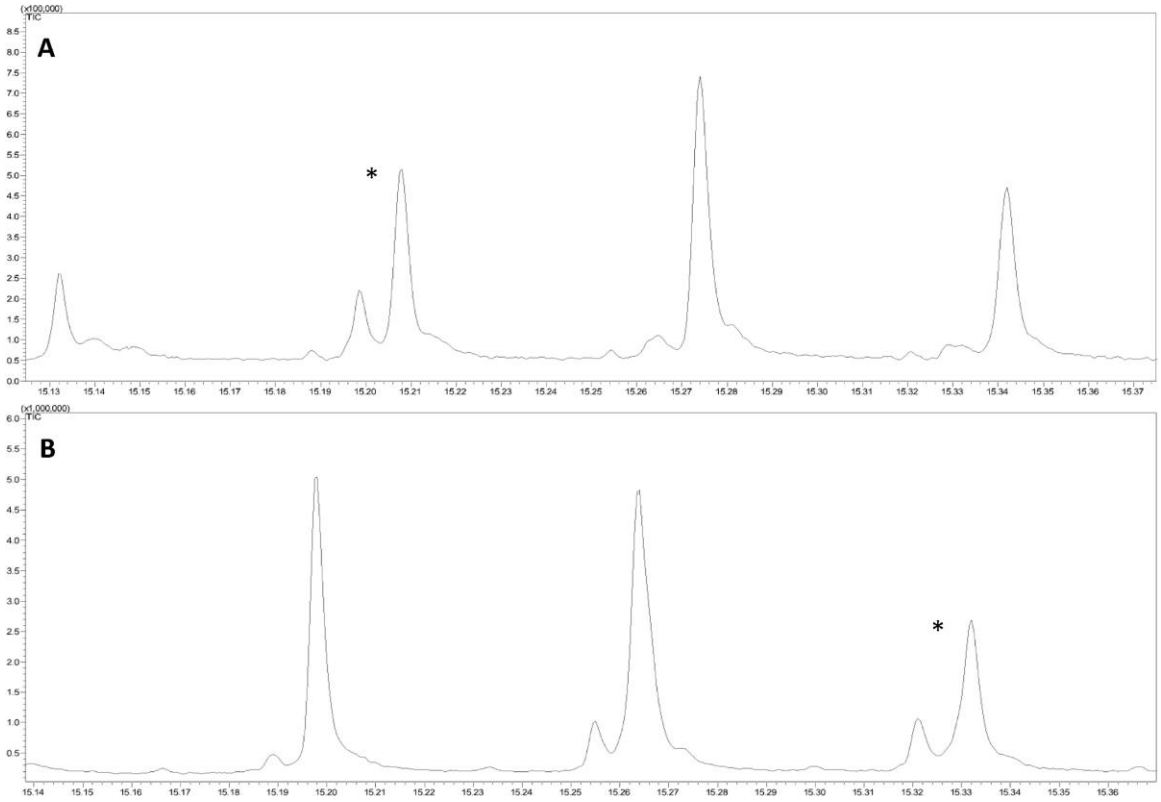

***Figure 5.4**. Cryogenically-modulated (in A) and flow-modulated (in B) GC×GC-MS untransformed chromatogram expansions relative to the analysis of coconut-derived bio-oil.*

The GC×GC profiles illustrated in *Figure 5.3*, even at a first glance, are very similar. As seen, such a fact was confirmed by measuring various chromatographic parameters, with focus on the ^{2}D separations, in particular. With regard to the ^{1}D separations, again these were entirely comparable as can be seen in the two 6.45 min expansions (range: 10.00-16.45 min) derived from the chromatograms shown in *Figure 5.3* (*Figure 5.5*).

***Table 5.2**. Capacity factor and theoretical plate number values for the 5 compounds indicated in the flow modulation and cryogenic modulation applications (Figure 5.3).*

Peak/Compound	**Cryogenic modulation**		**Flow modulation**	
	k	*N*	*k*	*N*
1. Phenol	1.8	2576	0.8	1909
2. Naphthalene-d_8	2.1	2326	1.1	2550
3. 2,6-Dimethoxyphenol	2.3	2856	1.3	3553
4. Acenaphthene-d_{10}	2.5	1911	1.4	2832
5. Syringylacetone	2.8	2904	1.7	4334
Average		*2515*		*3036*

Three dashed lines connect the same peaks (α, β, γ) in the two chromatogram expansions emphasizing the altogether similar elution profile along the *x* axis. The upper part of each dashed line was positioned at the peak apex in the CM result. The observation of the lower ends of the dashed lines highlight the fact that first dimension retention times for the three compounds were slightly lower in the FM analysis. However, in the two types of applications the retention time differences between compound β and α, as well as between compound β and γ, were very similar.

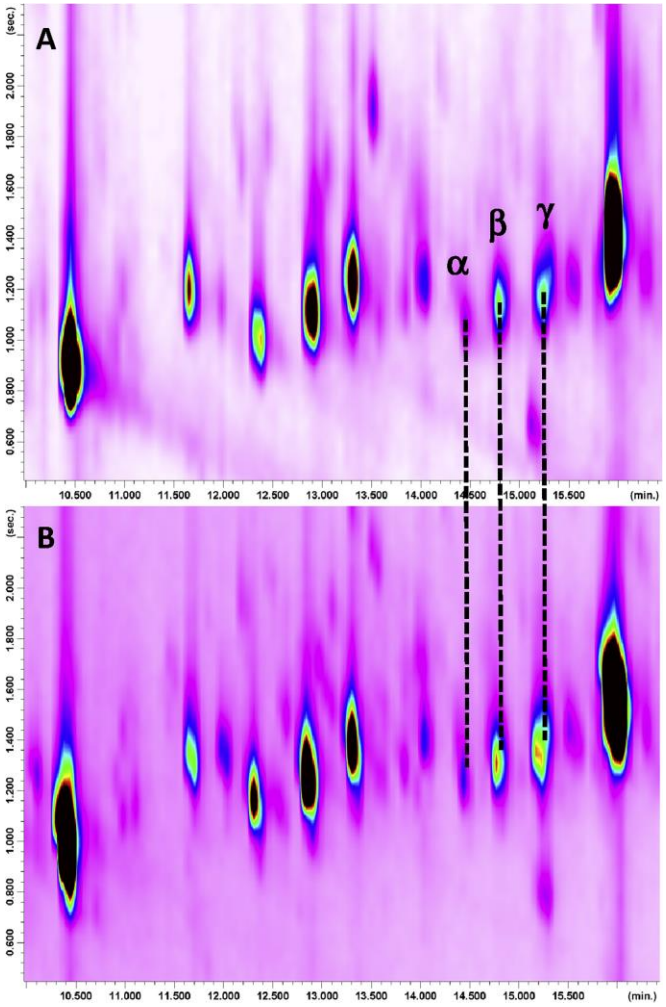

Figure 5.5. *Chromatogram expansions derived from the chromatograms shown in Figure 5.3. The CM and FM expansions are shown in A and B, respectively.*

5.1.4 Conclusions

A preliminary attempt to determine an equivalent standard column set for cryogenic and flow-modulation GC×GC-MS has been herein described. The term “preliminary attempt” is used because the CM and FM approaches provided an altogether similar, even though not equal, separation performance. Furthermore, the determination of “equivalence” would require a more in-depth evaluation of the GC×GC-MS fingerprints. Finally, a specific view on the analytical potential of FM GC×GC-MS, compared to the more powerful CM GC×GC-MS, has been given. In such a respect, obviously the use a ^{2}D 1.5 m × 0.10 mm ID × 0.10 μm d_f column would have provided a superior result (potentially 9,000,000 *N*), but such an evaluation would have been outside the scope of the present investigation.

5.2 Analysis of fragrance allergens by using flow- and cryogenic-modulation comprehensive 2D gas chromatography-mass spectrometry: obtaining similar chromatography performances [ii]

In the present research, very similar chromatography fingerprints were obtained by using finely-tuned cryogenic-modulation (CM) and flow-modulation (FM) comprehensive two-dimensional gas chromatography-mass spectrometry (GC×GC-MS) experimental conditions. The CM applications and the FM ones were performed by using the same systems described in the previous section (*Section 5.1*). A mixture of 64 cosmetic allergens was employed to measure different chromatography parameters, such as peak widths, resolution and signal-to-noise ratios. It is noteworthy that the FM combination of columns has been proposed as a standard column set, and the results herein reported confirm those previously attained in recent research (see *Section 5.1*). In the previous investigation, very similar chromatography fingerprints were obtained on a sample of coconut bio-oil by using finely-tuned FM and CM GC×GC-MS experimental conditions (*Section 5.1*). The aim of the present research was to confirm the results attained previously on an entirely different type of sample, namely a mixture of 64 cosmetic allergens.

5.2.1 Experimental

5.2.1.1 Standard compounds and sample preparation

Two solutions containing 24 (fragrance allergen mix A1) and 40 (fragrance allergen mix A2) contact allergens (*Table 5.3*) were kindly provided by Merck Life Science (Merck KGaA, Darmstad, Germany). The two solutions were mixed and diluted with methyl tert-butyl ether to a concentration of 10 mg L^{-1}.

[ii] This section has been adapted from the following publication: **B.Giocastro**, I. Aloisi, M.Zoccali, P.Q. Tranchida, L.Mondello in "*Cryogenic-and Flow-modulation comprehensive two-dimensional gas chromatography-mass spectrometry: obtaining similar chromatography performances". LC-GC-Europe, 2020, 33 (10), 512-520.*

5.2.1.2 Instrumentation

Cryogenic-modulation GC×GC-MS

The CM analyses were performed on a GC×GC-MS system (Shimadzu, Kyoto, Japan) consisting of two independent (GC2010) gas chromatographs, a cryogenic loop-type modulator and a single quadrupole mass spectrometer (QP2010 Ultra). The first GC was equipped with an AOC-20i auto-injector and a split-splitless injector (280 °C). The injected volume was 1.7 μL, at a split ratio of 10:1.

The first dimension, an SLB-5ms [SLB-5ms - silphenylene polymer with similar polarity to poly(5% diphenyl/95% dimethyl siloxane)] 30 m × 0.25 mm ID × 0.25 μm d_f, was connected to an 1.5 m × 0.18 mm ID uncoated capillary column, used as delay loop. The loop was then connected to a 1.5 m × 0.25 mm ID × 0.25 μm d_f [SLB-35ms - proprietary polymer with similar polarity to poly(35% diphenyl/65% dimethyl siloxane) second-dimension column. The column-loop connections were made using two Trajan SilTite mini-unions (Ringwood, Victoria, Australia).

GC conditions: temperature program was 50-330 °C at 6 °C min^{-1} (in both GC ovens).

Carrier gas (He) conditions: constant average linear velocities of about 18.5, 80.4, and 103.9 cm s^{-1}, were generated in the first dimension, the delay loop, and the second dimension, respectively. Modulation was carried out by using a liquid nitrogen free chiller unit Zoex ZX2 (under license from Zoex Corporation, Houston, TX, USA). Modulation period was 4000 ms, with a hot pulse (280 °C) duration of 200 ms.

Mass spectrometry conditions: the sample was analyzed in the scan mode (electron ionization at 70 eV) using a mass range of 45–360 *m/z*, and a spectra generation frequency of 33 Hz; interface and ion source temperatures were 250 °C. Data were collected by using the GCMS Solution software (Shimadzu). Data processing was performed in both CM and FM applications by using the ChromSquare software v. 2.3 (Shimadzu). The mass spectral database used was the FFNSC 3.0 (Shimdazu).

Flow-modulation GC×GC-MS

The FM applications were carried out on a single-oven Shimadzu GCMS-TQ8040 system. The GC was equipped with an AOC-20i auto-injector and a split-splitless injector (280 °C). The injected volume was 1.7 μL, at a split ratio of 10:1.

The ^{1}D column was an SLB–5 ms 20 m × 0.18 mm ID × 0.18 μm d_f, while an SLB-35ms 5 m × 0.32 mm ID × 0.25 μm d_f column was used as ^{2}D. The columns were heated by using the same temperature program as in the CM applications.

Modulation was performed by using a 7-port wafer chip. The 7-port wafer chip was located inside the GC oven and was connected to a three-way solenoid valve by using two symmetric 1.07 m stainless steel tubings of dimensions 0.97 m × 0.51 mm ID + 0.10 m × 0.25 mm ID. The gas flow was supplied to the solenoid valve through an auxiliary pressure control (APC) unit. The modulator loop (stainless steel) was of dimensions 40 cm × 0.51 mm ID (volume = 78.6 μL). The seventh port was blocked (used for a second detector, if necessary). Carrier gas (He) conditions: average ^{1}D gas velocity was 12.3 cm s^{-1} [gas flow was approx. 0.24 mL min^{-1} (injection pressure: ≈ 61 kPa) and 0.20 mL min^{-1} (injection pressure: ≈ 155 kPa) at the beginning and at the end of the analysis, respectively]; loop gas velocity was about 1.9 cm s^{-1} during accumulation and approx. 68.0 cm s^{-1} during re-injection; the average ^{2}D gas velocity was approx. 257 cm s^{-1} [gas flow was approx. 8.4 mL min^{-1} (re-injection pressure: ≈ 13 kPa) and 7.1 mL min^{-1} (re-injection pressure: ≈ 79 kPa), at the beginning and at the end of the analysis, respectively].

Modulation period was 4000 ms, with a re-injection period of 400 ms.

Mass spectrometry conditions: the sample was analyzed in the scan mode (electron ionization at 70 eV) using a mass range of 45–360 *m/z*, and a spectra generation frequency of 33 Hz; interface and ion source temperatures were 250 °C.

5.2.2 Results and Discussion

As aforementioned, in previous research very similar CM GC×GC-MS and FM GC×GC-MS chromatography performances were attained by finely tuning the experimental conditions. Applications involved a sample of coconut fiber bio-oil and were carried out by using a single quadrupole (CM) and a triple quadrupole mass spectrometer (FM), both in the scan mode (*Section 5.1*). It is noteworthy that the ion sources were the same in both MS instruments; moreover, the first quadrupole and the collision cell in the triple quadrupole system wereoperated only as “fly through” zones, while the operational conditions of the second quadrupole were the same as those used in the single quadrupole MS instrument. The same MS systems have been used in the present investigation.

The main objective of the present study was to confirm the results attained previously on an entirely different type of sample, namely a 10 mg L^{-1} mixture of cosmetic allergens

(*Table 5.3*). Injection conditions, temperature program, types of stationary phases and modulation period (4000 ms) were the same in the CM and FM methods.

***Table 5.3**. Information related to compound identity, MS similarities, peak widths at half height, and signal to noise ratios in the CM and FM analyses. Average values of the data listed in the columns are reported on the last line and are in italics.*

Peak	Compound	MS similarity %		w_h (ms)		*s/n*	
		CM	FM	CM	FM	CM	FM
1	α-Pinene	97	94	140	170		
2	Benzaldehyde	97	94	190	210	302	41
3	β-Pinene	96	95	150	160		
4	α-Terpinene	96	92	140	170		
5	Limonene	97	92	140	180		
6	Benzyl alcohol	96	82	200	270		
7	Salicylaldehyde	95	86	210	240		
8	Terpinolene	95	94	150	160	901	262
9	Linalool	96	87	150	180	708	123
10	Camphor	96	95	190	180		
11	Menthol	96	94	160	180		
12	Methyl-2-octynoate	95	93	150	210		
13	α-Terpineol	95	88	170	200	486	149
14	Methyl salicylate	91	83	200	260		
15	Citronellol	96	92	150	190		
16	Neral	96	85	170	190		
17	Linalyl acetate	96	87	140	150		
18	Geraniol	95	81	150	190		
19	Carvone	96	93	180	190	382	112
20	Geranial	94	86	180	240		
21	Cinnamaldehyde	95	83	220	440		
22	Hydroxycitronellal	95	82	160	210		
23	Anise alcohol	94	84	180	320		
24	*trans*-Anethole	97	96	210	200	297	116
25	Cinnamyl alcohol	97	84	210	490		
26	Dimethylbenzylcarbinyl Acetate	94	81	160	170	530	232
27	Eugenol	93	88	180	220		
28	Geranyl acetate	96	87	150	170		
29	Δ-Damascone	96	96	170	170		
30	β-Damascenone	94	91	170	180		
31	α-Damascone	95	95	160	170		
32	Vanillin	97	88	230	280		
33	β-Damascone	96	92	160	180		
34	Trimethyl-benzenepropanol	94	89	170	240		
35	β-Caryophyllene	96	95	160	150		
36	Ebanol 1	94	91	150	180		
37	Ebanol 2	93	93	160	180		

Table 5.3.

Cont.

Peak	Compound	MS similarity %		w_h (ms)		*s/n*	
		CM	**FM**	**CM**	**FM**	**CM**	**FM**
38	Isoeugenol	92	84	200	210		
39	Coumarin	94	90	260	290		
40	α-Isomethylionone	93	91	160	170	523	252
41	Eugenyl acetate	93	92	180	200		
42	Butylphenyl methylproponial	90	91	180	180		
43	Amyl salicylate	94	93	180	190		
44	3-Propylidene phthalide	95	94	220	240	163	59
45	Isoeugenyl acetate	94	92	180	210		
46	α-Amylcinnamaldehyde	95	93	190	210	332	147
47	Lyral 2	88	81	190	220		
48	ISO E (β)	82	92	170	210		
49	Lyral 1	93	86	190	200		
50	ISO E (α)	85	85	200	180		
51	α-Santalol	95	88	220	200		
52	α-Amylcinnamyl alcohol	92	82	200	280		
53	ISO E (γ)	90	82	200	240		
54	*trans*,*trans*-Farnesol	94	85	160	190		
55	β-Santalol	94	87	180	190	544	67
56	α-Hexylcinnamaldehyde	94	92	180	220	622	99
57	Benzyl benzoate	95	95	210	240		
58	α-Acetyl cedrene	94	89	180	200		
59 + 60	Galaxolide (1+2)	93	86	220	170		
61	Benzyl salicylate	96	91	220	230	340	22
62	Hexadecanolact-16-one	94	93	180	180		
63	Benzyl cinnamate	94	90	250	270	183	35
64	Sclareol	92	85	210	200	278	32
	Average	*94*	*89*	*181*	*213*	*439*	*117*

CM GC×GC-MS method

The CM GC×GC-MS instrument was operated in the constant average linear velocity (CALV) mode: the ^{1}D (low polarity, 30 m × 0.25 mm ID × 0.25 μm d_f) CALV was approx. 18.5 cm s^{-1}, leading to a void time of about 162 s. The delay loop (1.5 m × 0.18 mm ID) gas velocity was approx. 80 cm s^{-1}, enabling a dual-stage modulation process. The ^{2}D (mid-polarity, 1.5 m × 0.25 mm ID × 0.25 μm d_f) CALV was about 100 cm s^{-1}, leading to a void time of approx. 1.4 s. The phase ratio of both analytical columns was ≈ 250.

The CM GC×GC-MS result is shown in *Figure 5.6*, which contains two wrap-around corrected chromatogram expansions to better visualize the 2D separation.

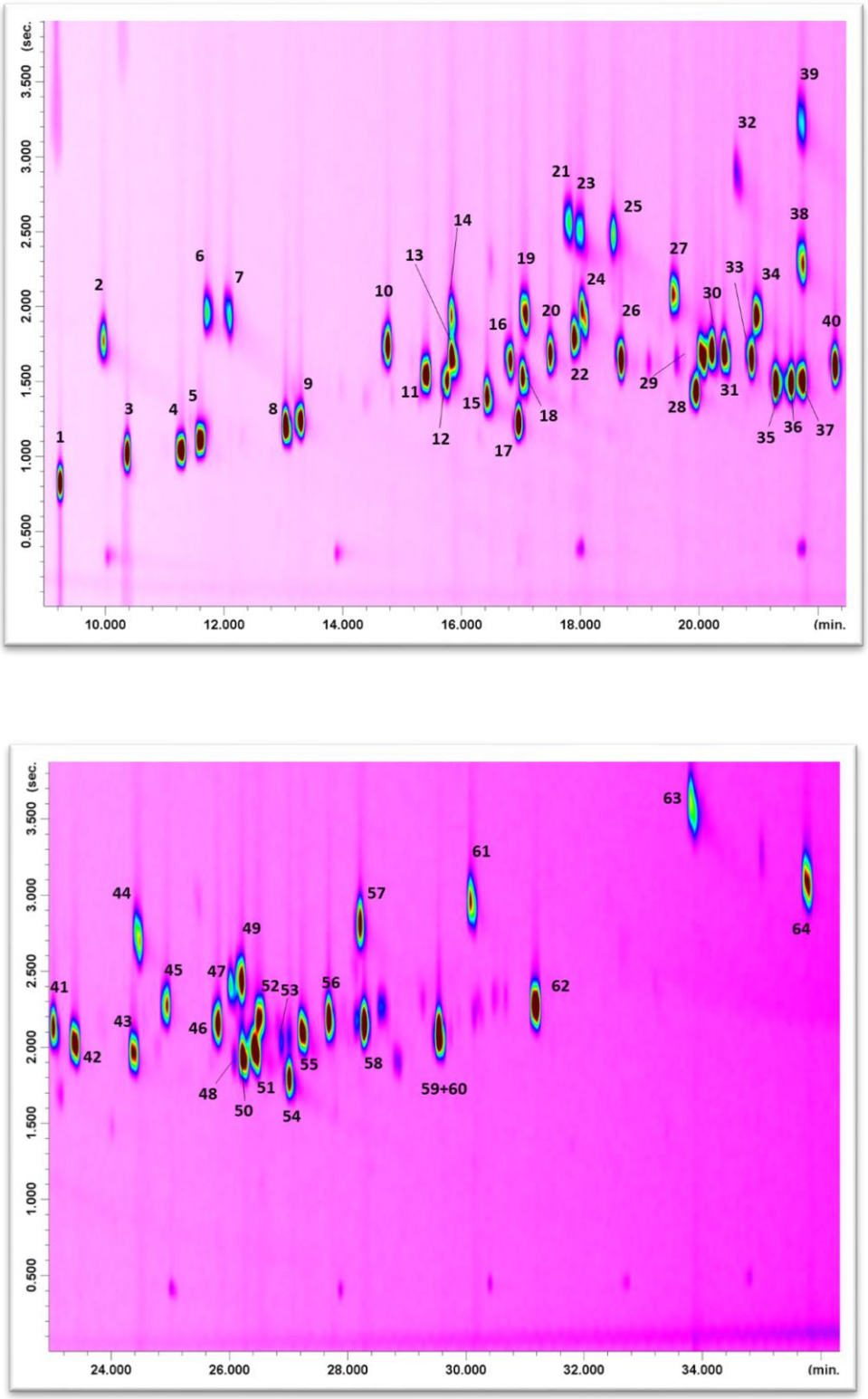

Figure 5.6. *Two cryogenically-modulated GC×GC-MS chromatogram expansions of 64 allergens. Peak identity can be found in Table 5.3.*

The ^{1}D retention time window in *Figure 5.6* is equal to approx. 27 min, or 405 modulations. Considering that the ^{2}D column, if operated under ideal chromatography conditions, could

generate about 6000 theoretical plates (*N*) [14], then this would lead to a potential overall *N* value of 2,430,000 (405 × 6000). The *N* value of the ^{1}D column again is not considered in such a calculation.

FM GC×GC-MS method

The FM GC×GC-MS system was operated as follows: the ^{1}D (20 m × 0.18 mm ID × 0.18 μm d_f) CALV was approx. 12.3 cm s^{-1}, leading to a void time of about 163 s (very similar to that of the CM method). The accumulation loop (40 cm × 0.51 mm ID) gas velocity conditions enabled two phases of accumulation and re-injection, thus a dual-stage process – two accumulation and two re-injection processes (see Section 2.2.2). The ^{2}D (5 m × 0.25 mm ID × 0.32 μm d_f) CALV was about 260 cm s^{-1}, leading to a void time of approx. 1.9 s. The phase ratios of the ^{1}D and ^{2}D columns were ≈ 250 and 320, respectively. The slightly higher ^{2}D void time in the FM method was, in part, counterbalanced by the higher column phase ratio, leading to a decrease in retention factors. The 7-port wafer chip was characterized by 5 ports on the front and 2 on the back for connections to the solenoid valve (Figure 1).

The FM GC×GC-MS result is shown in *Figure 5.7*, which again contains two wrap-around corrected chromatogram expansions. The ^{1}D retention time window is the same as that observed in the CM analysis. Considering that the ^{2}D column, if operated under ideal chromatography conditions, could generate *circa* 15,600 *N* [9], then this would lead to a potential overall *N* value of 6,318,000. Again, the efficiency of the ^{1}D column is not considered.

Comparison of the CM and FM results

A side-by-side measurement between MS similarities, peak widths at half height, and signal-to-noise ratios of both systems was made, with the results reported in *Table 5.3*.

The MS similarity, in both cases, is always higher than 80%, ranging between 82 and 97% for the CM system (with an average value of 94%), and between 81 and 96% for the FM system (with an average value of 89%). The higher values obtained in the CM analysis are due to the higher *s/n* values (see below). In fact, cryogenic modulation enables the ^{2}D injection of very narrow analyte bands, leading to enhanced sensitivity.

The average peak widths at half height were: 181 ms (ranging between 140-260 ms) for the CM system, and 213 ms (ranging between 150-490 ms) for the FM one.

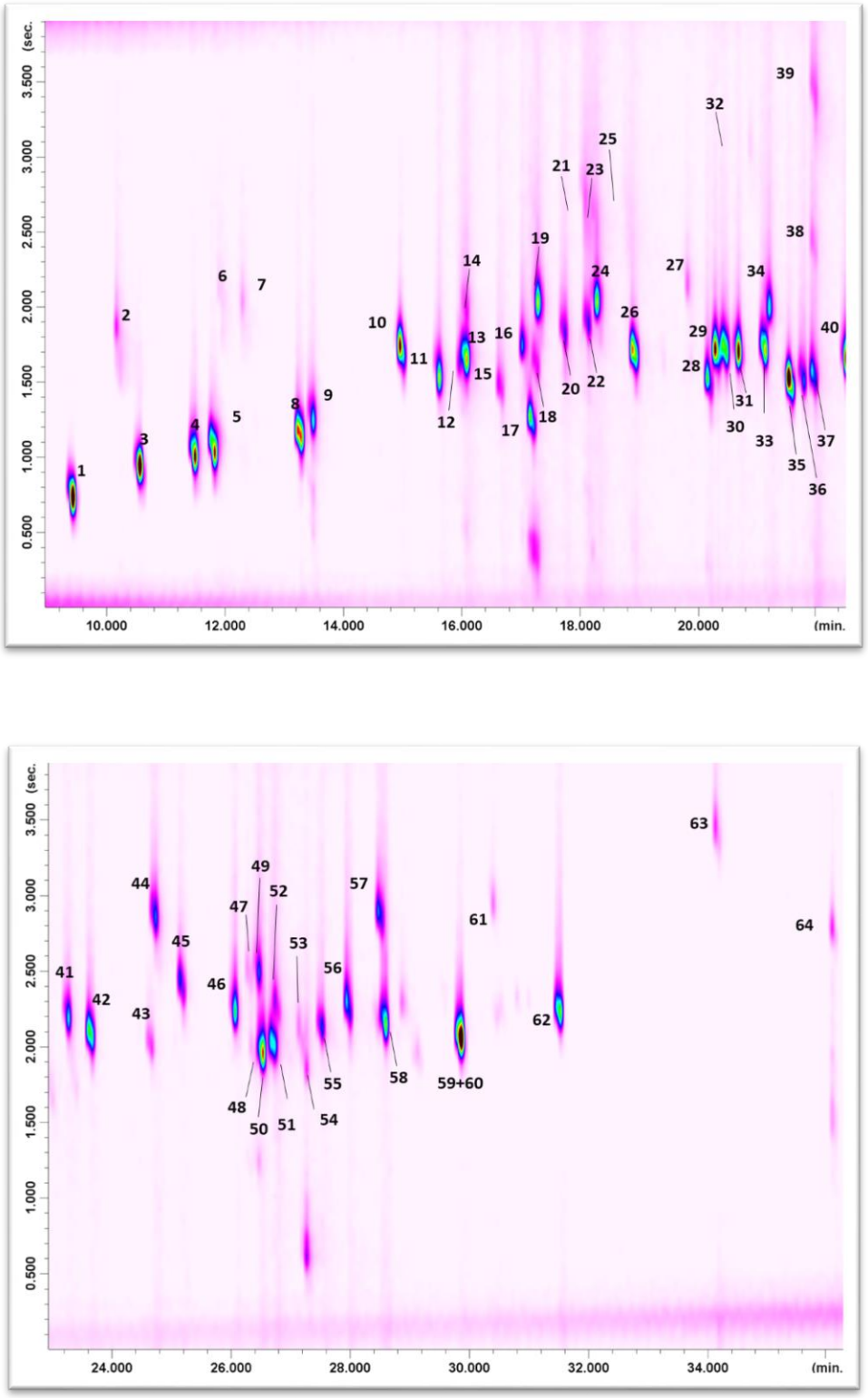

Figure 5.7. *Two flow-modulated GC×GC-MS chromatogram expansions of 64 allergens. Peak identity can be found in Table 5.3.*

The *s/n* values in *Table 5.3*, relative to 15 allergens, were the average values derived from three consecutive analyses. As expected, *s/n* values were always higher in the CM analysis, with an overall average increase by a factor of 3.8 (439 against 117).

First dimension retention times were similar, albeit slightly lower in the CM analysis: for eleven compounds (distributed over six pairs) spanning the chromatogram the minimum and maximum differences were 11.3 and 19.3 s, respectively (*Table 5.4*). Such retention time differences caused ^{1}D minimum and maximum elution temperature differences of about 1.1 and 1.9 °C, respectively (for the eleven compounds). Combining such a factor (increasing CM ^{2}D retention), with the lower CM ^{2}D column phase ratio (increasing retention) and the lower CM ^{2}D void time (reducing retention times), lead to a general increase in CM ^{2}D retention times. Again, considering the eleven compounds, the minimum and maximum differences were 0.47 and 0.72 s, respectively, leading to an increase in retention factor (*k*) values of just over a unit in the CM analysis *(Table 5.4).*

Table 5.4*. Information related to ^{1}D retention times ($^{1}t_R$), ^{2}D retention times ($^{2}t_R$) and related k values, N and resolution values (R_s) for six couples of compounds. Average N values are reported on the last line.*

Compound	CM					FM				
	$^{1}t_R$ (min)	$^{2}t_R$ (s)	*k*	*N*	R_s	$^{1}t_R$	$^{2}t_R$	*k*	*N*	R_s
13. Terpineol α	15.845	4.27	2.0	3495	0.8	16.099	3.55	0.8	1745	0.8
14. Methyl salicylate	15.845	4.54	2.1	2855		16.099	3.88	1.0	1234	
23. Anise alcohol	18.045	5.11	2.5	4465	1.5	18.233	4.6	1.4	1145	1.4
24. *trans*-Anethole	18.045	4.6	2.2	2658		18.299	3.94	1.0	2150	
37. Ebanol 2	21.778	4.12	1.9	3673	2.7	21.966	3.49	0.8	2083	2.6
38. Isoeugenol	21.778	4.93	2.4	3366		21.966	4.36	1.2	2388	
38. Isoeugenol	21.778	4.93	2.4	3366	2.4	21.966	4.36	1.2	2388	2.5
39. Coumarin	21.778	5.86	3.1	2814		21.966	5.41	1.8	1928	
51. α-Santalol	26.511	4.57	2.2	2391	0.8	26.699	3.97	1.0	2183	0.6
52. α-Amylcinnamyl alcohol	26.511	4.87	2.4	3285		26.766	4.21	1.2	1252	
57. Benzyl benzoate	28.311	5.44	2.8	3718	2	28.499	4.81	1.5	2225	1.9
58. α-Acetyl cedrene	28.311	4.78	2.3	4380		28.633	4.06	1.1	2283	
Average				*3372*	*1.7*				*1917*	*1.6*

Plate numbers were also calculated, and were always higher in the CM analysis: the average *N* values calculated for the eleven compounds in the CM and FM analyses were 3372 and 1917 respectively (*Table 5.4*).

Resolution was calculated for six pairs of compounds, the obtained values are reported in *Table 5.4*. As can be seen, the values for CM system are slightly higher with an average value of 1.7 (ranging between 0.8-2.7), while an average value of 1.6 was obtained for FM system (ranging between 0.6-2.6).

5.2.3 Conclusions

To conclude, it can be affirmed that the results attained in the present research confirm those reported previously (*Section 5.1*). In fact, the proposed standard FM GC×GC-MS column set provided an altogether similar chromatography result compared to that obtained by using a CM GC×GC-MS standard column set. The main difference relates to the average plate numbers, which were previously found to be slightly higher in the FM approach (average *N* values for 5 compounds: 2978 *vs.* 2680) (*Section 5.1*). Such a divergence could be due to the fact that, in the previous research, a 4× higher amount was analyzed in the FM analysis, to counterbalance the higher CM sensitivity. In the present research, equal sample amounts were subjected to analysis using the two methods, leading to lower signals in the FM analyses. Even so, and on the basis of the results attained, the FM GC×GC-MS column set proposed, can be potentially considered as a standard GC×GC column combination within the context of flow-modulated applications.

References

[1] Z. Liu, J.B. Phillips, J. Chromatogr. Sci. 29 (1991) 227.

[2] M. Edwards, A. Mostafa, T. Góreki, Anal. Bioanal. Chem. 401 (2011) 2335.

[3] H.D. Bahaghighat, C.E. Freye, R.E. Synovec, TrAC Trend. Anal. Chem. 113 (2019) 379.

[4] J.V. Seeley, N.J. Micyus, J.D. McCurry, S.K. Seeley, Am. Lab. 38 (2006) 24.

[5] P.Q. Tranchida, G. Purcaro, A. Visco, L. Conte, P. Dugo, P. Dawes, L. Mondello, J. Chromatogr. A 1218 (2011) 3140.

[6] M. Poliak, M. Kochman, A. Amirav, J. Chromatogr. A 1186 (2008) 189.

[7] P.Q. Tranchida, F.A. Franchina, P. Dugo, L. Mondello, J. Chromatogr. A 1255 (2012) 171.

[8] J.V. Seeley, S.K. Seeley, E.K. Libby, Z.S. Breitbach, D.W. Armstrong, Anal. Bioanal. Chem. 390 (2008) 323.

[9] P.Q. Tranchida, F.A. Franchina, P. Dugo, L. Mondello, Chromatogr. A 1359 (2014) 271.

[10] P.Q. Tranchida, F.A. Franchina, P. Dugo, L. Mondello, J. Chromatogr. A 1372 (2014) 236.

[11] L. Mondello, A. Casilli, P.Q. Tranchida, M. Lo Presti, P. Dugo, G. Dugo, Anal. Bioanal. Chem. 389 (2007) 1755.

[12] P.Q. Tranchida, M. Zoccali, F.A. Franchina, A. Cotroneo, P. Dugo, L. Mondello, J. Chromatogr. A 1314 (2013) 216.

[13] M.S. Klee, J. Cochran, M. Merrick, L.M. Blumberg, J. Chromatogr. A 1383 (2015) 151.

[14] F. David, D.R. Gere, F. Scanlan, P. Sandra, J. Chromatogr. A 842 (1999) 309.

Page intentionally left blank

Chapter 6

Research in the field of comprehensive 2D GC-MS using milder electron ionization conditions†

6.1 Introduction

The present research is based on the use of comprehensive two-dimensional gas chromatography-quadrupole mass spectrometry (GC×GC-QMS), using "milder" electron ionization (EI) conditions. The term milder refers to the use of 20-eV EI conditions, instead of the by-far-most-popular electron energy of 70 eV. The effects of using milder EI conditions were evaluated in the GC×GC-QMS analysis of a variety of different molecular-mass compounds with various polarities (*e.g.*, sterols, linear alkanes, fatty acid methyl esters, vitamin E, squalene, a linear alcohol, and a group of fifteen pesticides).

In general, the results attained indicate that milder EI conditions, and lower source temperatures, generate mass spectra with a higher relative abundance of ions at higher mass-over-charge (*m/z*) values, comprising the molecular ion, and reduced fragmentation at lower *m/z* values. The extent to which such a phenomenon occurred was obviously related to the chemical structure of each analyte. Spectral repeatability was also assessed, and was found to be satisfactory. Finally, with regard to analyte signalto-noise ratios these were generally comparable in applications involving different electron ionization energies.

† This Chapter has been adapted from the following publication: P. Q. Tranchida, I. Aloisi, **B. Giocastro**, M. Zoccali, L. Mondello.in "*Comprehensive two-dimensional gas chromatography-mass spectrometry using milder electron ionization conditions: a preliminary evaluation." Journal of Chromatography A, 2019, 1589, 134-140.*

In a recent review article focused on comprehensive two-dimensional gas chromatography-mass spectrometry (GC×GC-MS), covering the four-year period 2014-2017, it was found that 70-eV electron ionization (EI) was used in more than 90% of the published work [1]. Such a form of ionization is characterized by many well-known advantages and disadvantages, with the former consisting mainly in the generation of highly-repeatable, analyte-specific mass spectral fingerprints and by the fact that commercially-available MS databases are formed of 70-eV EI spectra. On the other hand, the excessive formation of low-mass fragment ions, and the reduced intensity, or the absence, of the molecular ion (MI) are two main drawbacks.

Considering the EI MS process of organic molecules, these are characterized by specific ionization efficiency curves, which most often have a maximum value at an ionization energy (IE) of 70 eV. The use of such an IE, widely in excess of that necessary to remove an electron from an analyte, will guarantee a high degree of ionization efficiency, but will often lead to excessive fragmentation; on the other hand, the use of a lower IE will lead to reduced fragmentation, at the cost of a lower ionization efficiency [2,3].

The combination of GC×GC, with various forms of 70-eV EI single-analyzer MS, forms a three-dimensional technology [4-7], with five possible levels (or points) of identification: I and II) retention values on the two GC columns (^1t_R and ^2t_R); III) the formation of chemical class patterns; IV) the entire mass spectral fingerprint; V) molecular mass. With regard to levels I, II and IV, these are always present, while level III depends mainly on sample composition (*i.e.*, presence or not of homologous series of compounds), and level V on the presence of the MI. The latter occurrence is often hindered by the 70-eV EI process [1]. A four-dimensional technology, with more than five levels of identification, can be generated by using a dual-analyzer MS system [8].

An ideal ionization process should maintain both the MS fingerprinting capability and the MI information; to pursue such an objective different “soft” ionization technologies have been exploited in the GC×GC-MS field, such as photoionization [9,10], chemical ionization [11], supersonic molecular beam EI [12-14], atmospheric pressure chemical ionization [15], variable EI [16], and field ionization [17]. In particular, the use of photoionization and supersonic molecular beam EI have been strongly-emphasized forms of soft ionization for GC×GC-MS analyses [9,10, 12-14]. Single photon ionization (SPI) is induced by using a pulsing laser, generating vacuum ultraviolet (VUV) photons with a sufficientenough energy to promote soft and universal ionization [9]. A GC × GC MS instrument, with the capability to provide both SPI and EI spectra, in an alternate manner during the same

analysis, has also been described [10]. With regard to the SMB EI process, an approach also defined as "cold EI", the ionization of vibrationallycooled compounds occurs in a fly-through EI ion source, producing particularly-evident MIs for analytes containing 15 or more atoms. Apart from soft ionization, other advantages of cold EI are represented by the possibility to operate at high gas flows (emphasized in flow modulation studies) and by a reduction of source-related peak tailing [12–14]. The use of milder EI conditions has been previously reported using modern MS instruments. For example, Shimma et al. analysed polychlorinated biphenyls using GC combined with miniaturized high-resolution time-of-flight mass spectrometry (GC-HR ToFMS) [19]. The GC-HRToFMS applications were performed at anEI energy of 18 eV (several EI conditions were evaluated), because it enabled a more intense signal for the quantification ion of heptachlorobiphenyl. In a very recent study, Polet et al. used GC combined with a quadrupole (Q)ToFMS system for the screening of doping agents in urine [20], using an EI energy of 18 eV, under both scan and MSMS conditions. With regard to the field of comprehensive two-dimensional GC, Wong et al. used GC × GC-QToFMS for the analysis of an oleoresin, with an EI energy of 30 eV, to increase the relative abundance of the molecular ions [21].

The use of GC×GC combined with single quadrupole mass spectrometry (QMS), under milder EI conditions (< 70 eV), is herein evaluated in applications involving the unsaponifiable fraction of a sample of extra-virgin olive oil, and homologous series of pure standard compounds (linear alkanes and fatty acid methyl esters). The mass spectral results attained were compared with those derived from GC×GC-QMS analyses, performed at an IE of 70 eV. To the best of the authors' knowledge, the evaluation of milder EI conditions, by using a classical EI source, has not been previously reported in the GC×GC-MS field.

6.2 Experimental

6.2.1 Sample, standard compounds, and sample preparation

A sample of genuine extra-virgin olive oil was provided by a producer from the Italian region of Puglia. The BSTFA [N,O-bis(trimethylsilyl)trifluoroacetamide] + 1% TMCS (trimethylchlorosilane) kit was supplied by Merck KGaA (Darmstadt, Germany). Powdered anhydrous sodium sulfate was purchased from AppliChem (Milan, Italy). The C_7-C_{30} alkane and C37 fatty acid methyl ester (FAME) mixtures, as well as the pesticides, were supplied by Merck KGaA.

Isolation and derivatization of the unsaponifiable fraction of the olive oil was performed by using a previously-used procedure [18].

6.2.2 Instrumentation

All GC×GC-QMS applications were performed on a system formed of two Shimadzu GC-2010 gas chromatographs, and a QP2020 quadrupole mass spectrometer (Kyoto, Japan). Data were acquired by using the GCMS solution software (Shimadzu). Bidimensional chromatograms were generated by using the ChromSquare software v. 2.3 (Shimadzu).
The first gas chromatograph (GC1) was equipped with an AOC-20i auto-injector, and a split–splitless injector. The first-dimension column was an SLB-5ms [(silphenylene polymer which can be considered equivalent in polarity to poly (5%diphenyl/95% dimethylsiloxane)] with dimensions 30 m × 0.25 mm ID × 0.25 μm d_f. The second-dimension column (housed in the second oven - GC2) was an SLB-35ms [(polymer which can be considered equivalent in polarity to poly (35%diphenyl/65% dimethylsiloxane)] with dimensions 3 m × 0.25 mm ID × 0.25 μm d_f. A 1 m segment of the ^{2}D column was used to create the delay loop, leaving approx. a 1.5 m segment for the analytical separations. All the columns used were provided by Merck KGaA. The connection between the columns was made by using a SilTite mini union (Trajan, Ringwood, Victoria, Australia).

Extra-virgin olive oil unsaponifiable fraction: helium was supplied at the GC1 inlet at a pressure of 60 kPa (constant linear velocity mode); volume and mode of injection (360°C): 1 μL in the split mode (30:1); GC1 temperature program: 90-280°C at 15°C min^{-1}, 280-330°C at 2.5°C min^{-1}, 330-360°C at 15°C min^{-1}; GC2 temperature program: +20°C offset (until 360°C, when an isothermal period of 1.3 min began).
Modulation was performed by using a cryogenic modulator (under license from Zoex Corporation); modulation period was 3.5 s (the heating step was performed at 360°C, for 0.3 s).
Mass spectrometry conditions: the temperature of the interface was 330°C; the ion source temperature was 250°C, with analyte fragmentation induced by electron ionization at different energies (70, 40, 20 eV), and the detector voltages set at different values through the autotuning process (see Results and Discussion). A mass range of *m/z* 50-520 and a spectral generation frequency of 33 Hz were applied.

Fatty acid methyl esters and linear alkanes: He was supplied at the GC1 inlet at a pressure of 45.6 kPa (constant linear velocity mode); volume and mode of injection (310°C): 1 μL in the split mode (50:1); GC1 and GC2 temperature programs: 50-300°C at 5°C min^{-1}. Modulation period was 2.5 s (the heating step was performed at 340°C, for 0.2 s).
Mass spectrometry conditions: the temperature of the interface was 300°C; the ion source temperature was 250°C, with analyte fragmentation induced by electron ionization at different energies (70, 40, 20 eV), and the detector voltages set at different values through the autotuning process. A mass range of *m/z* 50-500 and a spectral generation frequency of 33 Hz were applied.

Pesticides: helium was supplied at the GC1 inlet at a pressure of 76.8 kPa (constant linear velocity mode); volume and mode of injection (310 °C: 0.5 μL in the split mode (100:1); GC1 and GC2 temperature programs: 120–350 °C at 5 °C min^{-1}. Modulation period was 2.5 s (the heating step was performed at 340 °C, for 0.2 s).
Mass spectrometry conditions: the temperature of the interface was 310 °C; the ion source temperatures were 250 °C, 200 °C and 150 °C. Analyte fragmentation was induced by electron ionization at different energies (70 and 25 eV). A mass range of m/z 50–450 and a scan rate of 33 Hz were applied. In general, autotuning processes were performed every time an ion source condition was modified (EI energy or ion source temperature). The detector voltages (DVs) varied between the different types of applications (see Results and Discussion), and were obviously related to the tuning result.

6.3 Results and Discussion

The objective of the research was to evaluate mass spectral behaviours in GC × GC-QMS experiments, using milder ionization conditions. A series of applications were carried out at different EI energies. The DV values, set through the automatic tuning process, obviously tended to increase at lower EI energies, to contrast the reduction in analyte ionization efficiency, and thus in sensitivity. Below an EI of 50 eV, the ionization efficiency falls very rapidly [2,3].Allthe DVvalues used inthe present research were well below the maximum value recommended by the manufacturer (2.0 kV). The use of enhanced DVs can, however, reduce the lifetime of the detector. The scan rate was maintained constant in all the applications (33 Hz), it being sufficient for the generation of at least 10 data points per peak. The mass range varied slightly, in relation to the type of sample subjected to analysis.

It is herein defined, in an arbitrary manner and with the scope to facilitate a comparative study, that an“evident”molecular ion is one with a mass spectrum relative abundance of minimum 2.0%.

6.3.1 Phytosterols

The unsaponifiable fraction of a sample of extra-virgin olive oil was subjected to GC × GC-QMS analysis, with initial focus on the phytosterols, under the form of trimethylsilyl (TMS) ethers. The GC × GC-QMS applications were carried out at EI energies of 70, 40 and 20 eV, and DVs of 0.85, 0.88 and 1.10 kV, respectively. In all three experiments analyte signal-to-noise ratios (*s/n*) were rather similar [total ion current (TIC) result], with both the background noise and peak intensities increasing with the DV value.

Chromatogram expansions, related to the 70-eV and 20-eV analyses, are shown in *Figure 6.1*. Both chromatograms were obtained by setting the same values of minimum and maximum signal intensity (z-axis values). Four phytosterols, the presence of which is regulated in olive oils [23], are indicated in both expansions

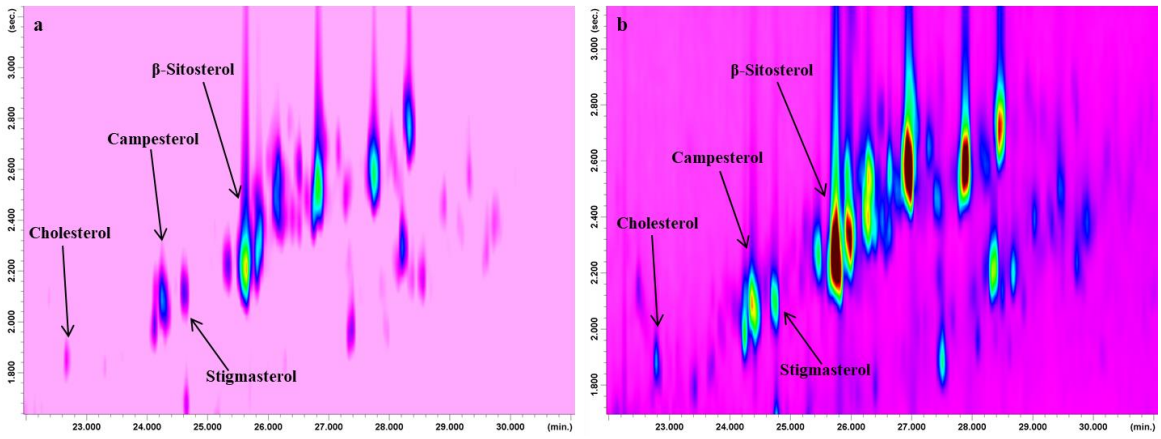

Figure 6.1. *Chromatogram expansions (reporting the sterol zone) relative to the GC×GC-QMS analysis of the unsaponifiable fraction of a sample of extra-virgin olive oil performed at ionization energies of 70 eV (a) and 20 eV (b). Minimum z-axis intensity: -14371; maximum z-axis intensity: 3.5155e +07.*

The *s/n* values (n = 3), calculated for the four phytosterols (the most intense modulated peak was considered) were comparable (as can be derived from the total average values), and are listed in *Table 6.1*.

Table 6.1. *Signal-to-noise ratio values (n = 3) for four phytosterols attained under different EI energies, along with the total average s/n values.*

	70 eV	**40 eV**	**20 eV**
Cholesterol	157	147	114
β-Sitosterol	1901	1271	1783
Campesterol	673	807	822
Stigmasterol	271	228	205
Average s/n	*751*	*613*	*731*

Having concluded that, under milder EI scan conditions, and for the specific analytes in question, there were no substiantial reductions in the *s/n* values, attention was focused on the mass spectral profiles. The averaged mass spectra for campesterol (the baseline noise was subtracted), under 70-, 40-, and 20-eV EI conditions, are shown in *Figure 6.2.* Attention was directed to seven ions (presumed identities are reported in *Table 6.2*), comprising the MI, and spanning the mass spectrum.

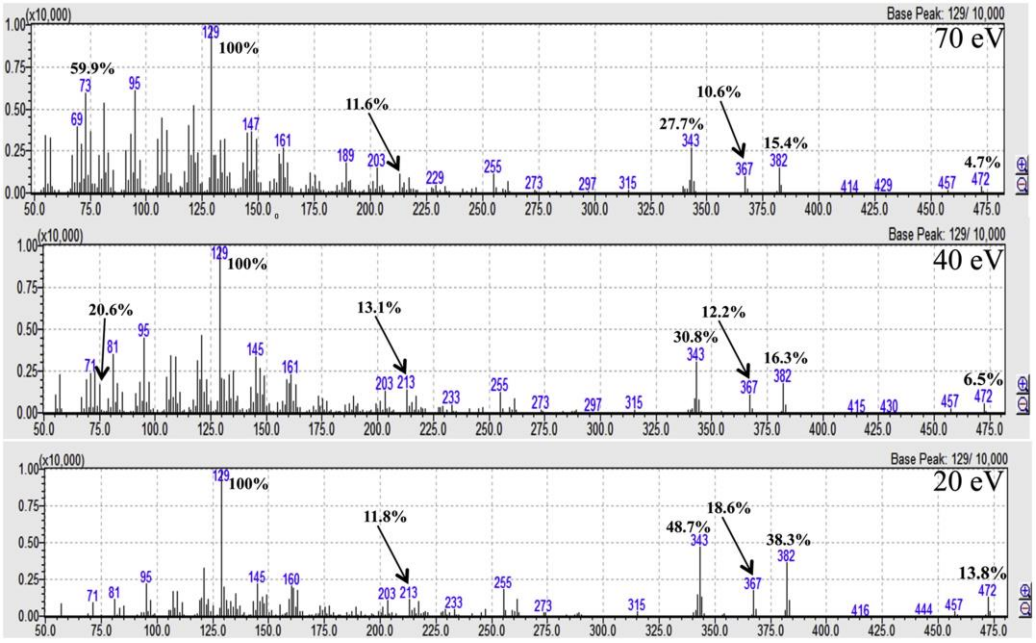

Figure 6.2. *Mass spectra for campesterol attained under 70-, 40- and 20-eV EI conditions; presumed identities of the indicated ions can be found in Table 6.2.*

As can be readily seen, the differences between the 70-eV and 40-eV mass spectra are only slight, with the main one being a reduced fragmentation below *m/z* 129 in the 40-eV spectrum. On the contrary, the differences were much greater between the 70-eV and 20-eV mass spectra: in the latter, the % value of the MI (*m/z* 472) increased by a factor of nearly 3, while other high-mass diagnostic fragments (*m/z* 382, 367, 343) were also

enhanced. Middle-mass ions, such as the *m/z* 213 and 129 (base peak) ions, remained basically unaltered, while fragmentation below *m/z* 129 is greatly reduced. For instance, the *m/z* 73 ion was the third most intense ion under 70-eV EI conditions, while it was not visible in the 20-eV EI spectrum. A similar (though not identical) trend was observed for the other three phytosterols, with the results attained under 70-eV and 20-eV conditions listed in *Table 6.2*. Considering the four MIs, the average degree of enhancement was by a factor of 2.8. On the other hand, the average degree of relative abundance reduction for the ion $[Si(CH_3)_3]^+$at *m/z* 73 was by a factor of approx. 33 (campesterol was not considered).

***Table 6.2**. Relative abundances for seven ions present in the 70- and 20-eV EI mass spectra of cholesterol, campesterol, β-sitosterol, and stigmasterol (the first values always refers to the 70-eV EI result), indicated in the two chromatogram expansions shown in Figure 6.1. Abbreviation: SC = side chain.*

Ion	Cholesterol%	Campesterol%	β-Sitosterol%	Stigmasterol%
1. $[M]^{+\bullet}$	4.7/8.6 (458)	4.7/13.8 (472)	6.5/24.5 (486)	3.1/8.9 (484)
2. $[M\text{-TMSOH}]^{+\bullet}$	12.7/30.7 (368)	15.4/38.3 (382)	22.1/64.5 (396)	5.2/16.1 (394)
3. $[M\text{-TMSOH-}CH_3]^+$	11.2/20.2 (353)	10.6/18.6 (367)	11.4/24.1 (381)	2.6/6.7 (379)
4. $[M\text{-}129]^+$	25.6/49.7 (329)	27.7/48.7 (343)	29.6/68.7 (357)	2.9/7.8 (355)
5. $[M\text{-SC-}42\text{-TMSOH}]^+$	11.8/11.9 (213)	11.6/11.8 (213)	10.4/12.6 (213)	9.3/13.9 (213)
6. $[C_6H_{12}SiO]^+$	100/100 (129)	100/100 (129)	100/100 (129)	41.8/54.3 (129)
7. $[Si(CH_3)_3]^+$	40.1/2.2 (73)	59.9/ - (73)	50.7/1.7 (73)	30.0/0.6 (73)

6.3.2 Fatty acid methyl esters

On the basis of the results attained on the phytosterols, GC×GC-QMS applications under 70-eV and 20-eV EI conditions were carried out on a standard mixture of thirty-seven FAMEs. As previously observed for the phytosterols, *s/n* values of the FAMEs in the two applications were similar, while substantial between-spectra differences were observed. Again, attention was directed to several ions across the mass spectra of the FAMEs. The results for five saturated FAMEs (C_{14}, C_{16}, C_{18}, C_{20}, C_{22}) are reported in *Table 6.3*, along with the presumed identity of the seven ions considered.

***Table 6.3**. Relative abundances for to seven ions present in the mass spectra of C14:0, C16:0, C18:0, C20:0, and C22:0 along with the peak s/n values, under 70- and 20-eV EI conditions (the first values always refers to the 70-eV EI result).*

Ion	$C_{14:0}$%	$C_{16:0}$%	$C_{18:0}$%	$C_{20:0}$%	$C_{22:0}$%
1. $[M]^{+\bullet}$	1.4/3.0 (242)	2.4/3.7 (270)	1.7/5.2 (298)	2.9/6.7 (326)	3.6/10.0 (354)
2. $[M\text{-}OCH_3]^+$	2.0/4.1 (211)	2.5/2.8 (239)	1.4/1.9 (267)	1.1/2.1 (295)	0.7/0.8 (323)
3. $[M\text{-}C_3H_7]^+$	7.4/9.5 (199)	6.0/9.5 (227)	6.8/10.1 (255)	4.5/9.4 (283)	3.8/7.6 (311)
4. $[M\text{-}C_5H_{11}]^+$	1.5/0.7 (171)	3.6/4.5 (199)	1.2/2.0 (227)	2.2/3.6 (255)	1.4/0.9 (283)
5. $[M\text{-}C_7H_{15}]^+$	15.0/24.3 (14	6.0/4.6 (171)	5.9/7.9 (199)	4.9/5.9 (227)	5.7/9.1 (255)
6. $[CH_3CH_2COOCH_3]^+$	85.5/62.8 (87	84.7/67.3 (87)	90.7/65.5 (87)	92.0/67.3 (87)	85.1/74.2 (87)
7. $[CH_2COHOCH_3]^{+\bullet}$	100/100 (74)	100/100 (74)	100/100 (74)	100/100 (74)	100/100 (74)
s/n	*103/139*	*158/189*	*100/92*	*69/53*	*87/47*

Higher-mass ions were more intense in the 20-eV EI spectra, while the opposite occurred for the lower mass ones (*e.g.*, $[CH_3CH_2COOCH_3]^+$). For the $[M\text{-}C_5H_{11}]^+$ ion the relative abundances were always increased in the 20-eV applications, except for C14:0 and C22:0; for the $[M\text{-}C_7H_{15}]^+$ ion, the relative abundances were always lower in the 70-eV applications, except for C16:0. Considering the five MIs of the saturated FAMEs, the average degree of enhancement was by a factor of 2.4. Additionally, in 2 cases the MI was characterized by an intensity lower than 2.0% under 70-eV EI conditions, and was always well over such an intensity level under milder EI conditions. The overall average s/n values, for the five saturated FAMEs, were 103 and 104, in the 70-eV and 20-eV applications, respectively (single TIC s/n values are reported in *Table 6.3*).

The mass spectra relative to the unsaturated FAMEs also differed, with the results for C14:1ω5, C18:1ω9, C20:1ω9, C18:2ω6, and C20:2ω6, listed in *Table 6.4*. Specifically, the percentages of three diagnostic ions were considerably increased using the milder EI conditions: average degrees of percentage enhancement were by factors of 11.2, 6.1, and 2.3, for the ions $[M]^{\bullet+}$, $[M\text{-}OCH_3]^+$ (plus $[M\text{-}32]^{\bullet+}$), and $[M\text{-}CH_2COHOCH_3]^{+\bullet}$, respectively.

***Table 6.4**. Relative abundances for three diagnostic ions present in the mass spectra of C14:1ω5, C18:1ω9, C20:1ω9, C18:2ω6, and C20:2ω6 along with the peak s/n values, under 70- and 20-eV EI conditions (the first values always refers to the 70-eV EI result).*

Ion	$C_{14:1\omega5}$%	$C_{18:1\omega9}$%	$C_{20:1\omega9}$%	$C_{18:2\omega6}$%	$C_{20:2\omega6}$%
1. $[M]^{+\bullet}$	0.9/5.4 (240)	0.1/2.7 (296)	0.3/2.3 (324)	0.8/2.3 (294)	0.7/8.6 (322)
2. $[M-32]^{+\bullet}$	5.9/30.9 (208)	5.9/47.5 (264)	6.2/20.1 (292)		
3. $[M-OCH_3]^+$				1.1/5.5 (263)	1.0/9.1 (291)
4. $[M-CH_2COHOCH_3]^{+\bullet}$	12.9/37.8 (166)	3.7/10.9 (222)	5.9/15.1 (250)	2.9/4.8 (220)	1.3/1.6 (248)
s/n	*72/91*	*50/53*	*46/25*	*25/21*	*44/33*

Moreover, in all cases the MI was characterized by an intensity lower than 1% under 70-eV EI conditions, and was always over the 2% level under milder EI conditions. As an example, the mass spectra for the FAME C14:1ω5 (molecular mass = 240.22 u), under hard and milder EI conditions, are reported in *Figure 6.3*.

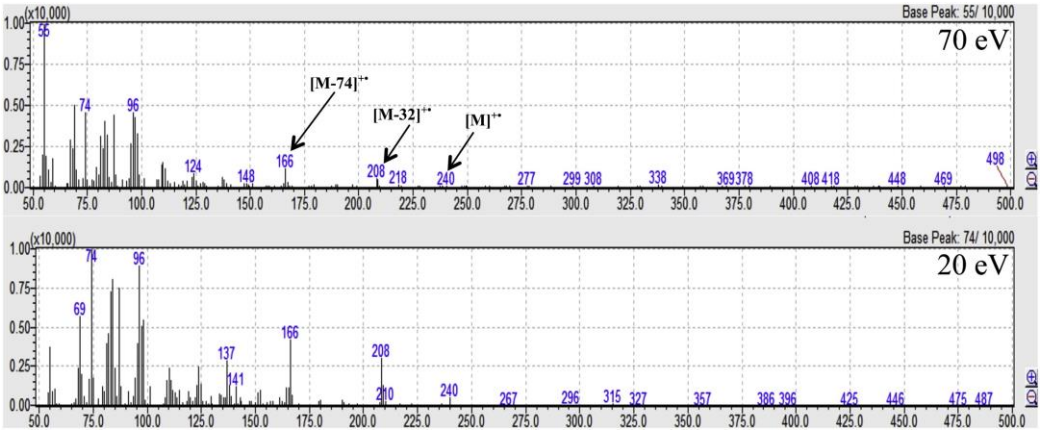

***Figure 6.3.** Mass spectra for the FAME C14:1ω5 attained under 70- and 20-eV EI conditions.*

As can be readily seen, all the diagnostic ions are more intense under 20-eV conditions, while the fragmentation profile is modified (rather than being reduced) at the low masses (below *m/z* 100). The overall average TIC s/n values, for the five unsaturated FAMEs, were 47 and 45, in the 70-eV and 20-eV applications, respectively (single s/n values are reported in *Table 6.4*)

6.3.3 Hydrocarbons, pesticides and other compounds

The mass spectral behaviour of linear alkanes, under 70-eV conditions, is well known, inasmuch that only the lower mass compounds present a distinguishable MI. Moreover, the intensity of the latter tends to diminish as the chain length increases [26]. A standard C7-C30 series of linear alkanes was subjected to GC×GC-QMS analysis, under hard and milder EI conditions; the relative abundances for the molecular ions, within the C10-C20

range, are listed in *Table 6.5*. As can be seen, the intensity of the $[M]^{\bullet+}$ ion gradually decreases with an increase in chain length, under both ionization conditions. However, for the C10 alkane the intensity of the molecular ion increased by a factor approx. 3.7, under 20-eV EI conditions. Moreover, C12 was the heaviest alkane with an evident molecular ion (2.0%), under hard ionization conditions, while C17 was the heaviest alkane with an evident molecular ion (2.1%), under milder ionization conditions. The 70-eV and 20-eV EI extracted-ion chromatograms (EICs), generated by using the eleven molecular ions across the C10-C20 alkane range, are shown in *Figure 6.4* (*m/z* values of the MIs are reported only for C10 and C20).

Both EICs were again visualized by using the same difference between minimum and maximum intensity levels. The differences between the signals in the two EICs are evident.

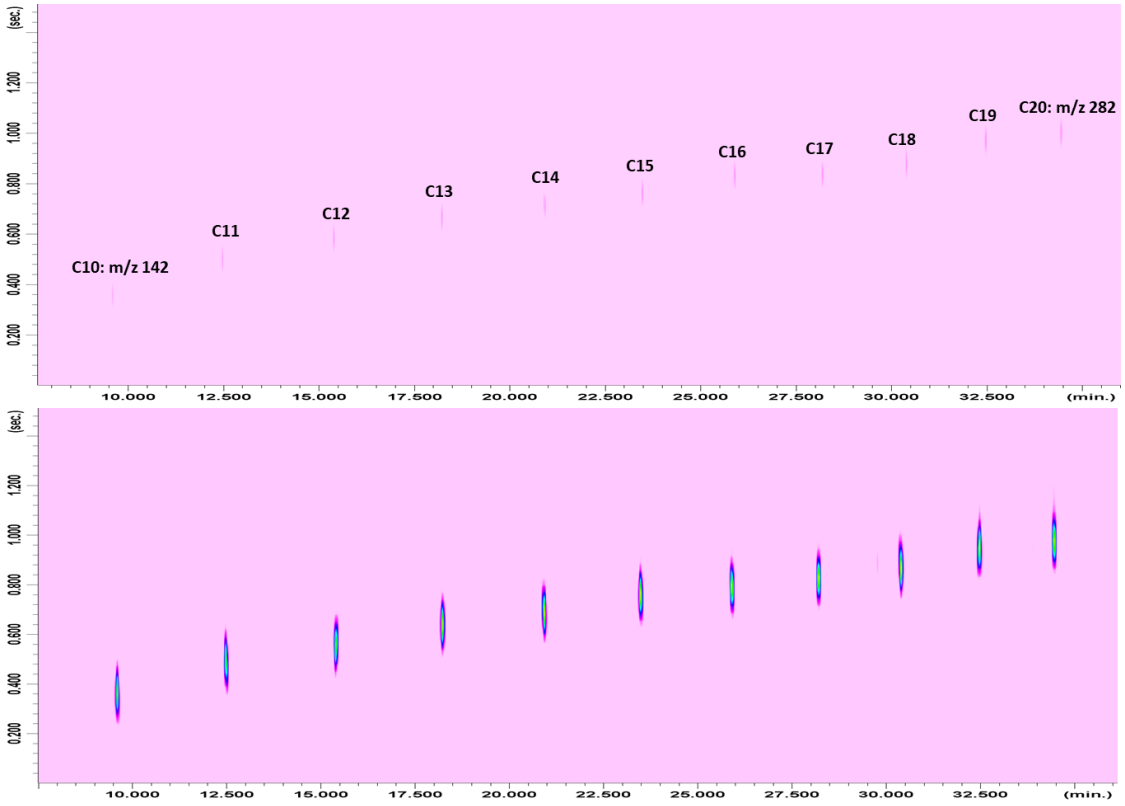

Figure 6.4. *Extracted-ion-chromatogram expansions relative to C10-C20 linear alkanes, analyzed under 70- and 20-eV EI conditions.*

To evaluate mass spectral repeatability, a 20-eV MS database was constructed by using the spectra of the C10-C20 alkanes; after, two consecutive GC×GC-QMS analyses were

performed, an MS database search carried out, with an overall calculated average MS similarity of 95% (min. 92%; max. 97%).

Table 6.5. *Relative abundances for the molecular ions present in the mass spectra of linear alkanes in the range C10-C20, along with average values, under 70- and 25-eV EI conditions and ion source temperatures of 250°C and 150°C (the first value always refers to the 70-eV EI result*).

Alkane	**$[M]^{+\bullet}$% - 250°C**	**$[M]^{+\bullet}$% - 150°C**
C_{10}	2.2/2.7	8.9/11.8
C_{11}	1.7/2.0	8.6/9.0
C_{12}	1.7/1.7	7.8/9.2
C_{13}	1.4/1.6	7.5/8.4
C_{14}	1.1/1.2	6.8/8.0
C_{15}	0.9/1.0	6.3/8.7
C_{16}	0.8/0.8	6.4/7.3
C_{17}	0.7/0.8	5.4/7.3
C_{18}	0.6/0.8	5.1/7.2
C_{19}	0.5/0.6	4.5/6.9
C_{20}	0.4/0.6	4.9/7.3
Average	*1.1/1.3*	*6.6/8.3*

Considering further compounds contained in the unsaponifiable fraction of extra-virgin olive oil, squalene is the most abundant constituent, and is a branched triterpene hydrocarbon with six double bonds ($C_{30}H_{50}$). With respect to linear hydrocarbons, branched ones generate more stable secondary and tertiary cations, normally leading to a low-intensity MI [26]. In fact, under 70-eV EI conditions, its MI reached an intensity of 0.1%, while it increased to a value of 2% under milder EI conditions. Additionally, MIs of very low intensity were observed for the TMS-derivatized aliphatic alcohol 1-octanosol (molecular mass = 482.49 u) under both ionization conditions; however, under milder ionization conditions the intensity of the diagnostic ion $[M\text{-}CH_3]^+$ was greatly increased, while the presence of lower MW fragments was considerably reduced (*Figure 6.5*). Finally, vitamin E, in the form of (TMS-derivatized) α-tocopherol was characterized by an evident MI (*m/z* 502; 13.3%) under 70-eV EI conditions; under milder EI conditions, the MI reached an intensity of 54.5%, while the ion at *m/z* 237 became the base peak (*Figure 6.6*).

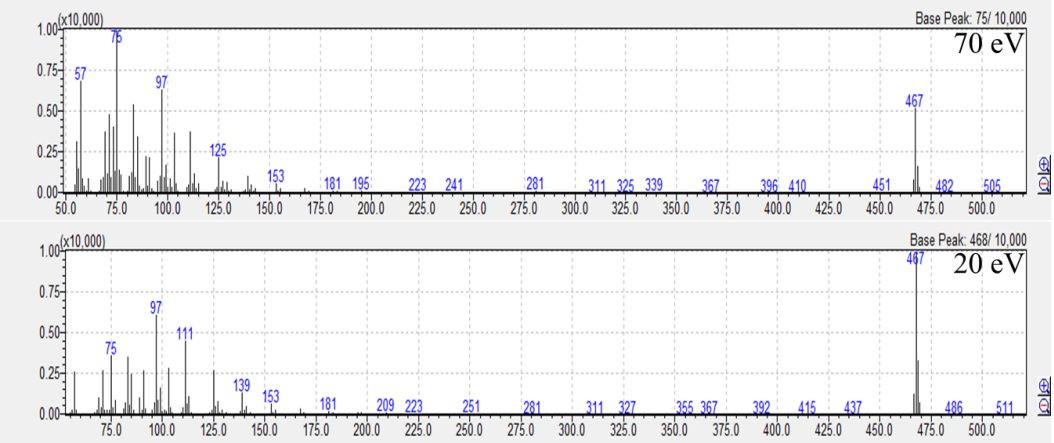

Figure 6.5. *Mass spectra for the TMS-derivatized 1-octanosol attained under 70- and 20-eV EI conditions.*

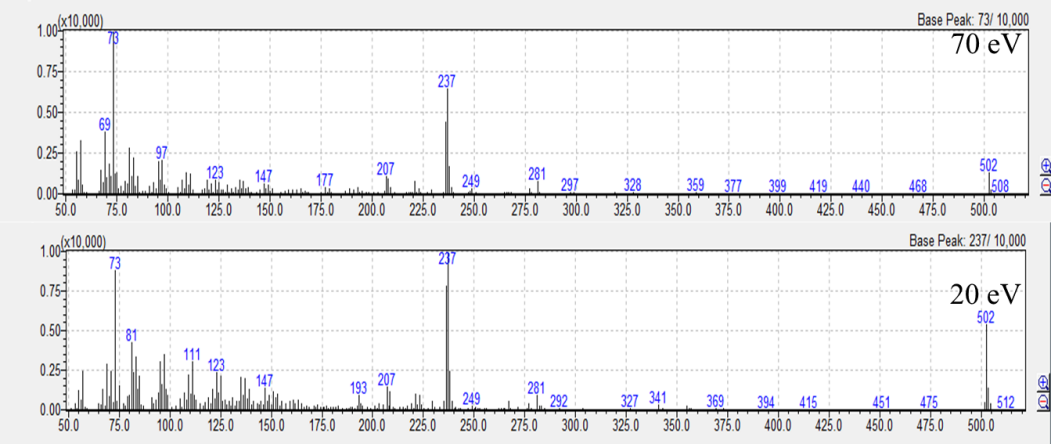

Figure 6.6. *Mass spectra for the TMS-derivatized α-tocopherol attained under 70- and 20-eV EI conditions.*

At this point of the research, the effects of two other MS operational conditions on the fragmentation process were investigated: the use of an EI energy slightly higher than 20 eV and the influence of the ion source temperature. As previously seen in the initial applications, the mass spectral differences between the 70- and 40-eV applications were limited. With regard to the source temperature, it is well-known that lower values promote reduced fragmentation, due to a reduction ofthe thermal vibrational energy [3,26]. The linear alkanes were again subjected to GC × GC-QMS analyses, this time under 70- and 25-eV EI energies, and at source temperatures of 250 °C and 150 °C. The 70 eV/250 °C results essentially confirmed those previously observed, in relation to the relative abundances of the C10-C20 MIs (*Table 6.5*). Furthermore, the use of 25 eV/250 °C conditions enabled only slight increases in the MI relative abundances: the average MI abundances were 1.1% and 1.3% under 70- and 25-eV EI conditions, respectively (*Table*

6.5). On the other hand, the use of a source temperature of 150 °C had a significant impact on the relative abundances of the MIs, with average values reaching 6.6% and 8.3% under 70- and 25-eV EI conditions, respectively (*Table 6.5*). For example, the MI of undecane (m/z 156) passed from a relative abundance of 1.7% to one of 9.0%, under 70 eV/250 °C and 25 eV/150 °C conditions, respectively. Although the scope of the present research is not a comparative one with other ionization technologies, it is noteworthy that the MI was the base peak in the spectrum of undecane with very limited fragmentation, when using GC × GC-SPI MS [10]. Moreover, in a flow-modulation GC × GC-SMB EI MS application on diesel fuel, the spectrum for a $C_{11}H_{24}$ hydrocarbon (presumably a branched alkane) was characterized by a base peak at m/z 156, while the general fragmentation profile was maintained [26]. Finally, a mixture containing 15 pesticides was subjected to GC × GC-QMS analyses, under 70- and 25-eV EI energies, and at source temperatures of 250 °C, 200 °C and 150 °C. Due to the differences in analyte chemistries, fragmentation behaviours varied greatly. However, distinct trends were again observed, with MI abundances reported in *Table 6.6*: the impact of using a source temperature of 150 °C, compared to one of 200 °C, was far greater than that observed between source temperatures of 200 °C and 250 °C. For example, under 25 eV EI conditions and at source temperatures of 250 ◦C, 200 ◦C and 150 °C, the average relative abundances of the MIs were 13.9%, 14.1%, and 18.9%, respectively. The combined use of a 25-eV EI energy and a source temperature of 150 °C enabled an increase in the average MI abundances of over 7%, with respect to 70 eV/250 °C conditions (11.6% →18.9%). In general, an increase in the abundance of higher mass ions, and a decrease of the lower mass ones, were observed. It must be noted, however, that source contamination increases when operating at lower temperatures, especially when high-boiling analytes are involved. Furtheromore, source-induced peak tailing can also occur [26].

***Table 6.6**. Relative abundances for the molecular ions present in the mass spectra of 15 pesticides, along with average values, under 70- and 25-eV EI conditions and ion source temperatures of 250°C, 200°C and 150°C.*

Compound	$M^{+\bullet}$	70 eV (250°C/200°C/150°C)	25 eV (250°C/200°C/150°C)
Dichlobenil	172	12.7/12.5/12.1	11.0/11.3/12.0
Pebulate	203	1.6/3.0/4.5	2.1/2.8/6.8
MCPA* methyl ester	214	57.3/64.1/69.8	70.6/77.0/93.2
Bromoxynil methyl	290	4.7/4.4/4.0	8.8/6.6/8.2
Chlorbufam	223	6.7/8.1/9.6	5.3/9.2/13.6
Terbacil	216	0.9/1.4/1.5	1.0/2.5/4.4
Dimethachlor	255	0.2/0.3/0.7	0.6/0.7/1.1
Orbencarb	257	0.3/0.6/0.9	0.2/0.6/1.0
Fluthiamid	363	0.4/1.1/2.1	0.5/1.2/2.4
Dimepiperate	263	0.7/1.6/3.0	0.8/1.9/3.1
Siduron isomer I	232	0.9/2.0/1.4	1.3/2.3/3.0
Nitrofen	284	46.0/42.7/54.5	42.2/43.9/57.2
Anilofos	367	0.4/0.7/1.0	0.5/0.7/0.5
Mefenacet	298	1.0/2.3/3.3	1.5/2.0/4.6
Fenoxaprop-P-ethyl	361	40.4/37.4/39.4	61.8/48.3/73.1
Average		*11.6/12.1/13.8*	*13.9/14.1/18.9*

**2-methyl-4-chlorophenoxyacetic acid*

6.4 Conclusions

The research herein described can be considered as a preliminary evaluation of the use of milder EI conditions, using cryogenically-modulated GC × GC-QMS. The results attained on various groups of chemically-diverse compounds can be considered as positive inasmuch that, compared to 70-eV EI, a general increase in the relative abundance of higher-mass diagnostic fragments was observed, along with a reduced relative abundance of the lower-mass fragments. Moreover, it was seen that a reduction of the source temperature favoured a further enhancement of the higher mass ions. Such characteristics are beneficial not only for the purpose of identification, but also for more selective targeted analysis, using extracted ions and selected-ion-monitoring. Apart from the outcome of the investigation, which was in part expected, a further underlying objective was to emphasize the need for highly-informative and sensitive softer ionization approaches

References

[1] P.Q. Tranchida, I. Aloisi, B. Giocastro, L. Mondello, TrAC Trends Anal. Chem. 105 (2018) 360.

[2] J.H. Gross, Mass Spectrometry - A Textbook 2nd Edition, Springer-Verlag Berlin Heidelberg, 2011, pp. 21.

[3] E. de Hoffmann, V. Stroobant, Mass Spectrometry - Principles and Applications Third Edition, John Wiley & Sons Ltd Chichester, England, 2007, pp. 15.

[4] N. Ochiai, T. Ieda, K. Sasamoto, Y. Takazawa, S. Hashimoto, A. Fushimi, K. Tanabe, J. Chromatogr. A 1218 (2011) 6851.

[5] D. Megson, R. Kalin, P.J. Worsfold, C. Gauchotte-Lindsay, D.G. Patterson Jr., M.C. Lohan, S. Comber, T.A. Brown, G. O'Sullivan, J. Chromatogr. A 1318 (2013) 276-.

[6] L. Mondello, A. Casilli, P.Q. Tranchida, M. Lo Presti, P. Dugo, G. Dugo, Anal. Bioanal. Chem. 389 (2007) 1755.

[7] W. Welthagen, S. Mitschke, F. Mühlberger, R. Zimmermann, J. Chromatogr. A 1150 (2007) 54.

[8] M. Zoccali, P.Q. Tranchida, L. Mondello, Anal. Chem. 87 (2015) 1911-1918.

[9] W. Welthagen, S. Mitschke, F. Muhlberger, ¨ R. Zimmermann, J. Chromatogr. A 1150 (2007) 54.

[10] M.S. Eschner, T.M. Gröger, T. Horvath, M. Gonin, R. Zimmermann, Anal. Chem. 83 (2011) 3865.

[11] J.D. Byer, K. Siek, K. Jobst, Anal. Chem. 88 (2016) 6101.

[12] M. Kochman, A. Gordin, T. Alon, A. Amirav, J. Chromatogr. A 1129 (2006) 95.

[13] M. Poliak, A.B. Fialkov, A. Amirav, J. Chromatogr. A 1210 (2008) 108.

[14] U. Keshet, A.B. Fialkov, T. Alon, A. Amirav, Chromatographia 79 (2016) 741.

[15] D. Megson, X. Ortiz, K.J. Jobst, E.J. Reiner, M.F.A. Mulder, J-C. Balouet, Chemosphere 158 (2016) 116.

[16] M.S. Alam, C. Stark, R.M. Harrison, Anal. Chem. 88 (2016) 4211.

[17] L.M. Dubois, K.A. Perrault, P.-H. Stefanuto, S. Koschinski, M. Edwards, L. McGregor, J.-F. Focant, J. Chromatogr. A 1501 (2017) 117.

[18] W. Genuit, H. Chaabani, Int. J. Mass Spectrom. 413 (2017) 27.

[19] S. Shimma, S. Miki, M. Toyoda, J. Environ. Monit. 14 (2012) 1664.

[20] M. Polet, W. Van Gansbeke, P. Van Eenoo, Anal. Chem. Acta., doi.org/10.1016/j.aca.2018.08.050

[21] Y. Foo Wong, T.M. Uekane, C.M. Rezende, H.R. Bizzo, P.J. Marriott, J. Chromatogr. A 1477 (2016) 91.

[22] P.Q. Tranchida, S. Salivo, F.A. Franchina, I. Bonaccorsi, P. Dugo, L. Mondello, Anal. Bioanal. Chem. 405 (2013) 4655.

[23] Regulation 2568/91 and modifications, European Commission, 11th July 1991.

[24] L.J. Goad, T. Akihisha, Analysis of Sterols, Chapman & Hall, London, 1997, pp. 152.

[25] J.H. Gross, Mass Spectrometry - A Textbook, 2nd edition, Springer-Verlag, Berlin Heidelberg, 2011, 249.

[26] A. Amirav, A. Gordin, M. Poliak, A.B. Fialkov, J. Mass Spectrom. 43 (2008) 141.

Page intentionally left blank

Chapter 7

Research in the field of fast comprehensive 2D GC-MS: concept, method optimization, and application †

7.1 Introduction

The present research is based on the concept of using a 10 m × 0.1 mm id column for cryogenic modulation fast comprehensive two-dimensional gas chromatography-quadrupole mass spectrometry separations. Specifically, an 8.9 m × 0.1 mm id low-polarity column was used as first dimension, while a 1.1 m × 0.1 mm id medium-polarity one was used as second dimension. The main scope of the investigation was to develop a high peak-capacity method, with an analysis time of approx. 10 min. Various aspects related to method optimization are discussed, as well as separation parameters such as peak capacity (in each dimension, and as a total value), peak widths, modulation ratio, sensitivity enhancement, and number of spectra per peak. The fast approach was evaluated in applications involving a mixture of cosmetic allergens, and a sample of perfume. The approach proposed enables high-resolution separations in a short time (across the C_8 to C_{23} alkane range), as well as a considerable reduction of the consumption of gases for modulation cooling and heating.

† This Chapter has been adapted from the following publication: **B. Giocastro**, M. Piparo, P. Q. Tranchida, L.Mondello.in "*Cryogenic modulation fast GC×GC-MS using a 10 m microbore column combination: concept, method optimization, and application.*"*Journal of Separation Science, 2018, 41, 1112-1117.*

Comprehensive two-dimensional gas chromatography (GC×GC) was first reported in 1991, by Liu and Phillips [1]. This now well-known multidimensional technology is commonly performed by using a conventional column (*i.e.*, 30 m × 0.25 mm id × 0.25 μm d_f) as first dimension (^{1}D), and a short micro-bore column segment (*i.e.*, 1-2 m × 0.1 mm id × 0.1 μm d_f) as second dimension (^{2}D) [2-4]. The analysis timeframes are about the same as those observed in one-dimensional GC applications (1-2 h), even though variations do exist. For example, the first published GC×GC experiment was carried out in a rapid manner (analysis times did not exceed 5 min), by using an accelerated temperature program (43°C min^{-1}) [1]. Furthermore, Bruckner et al. described the first flow-modulation experiment in 1998, it being performed by using a switching valve located between a 4.9m × 0.53 mm id × 3 μm d_f ^{1}D capillary, and a 0.85m × 0.18 mm id × 0.15 μm d_f ^{2}D one [5]. A GC×GC experiment was performed on a sample of white gas in 75 s. It is noteworthy that the investigations described by Liu & Phillips and Bruckner et al. were both achieved by using consumable-free forms of modulation [1,5].

Cryogenic modulation (CM) is currently the most efficient form of modulation, if both GC×GC peak capacity and sensitivity are considered [6]. However, the most popular versions of such modulators (loop-type and quad-jet) require cryogenic fluids, as well as high volumes of gas for the heating and cooling steps. Cryogenic modulators with no cooling fluid requirements have been developed, even though the necessity of cooling and heating gases still remains. As a consequence, one must bear in mind the effectiveness of cryogenic modulation, as well as the convenience of reducing the consumption of cryogenic fluids and/or that of cooling/heating gases. A simple manner to reach such an objective is to perform faster GC×GC applications.

Fast CM GC×GC applications, even though scarce, have been reported in the literature; for example, Adahchour et al. used a 4 m × 0.1 mm id × 3.5 μm d_f ^{1}D non-polar column, and a 0.5 m × 0.05 mm id × 0.05 μm d_f ^{2}D medium-polarity one, for the separation of diesel oil [7]. The temperature program was: 40°C (2 min) to 250°C (2 min) at 10°C min^{-1}, for a total analysis time of 25 min. A short modulation time of 3 s guaranteed 4-5 modulations per peak. Junge et al. carried out fast CM GC×GC by combining a 5m × 0.1 mm id × 0.1 μm d_f ^{1}D column, with a 0.3m×0.05 mm id × 0.05 μm d_f ^{2}D one [8]. A mixture of 29 compounds was separated through the application of the following temperature gradient: 80°C to 250°C (0.14 min) at 35°C min-^{1}, for a total analysis time of 5 min. Modulation time was very short, namely 1 s; under such conditions, ^{1}D peaks were sampled once or twice. Finally, Purcaro et al used a low-polarity 11.4 m × 0.1 mm id × 0.1 μm d_f ^{1}D capillary, linked to a

1 m × 0.05 mm id × 0.05 μm d_f ^{2}D one, for the analysis of bacterial fatty acid methyl esters [9]. It was reported that the last compound of interest eluted within 25 min.

The scope of the present research is obviously not to perform, for the first time, a rapid GC×GC analysis; rather, the investigation is focused on the development of a fast CM GC×GC method, combined with single quadrupole mass spectrometry (QMS), by using a low-polarity 8.9 m × 0.1 mm id × 0.1 μm d_f ^{1}D column, connected to a medium-polarity 1.1 m × 0.1 mm id × 0.1 μm d_f ^{2}D column. Thus, the analytical columns together, were equivalent to a 10 m micro-bore column. The latter are well-established tools to perform fast GC separations [10], and the concept is in part here moved to GC×GC.

7.2 Experimental

- **Standard compounds and sample**

The cosmetic allergens listed in *Table 7.1* were supplied by Merck Life Science (Merck KGaA, Darmstadt, Germany). A solution at the 1 mg L^{-1} level was prepared in *n*-hexane. A sample of commercial perfume was diluted 1:10 (*v/v*) in *n*-hexane.

- **Instrumentation**

All CM GC×GC-QMS applications were performed on a system formed of two Shimadzu GC-2010 gas chromatographs, and a QP2020 quadrupole mass spectrometer (Kyoto, Japan). Data were acquired by using the GCMS solution software (Shimadzu). The MS database used was the FFNSC v. 3.0 (Shimadzu). Bidimensional chromatograms were generated by using the ChromSquare software v. 2.3 (Shimadzu).

The first gas chromatograph (GC1) was equipped with an AOC-20i auto-injector, and a split–splitless injector (310°C). The ^{1}D column was an SLB-5ms [(silphenylene polymer which can be considered equivalent in polarity to poly (5%diphenyl/95% dimethylsiloxane)] with dimensions 8.9 m × 0.10 mm id × 0.10 μm d_f. A 1.5m × 0.10 mm id uncoated column was used to create the modulator loop. The ^{2}D column was an SLB-35ms [(polymer which can be considered equivalent in polarity to poly (35%diphenyl/65% dimethylsiloxane)] with dimensions 1.1 m × 0.10 mm id × 0.10 μm d_f. All the columns used were provided by Merck Life Science. The connections between the ^{1}D and ^{2}D columns, and the modulator loop, were made by using two SilTite mini unions (Trajan/SGE, Ringwood, Victoria, Australia). Helium was supplied at the GC1 inlet at a

pressure of 480.5 kPa; volume and mode of injection: 2 μL in the split mode (10:1), for the solution of allergens, and 2 μL in the split mode (100:1), for the perfume sample.

Gas chromatograph conditions: GC1 temperature program: 50-250°C at 17.5°C min^{-1}; GC2 temperature program: 65-265°C at 17.5°C min^{-1}. Modulation was performed by using a cryogenic fluid-free modulator; modulation period was 2.5 s (the heating step was performed at 350°C, for 0.3 s).

Mass spectrometry conditions: the temperature of the interface was 250°C; the ion source temperature was 220°C, with analyte fragmentation induced by electron ionization (70 eV). A spectral generation frequency of 50 Hz was applied.

7.3 Results and Discussion

The ^{1}D capillary was of low polarity, and of dimensions 8.9 m × 0.1 mm id× 0.1 μm d_f; the ^{2}D column was of medium polarity, and of dimensions 1.1 m × 0.1 mm id × 0.1 μm d_f. An uncoated 1.5 m × 0.1mm id capillary was used as delay loop. The initial objective was to develop a fast GC×GC method with a duration of approx. 10 min. Method development was rather complex because it involved a series of variables, namely the temperature program (in the two GC ovens - GC1 and GC2), constant gas velocities in the two dimensions and in the delay loop (automatically calculated by a software supplied with the instrumentation), modulation period (cooling and heating times), average number of modulations per peak, and MS spectral generation frequency. Optimization was carried by using a C7-30 alkane series and a mixture of cosmetic allergens, with a great number of applications involved. A 50- 250°C temperature range was applied in GC1 (and GC2), with a gradient of 17.5°C min-1 (analysis time: 11.4 min); the applied inlet pressure generated a gas velocity in the first dimension of 50 cm s^{-1}.

The alkane series was subjected to an unmodulated experiment: the elution range observed extended from alkanes C8 to C23. Peaks widths (wb - 4σ) for alkanes C10, C16, and C23 were 1.3, 1.6, 1.6 s, respectively. With an average peak width of 1.5 s (for the 3 alkanes), it would be necessary to have a modulation period of 0.5 s to attain 3-4 modulations per peak.

Table 7.1. *Identification, peak widths, linear retention index deviations (ΔLRI) with respect to MS database values, and S/N increase (compared to an unmodulated experiment), for compounds numbered in Figure 7.1. The last line reports average values. The average ΔLRI value is an absolute one.*

Peak/Compound	w_b (ms)	ΔLRI	*s/n* increase
1. Benzaldehyde	93	12	4
2. β-Pinene	93	5	
3. Benzyl alcohol	107	1	6
4. Linalool	93	0	
5. Camphor	107	2	4
6. Menthol	107	-8	
7. Methyl Salicylate	107	0	
8. Citronellol	107	-5	3
9. Neral (Citral isomer I)	93	0	
10. Carvone	107	-2	
11. (E)-Cinnamaldehyde	120	4	4
12. (E)-Anethol	93	0	
13. (E)-Cinnamyl alcohol	107	0	
14. α,α-Dimethylphenethylacetate	107	1	
15. Eugenol	133	1	9
16. Majantol	120	5	
17. Caryophyllene	120	-1	
18. Isoeugenol	93	1	
19. α-Isomethyl ionone	107	1	7
20. Lilial	107	-8	
21. 3-Propylidenephthalide	133	0	
22. α-Amyl cinnammaldehyde	120	6	
23. Lyral isomer 2	160	1	
24. α-Amyl cinnamyl alcohol	147	6	
25. β-Santalol	106	7	
26. α-Hexyl cinnamaldehyde	147	4	5
27. Benzyl benzoate	147	6	5
28. Galaxolide	120	7	
29. Benzyl salicylate	160	11	
30. 16-Hexadecanolide	160	1	3
Means	117	4 (absol.)	5

A series of modulation periods were tested and it was found that a cooling period of at least 2 s was necessary to efficiently trap the more volatile alkanes (≤ C10). The cryogenic fluid-free CM system used was capable of reaching operational temperatures of approx. -90°C. A modulation period, composed of a 2 s cooling step and a 0.3 s heating (350°C) one, was found to perform efficient entrapment/re-injection processes across the entire elution range. A mixture of cosmetic allergens (1 mg L^{-1} solution), characterized by a variety of molecular weights and chemistries, was subjected to fast GC×GC-QMS analysis. The allergens subjected to analysis have all been highlighted by the Scientific Committee on Consumer Safety (SCCS) as skin sensitizers [12].

When using equivalent temperature programs in both ovens, it was observed that rapid elution from the ^{1}D column was the cause of rather low ^{2}D analysis temperatures. Slight excessive stationary-phase retention lead to wrap-around of several polar compounds, them eluting in the low-polarity part of the chromatogram (^{2}D t_R < 0.75 s). It was found that the use of a positive offset of 15°C, applied in the GC2 oven, along with an extension of the modulation period (2.2 s cooling step), enabled a more appropriate occupation of the two-dimensional space. Thirty representative compounds, distributed across the entire separation space, are numbered in *Figure 7.1* (for identification refer to *Table 7.1*). Non-polar compounds, such as hydrocarbons (e.g., β-pinene peak 2; caryophyllene- peak 17), were situated in the lower part of the chromatogram, while the contrary was observed for the more polar compounds [*e.g.*, benzyl alcohol - peak 3; (*E*)- cinnamaldehyde - peak 11; benzyl salicylate - peak 29]. The applied inlet pressure generated gas velocities in the loop and in the second dimension of approx. 95 and 185 cm s^{-1}, respectively. Considering previous research, such an intra-loop velocity condition enables efficient re-injection conditions [13]. It is noteworthy that the use of columns with the same internal diameter enabled the generation of satisfactory He linear velocities (for the scopes of the research) in the first and second dimension, as well as in the delay loop. The benefits of using equal id columns, in the first and second dimensions, have been recently emphasized [14].

Even though the analyte positions in the two-dimensional were those expected, on the basis of polarity, the occurrence of wrap-around was investigated. Considerin the ^{2}D gas velocity, a dead time of circa 0.6 s would be expected; consequently, a compound such as β-pinene, with an apparent ^{2}D retention time of about 0.4 s, is certainly characterized by wrap-around. Furthermore, as the peak widths for the thirty compounds are rather similar (*Table 7.1*), it can be deduced that all such analytes undergo the same number of “wrap-arounds”. The general degree of wrap-around was evaluated by first doubling the modulation period to 5 s: β-pinene was still characterized by a retention time of approx. 0.4 s. After, a modulation period of 7.5s was applied: β-pinene presented a retention time of approx. 5.4 s. Such data indicated the occurrence of two “wrap-arounds”. The retention time of β-pinene was confirmed through the application of other extended modulation periods (e.g., 12.5 s, 15 s). So, it was concluded that it was necessary to add 5 s to the apparent ^{2}D retention times of the analytes listed in *Table 7.1* to attain their real retention times.

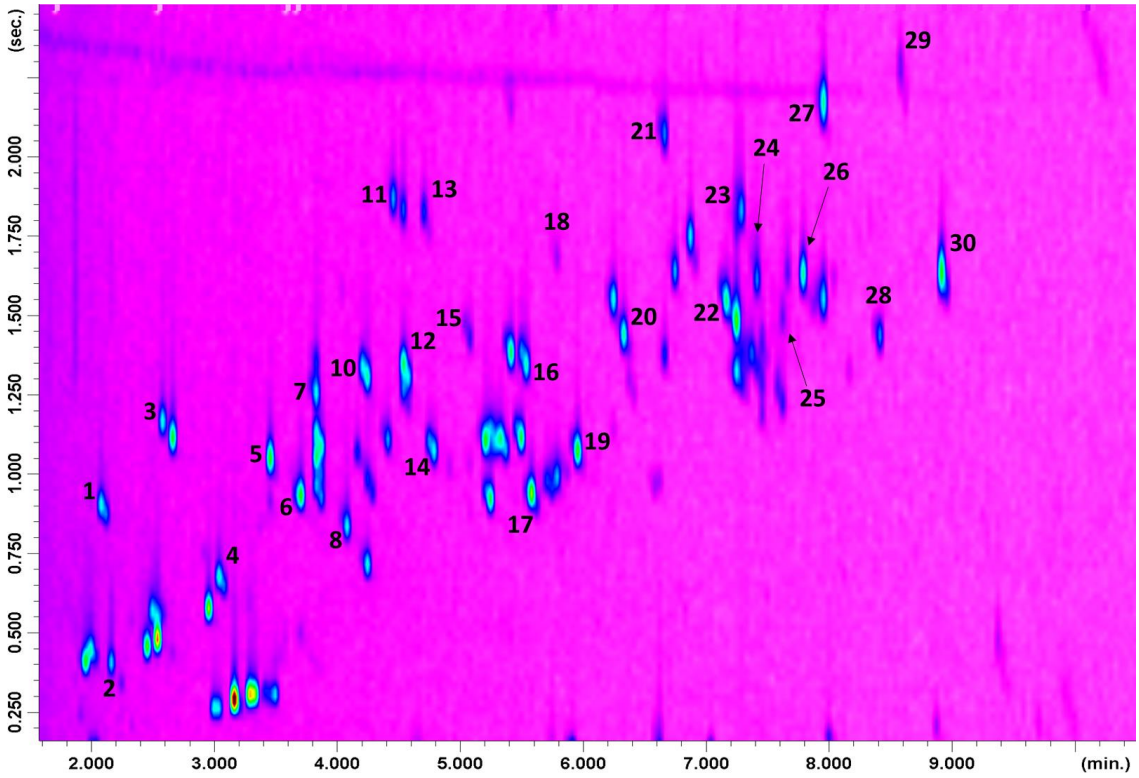

Figure 7.1. *Fast GC×GC-QMS chromatogram of a mixture of cosmetic allergens; the identity of the 30 numbered peaks is reported in Table 7.1.*

The method peak capacity was calculated by following a straightforward approach [11]: first-dimension peak capacity was roughly evaluated to be 420, it being calculated by dividing the elution time window (630 s) by the average width of the previously-mentioned non-modulated alkanes (1.5 s). Second-dimension peak capacity was roughly evaluated by calculating the average peak width value for the 30 allergens listed in *Table 7.1*.

Initially, 6σ peak width values were derived by counting the number of spectra contained in each peak, from the peak uprise to its return to the baseline. It was not possible to manually measure such a parameter on printed chromatograms, because the peaks were so narrow that the x-axis time intervals (expressed in minutes) did not accurately define peak widths. The QMS spectral production frequency was 50 Hz, with peaks reconstructed with 8, 9, 10, 11, 12 or 13 spectra, leading to a 6σ peak width range of 140-240 ms. The number of spectra generated per peak should be sufficient for the scopes of reliable quantification, if desired [16]. Four-sigma peak widths were derived from the 6σ values, and were calculated to be in the range of 93-160 ms, with an average approx. value of 117 ms.

Considering the entire modulation period, the void time was also considered because such space was occupied by wrap-around peaks - approx. 21 peaks could potentially elute one after another during each ^{2}D analysis. The product of the ^{1}D and ^{2}D peak capacities reaches a value of 8820. However, such a value must be corrected for undersampling: a “low” modulation ratio (MR) of 0.6 was calculated [17], considering the 1.5-s average peak width of the alkanes. Under the modulation conditions applied, ^{1}D peaks were sampled maximum once or twice, with such an event having a detrimental effect on ^{1}D resolution, and on the overall peak capacity. The reduction in peak capacity (β-correction) was calculated by exploiting theoretical considerations introduced by Davis et al. [18]. Specifically, a β value of 3.1 was calculated, leading to a corrected value of approx. 2850.

Apart from the negative impact on peak capacity, modulation undersampling should have a positive effective on sensitivity enhancement; very simply, ^{1}D peaks are distributed in a lower number of ^{2}D peaks (in this case one or two). The increase in sensitivity for 10 analytes, crossing the entire elution range, was evaluated by comparing S/N values in modulated and unmodulated experiments (n = 3). In the modulated experiment, and in the case of two modulations for a single compound, the most intense modulated peak was considered. In the unmodulated application, the spectral generation frequency was adjusted (5 Hz) to attain approximately 10 spectra per peak. Peak areas in the modulated and unmodulated experiments were also controlled to assure that similar sample amounts reached the ^{1}D column inlet. It is noteworthy that the general increase in signal intensities attained through the CM process was accompanied by a rather intense background noise, due to the 50-Hz spectral generation frequency; on the other hand, the background noise was much less in the unmodulated experiments. Moreover, it is obvious that the use of a short micro-bore ^{1}D column limited the extent of band broadening (compared to a conventional GC column). For such reasons, the S/N values were always higher in the GC×GC experiments, even though the enhancement was less than initially expected: S/N values were increased on average by a factor of approx. 5 for the 10 compounds, with minimum and maximum increases by factors of 3 and 9, respectively (*Table 7.1*). A final factor subjected to evaluation was the difference between experimental linear retention index (LRI) values and those present in the MS database used the latter being constructed by using a conventional GC column with the same stationary phase as that used in the first GC×GC dimension. As can be seen from the information listed in *Table 7.1*, the maximum LRI difference observed was that of 12 units for benzaldehyde; moreover, an absolute

average LRI difference of 4 units was calculated. As expected, a majority of positive LRI differences (19 compounds) were observed, due to the additional ^{2}D column retention. Such results indicate that the application of a tolerance range of ± 15 LRI units can be applied during the MS database search, to delete incorrect matches from the MS "hit" list.

Finally, a commercial perfume was subjected to fast GC×GC-QMS analysis (*Figure 7.2*); peak assignment was performed by using two filters, based on: i) a minimum spectral similarity of 90% ii) an LRI tolerance range of ± 15 units. The results of the MS database search are reported in *Table 7.2*: overall 36 peaks were assigned, with spectral similarities in the range 90-96%. Moreover, an absolute average LRI difference of 3 units was calculated, in good agreement with the data reported in *Table 7.1*. Eighteen compounds (reported in bold in *Table 7.2*), among the thirty-six, have been highlighted by the SCCS as skin sensitizers [12].

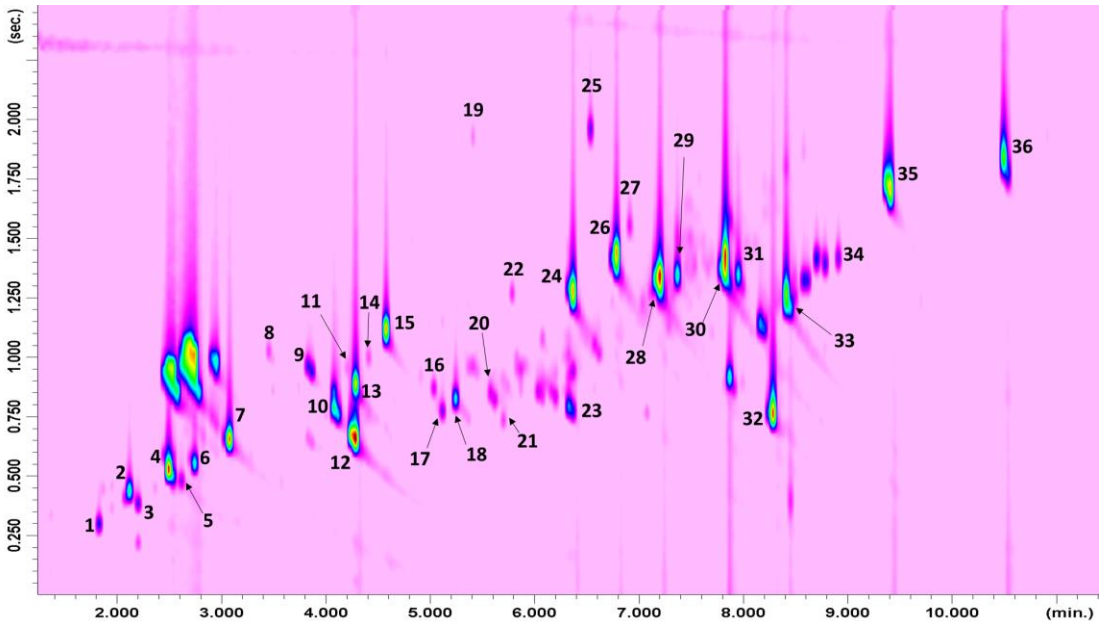

Figure 7.2. *Fast GC×GC-QMS chromatogram of a sample of commercial perfume; for peak assignment refer to Table 7.2.*

***Table 7.2**. Identification, linear retention index deviations with respect to MS database values, and spectral similarity values, for compounds numbered in Figure 7.2. Cosmetic allergens are reported in bold.*

Peak/Compound	ΔLRI	Similarity %
1. **α-pinene**	2	96
2. **β-Pinene**	-1	96
3. Myrcene	3	95
4. **Limonene**	-2	96
5. (*E*)-β-Ocimene	1	90
6. γ-Terpinene	4	95
7. **Linalool**	5	96
8. **Camphor**	1	93
9. **α-Terpineol**	1	94
10. **Citronellol**	0	94
11. **Neral (Citral isomer I)**	5	91
12. **Linalyl acetate**	3	96
13. **Geraniol**	1	94
14. **Geranial (Citral isomer II)**	2	90
15. **Hydroxycitronellal**	0	95
16. α-Terpinyl acetate	2	93
17. cis-Geranyl acetate	1	94
18. trans-Geranyl acetate	1	95
19. **Vanillin**	7	90
20. **Caryophyllene**	-1	95
21. α-Guaiene	1	90
22.1-(4-tert-Butylphenyl) propan-2-one	3	93
23.Hydroxycitronellal diethyl acetal	1	90
24. **Lilial**	2	92
25. Raspberry ketone	10	94
26. Phthalate diethyl	4	93
27. Isobutyl quinoline	7	92
28. cis-Methyl dihydrojasmonate	2	93
29. trans-Methyl dihydrojasmonate	5	94
30. **α-Hexyl cinnamaldehyde**	3	94
31. (*2Z*)-Hexyl cinnamaldehyde	2	95
32. Isopropyl myristate	3	95
33. **Galaxolide**	7	94
34. Ambrettolide	9	96
35. Ethylene brassylate	9	94
36. **Sclareol**	3	92
	3	

7.4 Conclusion

The scope of the present research was not to propose a fast GC×GC-QMS method, of general application, but to emphasize its concept, method optimization aspects, and potential. In fact, the approach herein developed can be applied to samples characterized by a C8-23 alkane boiling point range. The results described for the mixture of allergens and for the sample of perfume were certainly satisfactory. However, for other sample-types, one or more modifications of the many parameters which characterize a CM-GC×GC-QMS method would be necessary. In the case of fast GC-QMS experiments, using a 10 m × 0.1 mm id column, the main advantage over conventional GC-QMS applications, is the shorter analysis time. On the other hand, the benefits in the development of a fast CM GC×GC-QMS method are several, compared to a conventional approach. Apart from the obvious reduction in analysis time, there is also a decrease (in this investigation) of the consumption of heating and cooling gases. For CM systems using cryogenic fluids, there would be an additional economical advantage: the number of high-resolution GC separations, per unit volume of cryogenic fluid, would be much higher. Finally, the use of the same internal diameter in the first and second dimension, and in the delay loop, enables the generation of satisfactory gas velocities in all such zones.

References

[1] Z. Liu, J.B. Phillips, J. Chromatogr. Sci. (1991) 227.

[2] H.J. Cortes, B. Winniford, J. Luong, M. Pursch, J. Sep. Sci. 32 (2009) 883.

[3] P.Q. Tranchida, R. Costa, P. Donato, D Sciarrone, C. Ragonese, P. Dugo, G.Dugo, L. Mondello, J. Sep. Sci. 31 (2008) 3347.

[4] G: Purcaro, P. Q. Tranchida, L. Conte, A. Obiedzinska, P. Dugo, G.Dugo, L. Mondello, J. Sep. Sci. 34 (2011) 2411.

[5] C.A Bruckner, B.J. Prazen, R.E. Synovec, Anal. Chem. 70 (1998) 2796.

[6] M. Edwards, A. Mostafa, T. Górecki, Anal. Bioanal. Chem. 401 (2011) 2335.

[7] M. Adahchour., A.Taşöz, J. Beens, R.J.J. Vreuls, A.M. Batenburg, U.A.T. Brinkman, J. Sep. Sci. 26 (2003) 753.

[8] M. Junge, S. Bieri, H. Huegel, P.J. Marriott, Anal. Chem. 79 (2007) 4448.

[9] G. Purcaro, P.Q. Tranchida, P. Dugo, E. La Camera, G. Bisignano, L. Conte, L. Mondello, J. Sep. Sci.33 (2010) 2334.

[10] P. Donato, P.Q. Tranchida, P. Dugo, G. Dugo, L. Mondello, J. Sep. Sci. 33 (2007) 508.

[11] L.M. Blumberg, M. S. Klee, Anal. Chem. 70 (1998) 3828.

[12] Opinion on fragrance allergens in cosmetic products, SCCS/1459/11, June 2012.

[13] P.Q. Tranchida, M. Zoccali, F.A. Franchina, A. Cotroneo, P. Dugo, L. Mondello, J. Chromatogr. A 1314 (2013) 216.

[14] M.S. Klee, J. Cochran, M. Merrick, L.M. Blumberg, J. Chromatogr. A 1383 (2015) 151.

[15] B.D. Fitz, R.B. Wilson., B.A. Parsons, J.C. Hoggard, R.E.Synovec, J. Chromatogr. A 1266 (2012) 116.

[16] M. Adahchour, M. Brandt, H-U. Baier, R.J.J. Vreuls, A.M. Batenburg, J. Chromatogr. A 1067 (2005) 245.

[17] W. Khummueng, J. Harynuk, P.J. Marriott, Anal. Chem. 78 (2006) 4578.

[18] J.M. Davis, D.R. Stoll, P.W. Carr, Anal. Chem. 80 (2008) 461.

Chapter 8

Evaluation of a novel consumable-free thermal modulator: gas flow optimization aspects

8.1 Evaluation of different internal diameter uncoated modulation columns within the context of solid state modulator†

The present research is based on the use of a recently-developed comprehensive two-dimensional gas chromatography (GC×GC) thermal modulator, defined as solid state modulator (SSM). The SSM device was installed on top of a single GC oven, while benchtop low-resolution time-of-flight mass spectrometry (LR ToFMS) was used to monitor the compounds exiting the second analytical column. The SSM is a moving modulator which does not require heating and cooling gases to generate GC×GC data. The accumulation and re-mobilization steps occur on a trapping capillary, this being subjected to thermoelectric cooling and micathermic heating. In the present research, the effects on the modulation performance of the gas linear velocity, in particular, were evaluated by using two different uncoated trapping capillaries, *viz.*, 0.8 m × 0.25 mm id and 0.8 m × 0.20 mm id. Solid state modulator GC×GC-ToFMS applications were carried out on a standard solution containing *n*-alkanes (C_9, C_{10}, C_{12}), and on a sample of diesel fuel. The results indicated that the type of trapping capillary and gas velocity have a profound effect on modulation efficiency.

† This Section has been adapted from the following publication: M. Zoccali, **B. Giocastro**, P. Q.Tanchida, L. Mondello in *"Use of a recently-developed thermal modulator within the context of comprehensive two- dimensional gas chromatography combined with time-of-flight mass spectrometry: gas flow optimization aspects." Journal of Separation Science, 2019, 42, 691-697.*

8.1.1 Introduction

Comprehensive two-dimensional gas chromatography (GC×GC) is a very powerful technology, first described in 1991 by Liu and Phillips [1], and nowadays used in a variety of research fields [2-5]. The first modulator was a dual-stage one, and was constructed by looping the initial segment of the second dimension (^{2}D) outside the GC oven, and by coating it with gold paint. Compounds eluting from the first dimension (^{1}D) were subjected to phase-ratio focusing, because they were entrapped on a thick film (0.5 μm) of ^{2}D stationary phase, at ambient temperature. Electrical-heating of the gold coating enabled rapid thermal desorption of the entrapped chromatography bands [1].The longitudinally-modulated cryogenic system (LMCS), namely the first cryogenic modulator, was described in 1998 by Kinghorn and Marriott [6]. The LMCS is a moving CO_2-cooled cryo-trap, usually located at the head of the second dimension. The entrapment step occurs when the LMCS is immobile, while the re-injection step is performed when the cold column segment is exposed to the heat of the GC oven, through the longitudinal movement of the trap along the column. The "Phillips" modulator and the LMCS have been herein briefly described (the reader is directed to the literature if more details on modulation are required [7]) because they have both some characteristics in common with a consumable-free moving thermal modulator, recently described [8]. The transfer device, defined "thermal independent modulator" (TiM), was located on top of the GC oven, and used thermoelectric cooling and micathermic heating. The modulator position, and its consumable-free nature, were the main features in common with the "Phillips" modulator; analyte re-mobilization induced by column movement was the main characteristic shared with the LMCS. The ^{1}D and ^{2}D columns were connected by using a fused-silica modulation column (MC), with a 0.25 mm id. Cooling and heating processes were applied to a central segment of the MC. The TiM modulator is now commercially-available, and is defined with the term solid state modulator (SSM). In-depth optimization is a requisite for any type of modulation process, with such a topic being the focus of several studies [7]. The SSM was employed by Xiang et al. for the analysis of the volatile fraction of Dalbergia cochinchinensis Pierre samples [11], while Guan et al. developed a method for the analysis of highly volatile components (in the C_2 to C_{12} range) [12]. For such a purpose, a dedicated trapping column was employed, it being characterized by joining two pieces of uncoated column to each end of a porous layer open tubular column. Boswell et al. used the SSM within the context of group-type and biomarker analysis of Alberta oil sands bitumen [13]. An et al. reported

the use of the SSM within the context of quartz filter-based thermal desorption aerosol comprehensive two-dimensional gas chromatography -mass spectrometry [14].The SSM is a novel form of modulation, and as a consequence, details on optimization aspects are lacking. The present research can be located within such a context. In particular, the effects of the carrier gas average linear velocity (ALV) on the modulation performance were evaluated using two different uncoated MCs (0.8 m × 0.25 mm id and 0.8 m × 0.20 mm id).

8.1.2 Material and methods

- **Standard compounds and sample**

The *n*-alkanes (C_9, C_{10}, C_{12}) were supplied by Merck Life Science (Merck KGaA, Darmstadt, Germany). A solution at the 100 mg L^{-1} concentration level was prepared in *n*-hexane. A sample of diesel fuel was attained in a local petrol station (diluted 1:10 *v/v* in *n*-hexane).

- **Instrumentation**

All SSM GC×GC-time-of-flight(ToF)MS applications were carried out on a Master GC-ToFMS system, equipped with a Master AS autosampler and a split/splitless injector (280°C). (DANI Instruments SpA, Milan, Italy). Data were acquired by using the MasterLab solution software *v.* 4.1.5.5 (DANI Instruments SpA). Bidimensional chromatograms were generated by using the ChromSquare software *v.* 2.3 (Shimadzu, Kyoto, Japan).The primary column was an SLB-5ms [(silphenylene polymer, practically equivalent in polarity to poly (5% diphenyl/ 95 % methylsiloxane)], with dimensions 30 m × 0.25 mm id × 0.25 μm d_f. The secondary column was an SLB-35ms [(polymer which can be considered equivalent in polarity to poly (35%diphenyl/65% dimethylsiloxane)], with dimensions 1 m × 0.10 mm id × 0.10 μm d_f. Two different modulation columns - 0.8 m uncoated column segments with id values of 0.25 mm and 0.20 mm - were evaluated under different gas flow conditions (see Results and Discussion). All capillary columns used were kindly provided by Merck KGaA. The connections between the two analytical columns, and the MCs, were made by using two press fits. Modulation was performed by using a solid state modulator (SSM 1800 – J&X Technologies, Shanghai, China). Alkane

applications were carried out under isothermal condition (130°C): injection volume was 0.3 µl, using a split ratio of 100:1. Different modulation conditions were evaluated, in terms of carrier gas (He) flow and modulation period (see Results and Discussion). The SSM entry and exit zones were maintained at 130°C and 230°C, respectively, while the temperature of the cold zone was -51°C. The diesel fuel was analysed under the following conditions: injection volume was 0.2 µl, using a split ratio of 50:1. Initial inlet pressure: variable (see Results and Discussion). The GC oven was heated from 50°C to 280°C at 3°C min^{-1}. A modulation period (P_M) of 4 s was applied (2 s release time); the entry zone was heated from 50°C to 280°C at 3°C min^{-1}, while the exit zone was heated from 150°C to 300°C (26.6 min) at 3°C min^{-1}. Time-of-flight MS conditions, in all applications, were as follows: the temperature of the interface was 240°C; the ion source temperature was 200°C, with analyte fragmentation induced by electron ionization (70 eV). A mass range of *m/z* 50-360 and a spectral generation frequency of 50 Hz were applied.

8.1.3 Results and Discussion

The SSM is positioned on top of the GC oven, and is formed of a thermoelectric cooling (TEC) device located between two heated aluminium chambers (hot entry and hot exit). The two chambers are each linked to two transfers lines, enabling connections to the GC oven and to the TEC device (the reader in directed to *section 2.5.1.2* for further details related to the structure and mechanism of SSM). In the present research, the entry zone and the GC oven were always at the same temperature, while a +100°C offset was applied to the exit zone, to guarantee efficient re-mobilization.

The ^{1}D capillary herein used was of low polarity, and of dimensions 30 m × 0.25 mm id × 0.25 µm d_f, while the ^{2}D column was of medium polarity, and of dimensions 1 m × 0.10 mm id × 0.10 µm d_f. It is worthy of note that the SSM was supplied with two different MCs, one uncoated (with a 0.25 mm id), while the other contained a stationary-phase coating of mid-polarity (0.18 mm id). In the present study, the modulation performance of two uncoated MCs with a length of 0.8 m, but with different internal diameters (0.25 and 0.20 mm), was evaluated in relationship to gas velocity. The use of two uncoated columns from the same producer was preferred, against using the 0.25 mm id MC from the SSM supplier, and the 0.20 mm id MC from a different company.

Initially, a solution containing n-alkanes C_9, C_{10}, and C_{12} was subjected to analysis, under isothermal conditions (130°C), enabling an evaluation of the efficiency of SSM entrapment and release. Gas linear velocities were calculated using previously-described approaches [9,10].

8.1.3.1 0.20 mm id modulation column

Two MC gas ALVs were tested, namely 28 and 21 cm s^{-1}. In the former case, an inlet pressure of 133 kPa generated ^{1}D and ^{2}D gas ALVs of 15 and 169 cm s^{-1}, respectively. With regard to the slower application, an inlet pressure of 72.7 kPa generated ^{1}D and ^{2}D gas ALVs of 11 and 125 cm s^{-1}, respectively.Four modulation periods were evaluated in both types of application, *viz.*, 1 s (0.5 s release time), 2 s (1 s release time), 4 s (2 s release time), and 6 s (3 s release time). *Figure 8.1* illustrates the results attained, with non-efficient entrapment (peak splitting) occurring for n-alkane C_9 in all cases. Peak widths (at half height - w_h) for the three alkanes (the most intense modulated peak was considered), in all four applications, are listed in *Table 8.1*.

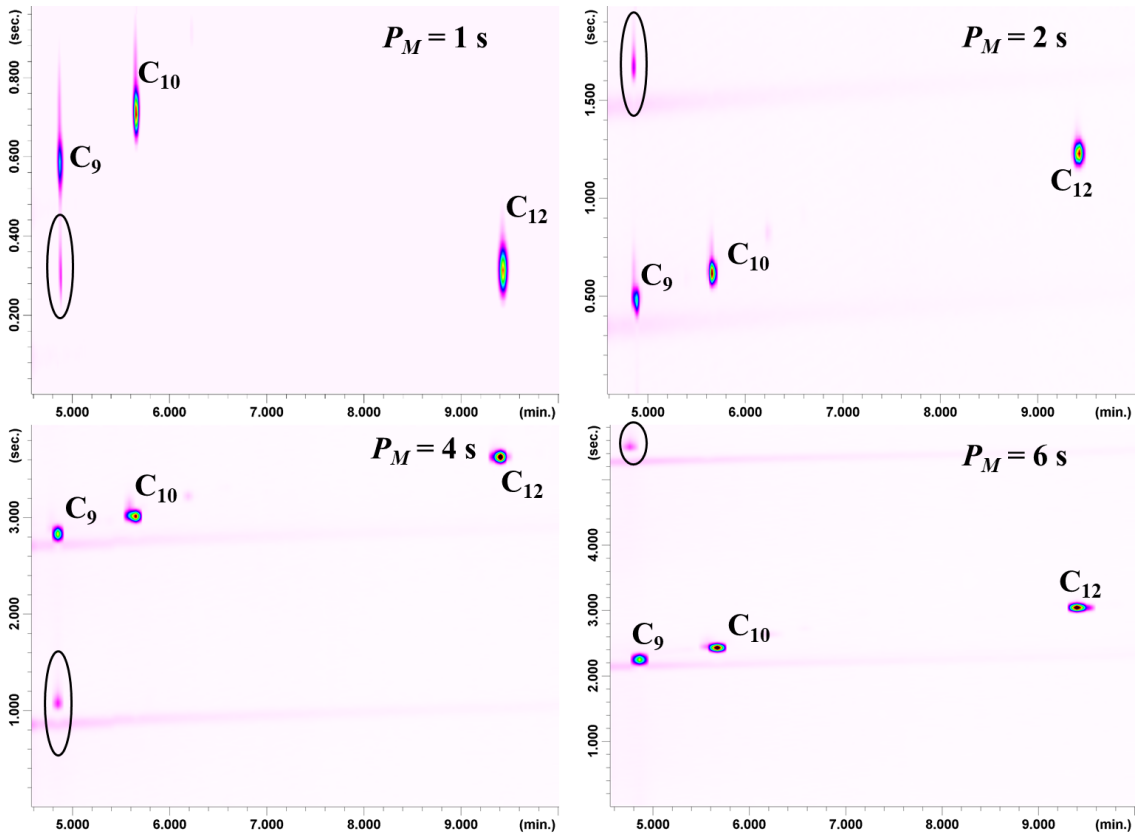

Figure 8.1. *Solid state modulation GC×GC-ToFMS chromatograms of n-alkanes C_9, C_{10}, and C_{12}, using 4 different modulation periods and an MC ALV of 28 cm s^{-1}. The breakthrough peak for n-alkane C_9 is circled.*

***Table 8.1**. Peak widths at half height for n-alkanes C_9, C_{10}, and C_{12} (average values are reported in italics), subjected to SSM GC×GC-ToFMS analyses (130°C) using a 0.8 m × 0.20 mm id MC, and different gas ALVs and modulation periods.*

MC ALV 28 cm s^{-1}			
P_M (s)	w_h C_9 (ms)	w_h C_{10} (ms)	w_h C_{12} (ms)
1	103	93	91
2	100	92	90
4	106	92	92
6	119	92	93
	103	*92*	*92*
MC ALV 21 cm s^{-1}			
P_M (s)	w_h C_9 (ms)	w_h C_{10} (ms)	w_h C_{12} (ms)
1	147	137	130
2	146	135	132
4	150	138	134
6	157	139	135
	148	*137*	*133*

The average w_h value for *n*-alkane C_9 was 103 ms, not considering the P_M of 6 s, because the compound was entrapped in a single modulation process causing slight peak overloading in the second dimension. For *n*-alkanes C_{10} and C_{12}, the average w_h value was 92 ms in both cases. The w_h values were slighter greater for n-alkane C_9, most probably due to non-efficient entrapment at the TEC temperature of -51°C. From such results it can also be concluded that the duration of the entrapment periods applied (50% of the modulation period) had no effect on peak width values.

It was presumed that peak splitting (or breakthrough) was caused by the MC gas ALV, and so the slower MC gas velocity was applied, using the same four modulation periods. *Figure 8.2* illustrates the results attained, with no breakthrough observed in all four applications. Such an outcome confirmed the relationship between breakthrough and MC gas velocity. Peak widths for the three alkanes, in all four "MC 21 cm s^{-1} ALV" applications, are listed in *Table 8.1*. The average w_h values for *n*-alkanes C_9 (again, the value at a PM of 6 s was not considered), C_{10} and C_{12} were 148, 137, and 133 ms, respectively. The higher w_h values, with respect to the faster analysis, can be related to the lower ^{2}D and MC gas ALVs [10].

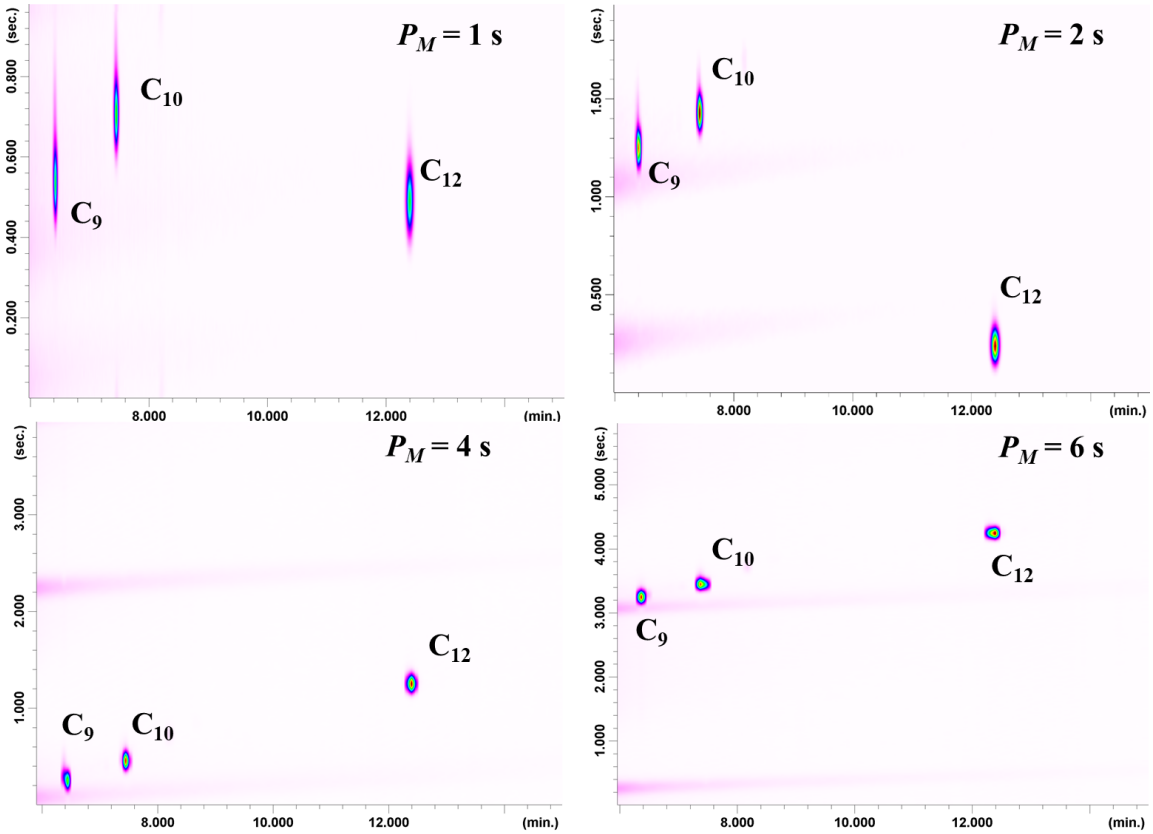

Figure 8.2. *Solid state modulation GC×GC-ToFMS chromatograms of n-alkanes C_9, C_{10}, and C_{12}, using 4 different modulation periods and an MC ALV of 21 cm s^{-1}.*

8.1.3.2 0.25 mm id modulation column

At this point, the 0.25 mm id MC was evaluated under a variety of experimental conditions. Specifically, MC gas velocities of 30 (inlet pressure: 286 kPa; ^{1}D and ^{2}D gas ALVs of 25 and 282 cm s^{-1}, respectively), 25 (inlet pressure: 218 kPa; ^{1}D and ^{2}D gas ALVs of 21 and 232 cm s^{-1}, respectively), and 15 (inlet pressure: 93 kPa; ^{1}D and ^{2}D gas ALVs of 13 and 141 cm s^{-1}, respectively) cm s^{-1} were generated, using a 2-s P_M. As can be seen in *Figure 8.3 a-c*, non-efficient entrapment occurred for *n*-alkane C_9 again in the faster application. Again peak widths at half height were calculated for the three alkanes in all four applications (*Table 8.2*), confirming the conclusions made for the 0.20 mm id MC, with respect to ^{2}D and MC ALVs.

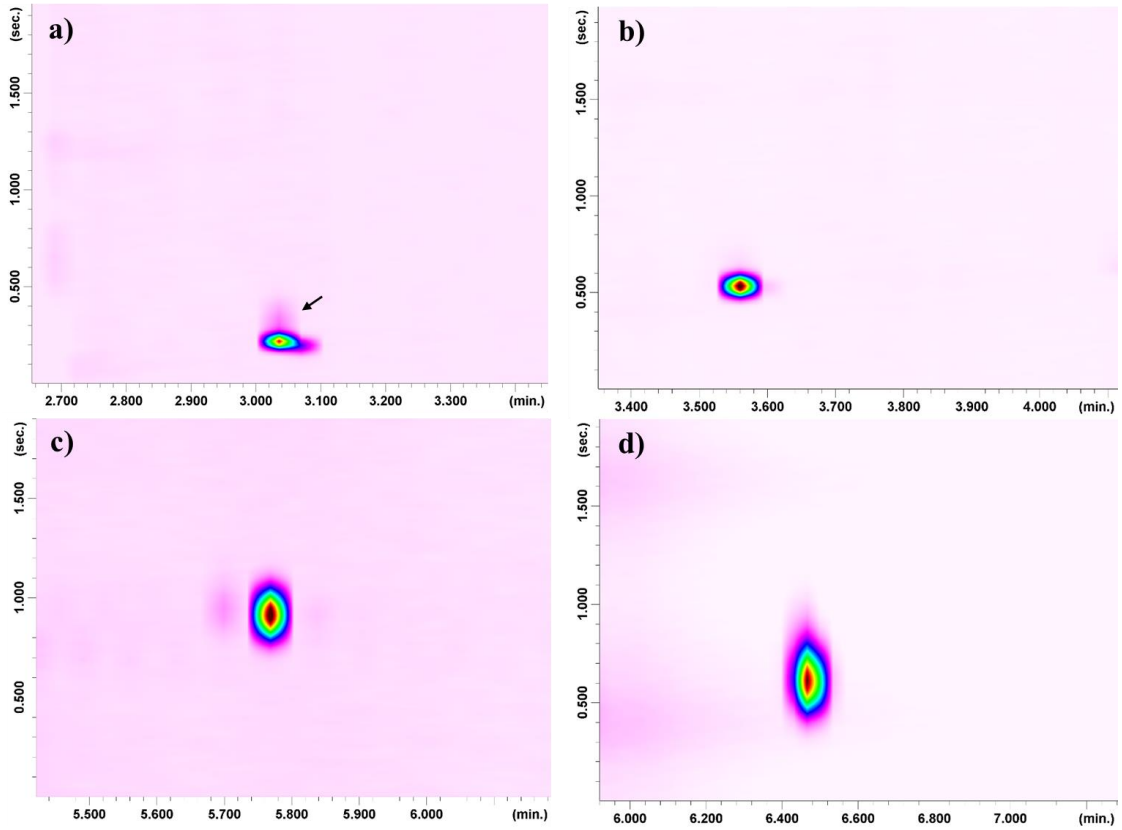

Figure 8.3. *Solid state modulation GC×GC-ToFMS chromatogram expansions showing n-alkane C_9, using MC ALVs of 30 cm s^{-1} (a), 25 cm s^{-1} (b), 15 cm s^{-1} (c), and 13 cm s^{-1} (d), and a 2-s modulation period.*

A fourth isothermal analysis was performed using an MC gas velocity of 13 cm s^{-1} (inlet pressure: 71 kPa), generating ^{1}D and ^{2}D gas ALVs of 11 and 125 cm s^{-1} (*Figure 8.3-d*). Such an experiment was performed to make a direct comparison with the 0.20 mm id MC analysis, carried out using an MC ALV of 21 cm s^{-1}, but with the same gas velocities in the first and second analytical column. In such a manner, the only differences between the two SSM GC×GC-ToFMS experiments were both the id and gas ALV of the MC.

Table 8.2*. Peak widths at half height for n-alkanes C_9, C_{10}, and C_{12}, subjected to SSM GC×GC-ToFMS analyses (130°C) using a 0.8 m × 0.25 mm ID MC, and different gas ALVs and a 2-s modulation period.*

MC ALV (cm s^{-1})	w_h C_9 (ms)	w_h C_{10} (ms)	w_h C_{12} (ms)
30	81	78	78
25	94	89	88
15	208	203	188
13	271	257	242

As observed in previous research [10], band velocity during the re-injection process can have a great effect on peak widths. In fact, the average w_h value for the three alkanes was 138 ms in the 0.20 mm id MC analyses, and 257 ms in the 0.25 mm id MC applications. An overlay of two modulated C_{12} alkane peaks, attained by using the 0.25 and 0.20 mm id MCs is shown in *Figure 8.4*. The benefits of using the 0.20 mm id column are evident. To be more specific, the increased peak widths were caused by the increased volume of the MC, from the point of entrapment to the ^{2}D column entrance, and by the lower MC gas velocity.

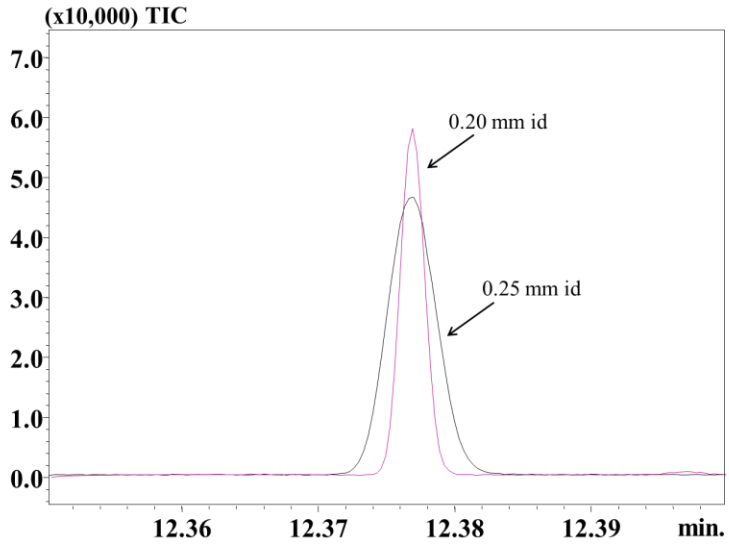

***Figure 8.4**. Overlay of two modulated C_{12} alkane peaks, attained by using the 0.25 and 0.20 mm id MCs, using MC gas ALVs of 13 and 21 cm s^{-1}, respectively.*

Finally, SSM GC×GC- ToFMS analyses were carried out on a real-world sample, namely diesel fuel, under temperature-programmed conditions (50°C to 280°C at 3°C min^{-1}). Four different MC gas ALVs were tested namely: 25 (inlet pressure: 175 kPa; ^{1}D and ^{2}D gas ALVs of 21 and 233 cm s^{-1}, respectively), 20 (inlet pressure: 119 kPa; ^{1}D and ^{2}D gas ALVs of 17 and 185 cm s^{-1}, respectively), 15 (inlet pressure: 62 kPa; ^{1}D and ^{2}D gas ALVs of 12 and 138 cm s^{-1}, respectively), and 13 cm s^{-1} (inlet pressure: 42 kPa; ^{1}D and ^{2}D gas ALVs of 11 and 121 cm s^{-1}, respectively). *Figures 8.5 a-d* report four chromatogram expansions (wrap-around corrected), highlighting the more volatile part of the sample.

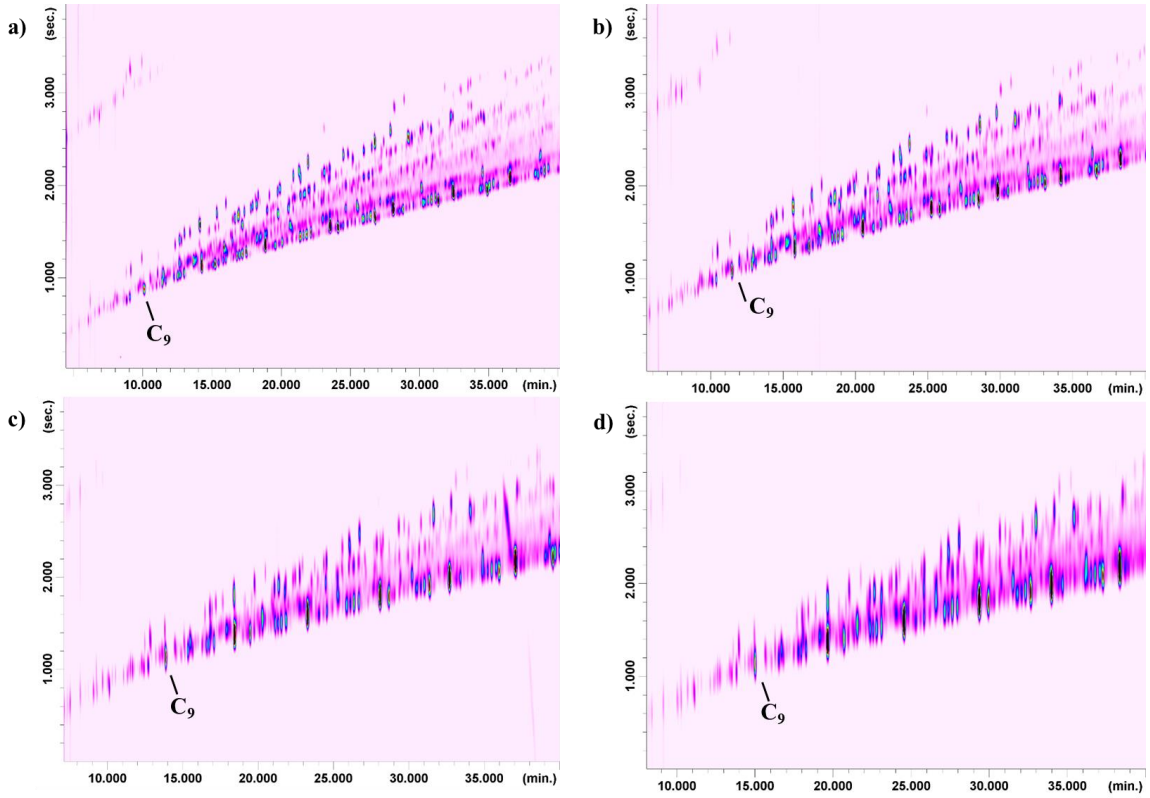

Figure 8.5. *Solid state modulation GC×GC-ToFMS chromatogram expansions of a diesel fuel, using MC ALVs of 25 cm s^{-1} (a), 20 cm s^{-1} (b), 15 cm s^{-1} (c), and 13 cm s^{-1} (d).*

As was previously observed, a decrease of the MC ALV lead to an improvement of the trapping of the more volatile compounds, thus reducing peak splitting. The position of the n-alkane C_9 is marked in all the chromatogram expansions. A series of double peaks was observed in the fastest analysis (*Figure 8.5-a*) which, on the basis of the MS information, were identified as C_8 alkanes (linear, branched and cyclic), and C_7/C_8 aromatic hydrocarbons. It is noteworthy that nonane was not found as double peak. Peak splitting was still present, albeit reduced, in the "20 cm s^{-1} MC ALV" application (*Figure 8.5-b*), and it involved C_8 alkanes (linear, branched and cyclic), and C_7/C_8 aromatic hydrocarbons. A further decrease in peak splitting can be observed in *Figure 8.5-c*, in this case involving the *n*-alkane C_7 (the slower ^{1}D ALV enabled elution of this compound beyond the solvent delay time) and C_8 alkanes (linear, branched and cyclic). Finally, only the C_7 *n*-alkane, along with branched and cyclic C_8 alkanes, were present as double peaks in the slowest application (*Figure 8.5-d*).

Apart from peak splitting, as expected the fastest application provided the best separation performance, due to a combination of adequate re-mobilization conditions, highest ^{2}D gas ALV, and lowest ^{2}D analyte elution temperatures.

8.1.4 Conclusions

The present work can be considered as a preliminary research, related to the operational optimization of the SSM. In general, GC×GC modulation optimization is characterized by a rather complex interplay of variables, and the SSM makes no exception. Among such variables, it has been herein demonstrated that the MC dimensions, along with the gas velocity conditions, can have a great impact on the modulation performance. In particular, higher intra-MC gas velocities cause incomplete entrapment of lower molecular weight compounds, and a better chromatography performance. On the other hand, more efficient analyte entrapment occurs at lower intra-MC velocities, at the cost of an inferior separation quality.

With regard to the 0.25 mm id and 0.20 mm id MCs, it was shown that, under equivalent ^{1}D and ^{2}D gas ALVs, the 0.20 mm id column provided a better performance. It is noteworthy that the SSM can accommodate an auxiliary gas flow, prior to the point of modulation, to improve the efficiency of the re-injection process. At the same time, however, an excessively-high ^{2}D gas flow can have a negative effect on analyte resolution. The auxiliary gas flow option will be evaluated in future research, along with the use of coated columns with a different IDs.

8.2 Evaluation of different internal diameter coated modulation columns within the context of solid state modulator

The aim of the present research is to evaluate the SSM modulation performance in relationship to different coated MC geometries. For such a purpose, two coated MCs with the same length, but with different ids (0.25 and 0.18 mm) were used. The effects of gas linear velocity (in particular), modulator temperature (exit zone) and modulation period were evaluated in several applications involving standard alkanes and a sample of diesel fuel. Fundamental gas chromatography parameters (peaks widths, resolution) were measured under the different experimental conditions. Detailed information is provided on gas flow optimization, with particular emphasis to the efficiency of chromatography band re-injection onto the second-dimension column. The results obtained from the present investigation highlight how the MC characteristics have a great impact on the overall GC×GC separation.

8.2.1 Experimental

- **Standard compounds and sample**

C_6, C_7 and C_8 *n*-alkanes, C_7-C_{30} *n*-alkane standard mixture, and solvents (*n*-hexane and dichloromethane), were provided by Merck Life Science. A sample of diesel fuel was attained from a local petrol station (diluted 1:10 *v/v* in *n*-hexane). A solution of C_6, C_7, and C_8 *n*-alkanes was prepared in dichloromethane at the 100 mg L^{-1} concentration level. The C_7-C_{30} *n*-alkane standard mixture was diluted in *n*-hexane at a concentration level of 100 mg L^{-1}.

- **Instrumentation**

All SSM GC×GC-FID applications were carried out on a Master GC system, equipped with a Master AS autosampler and a split/splitless injector (280°C) (DANI Instruments SpA, Milan, Italy). Data were acquired by using the MasterLab solution software *v*. 4.1.5.5 (DANI Instruments SpA). Two-dimensional chromatograms were generated by using the ChromSquare software *v*. 2.3 (Shimadzu, Kyoto, Japan).The primary column was an SLB-5ms [(silphenylene polymer, practically equivalent in polarity to poly (5% diphenyl/95 % methylsiloxane)], with dimensions 30 m × 0.25 mm id × 0.25 µm d_f. The secondary column was an SLB-35ms [(polymer which can be considered equivalent in polarity to poly (35%diphenyl/65% dimethylsiloxane)], with dimensions 1 m × 0.10 mm id × 0.10 µm d_f. Two different MCs coated with the same stationary phase (SLB-5ms) were evaluated under different gas (He) flow conditions (see Results and Discussion):

- 0.6 m × 0.18 mm id × 0.18 µm d_f
- 0.6 m × 0.25 mm id × 0.25 µm d_f

The MCs were connected with 0.2 m of uncoated column with the same id on the ^{2}D side using a SilTite µ-union (Trajan Scientific Australia Pty Ltd, Victoria, Australia). The µ-union was used to attach the MC to the gripper in the modulator exit zone. All capillary columns used were kindly provided by Merck Life Science.The connections between the two analytical columns, and the MC, were made by using two press fits (Restek Corporation, Bellefonte, USA). Modulation was performed by using a solid-state modulator (SSM 1810 – J&X Technologies, Shanghai, China). A scheme and details relative to the SSM can be found in *Figure 8.6*.The C_6, C_7, C_8 *n*-alkane applications were carried out under isothermal conditions (60°C): injection volume was 0.3 µl, using a split ratio of 100:1. Different modulation conditions were evaluated, in terms of gas flow, P_M,

and modulation temperatures (see Results and Discussion). The cold zone temperature was always -51 °C (in all the analyses). The C_7-C_{30} *n*-alkane applications were carried out under the following conditions: injection volume was 0.3 µl, using a split ratio of 100:1. The GC oven was heated from 50°C to 310°C at 3°C min^{-1}. The instrument was operated under constant average linear velocity conditions. A P_M of 6 s was applied (3 s release time). Different modulation conditions were evaluated, in terms of gas flow (see Results and Discussion). The diesel fuel was analysed under the following conditions: injection volume was 1 µl, using a split ratio of 100:1. The GC oven was heated from 50°C to 310°C at 3°C min^{-1}. A P_M of 6 s was applied (3 s release time). Different modulation conditions were evaluated, in terms of gas flow (see Results and Discussion). In all applications the FID temperature was 300°C, sampling frequency was 200 Hz, and gas flows were: 40 mL min^{-1} for hydrogen, 25 mL min^{-1} for nitrogen (make-up) and 280 mL min^{-1} for air, respectively.

8.2.2 Results and Discussion

8.2.2.1 Outline of the research

In-depth optimization is required for any modulation platform and a rather complex interplay of variables, which can affect the modulation performance, must be considered. The SSM is a relatively novel form of modulation, with information on optimization aspects still of interest.In previous work, the modulation performance was evaluated in relationship to gas velocity values by using two uncoated MCs, characterized by a different geometry (*viz.*, same length but different ids). It was observed that more volatile compounds suffered breakthrough (C_7-C_8-C_9 *n*-alkanes) under higher gas velocity conditions (*see Section 8.1*). The use of an MC with a stationary phase film will have a beneficial effect on the trapping of more volatile compounds. In this research, the low-polarity coated columns used were both 0.6 m long, with 0.25 and 0.18 mm ids, and film thicknesses of 0.25 and 0.18 µm, respectively. The phase ratio can be considered as the same in both cases. One side of each coated column was linked to a 0.2 m segment of uncoated column with the same id. The part containing the uncoated column was installed on the exit side in order to minimize band broadening due to the (unheated) transfer line between the modulator and the GC oven.

Initially, the effects of using MCs with different id on the modulation performance were evaluated. More specifically, five GC×GC-FID methods (A-E) characterized by different flow conditions and performed at the same constant temperature (60°C) were used. The modulation performance, when using the two MCs, was evaluated for each method for a total of 10 analyses. For each GC×GC-FID method the gas flow was maintained the same for the two analyses performed with the different MC. In each method, the (approximate) average linear velocity (ALV) values were equal or very similar in the ^{1}D and ^{2}D, and different in the MC exit zones (*Table 8.3*), in order to obtain the same elution temperature from the ^{1}D. In such a way, the only variable is the MC exit zone ALV. Once evaluated the modulation performances on the three volatile compounds (also in terms of P_M and exit zone temperature), the study was extended to a much wider volatility range, in temperature-programmed analyses.

***Table 8.3**. Analytical conditions applied for each SSM GC×GC-FID method. Inlet pressure (kPa), ^{1}D ALV (cm s^{-1}), ALV MC exit zone (cm s^{-1}), ^{2}D ALV (cm s^{-1}) and gas flow (mL min^{-1}).*

	0.25 mm id MC			0.18 id mm MC				
Method	Pressure	^{1}D ALV	ALV MC Exit zone	Pressure	^{1}D ALV	ALV MC Exit zone	^{2}D ALV	Flow
A	109	12	17	111	11	32	100	0.6
B	128	13	19	131	13	37	118	0.7
C	175	17	26	179	17	50	163	1.1
D	225	22	32	230	21	62	211	1.7
E	277	26	39	283	25	75	258	2.3

8.2.2.2 Isothermal analysis

The most important moments of the SSM process are the trapping and the re-injection steps, with the latter occuring in the exit zone (*Figure 8.6*). The cold zone is normally kept at its lowest possible temperature, namely −51 °C. The exit zone is usually held at a positive temperature offset with respect to the GC oven, in this case at +100°C. Initially, the effects of different P_M values on the modulation performance were evaluated. For such a purpose, three P_M values were applied, *viz.*, 2 s (1 s release time), 4 s (2 s release time), and 6 s (3 s release time). For inlet pressure and gas flow/velocity conditions refer to *Table 8.3*.

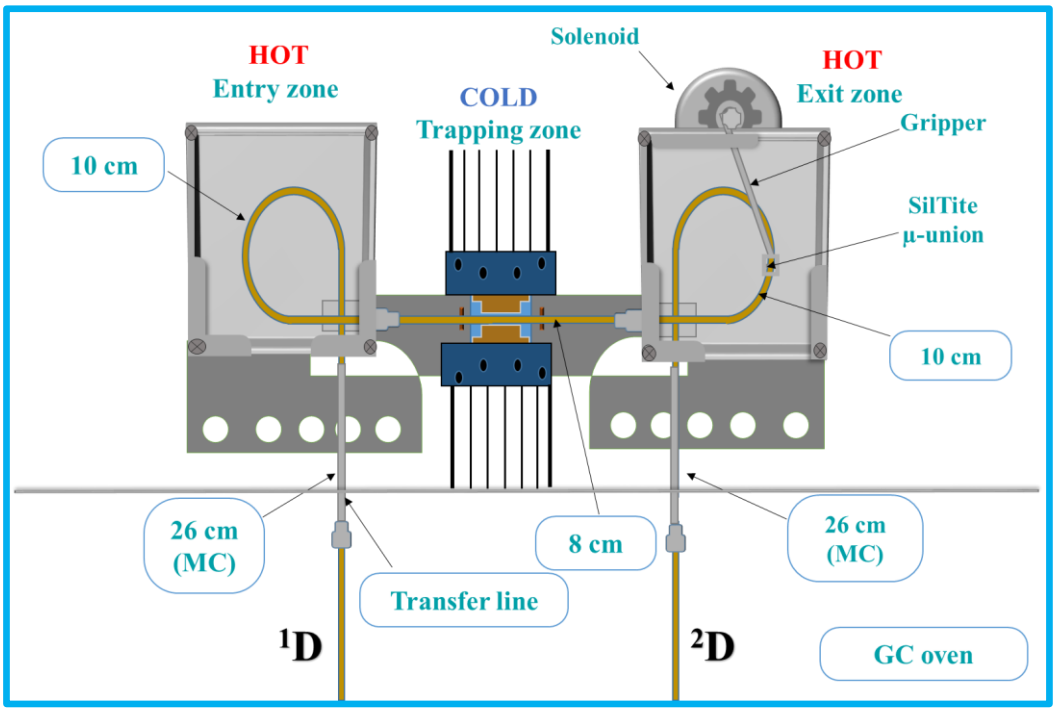

***Figure 8.6**. Scheme of the solid-state modulator.*

It was found that the use of different modulation periods had negligible effects on the peak full-width-at-half-maximum (fwhm) values (C_6, C_7, and C_8 *n*-alkanes) confirming the results observed in previous research (*Section 8.1*). The results hereafter described were attained by using a 4-s P_M. For the trapping process, apart from the temperature of the trapping zone, further experimentally-important aspects are the presence (or not) of a film of stationary phase in the MC and the MC ALV during analyte re-mobilization (exit zone). The use of a reduced-id MC (*e.g.*, 0.18 mm) will lead to a higher MC ALV in the exit zone, increasing the efficiency of re-injection and, at the same time, reducing the trapping capability (visible as breakthrough) for the more volatile compounds [15].

The use of the 0.25 mm id MC enabled the efficient trapping of all the hydrocarbons under all the conditions applied (*Tables 8.3* and *8.4*). Considering the fastest re-injection conditions (presumably the most efficient), achieved by using method E (ALV MC exit zone: 39 cm s^{-1}), the fwhm values for C_6, C_7, and C_8 *n*-alkanes were 80, 90 and 120 ms, respectively (*Figure 8.7a*).

Table 8.4. *Comparison of fwhm values (ms) using different id MCs and methods A-E. All applications were carried out under isothermal condition (60°C), applying +100°C in the modulator exit zone. For MCs ALVs please refer to Table 8.3.*

id MC	A - ^{2}D ALV 100 cm s^{-1}			B - ^{2}D ALV 118 cm s^{-1}			C - ^{2}D ALV 163 cm s^{-1}			D - ^{2}D ALV 211 cm s^{-1}			E - ^{2}D ALV 258 cm s^{-1}		
	C_6	C_7	C_8	C_6	C_7	C_8	C_6	C_7	C_8	C_6	C_7	C_8	C_6	C_7	C_8
0.25mm	230	230	290	190	190	240	130	140	180	100	100	140	80	90	120
0.18mm	120	120	150	100	110	130	80	80	110	-	70	90	-	70	90

The use of the 0.18 mm id MC enabled the efficient trapping of all the hydrocarbons using methods A-C (*Tables 8.3 and 8.4*). When using methods D-E only C_7 and C_8 *n*-alkanes were modulated efficiently; breakthrough occurred for C_6 *n*-alkane under the faster ALV MC conditions. Again, considering method E (ALV MC exit zone: 75 cm s^{-1}), the fwhm values for C_7 and C_8 *n*-alkanes were 70 and 90 ms, respectively. Compared to the 0.25 mm ID MC, and considering that the ^{2}D ALV values were the same (method E: 258 cm s^{-1}), a reduction of the fwhm values was obtained at the loss of modulation efficiency for C_6 *n*-alkane (*Figure 8.7 b*).

For the 0.18 mm id MC and this specific application, method C can be considered as a good compromise it providing both satisfactory modulation and chromatography performances (*Figure 8.7 c*). Hence, among all the 10 applications, it can be concluded that the best results were attained when using method C and the 0.18 mm id MC. It is noteworthy that the chromatograms in *Figure 8.7* have been all corrected for wrap-around by 1 s.

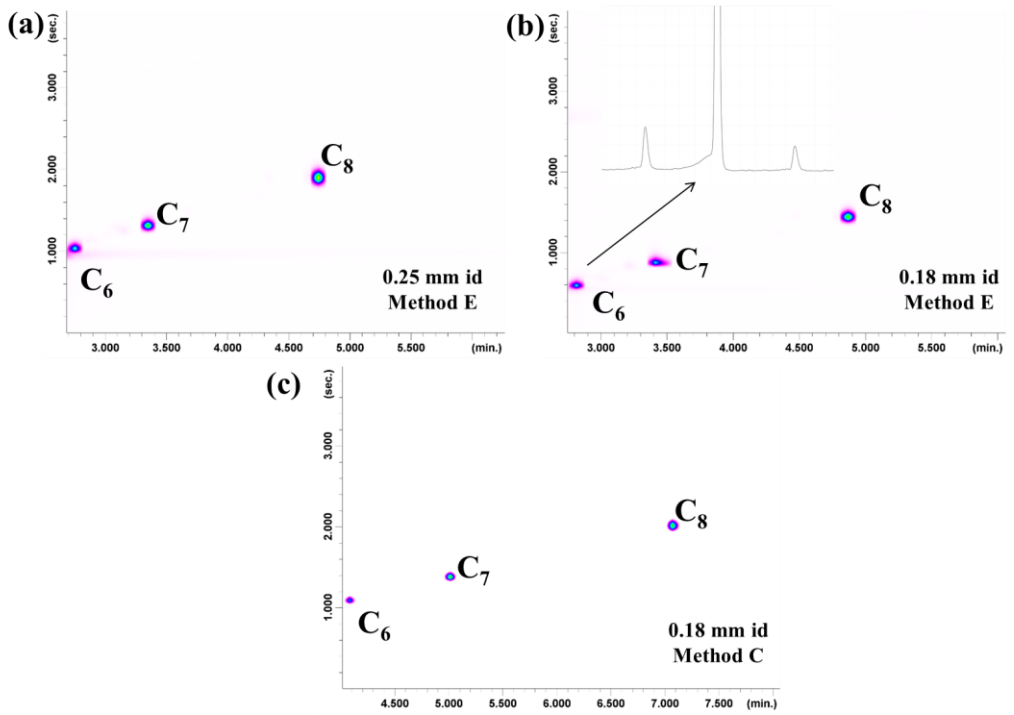

Figure 8.7. *SSM GC×GC-FID chromatograms of C_6, C_7 and C_8 n-alkanes using two different MCs under different conditions: a) 0.25 mm id MC - Method E; b) 0.18 mm id MC - Method E; c) 0.18 mm id MC - Method C. An untransformed chromatogram expansion for n-alkane C_6 is also shown in Figure 8.7b.*

Once established the effect of the different gas flows and MCs, attention was moved towards the evaluation of various exit zone temperatures during the re-injection step. The use of an exit zone +100°C offset on one hand provides general satisfactory re-mobilization, while on the other will cause enhanced MC bleed.

For such an evaluation, six different temperature offsets were applied to the exit zone: +0 °C (no offset compared to the GC oven), +25°C, +33 °C, +50 °C, +66 °C and +100 °C; in all cases a temperature of -51 °C was applied in the cold zone. What was considered the best method was used for each MC, for a total of 12 applications (*Table 8.5*). The 0.25 mm id MC was used under method E gas flow conditions. It was found that, apart from the use of no offset, fwhm values were always similar for C_6 and C_7 *n*-alkanes; on the other hand, fwhm values for C_8 *n*-alkane underwent a continuous increase as the offset was reduced (*Table 8.5*). For such a reason, the +100°C offset was chosen for the temperature-programmed analyses. The 0.18 mm id MC was used under method C gas flow conditions. Again it was found that, apart from the use of no offset, fwhm values were always similar for C_6 and C_7 *n*-alkanes; on the other hand, fwhm values for C_8 *n*-alkane underwent an increase when the offset was +33 °C and lower (*Table 8.5*). For such a reason, the +50 °C offset was chosen for the temperature-programmed analyses. The tendency observed in

analyte behaviour, in relation to the exit zone temperature, is obviously dependent on the thickness of the stationary phase. Specifically, a thinner stationary phase layer will require a lower SSM exit zone temperature.

Table 8.5. *Comparison of fwhm values (ms) using the best method for each MC (method E and method C for 0.25 mm and 0.18 mm id MCs, respectively). All applications were carried out under isothermal conditions (60°C) applying six different temperature offsets in the modulator exit zone. For ALV exit zone values please refer to Table 8.3.*

	0.25 mm id MC			**0.18 mm id MC**		
	E - ^{2}D ALV 258 cm s^{-1}			**C - ^{2}D ALV 163 cm s^{-1}**		
Offset	C_6	C_7	C_8	C_6	C_7	C_8
100°C	80	90	120	80	80	110
66°C	80	90	130	80	80	110
50°C	80	90	130	80	90	110
33°C	80	100	140	80	90	120
25°C	80	100	150	80	90	120
0°C	90	120	190	80	100	140

8.2.2.3 Temperature-programmed analysis

Once highlighted optimization aspects in isothermal applications on highly volatile alkanes, attention was directed to temperature-programmed analyses on samples characterized by a much wider volatility range. For such a purpose, a C_7-C_{30} *n*-alkane standard mixture and a diesel fuel sample were analyzed. All the experiments were carried out by applying the above-reported two exit zone temperatures and a P_M of 6 s. Gas linear velocity conditions underwent slight modifications in order to perform temperature-programmed analysis, and so the methods can still be defined as A-E. The ALVs related to the initial and final parts of the GC run are reported in *Table 8.6*: ^{1}D ALVs were constant across the temperature range, while both the MC exit zone ALVs and ^{2}D ALVs varied. It is noteworthy, in each method the ALV values were equal or very similar along the ^{1}D and ^{2}D for both MCs, thus maintaining constant the elution temperature.

***Table 8.6**. Analytical conditions applied for each temperature-programmed SSM GC×GC-FID analyses. ^{1}D ALV (cm s^{-1}), ALV MC exit zone (cm s^{-1}), ^{2}D ALV (cm s^{-1}) and gas flow (mL min^{-1}). The ALVs values at the start and at the end of the GC run (50°C-310°C) are reported. The ^{1}D ALVs were always constant and so a single value is reported.*

	0.25 mm id MC		0.18 id mm MC		
Method	^{1}D ALV	ALV MC exit zone	^{1}D ALV	ALV MC exit zone	^{2}D ALV
A	12	17-13	11	30-25	99-105
B	13	19-15	13	34-29	116-124
C	17	26-20	17	45-38	161-169
D	22	32-25	21	56-47	209-218
E	26	39-30	25	67-57	256-266

Again, ten experiments were performed on the C_7-C_{30} *n*-alkane mixture. With regards to the 0.25 mm ID MC, modulation was always satisfactory across the C_7-C_{24} *n*-alkane range. Above C_{24} *n*-alkane band broadening started to increase presumably due to the portion of unheated transfer line, connecting the exit zone to the GC oven. Considering methods B and C, the fwhm data have been plotted in two graphs shown in *Figure 8.8 a-b,* respectively. In the range C_7-C_{24}, the average fwhm was 173 and 124 ms, for methods B and C respectively; in the range C_{25}-C_{30}, the average fwhm was 262 and 195 ms, for methods B and C respectively (*Table 8.7*).

***Table 8.7.** Comparison of average fwhm values (ms) for C_7-C_{24} and C_{25}-C_{30} n-alkanes, using different id MCs and applying method B and C conditions. For ALVs please refer to Table 8.6.*

	Method B		Method C	
id MC	C_7-C_{24}	C_{25}-C_{30}	C_7-C_{24}	C_{25}-C_{30}
0.25 mm	173	262	124	195
0.18 mm	108	225	97	167

With regards to the 0.18 mm id MC, modulation was again always satisfactory across the C_7-C_{24} *n*-alkane range. Again, above C_{24} *n*-alkane band broadening started to increase. Considering methods B and C, the fwhm data is again shown in *Figure 8.8 a-b*. In the range C_7-C_{24}, the average fwhm was 108 and 97 ms, for methods B and C respectively; in the range C_{25}-C_{30}, the average fwhm was 225 and 167 ms, for methods B and C respectively (*Table 8.7*). It is noteworthy that methods B and C were selected because characterized by the same ^{1}D gas velocity for both MCs, and thus equivalent ^{2}D compound analysis temperatures.

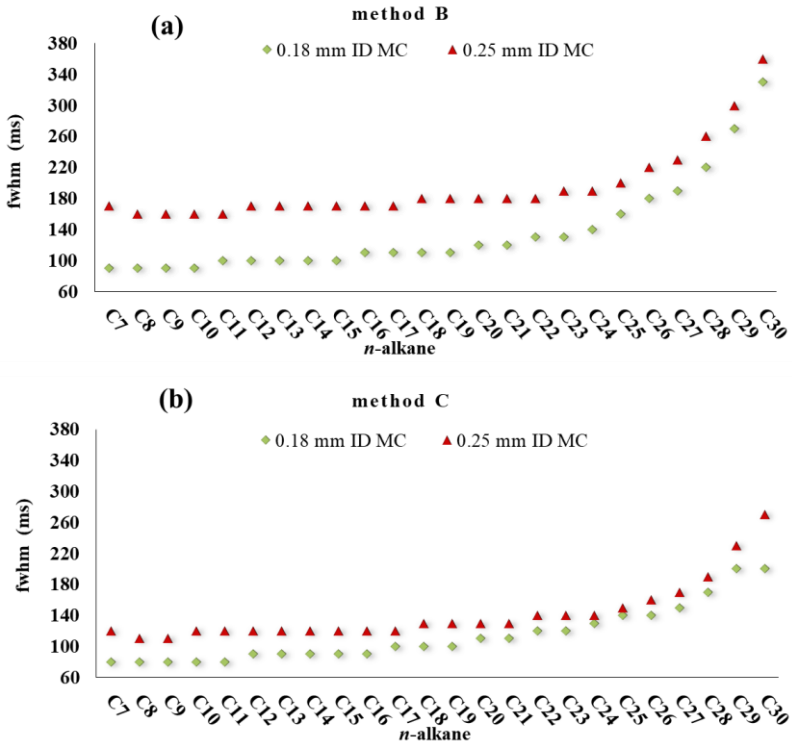

Figure 8.8. *Graphs constructed by using the fwhm (ms) values for the C_7-C_{30} n-alkane mixture using the two MCs and methods B (a) and C (b).*

The general chromatographic peak shape was herein evaluated in terms of asymmetry factor (*a*). Considering methods B and C, an average *a* value of 1.1 was found for both MCs, 0.25 and 0.18 mm ids respectively. At this point a sample of diesel fuel was subjected to analysis (carbon range: approx. C_6-C_{30}) using the two MCs, and methods B and C. The 2D chromatograms for the 0.25 mm id MC, relative to methods B and C, are shown in *Figures 8.9 a-b*, respectively.

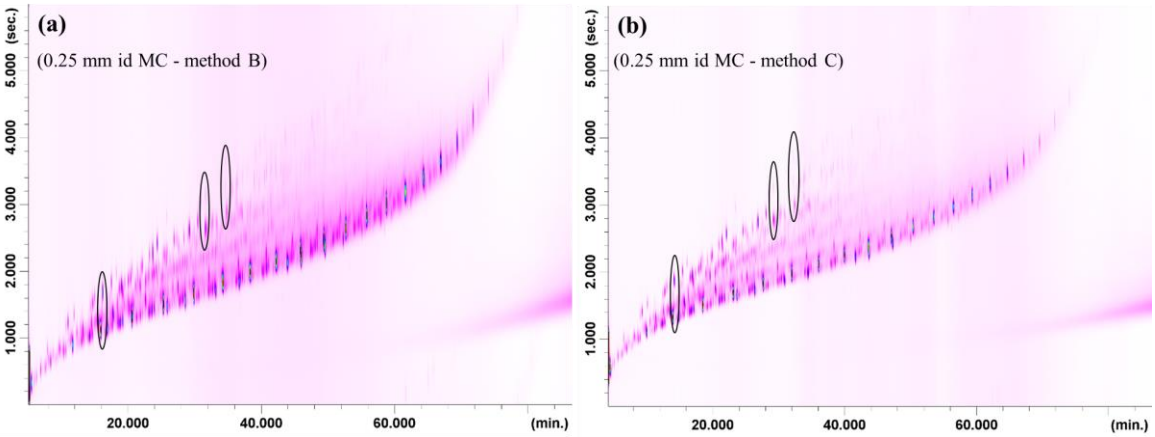

Figure 8.9. *SSM GC×GC-FID chromatograms of diesel fuel using the 0.25 mm id MC and methods B (a) and C (b).*

Resolution in the second dimension was measured for 3 pairs of compounds (classes C_{10}, C_{13}, and C_{14}), confined by ellipses in *Figures 8.9 a-b*. The results are reported in *Table 8.8*: for method C (compared to method B), resolution increased by 0.3 in two cases and decreased by 0.1 in one case.

***Table 8.8**. Second-dimension resolution values measured for 3 pairs of compounds (highlighted in Figures 8.9 and 8.10) using the two MCs and methods B and C. For ALVs please refer to Table 8.6.*

0.25 mm id MC		**0.18 mm id MC**	
B - ^{2}D ALV 118 cm s^{-1}	**C - ^{2}D ALV 163 cm s^{-1}**	**B - ^{2}D ALV 118 cm s^{-1}**	**C - ^{2}D ALV 163 cm s^{-1}**
1.3	1.6	2	2.1
1.2	1.5	1.9	2.2
1.5	1.4	1.7	1.8

The 2D chromatograms for the 0.18 mm id MC, relative to methods B and C, are shown in *Figure 8.10 a-b*, respectively. As can be seen, general resolution is slightly better in *Figure 8.10-b* (method C). Such an improvement was confirmed by measuring again resolution in the second dimension for the 3 pairs of compounds. The results are reported in *Table 8.8*. It is noteworthy that the chromatograms in *Figures 8.9* and *8.10* have been aligned (wrap-around corrected).

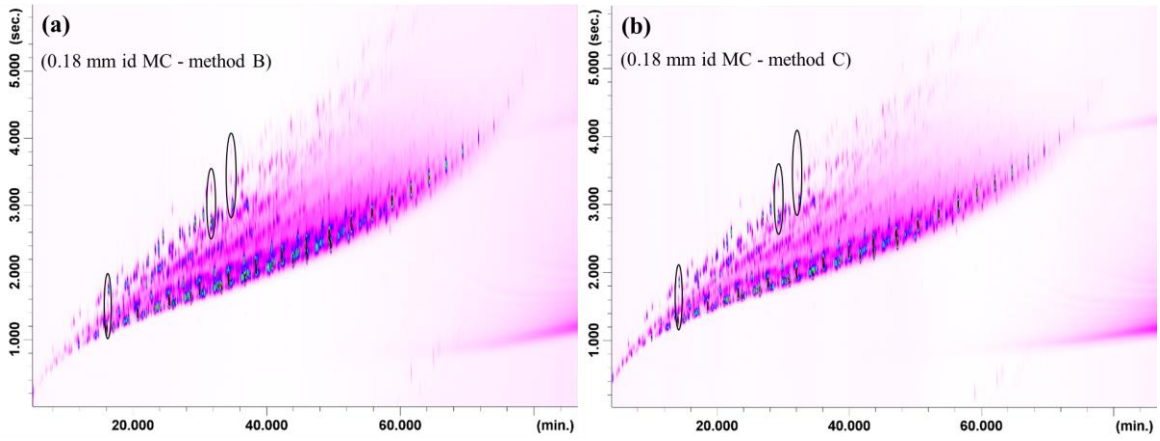

***Figure 8.10.** SSM GC×GC-FID chromatograms of diesel fuel using the 0.18 mm id MC and methods B (a) and C (b).*

8.2.3 Conclusions

Based on the results of the present research, it can be affirmed that MC geometries have a great impact on the SSM modulation performance. In particular, it has been demonstrated how the MC ID and film thickness both play an important role in both trapping and re-injection capabilities. A more efficient trapping of highly volatile compounds was reached using a thicker stationary phase film. On the other hand, a reduction of the MC id enabled more efficient chromatography band re-injection. Considering the results herein attained, the use of a 0.18 mm id × 0.18 μm d_f MC is certainly more advisable compared to a 0.25 mm id × 0.25 μm d_f one in the analyses described (C_7-C_{30} range). Specifically, the best results were achieved by using method C.

References

[1] Liu Z., Phillips J.B., J. Chromatogr. Sci. 29 (1991) 227.

[2] Tranchida P.Q., Franchina F.A., Zoccali M., Bonaccorsi I., Cacciola F., Mondello L., J. Sep. Sci. 36 (2013) 2746.

[3] Brokl M., Bishop L., Wright C.G., Liu C., McAdam K., Focant J.-F., J. Sep. Sci. 36 (2013) 1037

[4] Parastar H., Garreta-Lara E., Campos B., Barata C., Lacorte S., Tauler R., J. Sep. Sci. 41 (2018) 2368.

[5] Tranchida P.Q., Costa R., Donato P., Sciarrone D., Ragonese C., Dugo P., Dugo G., Mondello L., J. Sep. Sci. 32 (2008) 3347.

[6] Kinghorn R.M., Marriott P.J., J. High Resolut.Chromatogr. 21 (1998) 620.

[7] Bahaghighat H.D., Freye C.E., Synovec R.E, TrAC Trends Anal. Chem. https://doi.org/10.1016/j.trac.2018.04.016.

[8] Luong J., Guan X., Xu S., Gras R., Shellie R.A., Anal. Chem. 88 (2016) 8428.

[9] Harynuk J., Górecki T., J. Chromatogr. A, 1086 (2005)135.

[10] Tranchida P.Q., Zoccali M., Franchina F.A., Cotroneo A., Dugo P., Mondello L., J. Chromatogr. A 1314 (2013) 216.

[11] Xiang Z., Chen X., Zhao Z., Xiao X., Guo P., Song H., Yang X., Huang M., J. Sep. Sci. 4 (2018) 4315.

[12] Guan X., Zhao Z., Cai S., Wang S., Lu H., J. Chromatogr. A. 1587 (2019) 227.

[13] Boswell H., Carrillo K.T., Górecki T., Separations. 7 (2020) 13.

[14] An Z., Ren H., Xue M., Guan X., Jiang J., J. Chromatogr. A. 1625 (2020) 461.

[15] Tranchida P.Q., Zoccali M., Franchina F.A., Cotroneo A., Dugo P., Mondello L., J. Chromatogr. A. 1314 (2013) 216.

[16] Tranchida P.Q., Zoccali M., Franchina F.A., Dugo P., Mondello L., J. Sep. Sci. 36 (2013) 212.

List of Publications

- "Cryogenic-and Flow-modulation comprehensive two-dimensional gas chromatography-mass spectrometry: obtaining similar chromatography performances*."* **B. Giocastro**, I. Alosi, M. Zoccali, P. Q. Tranchida, L. Mondello. LC-GC (Europe) 33 (10) (2020) 512.
- "Towards the determination of an equivalent standard column set between cryogenic and flow-modulated comprehensive two-dimensional gas chromatography". I. Aloisi, T. Schena, **B. Giocastro**, M. Zoccali, P. Q. Tranchida, E. B. Caramão, L. Mondello, Anal. Chim. Acta 1105 (2020) 231.
- "Chemical characterization of unconventional palm oils from Hyophorbe indica and two other endemic Arecaceae species from Reunion Island." Y. Caro, T. Petit, I. Grondin, P. Clerc, H. Thomas, D. Giuffrida, **B. Giocastro**, P. Q. Tranchida, I. Aloisi, D. Murador, L. Mondello & L. Dufossé. Nat. Prod. Res.34 (2020) 93.
- "Comprehensive two-dimensional gas chromatography-mass spectrometry using milder electron ionization conditions: a preliminary evaluation." P. Q. Tranchida, I. Aloisi, **B. Giocastro**, M. Zoccali, L. Mondello, J. Chromatogr. A 1589 (2019) 134.
- "Use of a recently-developed thermal modulator within the context of comprehensive two-dimensional gas chromatography combined with time-of-flight mass spectrometry: gas flow optimization aspects." M. Zoccali, **B. Giocastro**, P. Q. Tranchida, L. Mondello, J. Sep. Sci. 42 (3) (2019) 691.
- "In-Depth Qualitative Analysis of Lime Essential Oils Using the Off-Line Combination of Normal Phase High Performance Liquid Chromatography and Comprehensive Two-Dimensional Gas Chromatography-Quadrupole Mass Spectrometry." M. Zoccali, **B. Giocastro**, I. L. Bonaccorsi, A. Trozzi, P. Q. Tranchida, L. Mondello, Foods, 8 (11) (2019) 580.
- "Current state of comprehensive two-dimensional gas chromatography-mass spectrometry with focus on processes of ionization." P. Q. Tranchida, I. Aloisi, **B. Giocastro**, L. Mondello, TrAC Trends Anal. Chem. 105 (2018) 360.
- "Cryogenic modulation fast GC×GC-MS using a 10 m microbore column combination: concept, method optimization, and application."**B. Giocastro**, M. Piparo, P. Q. Tranchida, L. Mondello, J. Sep. Sci. 41 (2018) 1112.